Demulsification Mechanism of Asphaltene Model Compounds- or Bitumen-Stabilized Emulsions by EO-PO Copolymers

By

Zhen Niu

A thesis submitted in partial fulfillment of the requirements for the degree of

Doctor of Philosophy

in

Chemical Engineering

Department of Chemical and Materials Engineering

University of Alberta

Abstract

The formation of stable water-in-oil (W/O) emulsions in the oil sands industry is highly undesirable because it poses great threats to the downstream operations, such as downstream upgrader corrosion, catalyst fouling, increased pumping cost, etc. To break the stable emulsions and to assist the separation of water from diluted bitumen, ethylene oxide-propylene oxide (EO-PO) polymeric demulsifiers are widely used. Understanding factors that affect emulsion stability and the role played by the demulsifiers in demulsification is of considerable importance to the oil industry. However, studying molecular mechanisms of stabilizing or destabilizing water-in-heavy oil emulsions is challenging due to the non-transparent nature of crude oil or bitumen even in diluted systems, as most measurements are based on visualization of the experimental systems. In comparison, measurement of interfacial properties using the oil-in-water (O/W) system is much easier, which is often practiced.

We aim to uncover the relationship between the measured interfacial properties of W/O and O/W systems using asphaltene model compounds C5Pe or C5PeC11, as their solutions have better optical transparency. The measured interfacial tension of the W/O system was always lower than that of the O/W system, indicating a larger amount of surface-active components adsorbed at the oil−water interface in W/O systems. The different amount of surface-active components adsorbed due to the reservoir effect (more C5Pe molecules are available for adsorption when oil is used as the continuous phase) affected the arrangement of molecules at the interface and hence the measured crumpling ratio, dilatational rheology, and coalescence time that could not be observed using flat oil−water interfaces. Although similar trends were observed in most situations, the O/W configuration could only give qualitative results for the W/O system.

The features of the W/O and O/W systems were also investigated when demulsifier is introduced. Specifically, the effect of the EO-PO demulsifier on the interfacial properties of the asphaltene model compounds C5Pe or C5PeC11 in xylene solution−water interface was studied, with the aim to understand the demulsification mechanism and investigate whether the EO-PO demulsifier could work similarly through adsorption replacement (the W/O system) and competitive adsorption (the O/W system). It was found the surface active EO-PO molecules could decrease the interfacial tension and interfacial film rigidity of the C5Pe/C5PeC11−water interface for both W/O and O/W systems. Interfacial pressure-area isotherm, AFM imaging, and shear rheology measurements were also carried out using diffusion (simulating adsorption displacement in the W/O system) and spreading (simulating competitive adsorption in the O/W system) protocols. The results confirmed that C5Pe molecules were responsible for the high interfacial film rigidity and the EO-PO demulsifier was able to destroy or avoid the formation of the C5Pe network interfacial film. Molecular dynamics simulation revealed that EO-PO molecules were more competitive for the interface and could replace most of the adsorbed C5Pe molecules, which made the interfacial film unstable. In addition, the adsorbed EO-PO molecules could form a new barrier at the interface, which inhibited the adsorption of the C5Pe molecules.

The demulsification performance of the EO-PO demulsifier on the water-in-diluted bitumen emulsions at elevated temperatures was investigated, while the reversed O/W emulsion systems were used for characterizing interfacial properties. Generally, better demulsification efficiency of the W/O emulsions by EO-PO copolymers was achieved at higher temperatures. As indicated by the interfacial tension results of the O/W system, the adsorption of the EO-PO molecules at the oil−water interface was enhanced at elevated temperatures. The droplet contraction experiment of the interfacial film using the O/W system revealed that EO-PO copolymers could significantly

soften the interfacial film formed at the oil−water interface, especially at elevated temperatures. The breakage of the interfacial film was observed with Brewster angle microscopy. Overall, the enhanced EO-PO adsorption could greatly soften and even break the interfacial diluted bitumen film at the oil−water interface at high temperatures, therefore promoting the coalescence of water droplets for efficient emulsion breakup.

Preface

Below is a statement of contributions to co-authored papers contained in this thesis that are either published or in preparation.

1. **Niu, Z**; Manica, R; Li, Z; He, X; Sjöblom, J; Xu, Z. Interfacial Properties Pertinent to W/O and O/W Emulsion Systems Prepared Using Polyaromatic Compounds. *Colloids Surf. A* **2019**, 575, 283-291. (Chapter 4)

I was responsible for designing and performing the experiments, data analysis, and drafting/revising the paper. Dr. Manica was involved in data interpretation and paper editing. Dr. Li was responsible for coalescence time measurement. Xiao He provided some helpful suggestions. Dr. Xu was involved in paper proofreading and editing.

2. **Niu, Z**; Yue, T; He, X; Manica, R. Changing the Interface Between an Asphaltene Model Compound and Water by Addition of an EO-PO Demulsifier through Adsorption Competition or Adsorption Replacement. *Energy Fuels* **2019**, 33, 5035-5042. (Chapter 5)

I was responsible for designing and performing the experiments, data analysis, and drafting/revising the paper. Tong Yue was involved in the experimental design. Xiao He was responsible for interfacial pressure-area isotherm measurement. Dr. Manica was involved in paper proofreading and editing.

3. **Niu, Z**; Ma, X; Manica, R. Yue, T. Molecular Destabilization Mechanism of Asphaltene Model Compound C5Pe Interfacial Film by EO-PO Copolymer: Experiments and MD Simulation. *J. Phys. Chem. C* **2019**, 123, 10501-10508. (Chapter 6)

I was responsible for designing and performing the experiments, data analysis, and drafting/revising the paper. Xiaomin Ma performed MD simulation. Dr. Manica and Tong Yue were responsible for paper proofreading and editing.

4. Effect of Temperature on Demulsification of Water-in-Heavy Oil Emulsions Using EO-PO Copolymer. In preparation. (Chapter 7)

I was responsible for designing and performing the experiments, data analysis, and drafting/revising the paper. Dr. Manica, Dr. Yan, and Dr. Xu were involved in paper proofreading and editing.

Acknowledgments

My deep gratitude goes first to my supervisor Prof. Zhenghe Xu for his professional guidance and support of the project. I appreciate all his contributions of ideas, funding, and time, which have allowed me to explore this topic in depth. Many times when I felt frustrated and unsure of my own work, it was Prof. Xu who never failed to offer advice and encouragement. I am also very thankful for the excellent model he has provided as a successful scientist and professor, which will influence me greatly on my scientific career in the future.

I appreciate Dr. Rogerio Manica, Dr. Zuoli Li, Dr. Ci Yan, and Dr. Zifu Li for their support on this project. Dr. Manica has provided numerous great suggestions for the improvement of all the papers and thesis writing. Dr. Zuoli Li has offered me not only countless valuable research advice but also generous help in my daily life. Her homemade sausage and Zongzi really made me feel warm in the cold Edmonton. Dr. Yan and Dr. Zifu Li have enlightened me on how to write a good paper.

I would also like to thank Mr. James Skwarok, Ms. Lisa Carreiro, Ms. Jie Ru, and Ms. Ni Yang for maintaining our great labs and providing timely help all the time. Great thanks also go to all members in the Oil Sands Research Group for their great help and suggestions on my work.

I would also like to thank the committee members for my candidacy exam, Dr. Qingxia Liu, Dr. Tony Yeung, Dr. Peichun Amy Tsai, and Dr. William McCaffrey, for their insightful questions during the exam, which gave me a good start of my PhD study.

I am grateful to the funding sources for my PhD work. Engineering Research Council of Canada (NSERC)-Industry Research Chair program in Oil Sands Engineering and Alberta Innovates-Energy and Environment Solutions have financially supported me during my whole PhD life.

Finally, I want to express my sincere appreciation to my family members. My parents have raised me with love and they are always supportive of all my pursuits. My sister has always been my best friend and tried her best to lessen the pressure in my life. I also appreciate my boyfriend for his faithful support and patience during the final stages of my PhD study. Without their strong support and selfless love, I would not have achieved what I have.

I will cherish this unforgettable experience at University of Alberta for my whole life.

Table of Contents

List of Figures

List of Tables

Chapter 1 Introduction

1.1 Importance of unconventional oil

Conventional oil is defined as the oil that can be economically extracted from deposits simply using standard drilling techniques. Because of this simplicity and relatively low-cost, the world has relied on the production of the conventional oil over the past several decades.[1-3] Decades of oil production have resulted in the extensive use of conventional resources, therefore, the less desirable unconventional oil has come to force as important resources. Unconventional oil such as heavy oil and bitumen resources is much more difficult to extract as specialized techniques and tools are needed. Although these materials are more expensive to produce and process than the most conventional petroleum reservoirs, they are available in abundance.[4] Alberta's oil sand resource is estimated at 1.7 trillion barrels, or 270 billion m^3 (ERCB ST98-2008) of crude bitumen, which represents one of the largest single deposit of oil in the world.

1.2 Oil sand

1.2.1 Oil sands formation

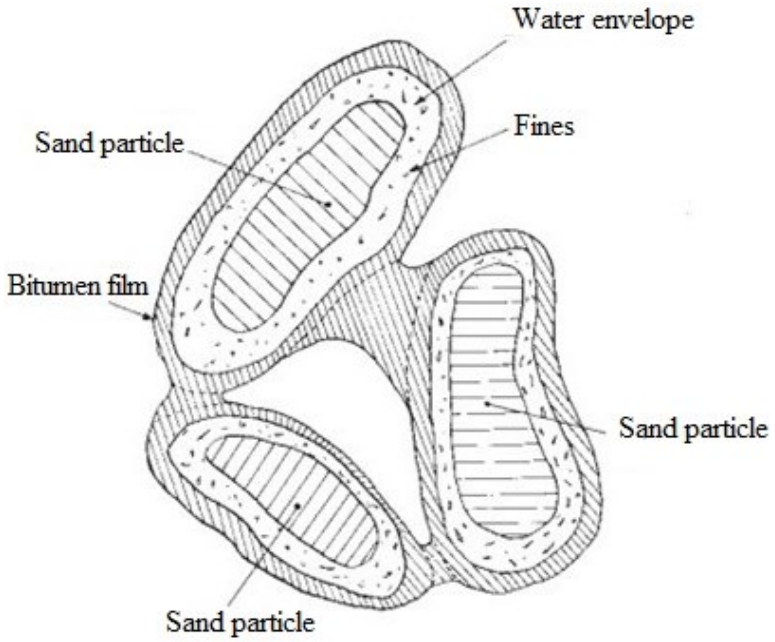

Figure 1-1 Composition of oil sands.

Oil sand is composed of quartz sand grains, covered by a film of water and clay, and embedded in the heavy oil called bitumen,[5] as schematically shown in **Figure 1-1**. It is widely accepted that the oil sands were formed many millions of years ago when Alberta was covered by a warm tropical sea. Marine life, mainly plankton and other marine animals, died and fell to the bottom of the sea and were embedded by sedimentary materials. Through pressure, heat, and time, their tiny bodies were transformed into bitumen products, which then seeped into the surrounding sands, forming oil sands.[4]

The bitumen content in deposits varies from 1% to 18%. More than 10 wt.% bitumen content is considered rich, while less than 6%-8% is considered poor and not economically feasible to mine, although it may be mined with a blended stock of higher grade oil sand.

1.2.2 Oil sands processing

There are three major oil sands areas in Alberta: Athabasca, Cold Lake, and Peace River. Each area is covered by a layer of overburden consisting of muskeg, glacial tills, sandstone, and shale. Based on the thickness of the overburden, two main methods are currently used to recover bitumen from oil sands: open pit mining and in situ[5] mining.

Open pit mining operations are applied to deposits of the overburden thickness less than 75 meters. It is estimated that among the oil sands deposits in Alberta, about 20% can be economically recovered by open pit mining technology.[4]

If the oil sand formation is deeper than 75 meters from the surface, the in situ technique is used. Since the oil sand content varies considerably from different deposits as well as within each deposit, no single method of in situ recovery can be applied to all oil sand deposits. Steam Assisted Gravity Drainage (SAGD) is the most common in situ process currently used. In this process, two parallel L-shaped wells are drilled into the deposit. Steam is injected through the top well. The injected steam heats the oil sand and reduces the viscosity of bitumen. The bitumen, together with the condensed steam, flows downwards into the bottom well and then pumped to the surface for further processing. Other in situ methods include Cold Heavy Oil Production with Sands (CHOPS), Vapour Extraction (VAPEX), and Cyclic Steam Stimulation (CSS), etc. CHOPS involves the deliberate initiation of sand influx into a perforated oil well, sustaining of sand influx during the productive life of the well, and separation of sand from the oil for disposal.

VAPEX is the same process as SAGD, except that a solvent vapor is injected to reduce the viscosity of the heavy oil. The diluted heavy oil will drain to the lower horizontal well by gravity, to be produced. CCS is predominately a vertical well process, involving the alternating injection of steam and production of oil with condensed steam from the same well. In the initial stage, steam is injected into a well. This is followed by a "steam soaking" period to heat the oil in the area, after which production is commenced. Then the cycle is repeated until production diminishes to noneconomic level.

1.3 Bitumen

1.3.1 Basics of bitumen

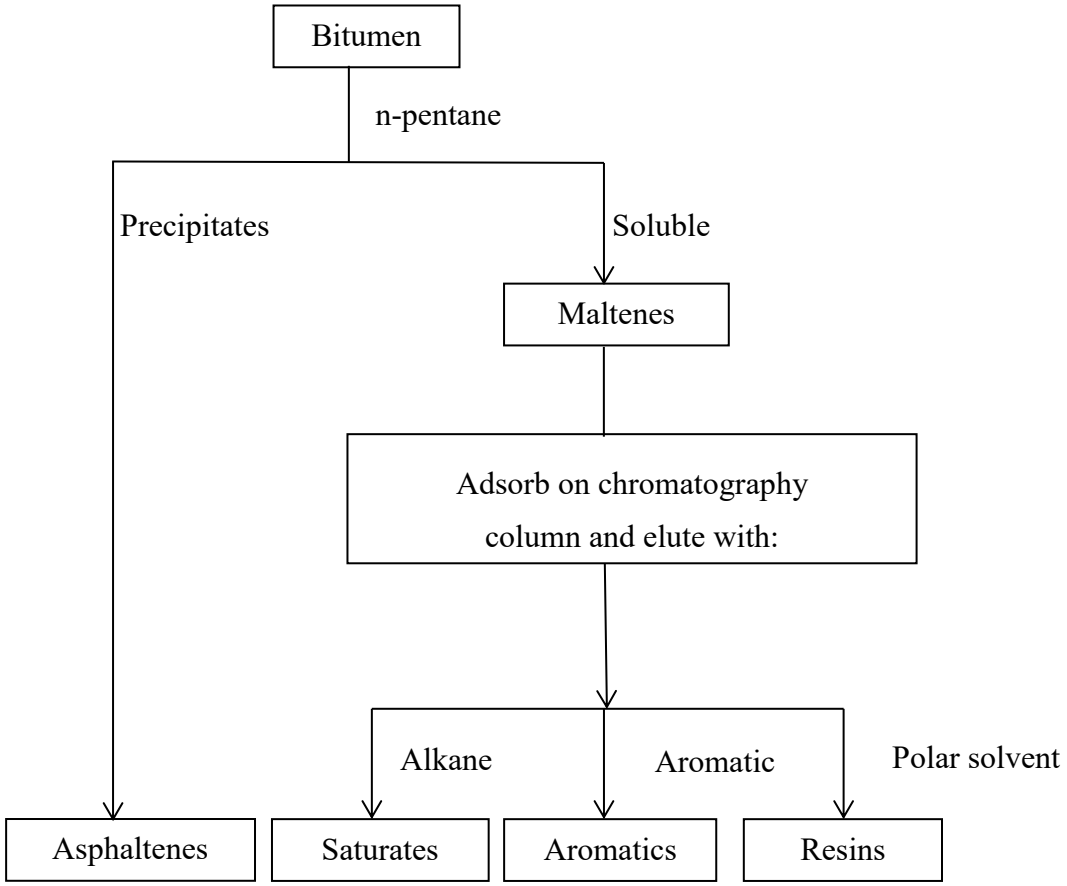

Figure 1-2 Basic flow sheet of SARA analysis.

Bitumen is a kind of extra-heavy oil in the oil sands and contains thousands of different hydrocarbon components. Bitumen is one of the most complex mixtures of molecules found in nature. The data in **Table 1-1** show the typical elemental compositions for some Alberta

bitumen.[5] The data of Athabasca bitumen composition illustrate that the bitumen composition depends on the exact origin of the sample and varies from one sample to another.

Bitumen	C	H	N	O	S
Syncrude	83.1	10.6	0.4	1.1	4.8
Suncor	83.9	10.5	0.4	1	4.2
Cold Lake	83.7	10.4	0.4	1.1	4.4

Table 1-1 Elemental composition of typical Alberta Athabasca bitumen (weight percent of the element; data from Speight).

Based on the solubility and adsorption characteristics, bitumen can be separated into several classes. Asphaltenes are defined as the bitumen or crude oil fraction that is soluble in aromatic solvents but insoluble in paraffinic solvents. Maltenes, also called deasphalted bitumen, contain all the soluble fractions of bitumen in n-pentane. The maltenes can be further separated into the following fractions by column chromatography: resins, aromatics, and saturates. A common acronym for this type of solubility and chromatographic separation protocol for petroleum is SARA analysis,[6] as schematically shown in **Figure 1-2**.

1.3.1.1 Asphaltene

Among all the components in bitumen or crude oil, asphaltenes are the most widely studied. The elemental analysis of Athabasca asphaltenes is shown in **Table 1-2**. Asphaltenes mainly consist of carbon, hydrogen, nitrogen, oxygen, and sulfur, and the hydrogen-to-carbon ratio is ~1.2. 40% of the carbon atoms are in aromatic rings and 90% of the hydrogen atoms are linked to saturated atoms in methyl and methylene groups, indicating a structure of condensed aromatic nuclei that carry alkyl and alicyclic chains with heteroatoms.

Table 1-2 Elemental compositions (wt.%) of Athabasca asphaltenes[7]

C	H	N	S	O	H/C
79.9	8.3	1.2	7.6	3.2	1.24

As mentioned in **1.3.1**, asphaltenes are typically defined as the fraction of bitumen or crude oil insoluble in paraffinic solvents (typically heptane, but also hexane or pentane) but soluble in aromatic solvents.[8-10] This definition inherently indicates that asphaltenes have undefined molecular structure and chemical composition. The average chemical formula of an asphaltene sample may be different between different sources.[11] Asphaltene model compound has been

widely used to investigate the mechanism of asphaltene behavior and emulsion stability,[12-14] where single and well-defined systems are used to have much higher control over the interfacial behavior and concentrations. Properties of asphaltene and asphaltene model compounds will be discussed in detail in **Chapter 2**.

1.3.2 Bitumen extraction

Bitumen from mineable oil sands ore can be recovered using the hot water extraction technique.[4] A typical bitumen extraction scheme is shown in **Figure 1-3**, where the mined oil sands ore is first crushed and then mixed with hot process water and chemical additives, such as caustic soda, to form the oil sands slurry. Usually, the slurry has a temperature of 35-55 °C and a pH of 8-8.5. The slurry is transported to the extraction plant to liberate bitumen. Air is then introduced into the slurry to aerate the liberated bitumen. The aerated bitumen has an apparent lower density than process water and hence floats to the top of the slurry to form a froth layer "rich" in bitumen. The recovered bitumen froth, on average, contains 60 wt.% bitumen, 30 wt.% water, and 10 wt.% solids. Most of the water is in a free form. The solids are entrained in the bitumen phase or accumulated at the oil−water interface.[15, 16] Most of the water and solids are then removed in the bitumen froth treatment plant prior to upgrading.

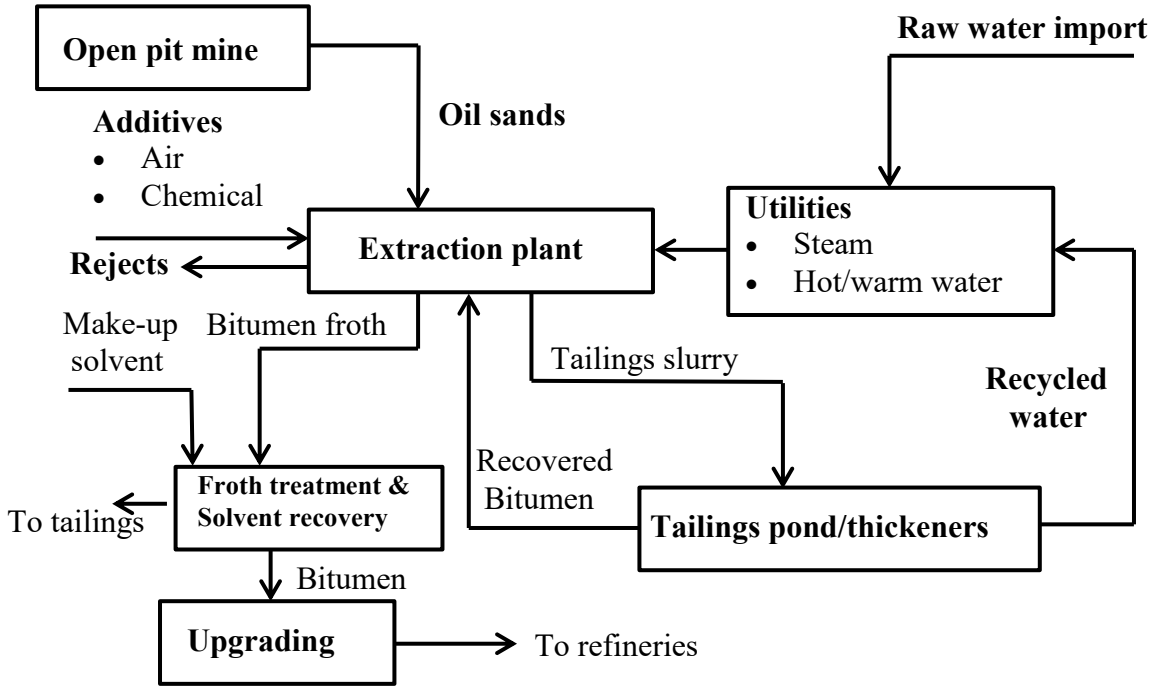

Figure 1-3 Schematic of the bitumen production process for mineable oil sands[4].

1.3.2.1 Bitumen froth treatment

Bitumen has almost the same density as water, therefore, a diluent is usually needed to create a density difference and reduce the viscosity of overall oil mixture. Based on the types of diluents used, two main technologies are currently used in commercial froth treatment operations: naphthenic froth treatment and paraffinic froth treatment, as shown in **Figure 1-4**.

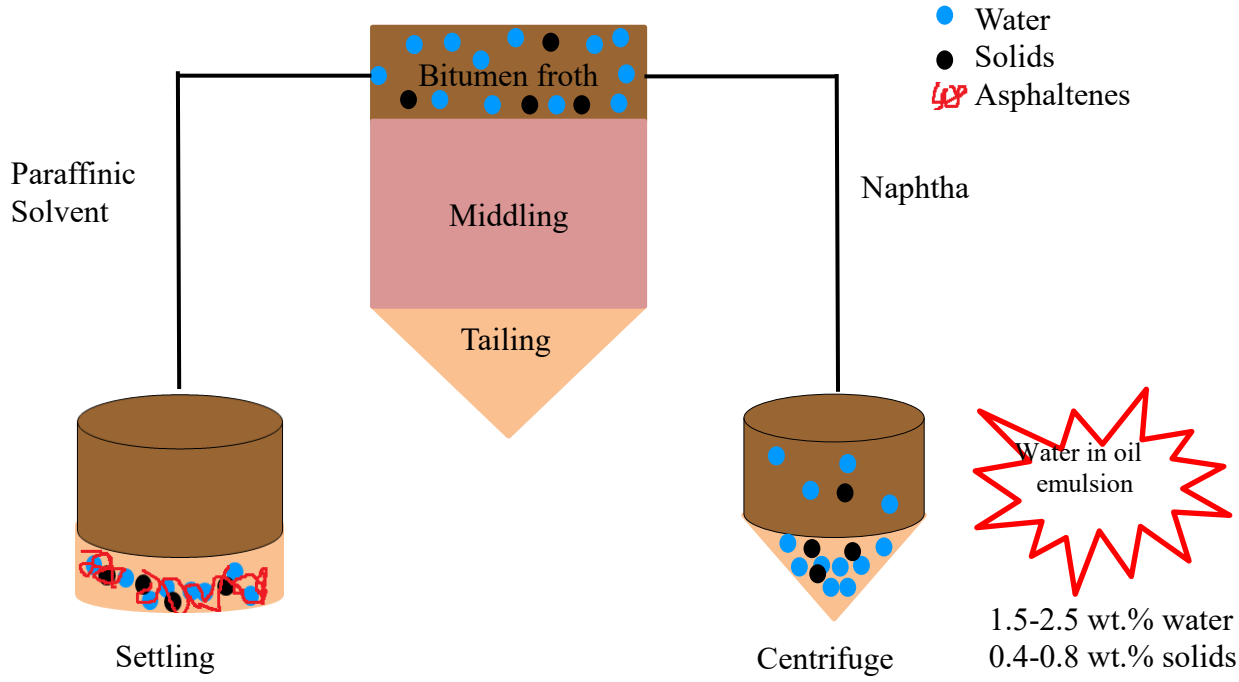

Figure 1-4 Bitumen froth treatment process.

Paraffinic froth treatment involves the addition of a paraffinic solvent, such as hexanes and pentanes, to reduce the viscosity and density of bitumen.[17] It usually requires a S/B (solvent to bitumen) ratio of about 2. Due to the low solubility of asphaltenes in paraffinic solvents, asphaltenes precipitate from bitumen, together with the dispersed water droplets and fine solids to form complex floccules or clusters of water-solids-asphaltene precipitates. The aggregates settle down quickly due to gravity to produce diluted bitumen with a negligible amount of water and solids. Thus, a very clean and dry oil product is obtained.

Naphthenic froth treatment uses hydrotreated or untreated naphtha, ranging from short-chain alkanes to aromatic hydrocarbons,[18] as the froth diluent. A S/B ratio of about 0.65-0.7 (by weight) is used. Mechanical separation equipment, such as hydrocyclone or centrifuge, is

employed to assist the separation of solids and water from diluted bitumen. After centrifugation, about 1.5 to 2.5 wt.% water and 0.4 to 0.8 wt.% solids remain in the diluted bitumen product.[4] The remaining water is in the form of stable emulsified water droplets (W/O emulsion) of several micrometers in size, which is very difficult to remove.

1.4 Emulsion

1.4.1 Basics of emulsion

An emulsion is a mixture of two immiscible liquids, one of which, the disperse phase, is suspended as stable droplets in the other, the continuous phase. Emulsions can be found in a variety of industries, such as food, pharmaceuticals, cosmetics, and petroleum. Two common types of emulsions are water-in-oil (W/O) and oil-in-water (O/W) emulsions (**Figure 1-5**).

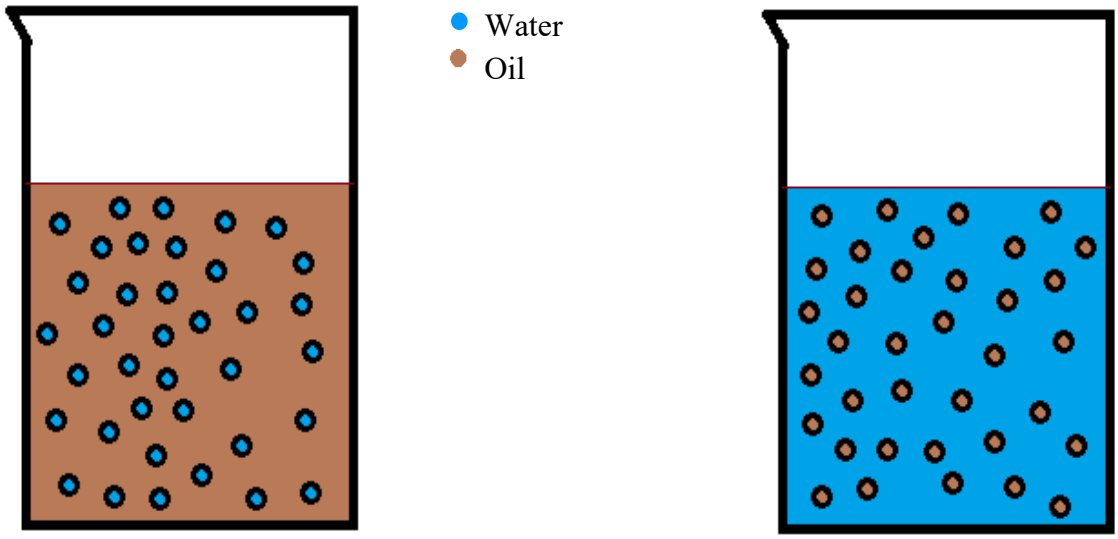

Figure 1-5 Water-in-oil (left) and oil-in-water emulsions (right).

1.4.2 Emulsions in the oil industry

In particular, W/O emulsions are often encountered during the production of crude oils and bitumen. In the crude oil industry, water-in-crude oil emulsions (W/CO) are usually formed when crude oil and water are intimately mixed at the wellhead, production well, valves, and pumps. The same is true in bitumen recovery by both in situ and open pit mining recovery methods. As mentioned in **1.3.2**, bitumen is first extracted using warm water, followed by a naphtha-based froth treatment and then a two-stage centrifugation, after which 1.5 to 2.5 wt.%

water remains in the final diluted bitumen product. The remaining water exists as emulsified water droplets that are hard to remove.

The formation of stable W/O emulsions in petroleum industry is highly undesirable because salts and fines carried with the emulsified water cause corrosion, poison catalysts, reduce throughput, and lead to equipment failure in downstream operations.[19] W/O emulsions can also significantly increase the pumping costs as a result of the dramatic increase in viscosity.[20-22] Understanding the emulsion stability and demulsification mechanisms is thus very important in petroleum industry.

1.4.3 Stability of emulsions

Emulsions are thermodynamically unstable because their formation creates a large specific interfacial area, with the total energy change given by Equation (1-1),

$$\Delta G = \gamma_{o/w} \Delta A \tag{1-1}$$

where $\gamma_{o/w}$ is the oil−water interfacial tension. Since the interfacial tension is positive in general, an increase in the interfacial area by emulsification increases the total system energy, making the system thermodynamically less stable. Consequently, phase separation, or what we call emulsion breaking, should occur spontaneously, because it can reduce the system energy. Generally, an emulsifier or emulsifying agent is needed to stabilize the emulsion. These components may stabilize the emulsion by preventing direct emulsion droplet contact or drainage of the thin liquid film between emulsion droplets.[23, 24] There are three general types of emulsifiers: macromolecules (such as synthesized polymers, natural proteins, and so on), colloidal solids, and surfactants. One of the most important properties of a surfactant is its amphiphilicity. Surfactant is known to have two well-defined regions: a hydrophilic head group and a hydrophobic tail. The most common emulsion stabilization is due to the adsorption of surfactants at the oil−water interface. When adsorbed, the hydrophilic part of the surfactants stays in the polar phase (such as water) while the hydrophobic part remains in the hydrocarbon phase (such as bitumen or crude oil). The adsorbed surfactants will change the properties of the interfacial film significantly, such as reducing the interfacial tension, the film rigidity, and viscoelasticity, etc., thereby altering the emulsion stability. Water-in-diluted bitumen emulsions in the petroleum industry are very stable. It is widely accepted that the emulsion stability is due to the formation of a mechanically strong,

rigid, and viscoelastic interfacial film by the accumulation of surface-active molecules (such as asphaltenes, resins, naphthenic acids, and inorganic solids from bitumen, as shown in **Figure 1-6**) around the water droplets. This protective interfacial film prevents coalescence of the emulsion droplets in case of collision.

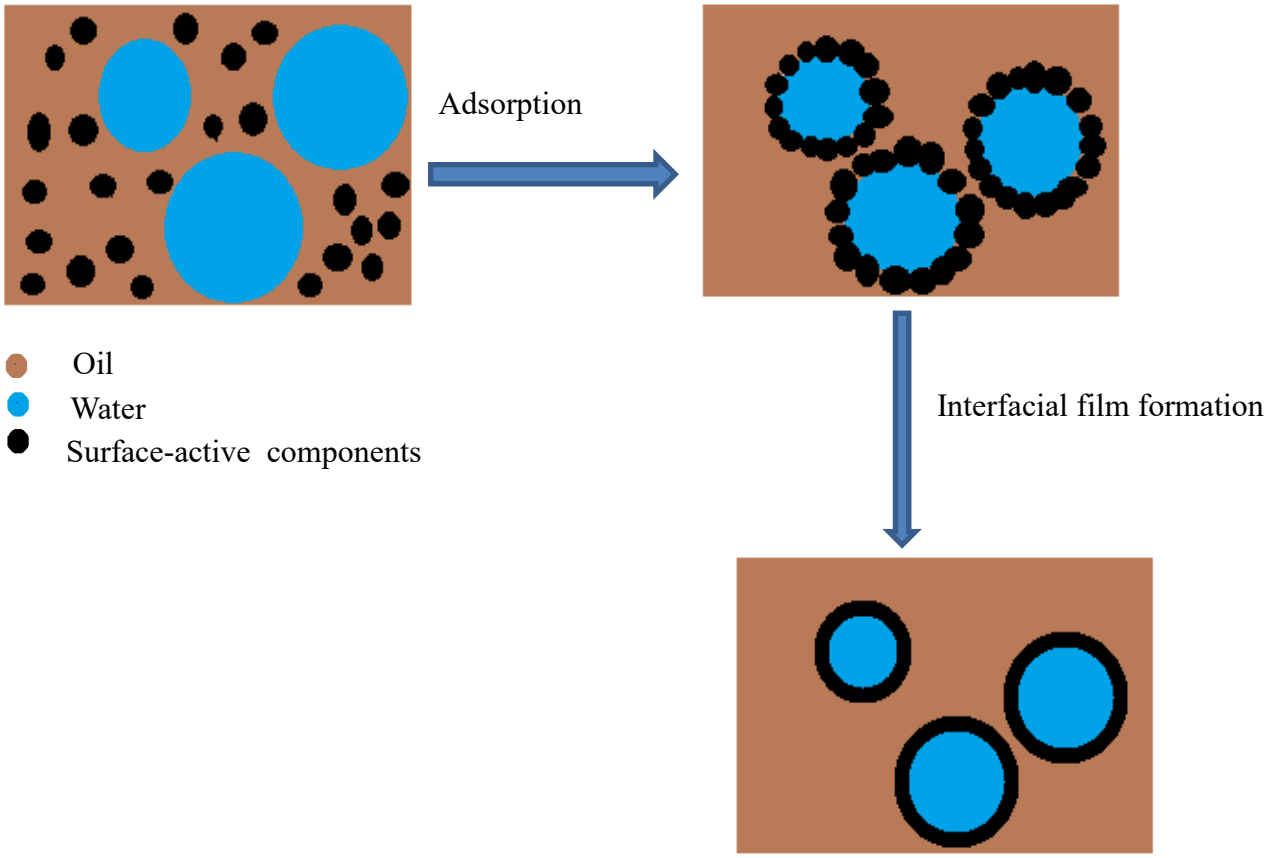

Figure 1-6 Interfacial film formation process.

1.4.4 Demulsification and demulsifiers

1.4.4.1 Demulsification

The stability of an emulsion indicates its resistance to aggregation (such as creaming, flocculation, etc.) or coalescence. For breaking of an emulsion, there are typically two steps: collision of the emulsion droplets, followed by destabilization. For destabilization of the emulsions, coalescence and/or flocculation should occur (**Figure 1-7**). During the flocculation process, droplets are brought together to form large aggregates or flocs while maintaining their individual drop size. Because of the larger size, the flocs can be removed more easily than individual droplets. Coalescence is a process of emulsion droplets merging at contact, resulting

in an increase of droplet size and a decrease in droplet counts, which is always desirable if we want to break the emulsion.

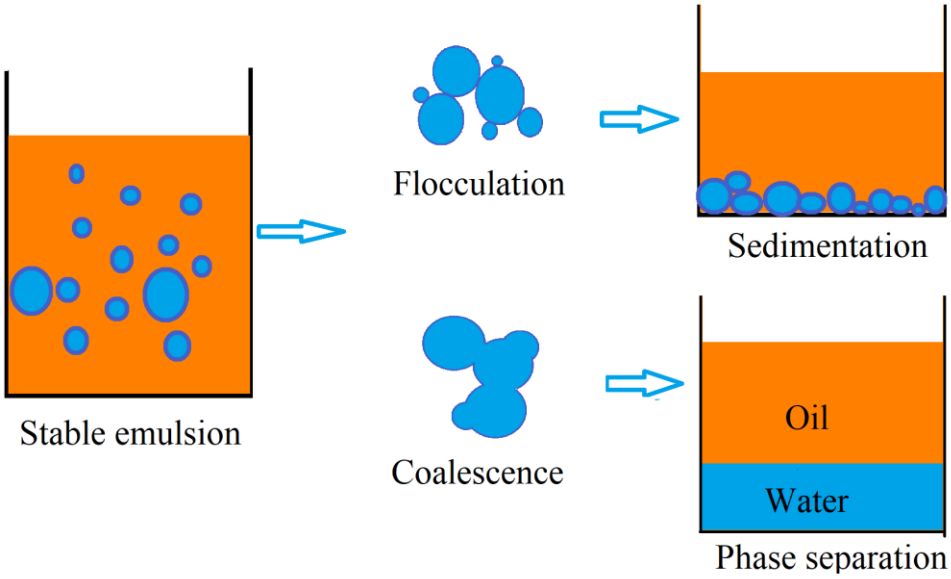

Figure 1-7 Emulsion destabilization.

To achieve efficient breakup of W/O emulsion, heat, electricity, and chemicals are usually used to enhance gravity settling of the emulsified water in industry. The use of heat is very effective in breaking W/O emulsions by reducing the viscosity of the oil and changing the solubility of the natural emulsifiers in the oil.[25] Usually, interfacial materials such as solids still stay in the treated oil after evaporation of water, which lowers bitumen quality. Alternatively, electrical approaches apply an electrical field in the emulsion system.[26] Electrostatic coalescence causes charge separation at the droplet surface and the droplets act as dipoles. The aligning of the dipoles brings the droplets together. The dipole in a droplet also causes the droplet to elongate, which stretches the interface and potentially creating pathways for rupture.[27] Either of these two ways can enhance the coalescence of water droplets. Chemical demulsification consists of the addition of a small amount of demulsifiers (usually 1-1000 ppm), usually surfactants, polymers, pure solvents, or their mixture,[26] to enhance phase separation. It works mainly by weakening the interfacial layer on water droplet surfaces. The use of demulsifiers to break W/O emulsions has been regarded as an economical and efficient method and is widely applied in petroleum industry.[28, 29]

1.4.4.2 Demulsifier

To break W/O emulsions successfully, demulsifiers must have:[30-35] 1) strong affinity to the oil−water interface with the ability to destroy or at least substantially weaken the protective film around the droplets and/or change the wettability of solids; 2) the ability to flocculate or coalesce the droplets.

Chemical demulsifiers destabilize emulsions by three major mechanisms: (1) They exhibit greater interfacial activity compared with the stabilizing species and can thus penetrate stabilizing films at the oil−water interface.[36, 37] (2) They disrupt and soften (i.e., lower the viscoelastic moduli) the stabilizing interfacial film.[36, 38, 39] (3) They suppress the interfacial tension gradient and the Marangoni-Gibbs stabilizing effect, thus accelerating the rate of film drainage and promoting coalescence.[33]

Modern demulsifiers are usually mixtures of surface-active macromolecular chemicals, such as acid- or base-catalyzed phenol-formaldehyde polymers, ethoxylated and/or propyloxylated polyamines, di-epoxides, polyols, and silicone copolymers.[40, 41] Most of the active ingredients in the chemicals used as demulsifiers are copolymers of ethylene oxide (EO) and propylene oxide (PO) of various molecular weights and EO-to-PO ratios.[30, 42-46] Three different molecular structures are shown in **Figure 2-3**, representing the linear, star, and branched structures. It is reported that the best demulsification performance was achieved by demulsifiers of branched molecular structures.[44] For EO-PO copolymers, the EO groups in the structure confer hydrophilic properties and the PO groups add hydrophobic properties to the demulsifier molecule. Therefore, increasing the EO content makes the polymer more hydrophilic, while increasing the PO content makes it more hydrophobic. The amphiphilicity of the EO-PO copolymer enables it to adsorb at the oil−water interface, thus affecting the properties of the interfacial film.

1.5 Objectives and outline of the thesis

The research performed in this thesis has four goals: (1) To investigate the relationship between W/O and O/W systems using asphaltene model compounds as the oil samples, which have better optical transparency for both systems. (2) To study the effect of the EO-PO copolymer on the water−xylene diluted asphaltene model compound interface, in order to reveal the demulsification mechanism and provide some information on the feasibility of using the reverse O/W system to study the interfacial properties of the W/O system when demulsifier is

introduced. (3) To provide insights into the destabilization mechanism of the C5Pe interfacial film by the EO-PO copolymer and to study how different groups of the EO-PO demulsifier behaved at the interface using molecular dynamics simulation, so as to provide information on how to design efficient demulsifier for dewatering. (4) To understand the influence of the demulsifier dosage, water pH, and temperature on breaking water-in-diluted bitumen emulsions using EO-PO copolymer as the demulsifier and to uncover the corresponding destabilizing mechanisms using the reverse diluted bitumen-in-water system. To realize those goals, an array of experimental techniques was used, including focused beam reflectance measurement (FBRM), interfacial film drainage apparatus (ITFDA), Theta Optical Tensiometer (T200), rheometer, Brewster angle microscope (BAM), atomic force microscope (AFM), Langmuir trough, and Karl Fisher titrator. Among these techniques, FBRM allows in situ and real-time particle size measurement, which helps us to gain insight into the kinetics of demulsification. ITFDA is an in-house apparatus that allows us to measure the film drainage time under a well-controlled external force. Tensiometer can be used for the interfacial tension, film rigidity, and interfacial dilatational rheology measurements. An AR-G2 rheometer is used to investigate the interfacial shear rheology of the interfacial film. BAM and AFM can image the morphological changes of films at the oil−water interfaces with demulsifier addition. Langmuir trough can be used to investigate the compressional behavior of the interfacial film by measuring the interfacial pressure−area isotherm. The remaining water content in the emulsion sample can be measured by the Karl Fisher titrator. In addition, molecular dynamics simulation was used to model the demulsification mechanism at the molecular level.

The theme of this research is presented in the following chapters.

Chapter 1: This chapter provides the background and objectives of this study. A brief introduction is given on how oil sands ore is processed, how stable emulsions are formed, and how to get rid of the emulsions.

Chapter 2: Several mechanisms by which W/O emulsions are stabilized and destabilized are briefly reviewed in this chapter. The correlation between chemical demulsifier performance and properties such as molecular weight (MW), relative solubility number (RSN), hydrophile-lipophile balance (HLB), molecular structure, etc., are also presented. Properties of asphaltene and asphaltene model compounds are also reviewed.

Chapter 3: A detailed description of the related techniques used in this work is presented. The introduction of the pendant drop technique for the dynamic interfacial tension measurement and Du Noüy ring method for the static interfacial tension measurement is given. Characterization of the skin formation at the oil−water interface is conducted by crumpling ratio and dilatational rheology measurements using Tensiometer and the corresponding principles are provided. Rheometer, BAM, and AFM, which are used for characterizing the shear rheology and morphology of the interfacial film, are introduced. Techniques to evaluate the efficiency of demulsification, such as droplet size and count measurement by FBRM, coalescence time measurements by ITFDA, and remaining water content measurement by Karl Fisher Titrator, are also provided. This chapter aims to provide theoretical background information for the following chapters.

Chapter 4: In this chapter, the relationship between W/O and O/W systems is studied, to obtain the conditions where we can perform optical measurements using the reverse system, i.e., diluted bitumen or crude oil in water, which has better visualization.

Chapter 5: In this chapter, the effect of the EO-PO demulsifier on the interfacial properties of the C5Pe/C5PeC11−water interface is studied to provide new insights into the molecular mechanism of emulsion destabilization. This chapter also provides information on the feasibility of using reverse O/W system to study the interfacial properties of the W/O system when demulsifier is introduced. In addition, this chapter provides further justification for using C5Pe as the asphaltene model compound by investigating whether asphaltene model compound could interact with demulsifier molecules in a similar way as that of real asphaltenes and demulsifier molecules.

Chapter 6: Molecular dynamics simulation was used to study the effect of the EO-PO copolymer on the C5Pe interfacial film to provide a perspective of the demulsification mechanism at the molecular level. In addition, the behavior of different groups of the demulsifier at the interface was also studied.

Chapter 7: In this chapter, EO-PO copolymers are added to a water-in-naphtha diluted bitumen emulsion, and the effectiveness of the copolymers in dewatering water-in-naphtha diluted

bitumen emulsions at high temperature is investigated, while the reverse O/W emulsion systems were used for characterization of the interfacial properties.

Chapter 8: This chapter draws the overall conclusions and provides recommendations for future work.

Chapter 2 Literature Review

2.1 Emulsion stabilization mechanisms

There are at least four mechanisms by which emulsions are stabilized: (1) electrostatic repulsion; (2) steric repulsion; (3) the Marangoni Gibbs effect, which retards film drainage; and (4) thin film stabilization. A brief review of each of these mechanisms is given below.[47]

2.1.1 Electrostatic repulsion

Electrostatic repulsion refers to two particles or droplets of the same charge that repel each other. For W/O emulsions, electrostatic forces do not play a significant role in the emulsion stabilization because that ions are not soluble in the oil phase.[47]

2.1.2 Steric repulsion

Steric repulsion is known as the resistance of the interactions between the adsorbed species on different droplet interfaces. In other words, steric repulsion arises from the fact that each atom within a molecule occupies a certain amount of space. If atoms are brought too close to each other, there is an associated energy cost due to the overlapping of the electron clouds. In W/O emulsions, the dispersed water droplets are covered by surfactant molecules and the surfactant tail adsorbed at the interface prevents the close contact of the droplets. Therefore, steric repulsion may play a significant role in stabilizing W/O emulsions.

2.1.3 Marangoni-Gibbs effect

When the continuous liquid phase between the emulsion droplets drains out, an interfacial tension gradient (a surfactant concentration gradient) is produced as the surfactants at the droplet interface are pulled outward with the draining liquid. Because of the surfactant depletion, a diffusion flux is then generated in the opposite direction of the drainage to slow this process. This phenomenon is called the Marangoni-Gibbs effect.[47-49] In other words, the Marangoni-Gibbs effect can stabilize emulsions by preventing the drainage of the continuous phase from between two nearby droplets. To enhance coalescence by the demulsifier, the interfacial activity of the adsorbed demulsifier molecules at the interface must be high enough to suppress or even reverse this interfacial tension gradient so as to enhance the liquid drainage.[49-53] It has been reported by Mukherjee et al.[54] that the interfacial shear viscosity must be low to achieve efficient emulsion breakage. Since the formation of the viscoelastic interfacial film results in the high

interfacial viscosity of the asphaltene-containing systems, this stabilization mechanism is unlikely to be significant for water-in-crude oil or water-in-diluted bitumen systems.[47]

2.1.4 Thin film stabilization

It is widely accepted that emulsion stability is mainly due to the formation of the mechanically strong, viscoelastic, and rigid interfacial film around the emulsion droplets, and this film is produced by the accumulation of the surface-active molecules and inorganic solids from crude oil or bitumen.[47, 55-59] The presence of surface-active chemical species (such as asphaltenes, resins, and acids as well as fine solid particles) at the oil−water interface on water droplets has been reported extensively. This film has been proven to be able to resist droplet coalescence.[60]

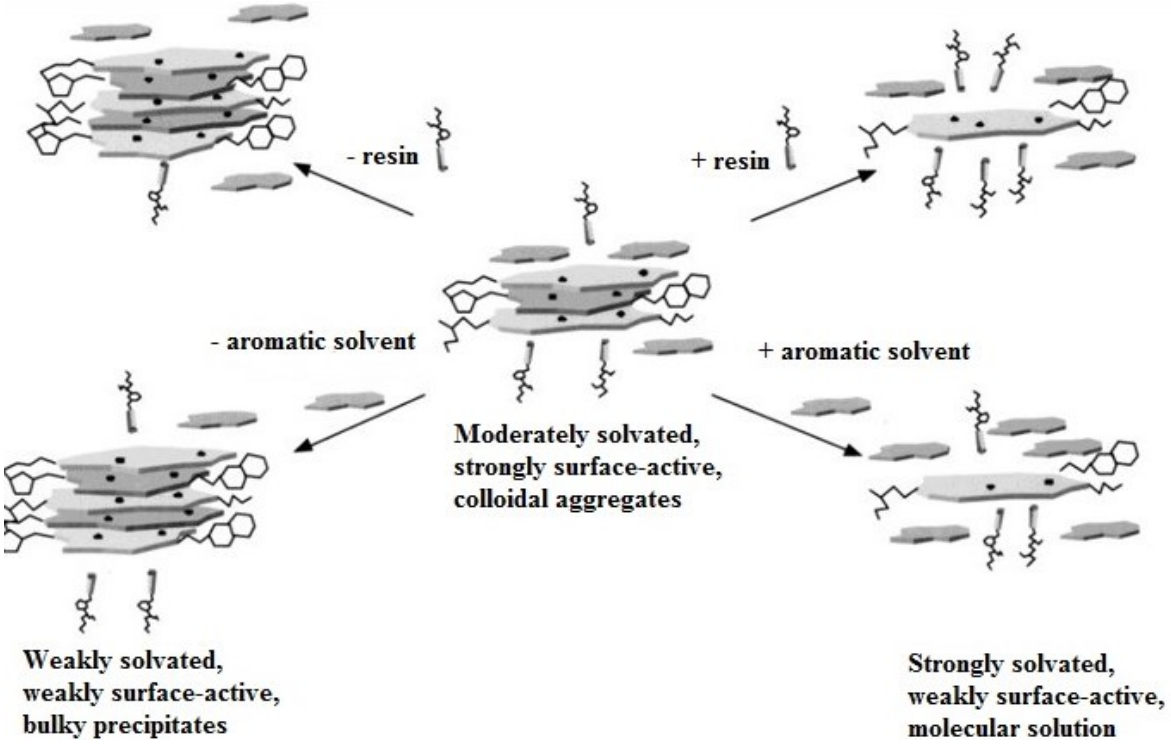

Figure 2-1 Effects of solvent composition and resin concentration on the surface activity and solvency of asphaltene. [47]

Asphaltenes are reported to be one of the primary causes of emulsion stability in petroleum industry.[61, 62] The interactions between the polar cores of different asphaltene molecules and between the polar cores of the resins with the polar cores of asphaltenes result in the formation of the asphaltenic aggregates solvated with resins.[47] To form an interfacial film, the asphaltene aggregates should be small enough to be held at the interface. The degree of the asphaltene

aggregation depends on both the resin concentration and the aromaticity of the crude oil medium or diluted bitumen. Reduced aromatic solvent content or resin concentration encourages asphaltene aggregation. Under the condition of moderate asphaltene solvation, a cross-linked interfacial network of asphaltenes can be formed at the oil−water interface, leading to the maximum emulsion stability, as shown in **Figure 2-1**.[47]

Acids in crude oil and bitumen are also known to play an important role in W/O emulsion stabilization. The adsorption of carboxylic acids and their anions, depending upon conditions of pH, can dramatically lower the interfacial tension, thus stabilizing the W/O emulsion. Naphthenic acids are reported to stabilize W/O emulsions through the formation of a lamellar liquid crystalline phase.[63] ARN acids, which are tetra-acids of roughly 1227-1235 molecular weight[64] appear to stabilize W/O emulsions through the formation of a cohesive film. This film is firmly anchored at the interface by binding with divalent cations (such as calcium ions). Acidic components of asphaltenes are found to be very interfacial active and can dramatically stabilize W/O emulsion films after adsorbing at oil−water interfaces.[65]

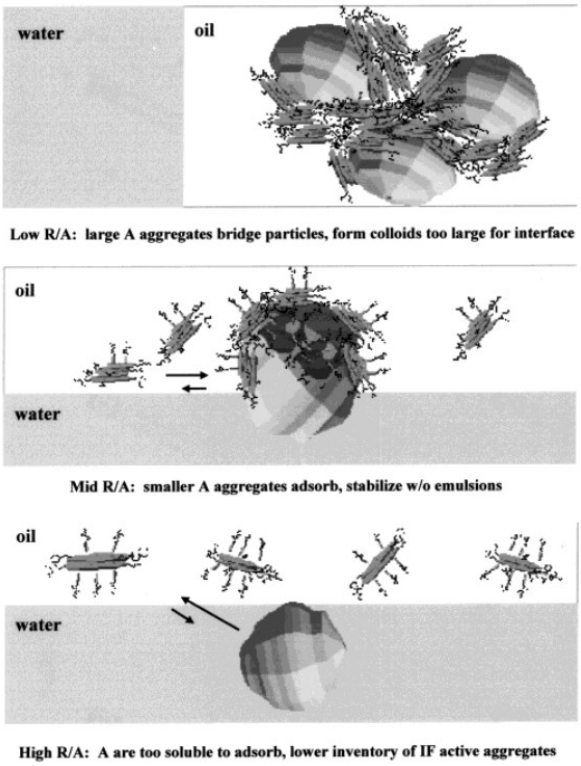

Figure 2-2 Effect of the solubility of asphaltenes in resin on particle modification.[47]

An enhancement mechanism for the stabilization of crude oil emulsions has also been brought up. The W/O emulsion stability can be significantly enhanced by the adsorption of very small inorganic solid particles (with only a few μm or even less in size) at the interfaces. It has been reported that silica, clay fines, iron oxides, and some other inorganics are capable of enhancing W/O emulsion stability.[47] Sullivan et al.[47] concluded that these fine inorganic particles can lead to dramatically enhanced emulsion stability when suitably modified through the adsorption of polar species, such as resins or asphaltenes from crude oil. The adsorption of the organic components changes the wettability of these inorganic particles and makes them interfacially active.[56, 57, 59] The wettability of the particles plays an essential role in stabilizing W/O emulsions and the most stable emulsions can be yielded with the smallest particles. The effect of the resin/asphaltene ratio on the adsorption ability of asphaltene on the fine particles was also demonstrated (**Figure 2-2**[47]).

2.2 Emulsion destabilization

Chemical demulsification has been regarded as an economical and efficient method and is widely used in petroleum industry. Correlations between demulsifier performance and properties such as molecular weight (MW), hydrophile-lipophile balance (HLB), relative solubility number (RSN), demulsifier structure, and EO/PO ratio are reviewed here. HLB of surfactant is a measure of its hydrophilicity or hydrophobicity and higher HLB indicates higher hydrophilicity of the surfactant. Similar to HLB, higher RSN value represents greater hydrophilicity of the surfactant.

2.2.1 Chemical demulsifier

2.2.1.1 Effect of MW on demulsification efficiency

MW shows a significant effect on the demulsification performance. In general, polymeric demulsifiers with low MW are highly interfacial active and can adsorb irreversibly at the oil−water interface, resulting in the coalescence of the emulsion water droplets. Polymeric demulsifiers with low MW destabilize emulsions by flocculating nearby water droplets.[66] From the flocculation point of view, an increase in the MW of the demulsifier will increase the flocculation opportunities of the water droplets, resulting in better dewatering efficiency. Pelssers et al. reported that poly (ethylene oxide) flocculants must have a MW higher than 10^6 g/mol for successful flocculation of the polystyrene latex particles in water.[67]

Kailey et al.[68] systematically studied the effect of MW of EO-PO copolymers on dewatering of water-in-diluted bitumen emulsions. They concluded that by increasing the MW of EO-PO copolymers, the demulsification efficiency increased. Wu et al.[30] found that when the MW of a demulsifier is less than 4000, the demulsifier is not effective regardless of the RSN values. High performance of the demulsifier was achieved for an RSN between 7.5 and 12.5 and a MW between 7500 and 15000 g/mol, which is consistent with Kailey's work as the MW of the demulsifier that Kailey et al. used was all under 15000 g/mol. It should be noted that the demulsifiers with a MW higher than 15000 g/mol were not tested in Wu's study. Ethylcellulose (EC) is also effective in breaking water-in-diluted bitumen emulsions. Feng et al.[69] found that over the MW range of 40000 to 180000 g/mol, a better demulsification efficiency was obtained for EC with a higher MW. Therefore, it is safe to say that the dewatering efficiency of the demulsifier is directly correlated with the MW of the demulsifier. At least for commonly used demulsifiers, such as EO-PO copolymers and EC, an increase in the MW results in a higher demulsification performance.

2.2.1.2 Effect of HLB or RSN on demulsification efficiency

HLB is an important parameter for the characterization of nonionic surfactants. Because HLB is difficult to determine experimentally, RSN is usually used to characterize HLB. Wu et al.[70] found that within the same surfactant family, RSN value has a good linear relationship with classic HLB value. Wu et al. established an empirical relationship (Equation (2-1)) between RSN and HLB values for the Brij (PEO alkyl ether), Igepal (PEO alkyl phenyl ether), Span (sorbitan ester), and Tween (PEO sorbitan ester) surfactant families:[70]

$$HLB=A\times RSN+B \tag{2-1}$$

where A and B are empirical constants varying with the surfactant family.

Similar to HLB, RSN demonstrates the hydrophilic and hydrophobic properties of the surfactant. The higher the RSN value, the greater the hydrophilicity of the surfactant. The correlation between the demulsification efficiency and the RSN value of a demulsifier has been widely investigated. Kailey et al.[68] proved that demulsification efficiency increased as the RSN value increased. Xu et al.[29] concluded that for EO-PO copolymers which contain a fixed number of the PO units, the demulsification efficiency increased when increasing the EO number in the

molecules. Wu et al.[70] reported an optimal RSN value for the demulsification efficiency of the surfactant in the same family. For polymerized polyol, oxyalkylated alkylphenol-formaldehyde resin, and oxyalkylated alkyl resin, a significant relationship between the percentage of water removed and the RSN value in each of the given demulsifier families was reported by Wu et al.[30] For polymerized polyols, demulsifiers with low RSN values from 4 to 5 showed no effect on dewatering, while the one with RSN values in the range of 7 to 8 removed water effectively. For the alkylphenol-formaldehyde resin family, a bell-shaped curve was obtained, indicating an optimum RSN value for dewatering. Similar results were also obtained for the oxyalkylated alkyl resin family.

The results discussed above show that there is no overall correlation between water removal and the RSN values of the demulsifiers when taking all types of surfactants into consideration. However, a noticeable correlation is observed between dewatering performance and RSN values within a given demulsifier family. An optimal RSN range exists in which dewatering efficiency reaches its maximum.

2.2.1.3 Effect of demulsifier structure on demulsification efficiency

The effect of the demulsifier structure on the dewatering efficiency of W/O emulsions has been extensively investigated from different aspects.

Ramalho et al.[44] found that for PEO-b-PPO demulsifiers, the demulsifier with a branched molecular structure showed the best dewatering performance, followed by the star and the linear structures, as shown in **Figure 2-3**. They also concluded that compared with the star and linear structures, the branched demulsifiers had higher interfacial activity and could decrease the interfacial tension to the lowest value. Kailey et al.[68] reported that the higher the branching, the more efficient the dewatering. EO-PO demulsifiers with five EO-PO branches showed better performance on dewatering than that with three EO-PO branches. Sun et al.[34] demonstrated that the demulsifiers with branched structures were more effective than the linear demulsifiers because they left smaller vacancies at the oil−water interface, making it hard for the surface-active components in the crude oil or bitumen to adsorb at the interface again. Abdel et al.[45] synthesized two types of EO-PO demulsifiers based the structure of the amines used for the synthesis and systematically studied the effect of the structural changes in the prepared demulsifiers on their dewatering efficiency of W/O emulsions. They concluded that the

demulsification efficiency could be enhanced by increasing the number of EO-PO branches. In addition, the disubstituted EO-PO aromatic amine was superior to their monosubstituted counterparts in dewatering water-in-benzene emulsions.

(a)

$HO\text{-}CH_2CH_2[\text{-}O\text{-}CH_2CH_2]_{n\text{-}1}[\text{-}O\text{-}CH(CH_3)CH_2]_m\text{-}O\text{-}CH(CH_3)CH_2\text{-}O\text{-}[CH_2(CH_3)CH\text{-}O\text{-}]_m[CH_2CH_2\text{-}O\text{-}]_{n\text{-}1}CH_2CH_2\text{-}OH$

(b)

$$\begin{array}{l} H_2C\text{-}O\text{-}[CH_2(CH_2)CH\text{-}O\text{-}]_3[CH_3CH2\text{-}O\text{-}]_2CH_2CH_2\text{-}OH \\ | \\ HC\text{-}O\text{-}[CH_2(CH_2)CH\text{-}O\text{-}]_3[CH_3CH2\text{-}O\text{-}]_2CH_3CH_2\text{-}OH \\ | \\ H_2C\text{-}O\text{-}[CH_2(CH_2)CH\text{-}O\text{-}]_3[CH_3CH2\text{-}O\text{-}]_2CH_3CH_2\text{-}OH \end{array}$$

(c)

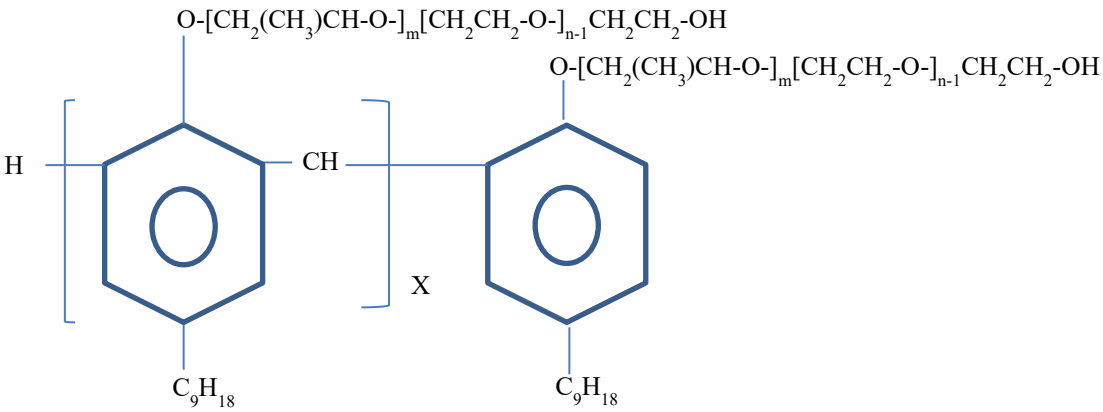

Figure 2-3 Basic molecular structure of commercial demulsifiers: (a) linear, (b) star, and (c) branched.

Wu et al. investigated the effect of position isomerism of the nonionic surfactants on demulsification performance.[43] They reported that the sequential block copolymers containing more than 40% EO were effective in breaking W/O emulsions and the demulsifier with higher EO percentage performed better on emulsion breakage. The reverse sequential copolymers, regardless of EO percentage, merely showed little effect on breaking the W/O emulsions. The difference in the demulsification performance of the sequential and the reverse sequential copolymers should be attributed to the different HLB (RSN), interfacial properties, and steric effect between them.

Xu et al.[29] used polyoxyalkylenated diethylenetriamine (DETA) based demulsifiers with various EO to PO ratios to destabilize W/O emulsions. They found that the performance of the demulsifier is closely correlated with its EO and PO numbers: 1) If the number of PO >> EO, the

demulsifier was only effective at high dosage for breaking W/O emulsions; 2) If the number of EO > PO, only a low demulsifier dosage was required for efficient emulsion breakage. However, the demulsification performance decreased at high demulsifier dosage, showing an overdose effect; 3) If the number of PO ≈ EO, the demulsifier could break the emulsion quickly and effectively at a low dosage and no overdosing was observed.

2.2.1.4 Effect of demulsifier concentration

An increase in the bulk concentration of the demulsifier can affect the interfacial properties of the oil−water interface in two ways: one is to increase the interfacial demulsifier concentration, and the other is to enhance the diffusion of the demulsifier molecules from bulk to new interfaces.

Abel-Azim et al.[45] studied the influence of PPPEA concentration on its demulsification efficiency. An optimum concentration existed at which the PPPEA demulsifier showed the best demulsification performance. At the optimum concentration, the demulsifier molecules could replace the asphaltene molecules at the benzene−water interface, which made the protecting film around the water droplets to thin and eventually to rupture, providing opportunities for the coalescence of the water droplets. A higher concentration may result in the aggregation of the demulsifier molecules at the interface, forming a new protective film with greater mechanical strength. Pensini et al.[71] also reported that overdose of the EO-PO copolymer appeared when increasing the demulsifier dosage from 2.3 ppm to 28.8 ppm for the destabilization of the asphaltene stabilized W/O emulsions. By investigating the morphology of the interfacial film using Brewster angle microscopy, they concluded that the large irregular structures at the toluene−water interface, which indicates the presence of steric repulsion, are responsible for the overdose effect.

2.2.2 Effect of temperature on demulsification

2.2.2.1 Effect of temperature on viscosity and density

It is reported that increasing temperature results in a significant decrease in the bulk viscosity and density of the diluted bitumen. Romanova et al.[72] studied the viscosity and density of diluted bitumen (Athabasca coker-feed bitumen) at elevated temperatures. As shown in **Table 2-1**[72], a decrease of both the viscosity and density is observed at elevated temperatures, which is favorable for the settling of the water droplets. In fact, the settling process depends on the

balance between the forces of gravity and viscosity, which can be expressed as R_{gv}[72] (Equation (2-2)):

$$R_{gv} = \frac{d^3 a(\rho_p - \rho_m)}{\mu u d} \quad (2\text{-}2)$$

where d is the diameter of the settling particle or droplet, a is the acceleration, ρ_p is the density of the particle or droplet, ρ_m is the density of the medium, μ is the viscosity of the medium, and u is the velocity of the particle or droplet. A higher R_{gv} means that it is much easier to obtain an effective separation. When evaluating the effect of temperature on demulsification, the varied parameters are ρ and μ. Assuming that the changes of other parameters are negligible, Equation (2-2) can be simplified to Equation (2-3):

$$R = \frac{(\rho_p - \rho_m)}{\mu} \quad (2\text{-}3)$$

Table 2-1 Density and viscosity of diluted Athabasca coker-feed bitumen.

	Density (g/mL)		**Viscosity (mPa·s)**	
S/B, wt/wt	60 °C	23 °C	60 °C	23 °C
		Toluene		
0.09	0.9861	0.9923	486	1381
0.43	0.9242	0.9592	9.4	24.6
0.61	0.9214	0.9478	4.4	9.8
0.87	0.9079	0.9357	1.4	3.4
1.30	0.8926	0.925	0.6	1.5
1.73	0.8825	0.9128	0.6	0.9
		n-heptane		
0.07	0.9574	0.975	188.6	8615
0.27	0.8987	0.9137	20.4	167.8
0.41	0.8703	0.8841	7.8	58.8
0.62	0.8392	0.8518	2.8	23.6
0.82	0.8176	0.8292	1.3	12.8
1.16	0.7644	0.8025	0.5	4.8

❖ S/B indicates solvent to bitumen ratio

2.2.2.2 Effect of temperature on interfacial properties

Menon et al.[73] found that the interfacial shear viscosity of the shale oil−water interface can be reduced by increasing temperature, as shown in **Figure 2-4**.[73] The reduction in the interfacial

shear viscosity could accelerate the film drainage rate between nearby droplets, thereby making it possible for coalescence.

2.2.2.3 Effect of temperature on collision rate of dispersed droplets

Increasing temperature also increases the number of collisions between two dispersed water droplets. This should be due to the increased intensity of Brownian motion at high temperature.

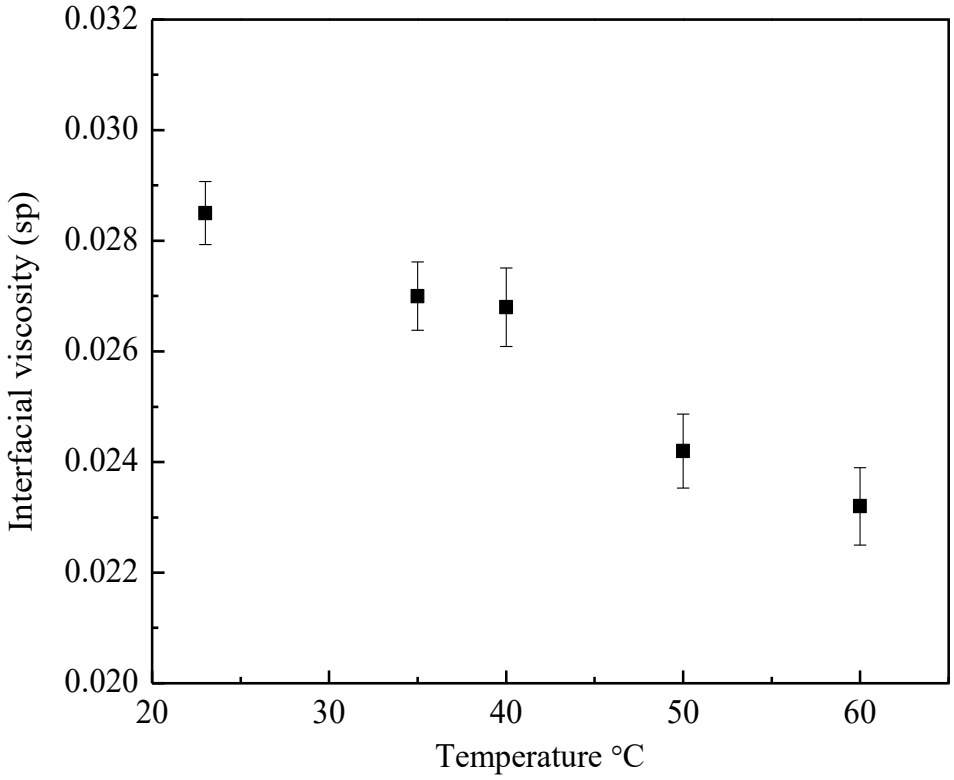

Figure 2-4 Effect of temperature on interfacial shear viscosity of a shale oil−water interface.

2.3 Asphaltene and asphaltene model compound

2.3.1 Asphaltene

2.3.1.1 Molecular weight of asphaltene

The determination of the molecular weight (MW) of asphaltenes has been a controversial object for decades.[74] The obtained results vary from a few hundred to several hundreds of thousands of g/mol. Previous reported asphaltene molecular weight is in the range of 1,000 to 30,000 g/mol. Techniques such as vapor pressure osmometry (VPO),[75] gel permeation chromatography (GPC),[76] and mass spectrometry (MS)[75, 77] have been used for the characterization of the MW of asphaltenes. However, both VPO and GPC suffer from large uncertainties. It is known that asphaltene molecules tend to aggregate in their solutions to form dimers, trimers, and so on. To

estimate the 'true' MW of the asphaltene in VPO, the solutions should be highly diluted so that the degree of association can be regarded as zero.[75] However, large experimental errors are introduced at high dilutions as the vapor pressure of the highly diluted solution is very close to that of the pure solvent. GPC can be used to estimate the molecule size distribution based on the elution time of the studied material from a porous column. GPC also suffers from asphaltene aggregation as the association of asphaltene makes the molecules bigger. The results at infinite dilution can be obtained by extrapolating the results for more concentrated solutions, which also results in large experimental errors. It was not until 1999 that reliable results, accounting for the molecular aggregation at low dilution, became available. Mass spectrometry[75, 77] (MS) is used based on the mechanism that the mass-to-charge ratio is measured directly. Fluorescence depolarization technique[78, 79] is able to deal with highly diluted asphaltene solutions. Asphaltene molecular mass obtained using these modern techniques are in the range of 400 to 1500 g/mol, with an average value of around 750 g/mol.

2.3.1.2 Asphaltene structure

Two main models of asphaltene structure exist in the literature, known as archipelago and island models. According to the archipelago model, asphaltenes should have several poly-condensed aromatic rings which are connected together via alkyl chains or sulfide bridges.[80] All the molecular values based on this model are close to those obtained for the acetone-extracted Athabasca asphaltenes.[81] In the island model, asphaltenes are believed to have a polyaromatic core containing condensed aromatic rings with side chains attached.[82] The polyaromatic part of the island structure contains about seven fused aromatic rings, which is supported by direct molecular imaging with high-resolution transmission electron microscopy[83] and by studying the UV-visible spectra of asphaltenes coupled with molecular orbital calculations.[84]

2.3.1.3 Asphaltene aggregation

Asphaltenes are known to self-associate both in crude oils[85] and in model solvents such as toluene. The self-association properties of asphaltenes have been extensively studied. It was reported that the self-association behavior of asphaltenes depends on thermodynamic conditions such as the nature of solvents, temperature, pressure, and the presence of co-solute such as resins,[86-89] and so on. Several molecular association models have been proposed previously to

explain the observed self-association of asphaltenes molecules and some models are briefly discussed here.

Yen[90] and later Mullins et al.[91] proposed a hierarchical asphaltene aggregation model. The "Yen model"[90] was developed at a relatively early stage involving structures of different length scales. Yen et al.[90] assumed that asphaltene molecules firstly aggregate into "particle" by π-π stacking of the polyaromatic parts. Several asphaltene particles further self-associate to form micelles. The Yen model has been very useful for most contributors in the field. With the improvement in the understanding of asphaltenes, a much-refined asphaltene model, "the modified Yen model",[91] has been proposed. The main asphaltene structure is described as a single condensed aromatic ring of moderate-size with peripheral alkyl chains. The asphaltene molecules can form asphaltene nanoaggregates with aggregation numbers of ∼6 asphaltene molecules and the asphaltene nanoaggregates can further aggregate to form clusters with aggregation numbers of ∼8 asphaltene nanoaggregates. The modified Yen model provides a framework to treat large numbers of diverse asphaltene studies.

Agrawala et al[216] reported a linear polymerization-like asphaltene association model. They described the polymerization-like association "reactions" in terms of terminators and propagators. The key concept in this model is that molecules with multiple active sites act as propagators, which is capable of linking with other molecules, and molecules with single active sites act as terminators. Asphaltenes are primarily composed of propagators. Resins, which are known to affect asphaltene association,[47] consist primarily of terminators.

Recently, Gray et al.[92] proposed a "supramolecular assembly model", in which multiple interactions, such as π-π stacking, metal coordination complexes, hydrogen bonding, cooperative binding by Brønsted acid-base interactions, and interactions between alkyl and cycloalkyl groups to form hydrophobic pockets, etc., are believed to lead to a range of architectures of asphaltene aggregates, including host-guest complexes and porous networks. From their perspective, the ionic association represents (acid-base interaction) the strongest driving force for asphaltene aggregation.

In a recent review, Yarranton et al.[93] discussed an array of experimental techniques to investigate the possible size and structure distributions of asphaltene monomers and aggregates. They

reported that asphaltenes nanoaggregates have a loose and highly polydisperse structure with sizes ranging from 2 to 20 nm.

2.3.2 Asphaltene model compound

Asphaltenes are widely reported to be polyaromatic hydrocarbons with amphiphilic properties, which consist of fused aromatic rings with alkyl branches attached to the periphery.[94-97] Based on this structure, several polyaromatic surfactants have been synthesized as the asphaltene model compounds by attaching hydrophobic chain(s) to one and alkyl chain(s) of hydrophilic groups to the other end of a perylene core.[98-100] The synthesized model compounds exhibit similar interfacial activities as asphaltenes and Norfgard et al. have reported that both W/O and O/W emulsions can be stabilized by the polyaromatic surfactants.[98-100]

C5Pe (**Figure 2-5**, N-(1-hexylheptyl)-N′-(5-carboxylicpentyl) perylene-3,4,9,10-tetracarboxylic bisimide), as one of the model compounds, is composed of fused aromatic rings connected via cyclic rings containing heteroatoms of O and N. A pentyl carboxylic acid chain and a hexyl-heptyl double chain are attached to the fused aromatic rings through nitrogen atoms. The molecular weight (MW) of C5Pe (MW of 689 g/mol) falls into the well-accepted MW range of asphaltenes. The amphiphilic nature and polyaromatic structure of C5Pe simplify the complicated asphaltene nature and structure.[101, 102] Both C5Pe and C5PeC11 (**Figure 2-5**) are reported to be suitable asphaltene model compounds.[99, 103-106] These model compounds have been extensively studied and their properties are briefly reviewed here.

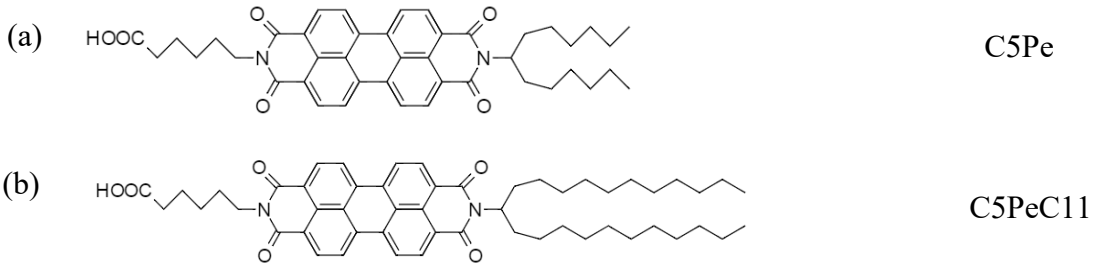

Figure 2-5 Molecular structure of polyaromatic surfactant C5Pe (MW=689 g/mol) and C5PeC11 (MW=827.12 g/mol).

2.3.2.1 Interfacial properties

The interfacial properties of C5Pe molecules can be assessed by measuring the interfacial tension of the C5Pe in toluene solution−water (pH=9) interface. C5Pe molecules (1-20 μM) can significantly reduce the interfacial tension of the toluene−water interface, indicating high

interfacial activity of C5Pe.[98, 106] As indicated by the fluorescence spectroscopy results of the Langmuir-Blodgett films, C5Pe adopts a head-on conformation at the interface with a face-to-face packing of the molecules,[98] which accounts for the high interfacial activity of the C5Pe model compound. C5PeC11 exhibits pH-dependent surface activity. Increasing pH could deprotonate the carboxylate functional group of C5PeC11, thereby increasing surface activity. The deprotonation could also decrease the molecular tilt at the interface.[107] C5Pe also shows pH-dependent surface activity.

2.3.2.2 Asphaltene model compound as the emulsion stabilizer

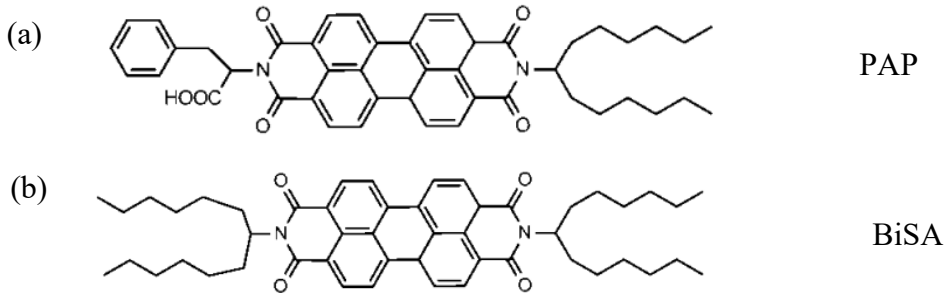

Figure 2-6 Molecular structure of PAP (MW=723 g/mol) and BiSA (MW=755 g/mol).

Nordgård et al.[98] compared the stability of emulsions stabilized by C5Pe, PAP, and BisA. The structures of PAP and BiSA are shown in **Figure 2-6**. BisA was not able to form stable emulsions while PAP and C5Pe showed good performance on emulsion stabilization, though PAP was shown to stabilize emulsions to a less extent than C5Pe. Grimes et al.[108] reported that when the concentration of C5Pe was more than 0.08 mM, the prepared emulsions were very stable and only a very small amount of water was separated even over a long period of about 6500 min. They also measured the equilibrium interfacial tension as a function of the C5Pe concentration and found that the data could be well-fitted by the Gibbs adsorption equation[109] and Langmuir isotherm. Jiebin et al.[106] systematically investigated the interfacial properties of the C5Pe interfacial film and its role in the stabilization of the W/O emulsions. BAM and AFM images showed that the C5Pe aggregates would accumulate at the interface and form a thick interfacial layer. The continual accumulation and the time-dependent rearrangement of the C5Pe aggregates contributed to form an elastic and rigid interfacial layer, which is essential to prevent coalescence of the emulsion droplet.

2.3.2.3 Molecular association and interaction

Wang et al.[104] studied the interfacial behavior of C5Pe molecules on mica surfaces and the interactions between the adsorbed C5Pe layers in different organic solvents. They reported the formation of the C5Pe aggregates and the irreversible nature of the aggregation. In addition, it was also found that the organic solvents can dramatically influence the aggregation behavior and molecular interactions of the C5Pe molecules. Weaker or even no adhesion was detected in toluene, whereas strong adhesion forces were measured in heptane for the interactions of C5Pe films.

Wang et al.[105] investigated the influence of the solution conditions including pH, salinity (electrolyte), and cation (Ca^{2+}) addition on the molecular behavior of C5Pe. In basic solutions, the carboxylic acid (–COOH) head group of C5Pe will be ionized. The ionization of the -COOH group increased the hydrophilicity of the adsorbed C5Pe films, thereby reducing the attractive hydrophobic force. In addition, at high salinity, the electric double layer was compressed and the hydrophobic forces were weakened, which led to the reduction in. Ca^{2+} ion could bine strongly with two –COOH groups and bridge two small C5Pe aggregates, which resulted in the formation of large aggregates.

Liu et al.[110] studied the nanoaggregation behavior of the asphaltene model compounds. They found that the aggregation number (n) of C5Pe in solution fell into the range of 1 to 31, with a large fraction of relatively small nanoaggregates ($2 \leq n \leq 11$). Compared to that in toluene, C5Pe molecules tended to form smaller aggregates in xylene (n=2, 3, 5, and 6), which should be attributed to the stronger interactions between C5Pe and xylene via π-π stacking and the larger steric effect of xylene. Naphthenic acids could interact with C5Pe to reduce its aggregation level, and the strength of the interaction depended on the size and structure of the naphthenic acid molecules.

Pradilla et al.[107] investigated the sorption of C5PeC11 at the interface. The adsorption of the C5PeC11 molecules at the decane−water interface was found to be reversible. In addition, the presence of interactions (aggregation) among the C5PeC11 molecules at both the oil−water and air−water interfaces was confirmed by the surface pressure−area (Π-A) isotherms. These interactions are most likely due to the π−π stacking and hydrogen bonding forces.

2.3.2.4 Molecular dynamics simulation

Molecular dynamics (MD) simulation has been widely used to study the self-association properties of the asphaltene model compounds.[111-114] Teklebrhan et al.[111] studied the adsorption and association behavior of five uncharged polyaromatic surfactants (C5Pe, PAP, TP, PCH, and BisA) at the oil−water interface using MD simulation. In both toluene−water and heptane−water systems, C5Pe molecules tend to predominantly concentrate and position at the interface, forming large nanoaggregates. Gao et al.[115] reported the formation of the hydrogen bonding between the oxygen atom in the carboxyl groups of C5Pe and the hydrogen atoms, which lead to aggregation of C5Pe molecules. Jian et al[116] investigated the adsorption behavior of the polycyclic aromatic compounds (PAC) molecules onto the water droplet in different organic solvents. In heptane, the adsorbed PAC aggregates render a straight one-dimensional (1D) rod-like structure on the small water droplet (radius of 1.86 nm) and a bent 1D structure on the large droplet (radius of 1.86 nm). In toluene, evident adsorption of the PAC molecules could only be observed in the case of large PAC concentration and large water droplet.

The orientation of the polyaromatic molecules at the oil−water interface was also studied extensively. Teklebrhan et al.[111] reported a side-on or head-on orientation of the uncharged polyaromatic molecules at the oil−water interface. Jian et al.[116] reported that the aggregates of the PAC molecules tend to have a perpendicular orientation to the water surface where contact occurs. Andrews et al.[117] also observed a perpendicular orientation of the polyaromatic cores of Violanthrone-78 at the solvent−water interface.

2.4 Summary of the literature review

Previous studies revealed that the stability of W/O emulsions in petroleum industry is most likely due to the formation of a mechanically strong, rigid, and viscoelastic interfacial film by the accumulation of surface-active molecules and inorganic solids from crude oil or bitumen[47, 55-59] at the interface. Chemical demulsification is both an effective and economy-efficient method to break emulsions. The molecular weight, HLB, relative solubility number, structure, and concentration of the demulsifier play important roles in breaking emulsions. Among all the demulsifiers, EO-PO copolymer has been extensively investigated[29, 30, 42-46] and previously reported as an effective additive in breaking asphaltene-stabilized W/O emulsions.[71] Temperature can also affect the demulsification efficiency by lowering the viscosity and density

of the oil, changing the interfacial properties of the oil−water interface, and increasing the collision rate of dispersed droplets. It is meaningful to study whether chemical demulsification can be combined with temperature treatment to induce better demulsification efficiency. The effect of temperature on the demulsification performance of EO-PO copolymers is therefore studied in this thesis.

C5Pe is considered as a suitable asphaltene model compound, which resembles asphaltene in terms of structure, molecular weight, interfacial activity, self-association behavior, etc. The use of C5Pe asphaltene model compound simplifies the original bitumen system, which is helpful in providing a deep understanding of the demulsification mechanism. It should be noted that there remains a gap between the two model systems and real crude oils comprising a mixture of different types of hydrocarbons.

Chapter 3 Experimental Techniques

3.1 Emulsion droplet size and counts determination by Focused Beam Reflectance Measurement (FBRM)

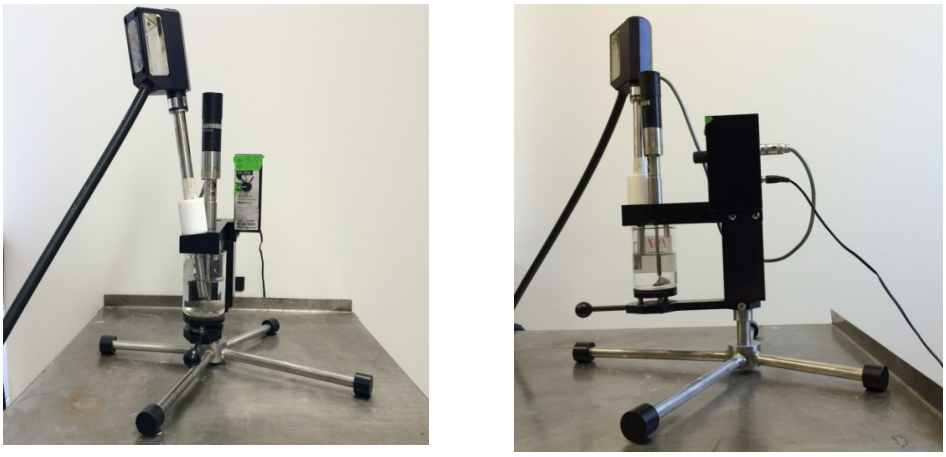

Figure 3-1 Front view (left) and side view (right) of the FBRM system

FBRM is designed to provide in situ particle or droplet size determination in real time. It can be used at operating pressures from vacuum to 150 psi over the operating temperatures of 41°F to 194 °F. In this study, FBRM was employed to measure the size of the emulsion droplets as a function of time under different experimental conditions. The emulsion droplet count in specific size range was also given by FBRM.

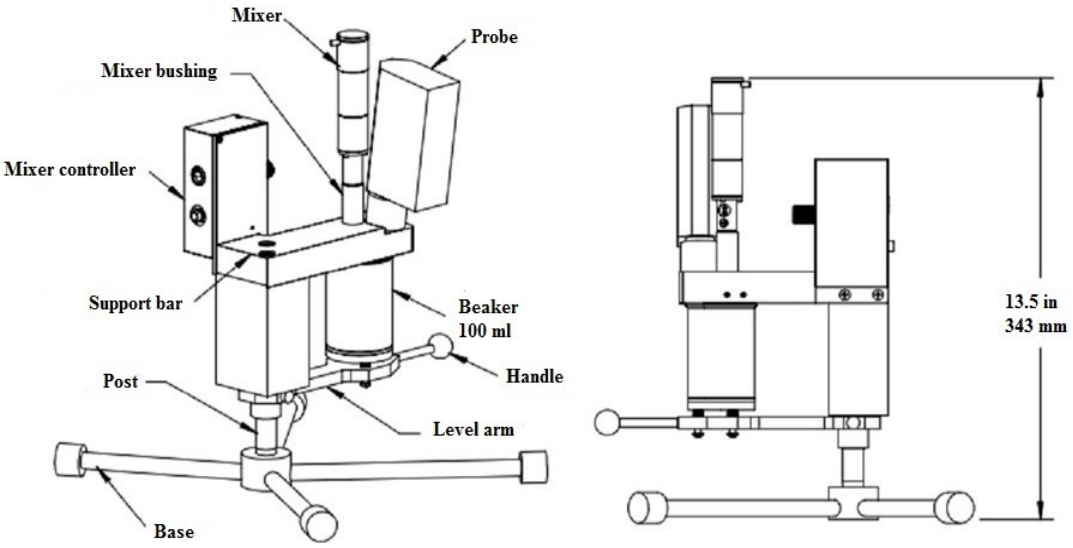

Figure 3-2 Front view and side view of the fixed beaker stand

All Lasentec S400 probe systems include a Fixed Beaker Stand (FBS) and overhead mixer for instrument calibration verification. The whole system is shown in **Figure 3-1**.

The fixed beaker stand comes in four separate parts: the base, the support bar with a mixer attached, bushings for the probes, and the probe itself (**Figure 3-2).**

3.1.1 FBRM probe working principle

A cut-away schematic of the FBRM probe is shown in **Figure 3-3**.[118] The probe is inserted into a flowing process medium. A laser source in the field unit travels down through a set of fiber optics into the probe and another set of optics at the tip of the probe focuses the laser beam to a very small spot. This is how the focused beam is defined. A motor is used to rotate the set of optics at the probe tip so that the focused beam scans a circular path at a constant speed. The focused beam usually moves at a high speed between 2 m/s to 8 m/s, depending on the application. In this manner, the motion of droplets or particles is insignificant to the measurement.

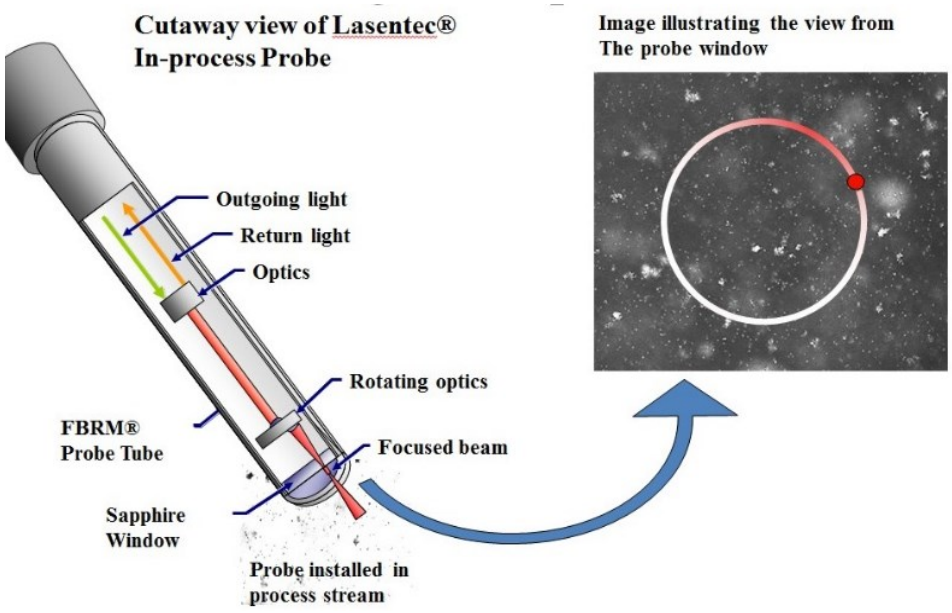

Figure 3-3 Cutaway view of the Lasentec in-process probe

3.1.2 FBRM probe data collection[119]

When a particle or droplet flows across the window, the focused beam intersects the edge of a particle or droplet. The particle or droplet then start to backscatter laser light until the focused beam reaches the opposite edge (**Figure 3-4**[118]). The pulses of backscattered light are collected

and then converted to chord lengths based on the simple calculation of the pulse width (time) multiplied by the scan speed (velocity). A chord length[120-122] is simplify defined as the straight-line distance between any two points on the edge of a particle or droplet. This chord length, in general, is not equal to the true particle or droplet size. However, with thousand times measurements of the chord lengths per second, it is a still good representation of the particle or droplet size statically.

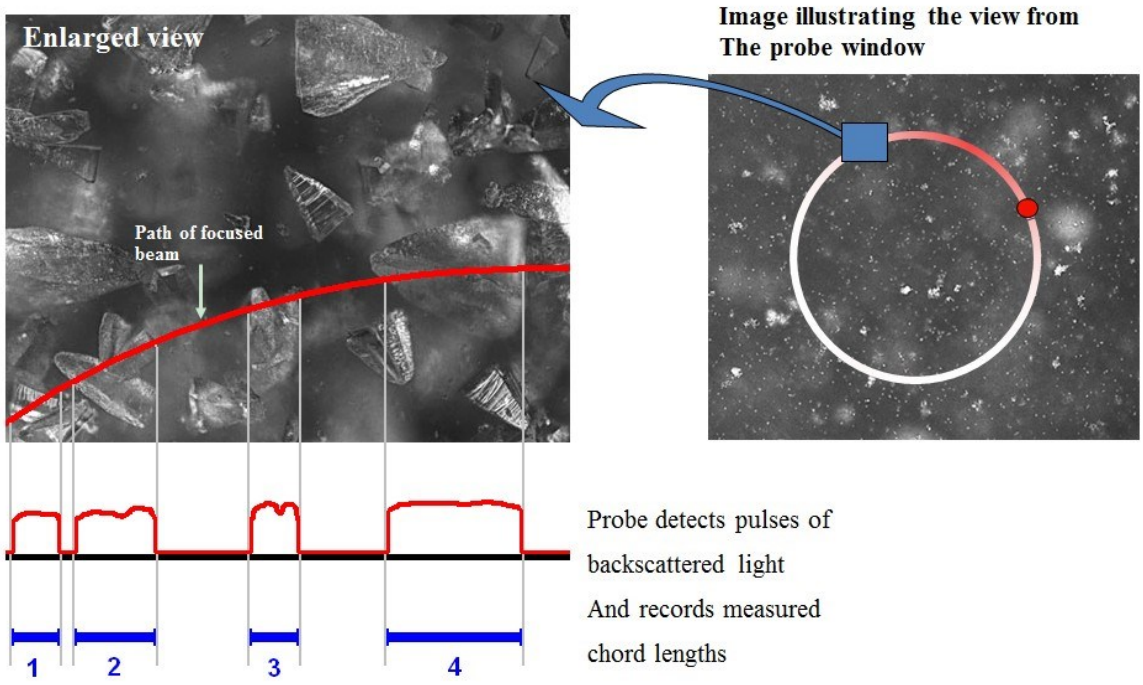

Figure 3-4 Working principle: probe detects pulses of backscattered light and records measured chord lengths

Two kinds of chord length from FBRM can be obtained: unweighted chord length (UWT CL) and square weighted chord length (SWT CL), which can be calculated using Equations (3-1) and (3-2).[123]

$$\overline{CD_u} = \frac{\sum_{i=1}^{k}\left[\left(\frac{n^i}{\sum_{i=1}^{k} n_i}\right)M_i\right]}{\sum_{i=1}^{k}\left(\frac{n^i}{\sum_{i=1}^{k} n_i}\right)} = \frac{\sum_{i=1}^{k} n_i M_i^1}{\sum_{i=1}^{k} n_i M_i^0} \tag{3-1}$$

$$\overline{CD_s} = \frac{\sum_{i=1}^{k}\left[\left(\frac{n^i M_i^3}{\sum_{i=1}^{k} n_i M_i^3}\right)M_i\right]}{\sum_{i=1}^{k}\left(\frac{n^i M_i^3}{\sum_{i=1}^{k} n_i M_i^3}\right)} = \frac{\sum_{i=1}^{k} n_i M_i^4}{\sum_{i=1}^{k} n_i M_i^3} \tag{3-2}$$

where k is the channel number (the data detected by FBRM are split into 90 channels of different size ranges in a logarithmic progression.), n_i is the counts in each individual channel, and M_i is the midpoint chord length of each individual channel.

The UWT chord length is number sensitive, which emphasizes the presence of fines in the studied samples. On the other hand, a SWT chord length distribution accentuates the contribution of larger particles or droplets of a dispersion system.

3.1.3 FBRM used at high temperature and pressure

The autoclave was employed to create a high-temperature and high-pressure emulsion system. With the help of the autoclave, solvent evaporation is avoided and the high-pressure condition is achieved. In order to mount the probe in the autoclave reactor, a branch was made on the side of the reactor (**Figure 3-5**). The best orientation is achieved when the angle of the probe window is between 30° and 60° to the flow, though 45° is the optimum angle. Therefore, a 45° angled branch was used to mount the probe.

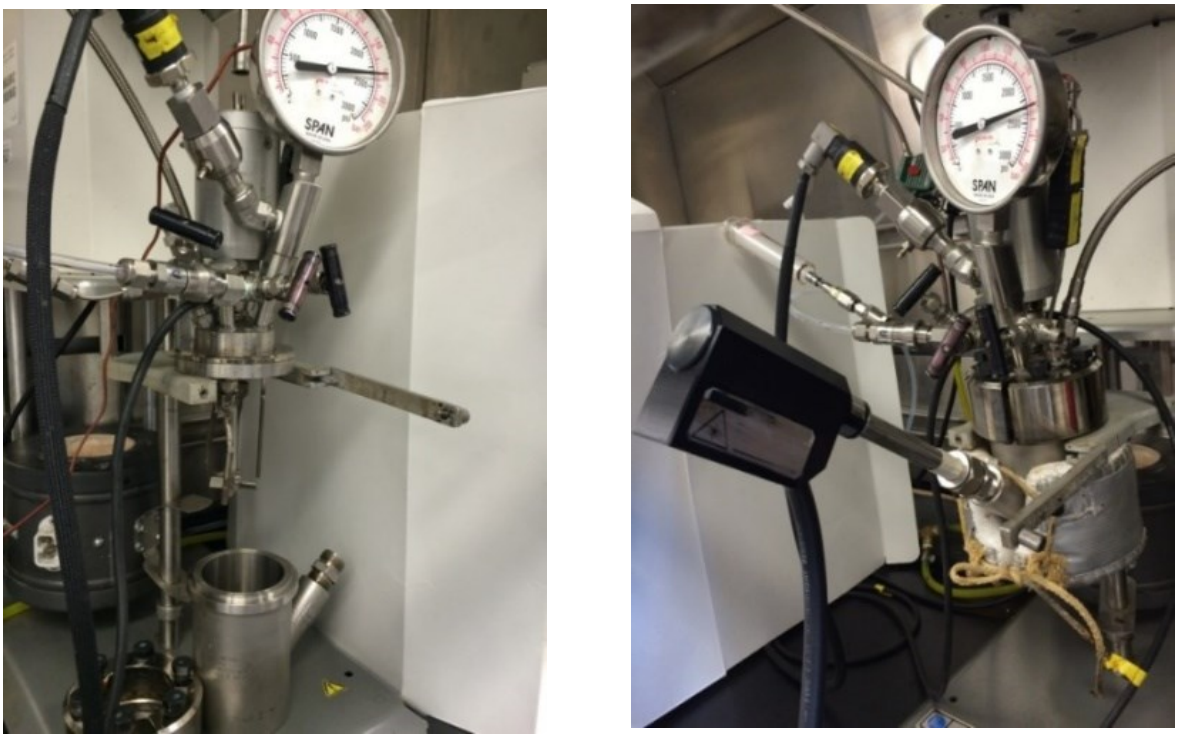

Figure 3-5 Autoclave with a 45° angled branch for FBRM

3.2 Coalescence time measurement by integrated thin film drainage apparatus (ITFDA)

To investigate the drainage of the thin liquid film between two droplets, a custom-built integrated thin film drainage apparatus (ITFDA) was used to measure the drop-drop coalescence time. **Figure 3-6**[124] shows a schematic view of the instrument. Details on the instrument setup and applications have been provided in other literature.[124] The operating procedures will be explained in detail in related chapters.

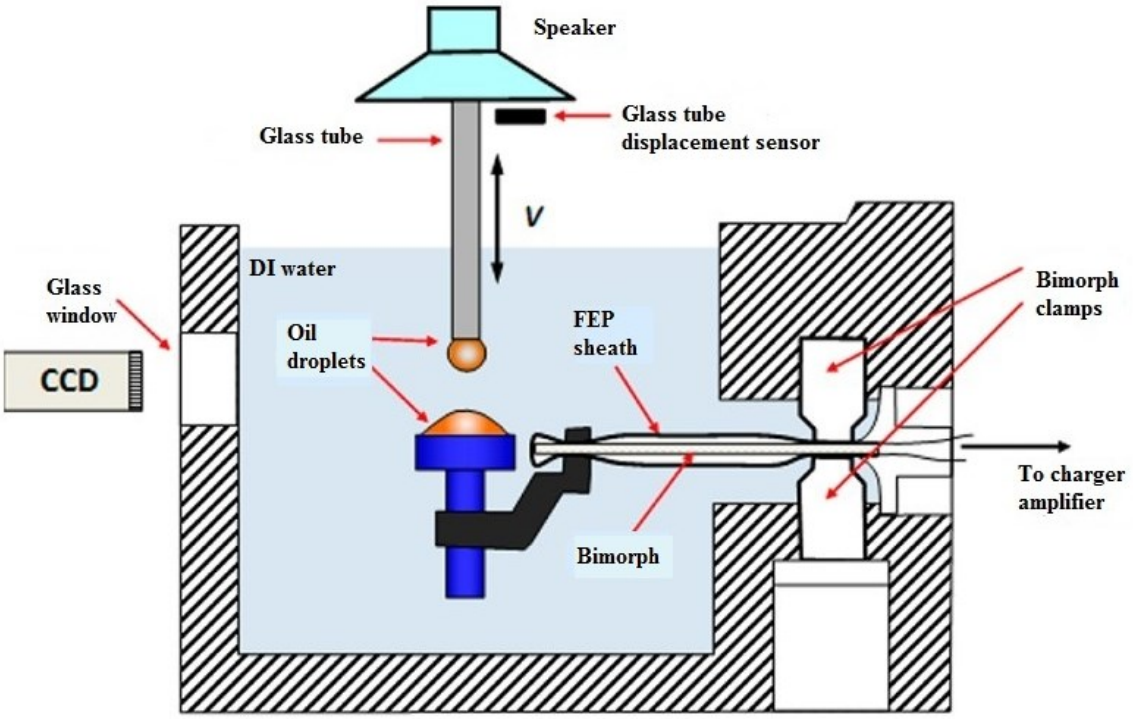

Figure 3-6 Schematic view of the integrated thin film drainage apparatus.

3.3 Static interfacial tension measurement by Du Noüy ring method

The static interfacial tension (IFT) of the oil−water interface can be measured using the Du Noüy ring method. **Figure 3-7**[125] is a cutaway view, which explains the mechanism of the Du Noüy ring method (1919). The water phase is loaded in the cell first (liquid 1) and the ring is immersed in it. Then the water phase is covered by the oil phase (liquid 2). The immersed ring is gradually directed towards the interface by lowering or raising the sample holder while monitoring the force applied on the ring. At the point when the liquid interface is vertical (as shown by the dotted lines in **Figure 3-7**), the largest detachment force can be detected by the electronic

balance, which can be converted to IFT by the software automatically, using Equations (3-3) to (3-6). It should be noted that all the measurements using the Du Noüy ring method are one-offs.

$$F = \gamma L \tag{3-3}$$

$$L = 2\pi(R+r)+2\pi(R-r)=4\pi R \tag{3-4}$$

$$F_{tol} = G_{ring} + F \tag{3-5}$$

$$\gamma = \frac{F_{tol} - G_{ring}}{4\pi R} \tag{3-6}$$

where F is the surface or interfacial tension force, F_{tol} is the total force measured using an electronic balance, G_{ring} is the gravity force of the ring, r is the radius of the ring, and R is the middle radius of the ring.

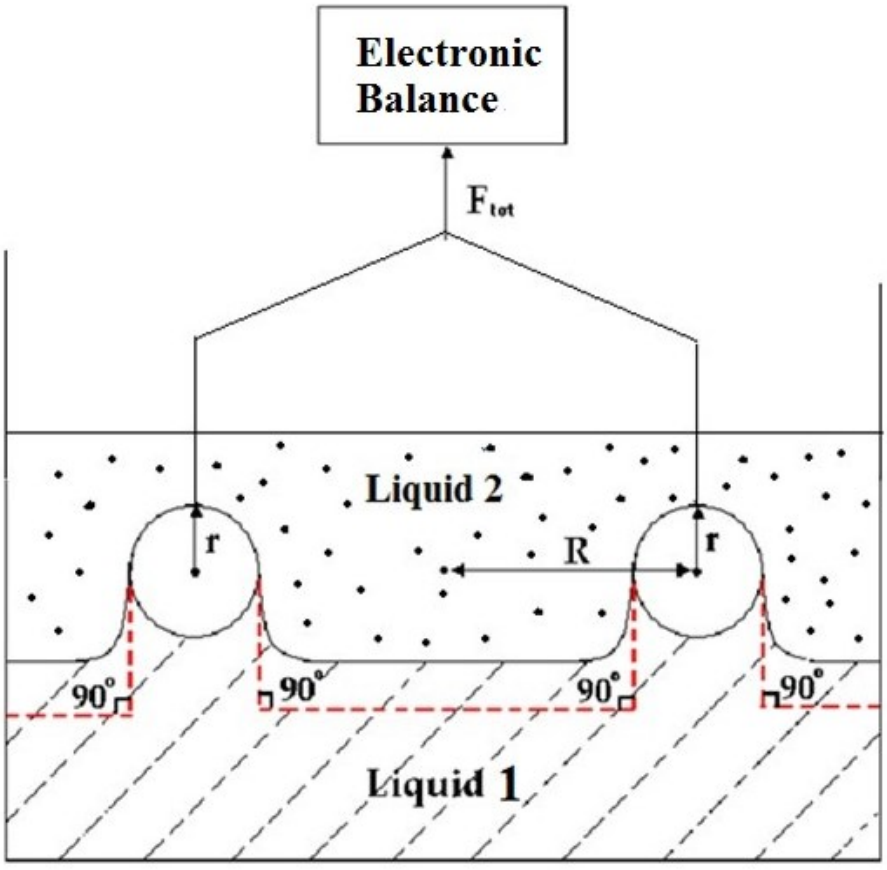

Figure 3-7 Cutaway view of the Du Noüy ring method.

3.4 Dynamic interfacial tension (DIFT) measurement by Theta Optical Tensiometer

Using the pendant drop technique, the DIFT of the oil−water interface can be measured. The IFT is calculated using the Young-Laplace equation:

$$\Delta P = \gamma \left(\frac{1}{r_1} + \frac{1}{r_2} \right) \quad (3\text{-}7)$$

$$\gamma = \Delta\rho \, g \frac{R_o^{\,2}}{\beta} \quad (3\text{-}8)$$

where γ is the IFT, $\Delta\rho$ is the density difference between the fluids, g is the gravitational constant, R_0 is the radius of the droplet at the apex, and β is the shape factor obtained by comparing the solution of the Young-Laplace equation with the shape of the drop. The Young-Laplace equation can be expressed as a system of dimensionless first-order equations as shown in **Figure 3-8**.[126]

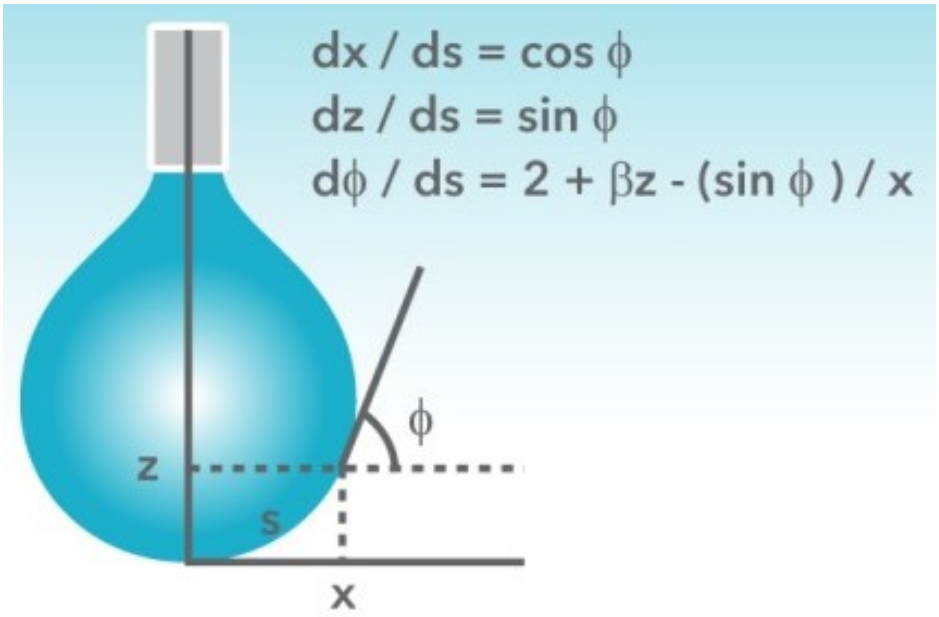

Figure 3-8 Pendant drop.[126]

3.5 Crumpling ratio measurement by Theta Optical Tensiometer

The stability of water-in-diluted bitumen emulsions has been attributed to the skin formation at the interface. The existence of this steric layer has been observed experimentally (**Figure 3-9**)[55, 58, 127-129] and can be quantitatively characterized using the volume contraction experiment.

When retracting the droplet, the volume of the droplet decreases smoothly with the shape of it remained spherical if the droplet surface remains fluid. However, a sudden crumpling of the oil−water interface may occur during the contraction process if a rigid skin is formed at the droplet surface. Crumpling behavior is the out-of-plane deflections of the rigid film due to its incompressible nature. To quantify the skin formation, a crumpling ratio (CR), was introduced[128] as Equation (3-9):

$$CR = \frac{A_f}{A_i} = \frac{\pi R_f^2}{\pi R_i^2} = \frac{R_f^2}{R_i^2} \tag{3-9}$$

where A_i is the initial projected area of the water droplet, A_f is the projected area of the oil droplet right before the point when crumpling was first observed. The larger the crumpling ratio, the more rigid the skin on the droplet surface.

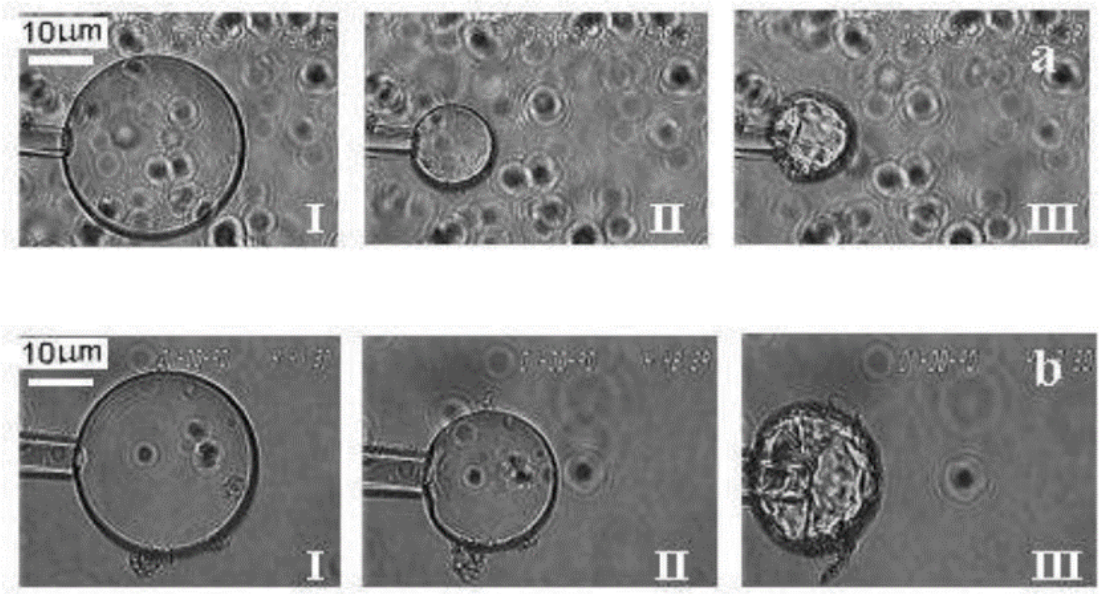

Figure 3-9 Skin formation (steric layer) at water droplet surfaces in (a) 0.1 wt.% bitumen and (b) 0.001 wt.% bitumen

3.6 Dilatational rheology measurement by Theta Optical Tensiometer

The study of interfacial dilatational properties is a powerful technique for probing the interfacial adsorption behavior, which is useful for a better understanding of the viscoelasticity of an interfacial film.[130] The pulsating droplet module (PD 200) was used to measure the dilatational viscoelastic complex modulus (E) and hence the dilatational elastic modulus (E') of the

oil−water interface. The complex surface dilatational modulus is related to the change of surface area (A) and interfacial tension (γ) of the pendant drop, which is defined as Equation (3-10):

$$|E| = \frac{d\gamma}{d \ln A} \tag{3-10}$$

This complex surface dilatational modulus can be decomposed into the elastic and viscous moduli as shown in Equation (3-11), and δ is the phase angle.

$$E' = |E| \sin \delta \qquad E'' = |E| \cos \delta \tag{3-11}$$

When measuring the surface dilatational modulus by the oscillating drop technique, a small drop was formed at the end of the capillary tip and harmonically oscillated by a membrane in the PD 200 module. **Figure 3-10**[131] shows sample responses of the bubble surface area and surface tension for a sinusoidal perturbation of a pendant drop and sample adsorption kinetics of surfactant on the surface of a pulsating drop.

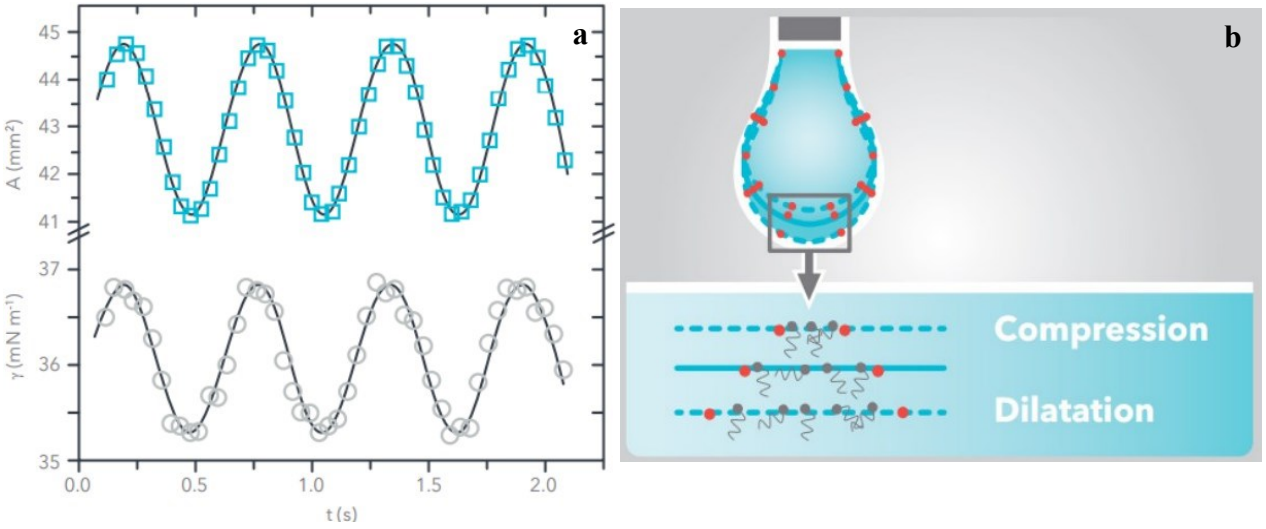

Figure 3-10 (a) Interfacial tension (grey circles) follows the change in droplet area (turquoise squares) and (b) deformation to the adsorbed molecular layer is caused by dilation or compression of the droplet.

3.7 Interfacial shear rheology measurement by Rheometer

Interfacial rheology studies the flow behavior of liquid interfaces, which determines the stability and behavior of emulsions, suspensions, foams, and froth, etc. A rheometer is normally used for interfacial shear rheology characterization and the basic principle of an oscillatory rheometer is to induce a sinusoidal shear deformation of an interface and measure the resultant stress response.

[132] The double wall ring (DWR) setup that is depicted in **Figure 3-11**[133] was used in this study. The trough, which contained the samples, was directly placed on the bottom plate and the circulation water flowed through the plate to control the experimental temperature. There are stepwise edges at the outer and inner sides of the trough to pin the interface and reduce the meniscus effect. After injecting the heavy phase in the trough (liquid 1), the double wall ring that is connected to the rheometer was positioned at the oil−water interface.[39] After washing the ring using acetone, toluene, and water, the organic contaminants on the ring were thoroughly removed with a flame prior to use. The trough has an outer radius of 39.5 mm and an inner radius of 31.0 mm. The outer and inner radii of the ring are 35.5 mm and 34.5 mm, respectively, with a thickness of 1 mm. The ring has a square-shaped cross-section with sharp edges in order to create a planar interface.

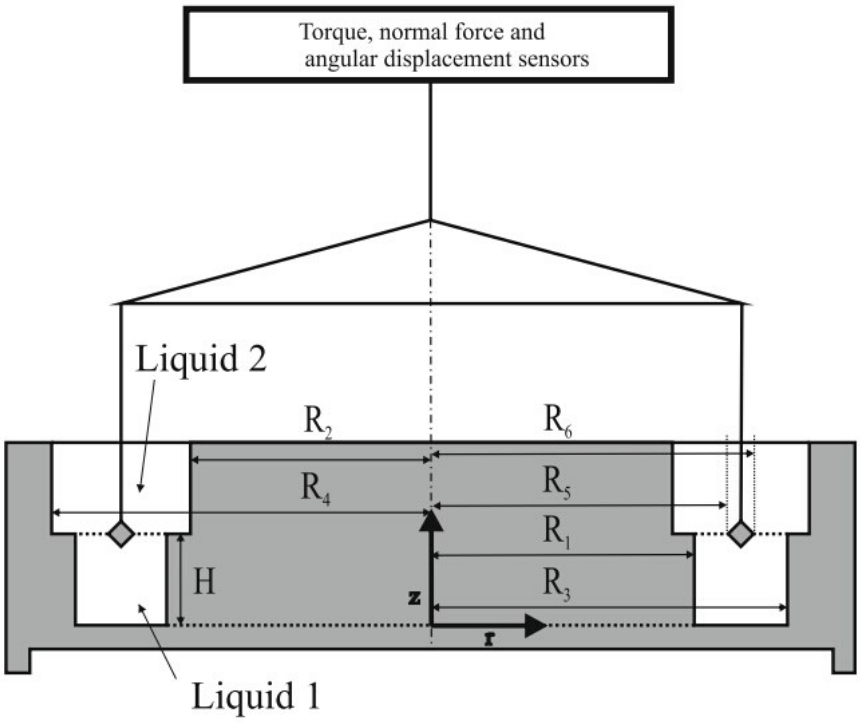

Figure 3-11 Schematic cross section of the DWR setup.

In interfacial shear rheology, shear deformation is applied at the interface while keeping the interfacial area constant. During the oscillation test, the functional relationship between shear stress (γ (t)) and shear strain (σ (t)) as a function of time is established. Shear stress is the force applied on the interface and shear strain is the deformation of the interface:[39]

The overall resistance of a material to deformation is defined as complex modulus, G*, and is given by Equation (3-14):

$$G^* = \gamma(t) / \sigma(t) \tag{3-14}$$

G* can be broken down into its component parts: storage modulus (G') and loss modulus (G"), as shown in Equations (3-15) and (3-16):

$$G' = \frac{\gamma(t)}{\sigma(t)} \cos(\delta) \tag{3-15}$$

$$G'' = \frac{\gamma(t)}{\sigma(t)} \sin(\delta) \tag{3-16}$$

which describe the elasticity and viscosity of the film, respectively. δ is the phase angle. If δ is greater than 45°, the interface shows more fluid-like properties, while the interface shows more solid-like properties if δ is less than 45°.

3.8 Pressure−area isotherm measured by Langmuir trough

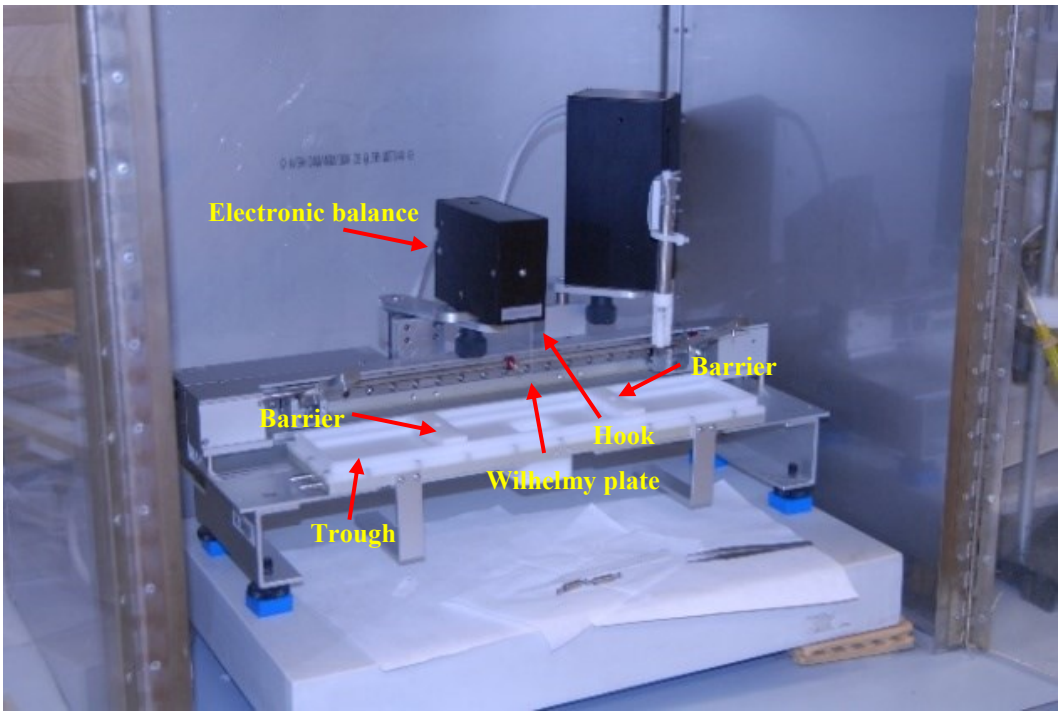

Figure 3-12 Langmuir interfacial trough set up.

Langmuir trough (KSV M1200) with a trough area of 243 cm^2, which is shown in **Figure 3-12**, was used in this study to investigate the compressional behavior of the interfacial films at the oil−water interface. The instrument consists of a two-compartment trough and two symmetrical barriers for compression of the interface or surface. The oil−water interface is located at the intersection between the two compartments. The interfacial pressure was measured using a Wilhelmy plate hang on the hook connected on the electrobalance. The Wilhelmy plate was partially immersed in the subphase. The interfacial pressure (π) is defined as the difference between the interfacial tension of the clean interface (σ_0) and the interfacial tension of the interface with surface-active materials (σ), which is given by $\pi = \sigma_0 - \sigma$.

3.9 Surface topography studied by atomic force microscope (AFM)

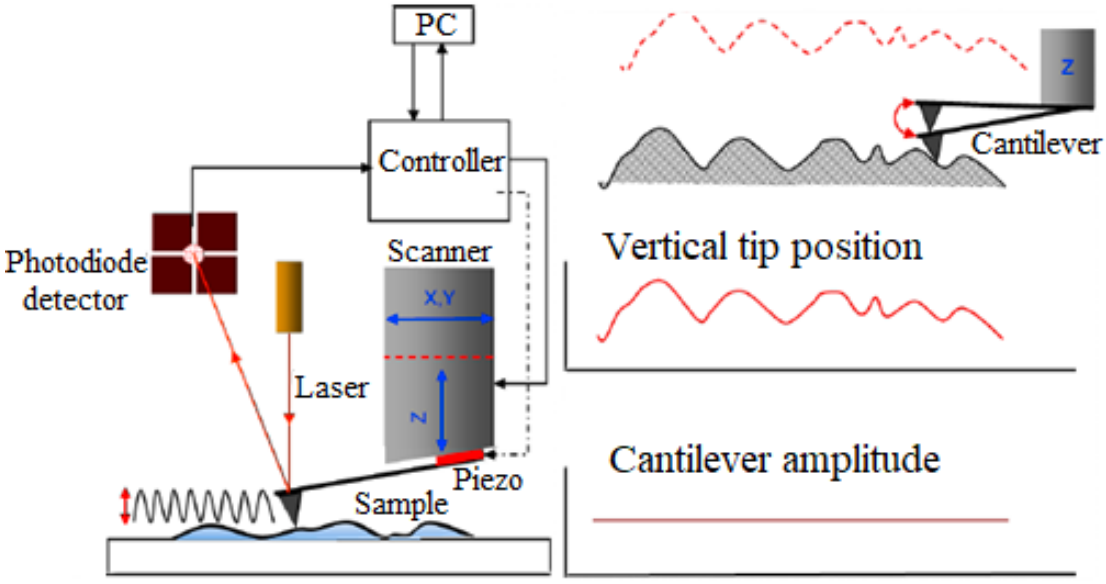

Figure 3-13 AFM imaging

AFM images of the interfacial films deposited on silicon wafers were obtained using a Dimension Icon Atomic Force Microscope (Bruker Dimension Icon-PT, Bruker Corporation) under tapping mode in air at 23 ˚C. Silica tips (NCHV) were used for imaging. **Figure 3-13** shows the basic mechanism for AFM imaging under tapping mode. In this mode, the cantilever is driven to oscillate up and down at or near its resonance frequency. When the spring-like cantilever is brought into proximity of a sample surface, the amplitude of the cantilever's oscillation will change due to the interaction forces between the cantilever tip and sample. A piezo is used to adjust the height of the cantilever above the sample to keep the

oscillation amplitude of the cantilever constant. The surface topography of the sample is therefore obtained by recording the height of the cantilever that corresponds to the constant cantilever tip−sample interaction.

3.10 Morphology of the interfacial film studied by Brewster angle microscopy (BAM)

Brewster angle microscopy as shown in **Figure 3-14** (Model EP3, Accurion GmbH, Goettingen, Germany) is used in this study to investigate the morphology of the oil−water interface. An advantage of this technique is that BAM is capable of determining the morphological changes of the interfacial films at the oil−water interface by demulsifier addition in real time and without transferring the film to a solid substrate. At the Brewster angle, θ_B, the p-polarized light is not reflected from the clean interface, while once the interface supports a film, the light will be reflected to the detector. Capture of this reflected light provides an image of the film, which serves as a representation of the interface. Further details about this technique and its application for interface imaging can be found elsewhere.[134, 135]

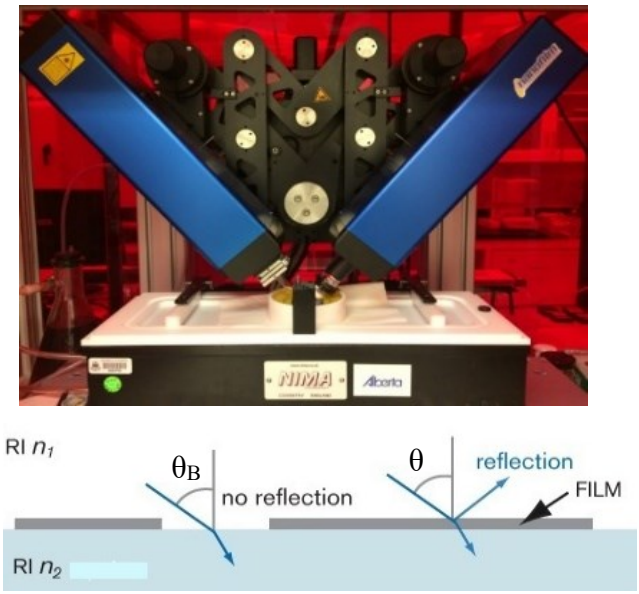

Figure 3-14 Brewster angle microscope

BAM used in this study was equipped with a CCD camera to image the morphology of the interfacial films at the oil−water interface at a 5X magnification. A wedge-shaped reflection plate in black was placed at the bottom of the trough to eliminate the influence of the refracted light from the surface and the reflected light from the bottom of the trough. All the images were collected using the EP3View2.x software (Accurion GmbH, Germany).

3.11 Water content measurement by Karl Fisher Titration

The demulsification efficiency of EO-PO demulsifiers was evaluated by measuring the water content at a depth of 2.5 cm from the emulsion surface. In this study, a Karl Fisher titrator (Cou-Lo 2000, GR Scientific Canada), as shown in **Figure 3-15**, was used to determine the water content. An average value of three measurements was reported.

$$B{\cdot}I_2 + B{\cdot}SO_2 + B + H_2O \rightarrow 2BH{+}I^- + BSO_3$$

Figure 3-15 Karl Fisher titrator

Chapter 4 Interfacial Properties Pertinent to W/O and O/W Emulsion Systems Prepared Using Polyaromatic Compounds

4.1 Introduction

Water-in-crude oil or diluted bitumen (W/O) emulsions encountered during crude oil production and bitumen processing are known to be very stable and the emulsified small water droplets are hard to remove. Such emulsions are undesirable for a number of reasons, such as additional volume (cost) for transportation, equipment corrosion, and catalyst fouling at downstream refineries.[136] Therefore, these emulsions have to be treated to remove the dispersed water droplets and associated inorganic salts to meet the specifications for transportation, further refining, upgrading, storage, and export.

Unlike microemulsions, macroemulsions are generally anticipated to be thermodynamically unstable and hence to be phase separated with time.[137, 138] Persistent stability of W/O emulsions encountered in the oil industry is often attributed to a rigid, viscoelastic, and mechanically strong interfacial film that surrounds water droplets and prevents their coalescence.[128, 137, 139-141] Destabilization of the emulsions can be realized by the use of chemical, heating, mechanical, and/or electrical treatments. Among these methods, chemical demulsification is considered to be the most efficient and cost-effective, which has been widely used in the oil industry.[28, 142, 143] However, the excess use of the chemicals is a serious concern that not only increases the cost of operations but is also sensitive to process conditions that may not always be effective.

The interfacial properties of emulsions and coalescence mechanisms of the water droplets have been investigated with the aim to improve the design of efficient and robust demulsifier chemicals.[71, 144-146] Through interfacial tension measurement, X-ray photoelectron spectroscopy characterization, micropipette experiment, and shear rheology measurement, Pensini et al.[71] proved that the ethylene oxide-propylene oxide (EO-PO)-based polymeric demulsifier is more interfacially active than asphaltenes (0.25 g/L) and can compete effectively with asphaltenes at the interface, penetrating and softening interfacial asphaltene films. The dilatational viscoelastic behavior of the W/O interface formed with 0.044 wt.% surface-active fractions extracted from an Iranian heavy oil was studied by Sun et al.[144] Their results showed that the adsorption of demulsifier molecules at the oil−water interface leaves small voids at the interface of water

droplets, providing opportunity for droplet coalescence. Ese et al.[145] investigated surface pressure−area isotherms and concluded that increased compressibility (reduced rigidity of the film) after demulsifier addition seems to be an important feature when breaking a stable emulsion.

In fact, interfacial tension has been widely studied in the oil industry[147, 148] as a good indicator of the adsorption of surface-active molecules at the oil−water interface. While the crumpling ratio (CR) of the droplets reflects the degree of steric layer (skin) formation at the interface,[128] dilatational rheology characterizes the viscoelasticity of the interfacial film.[149, 150] Studying interfacial dilatational rheology is a powerful tool to probe the adsorption and association of surface-active molecules at the oil−water interface, providing a better understanding of the microscopic properties of an interfacial film.[130] The stability of the thin liquid film between two liquid droplets is reported to be critical for emulsion stability,[151] while the coalescence time characterizes the stability of this thin liquid film.[152, 153]

Investigations using optical methods are normally performed on an oil droplet in an aqueous phase as the measurements require the continuous phase to be transparent for good optical visibility of studied objects and non-transparent crude oil prohibits the measurement of water droplets in crude oil, which is more relevant to W/O petroleum emulsions. Asphaltenes of polyaromatic cores are recognized as the main components to stabilize W/O petroleum emulsions. However, the asphaltene solutions are non-transparent even at low asphaltene concentrations. Perylene family compounds such as C5Pe and C5PeC11 are of similar structural characteristics (containing a fused polyaromatic core) of asphaltene molecules and exhibit similar interfacial activities.[101, 102] Since the transparent solutions of C5Pe and C5PeC11 can be made to reasonable concentrations, they are used in this study as asphaltene model compounds.[99, 103-106] It should be noted that there remains a gap between the two model systems and real crude oils comprising a mixture of different types of hydrocarbons.

The current study aims to uncover the relationship between the measured interfacial properties using W/O and O/W systems. The objective of this study is to confirm whether the measurement of interfacial properties using the reverse (O/W) system could provide insights on stabilization mechanisms of W/O emulsions. To achieve this goal, interfacial tension, crumpling ratio, dilatational rheology, and coalescence time measurements were conducted using xylene

containing surface-active polyaromatic compounds C5Pe and C5PeC11 as the oil phase which is of good optical transparency.

4.2 Materials and Methods

4.2.1 Materials

C5Pe (N-(1-hexylheptyl)-N′-(5-carboxylicpentyl) perylene-3,4,9,10-tetracarboxylic bisimide) and C5PeC11 (N-(1-undecyldodecyl)-N′-(5-carboxylicpentyl) perylene-3,4,9,10-tetracarboxylic bisimide) were used as asphaltene model compounds (**Figure 2-5**). The only difference in molecular structure between C5Pe and C5PeC11 is longer aliphatic chains of C5PeC11 that enhances its solubility in xylene. The protocols utilized to synthesize C5Pe and C5PeC11 have been described in detail elsewhere.[154]

Solutions of C5Pe or C5PeC11 in xylene (≥98.5%, ACS grade, Fisher Scientific, Canada) were used as model oil in this study. C5Pe or C5PeC11 in xylene solutions were prepared by sonicating (Crest 275DA Ultrasonic Cleaner, 50/60 Hz) a given amount of C5Pe or C5PeC11 in xylene for 30 min. Deionized (DI) water of resistivity > 18.5 MΩ·cm was purified with a Millipore system and used throughout this study. Buffer solutions of pH 7 were provided by Fisher Scientific and used as received.

4.2.2 Methods

A Theta Optical Tensiometer T200 (Attention, Biolin Scientific, Finland) was used to study the interfacial properties of the C5Pe or C5PeC11 in xylene solutions (oil)−water interface by measuring the interfacial tension, crumpling ratio, and interfacial dilatational rheology. An integrated thin film drainage apparatus (ITFDA)[124] was used to determine the coalescence time of water droplets in oil or oil droplets in water, which provides information on the rupture of the thin liquid film.

4.2.2.1 Interfacial tension

The pendant drop technique was used to determine the dynamic interfacial tension of W/O (water droplets in C5Pe or C5PeC11 in xylene solution) and O/W (droplets of C5Pe or C5PeC11 in xylene solution in water) systems. For W/O systems, a water droplet of 10 μL in volume generated by a gastight syringe (Hamilton Co., USA) was immersed in 3 mL C5Pe or C5PeC11 in xylene solution placed in a quartz cuvette. For O/W systems, an oil droplet of 10 μL in volume

was immersed in 3 mL water. The interfacial tension was recorded after the droplets were in contact with the continuous phase for 10 min and 30 min, respectively.

For comparison, the interfacial tension of the oil−water interface was also measured using the Du Noüy ring method. In this case, 20 mL of water was loaded in the measurement cell first while the ring was immersed in water. The water phase was then covered by 15 mL of the oil phase. After aging the interface for a desired period of time, the immersed ring was gradually pulled towards the interface while monitoring the force exerting on the ring. At the point when the liquid interface was vertical, the largest detachment force was detected by the electronic balance, which was converted to the interfacial tension.

4.2.2.2 Crumpling ratio

Similar to interfacial tension measurements, the size of the water (or oil) droplets was controlled to 10 μL in volume for crumpling ratio measurements. After aging of the droplets for a desired period of time, the water (or oil) droplet was retracted steadily into the syringe while the whole process was recorded. The crumpling ratio was quantified by dividing the projected area of the droplet at the point when wrinkles (crumpling) were first observed on this droplet (Af) by the projected area of the initial droplet (Ai). The point where the crumpling began was determined by analyzing the video frame by frame.

4.2.2.3 Dilatational Rheology

The pulsating droplet module (PD 200) was used to measure the dilatational viscoelastic complex modulus (E) and hence the dilatational elastic modulus (E') of the oil−water interface. A water (oil) droplet of 5 μL in volume was generated at the tip of the syringe needle and immersed in 3 mL of oil (water) placed in a quartz cuvette. The droplet was sinusoidally oscillated and the change in the interfacial tension and surface area was recorded. In this study, the maximum change in droplet volume was set to be 10% and the oscillation frequency was set at 0.1 Hz, which is in the linear viscoelastic region as shown by the results in Figure **4-9**. This frequency was used to avoid the loss of accuracy at higher frequencies.[155] Each measurement was set to include ten oscillations with a 10 s delay between consecutive measurements.

4.2.2.4 Coalescence time

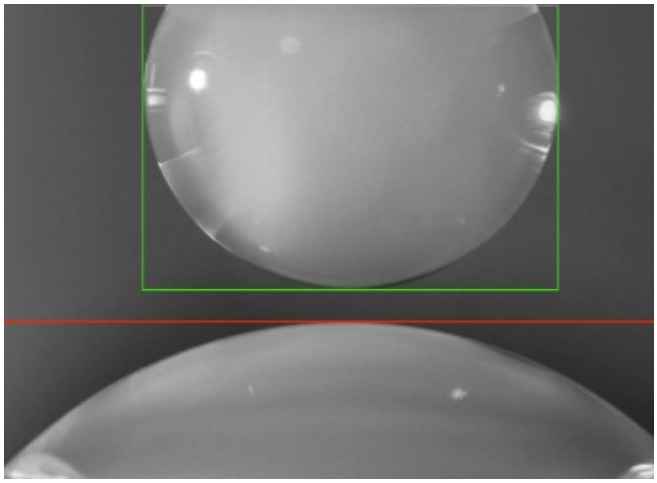

Figure 4-1 Two water (or oil) droplets are placed close to each other before the coalescence time measurement for aging of the droplets. The square and horizontal lines are used to make sure the size of the droplets and initial distance are the same throughout different experiments. The radii of the droplets are R_1~1.3 mm (measured by the maximum horizontal dimension of the top droplet) and R_2~2.8 mm (calculated from the curvature of the semicircular bottom droplet).

A custom-built integrated thin film drainage apparatus (ITFDA) was used to measure the coalescence time of two water droplets in oil or two oil droplets in water. Details of the instrument setup can be found in Wang et al.[124] Initially, a bottom water (or oil) droplet with semicircular shape was generated on a holder made of glass (for water droplet) or Teflon (for oil droplet). A top water (or oil) droplet was produced immediately by the capillary tube with the help of a gastight syringe. The droplets were held apart at a separation distance of 200 ± 10 μm in oil (or water) as shown in **Figure 4-1**. During the aging period of 10 min, the two droplets were aligned. Right after aging, the top droplet was driven downward at a constant velocity of 313 μm/s for a fixed distance of 313 μm so that the two droplets were brought in contact with an overlap of 119 μm. The drop−drop interaction process was recorded by a high-speed video camera for a period of 2 min. During the holding period, the droplets could coalesce or remain as individual droplets. The coalescence time was determined as the time from the moment that contact between the droplets was observed until their coalescence. In the case that coalescence did not occur, the droplets were considered stable. The coalescence time for the former case was determined by counting the time during the video playback. For repeating tests, fresh droplets were produced in a similar manner as described above. Although care was taken to use droplets of the same size, it was not possible to get exactly the same size every time, especially the shape

of these large drops could change considerably when the interfacial tension was low due to the addition of surface-active molecules such as C5Pe or C5PeC11.

4.3 Experimental Results

4.3.1 Interfacial tension measurement

The optimum volume of droplets for IFT measurement using Theta Optical Tensiometer is the largest volume of the droplet that does not fall down from the tip of the syringe needle. In general, the lower, the IFT, the smaller, the optimum droplet volume. A droplet of 10 µL is the upper size limit for the largest concentration of 150 mg/L C5Pe with the lowest IFT in our case. This is the basis for us to use 10 µL volume of droplets in all IFT measurements in this study. To confirm that the measurements were consistent, we investigated the effect of volume on the IFT for the cases of lower concentrations (30 mg/L) and obtained the same results at different volumes as shown in **Figure 4-2**.

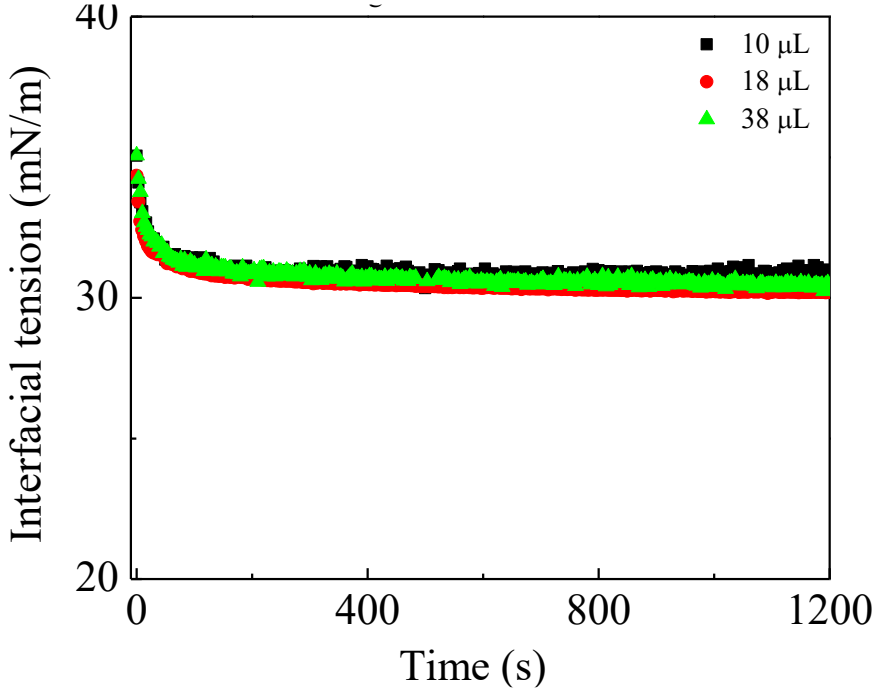

Figure 4-2 Effect of the droplet volume on interfacial tension of the 30 mg/L C5Pe solution−water interface.

The results of interfacial tension measurements using the pendant drop technique as a function of C5Pe/C5PeC11 concentration in xylene are shown in **Figure 4-3** and **Figure 4-4**. The pH of the aqueous phase and droplet aging time were varied in this set of measurements. To improve the

confidence of the results, each experiment was repeated for at least three times, and the interfacial tension difference between different measurements under the same condition was less than 0.2 mN/m.

In **Figure 4-3** and **Figure 4-4**, a decrease in interfacial tension with increasing the concentration of C5Pe or C5PeC11 in xylene is observed, which implies that more C5Pe or C5PeC11 molecules can be adsorbed at the oil−water interface at higher C5Pe or C5PeC11 concentrations. The interfacial tension of water droplet in C5PeC11 solutions shows almost no changes upon aging from 10 min to 30 min, while the interfacial tension of the water droplet in C5Pe continues to decrease with aging from 10 min to 30 min, indicating further adsorption of C5Pe molecules at the interface with aging. The dynamic interfacial tension changes of the W/O and O/W systems are shown in **Figure 4-5**.

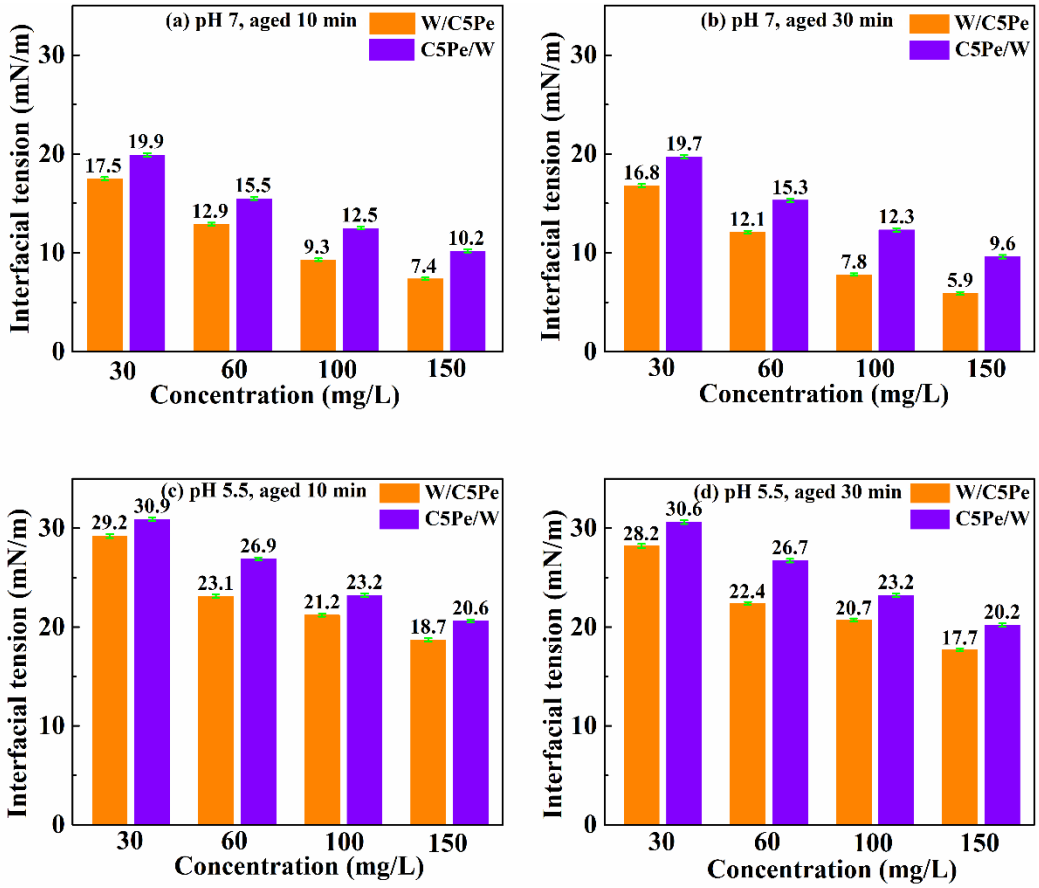

Figure 4-3 Interfacial tension as a function of C5Pe concentration for pH 7 water−C5Pe in xylene solution: (a) aged for 10 min and (b) aged for 30 min; pH 5.5 water−C5Pe in xylene solution: (c) aged for 10 min and (d) aged for 30 min.

Figure 4-3 (a) and (b) shows that over the C5Pe concentration range in xylene from 30 mg/L to 150 mg/L, the interfacial tension of the W/O system is always lower by 1~4 mN/m than that of the O/W system (at water pH of 7), indicating that the oil−water interface in the W/O system can accommodate more C5Pe molecules and/or lead to a tighter packing of C5Pe molecules as the surface area is the same for W/O and O/W systems. Despite small, such difference between the two systems may have a significant impact on film rigidity of the two systems as will be seen from the crumpling ratio and dilatational modulus discussed in the following sections. The same trend of the interfacial tension is obtained in **Figure 4-3** (c) and (d) for the same systems but at pH 5.5 of the aqueous phase, although the interfacial tension values are much higher than that for the systems at pH 7. The Zeta potential of the xylene diluted C5Pe in water emulsions at different pH was also measured in this study and the results are shown in Error! Reference s ource not found.. The pKa of C5Pe (at 30 mg/L) is at pH 6, which agrees with Wang et al.[156] In addition, it was found that the zeta potential of the xylene diluted C5Pe in water emulsions at water pH of 7 did not change with C5Pe concentrations (i.e., at 60, 100, and 150 mg/L). It can be inferred that C5Pe is fully protonated at pH 5.5 while it is probably partially or even fully ionized at pH 7. The ionized C5Pe molecules are clearly much more interfacially active as anticipated, leading to the observed lower interfacial tension at higher pH.

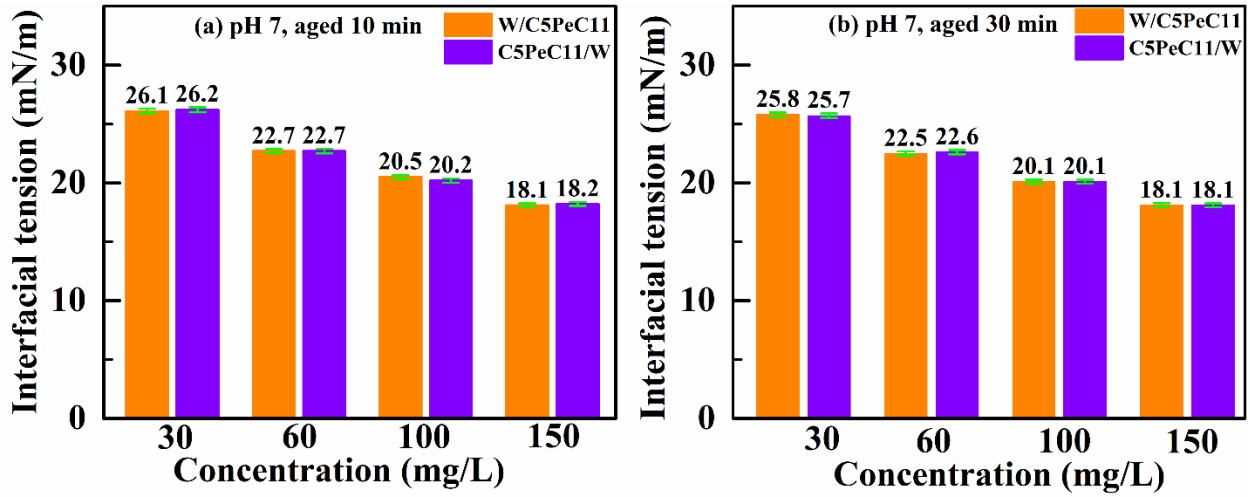

Figure 4-4 Interfacial tension as a function of C5PeC11 concentration for pH 7 water−C5PeC11 in xylene solution: (a) aged for 10 min and (b) aged for 30 min.

As shown in **Figure 4-4** for C5PeC11, the interfacial tension becomes constant after 10 min of aging for both W/O and O/W systems for all C5PeC11 concentrations examined. This result

suggests that the interface in the C5PeC11 system reaches equilibrium after 10 min, which is much faster than that in the corresponding C5Pe system. However, the xylene−water interfacial tension in the C5PeC11 system is much higher than that in the C5Pe system, indicating less surface-active nature of C5PeC11 than C5Pe. More interestingly, the interfacial tensions for a given C5PeC11 concentration are the same for W/O and O/W systems, which is different from the C5Pe case. The same interfacial tension for O/W and W/O in C5PeC11 system appears to be the result of less C5PeC11 molecules at the xylene−water interface due to its better solubility in xylene. In this case, the amount of surface-active C5PeC11 molecules at the oil−water interface is essentially the same for the two systems.

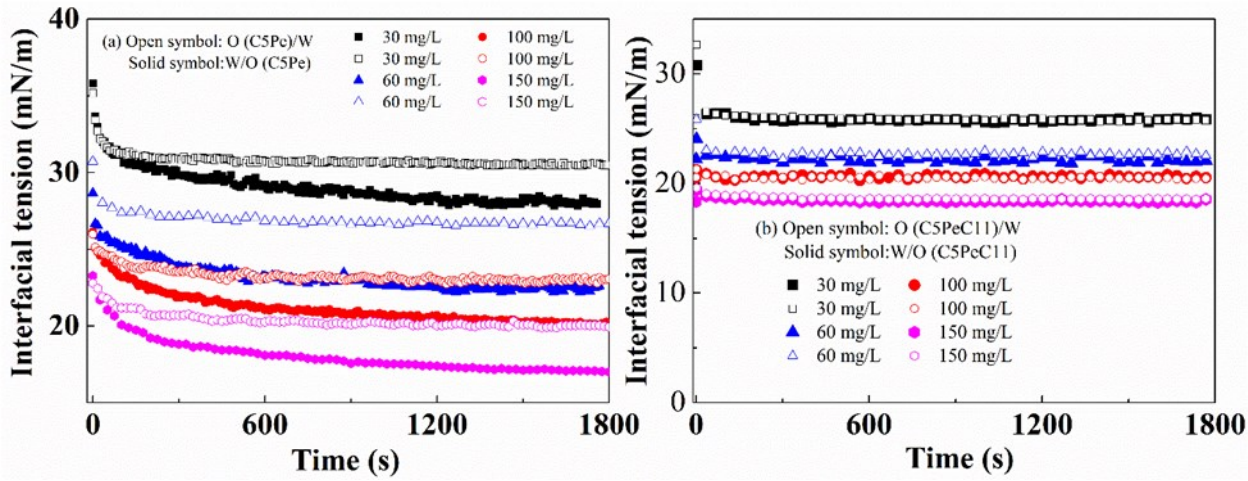

Figure 4-5 (a) dynamic IFT of C5Pe−water (pH 5.5) interface and (b) dynamic IFT of C5PeC11−water (pH 7) interface.

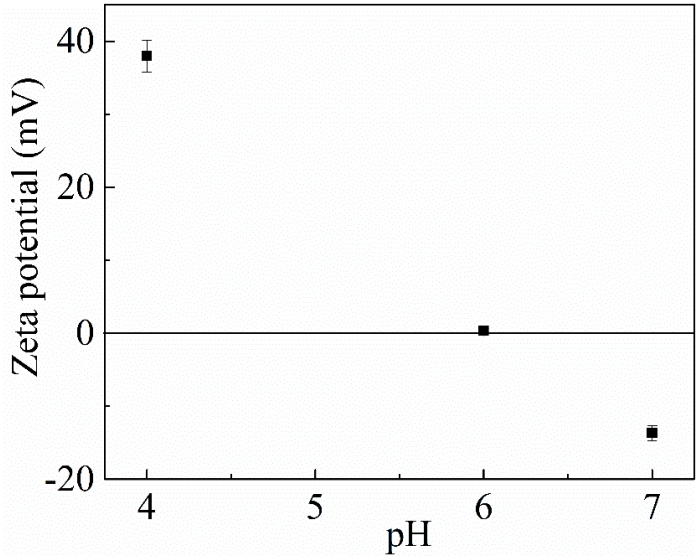

Figure 4-6 Zeta potential of xylene diluted C5Pe in water emulsions as a function of pH.

The observed difference in interfacial tensions of C5Pe systems in **Figure 4-3** obtained using the pendant drop method might be attributed to the reservoir effect, i.e., more C5Pe molecules are available for adsorption in the W/O system than in the O/W system. To check this hypothesis, interfacial tension measurements were also performed using the Du Noüy ring method for planer oil−water interface. The measured interfacial tensions match well with that measured using the W/O case (**Figure 4-7** (a)), showing that the larger amount of C5Pe in the continuous phase indeed provides more material to attach to the interface. For C5PeC11, the interfacial tensions measured using Du Noüy ring method for planer oil−water interface match well with that measured using O/W and W/O systems (**Figure 4-7** (b)), as anticipated. In fact, by studying 12 different ionic and non-ionic surfactants, Miller et al.[157] reported that in solutions of highly surface-active surfactants (especially at low concentration), the concentration within the drop becomes essentially lower as compared to the initial concentration due to the adsorption of the surfactant molecules at the drop surface, while surfactant depletion due to adsorption does not occur with the bubble profile (or Du Nouy ring, or Wilhelmy plate method), where the volume of the studied solution is large. In addition, for surfactant of low surface activity, no difference is found, as in the case of C5PeC11 in this research. Overall, the reservoir effect leads to the difference in the interfacial tensions of W/O and O/W systems.

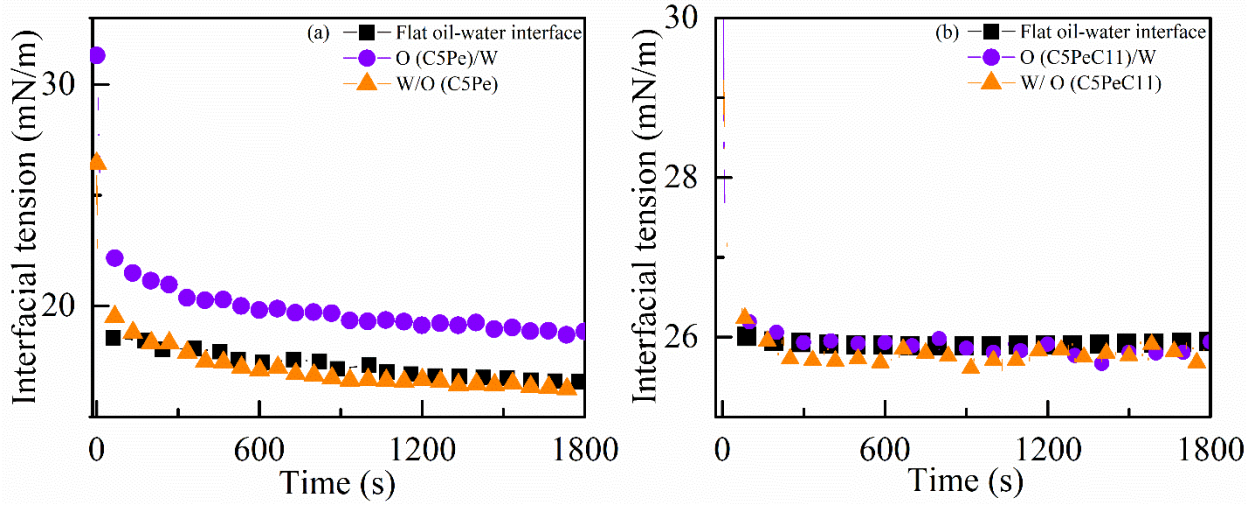

Figure 4-7 Comparison of interfacial tensions measured using the pendant drop and Du Noüy ring methods: (a) for water−C5Pe in xylene solution and (b) for water−C5PeC11 in xylene solution, both aged for up to 30 min. Note: V_{water}:V_{oil}=4:3 for Du Noüy ring method; V_{water}:V_{oil}=1:300 in W/O case and 300:1 in O/W case for the pendant drop method.

4.3.2 Crumpling ratio

The contraction behavior of asphaltene films at the oil−water interface has been shown to shed light on the role of asphaltene films in stabilizing water droplets from coalescence in emulsions.[58, 158, 159] Similarly, the adsorption of C5Pe or C5PeC11 molecules at the xylene−water interface was investigated by crumpling experiments. The arrangement of surface-active species, such as asphaltenes, resins, and inorganic solids, at the liquid−liquid interface, can create a 'skin-like' interfacial layer around the droplet. Upon removal of the liquid inside the droplet, the area of the skin becomes larger than the area of a Laplacian droplet of the reduced volume and the interface crumples as a result of irreversible adsorption and/or assembling of adsorbed species at the interface. The projected area of the droplet surface when crumpling becomes visually evident divided by the projected area of the initial droplet is defined as the crumpling ratio.

The results of volume contraction experiments are summarized in **Figure 4-8**. Each data point in **Figure 4-8** is an average of at least three independent measurements and the error bars represent the standard deviation of all the measurements. Only crumpling ratio of C5Pe−water system is shown here as no crumpling was detected for C5PeC11−water system up to 150 mg/L C5PeC11 concentration for both W/O and O/W systems. The absence of the crumpling of water−C5PeC11 in xylene solution interface indicates the absence of C5PeC11 skins at the xylene−water interface, most likely as a result of more reversible nature of C5PeC11 adsorption and/or minimal molecular association between C5PeC11 molecules at the interface due to steric hindrance of longer aliphatic tails[160] and its high solubility in xylenes. Compared with C5PeC11, less bulky hydrophobic tails of C5Pe molecules which has weaker steric repulsion in xylene allows stronger association with each other by attractive forces such as π-π stacking, forming an inter-linked crumpling C5Pe interfacial film.[156]

It is interesting to note a much higher crumpling ratio for the W/O system than that for the O/W system (Figure **4-8**), despite the same chemistry of both systems. Such a significant difference in the crumpling ratio of the two systems is most likely linked to the amount and irreversible nature of the adsorption that leads to different packing patterns of C5Pe molecules at the oil−water interfaces. According to interfacial tension results, more C5Pe molecules are adsorbed at the oil−water interface for W/O systems than for O/W systems due to the reservoir effect, leading to tighter packing of the C5Pe molecules at the interface. The tighter packing results in a stronger

association of C5Pe molecules of the W/O systems. As the film is contracted during the retraction of the water droplets as in the W/O system, the bulky hydrophobic tails of C5Pe molecules are more easily jammed up (squeezed), leading to crumpling at relatively small volume reduction of the droplet (i.e., large crumpling ratio) due to the irreversible nature of the interfacial film. For the O/W system, the relatively loose packing allows more contraction of the droplets before the steric repulsion among the hydrophobic tails in xylene comes into play, leading to a smaller crumpling ratio. Such differences in crumpling ratio also confirm the formation of interfacial layers of elastic nature as illustrated by the results of interfacial rheology shown in **Figure 4-10**. It is not surprising to see higher crumpling ratio at higher C5Pe concentrations in xylene as more C5Pe molecules are expected to adsorb at the xylene−water interface as shown in **Figure 4-3**. When much less reversibly adsorbed molecules are at the O/W interface, which is the case for C5PeC11, crumpling will not occur. Overall, the difference in the C5Pe adsorption amount at the oil−water interface plays a big role in the crumpling of the interface.

In addition, an obvious increase in the crumpling ratio is observed with increasing aging from 10 min to 30 min for the W/O system, while the crumpling ratio increases slightly for the O/W system. This trend corresponds well with the change in interfacial tension as shown in **Figure 4-3**: the interfacial tension of the O/W system almost reaches equilibrium after 10 min aging whereas the interfacial tension of the W/O system continues to decrease. Therefore, the more adsorbed C5Pe molecules at the interface for longer aging lead to the higher crumpling ratio.

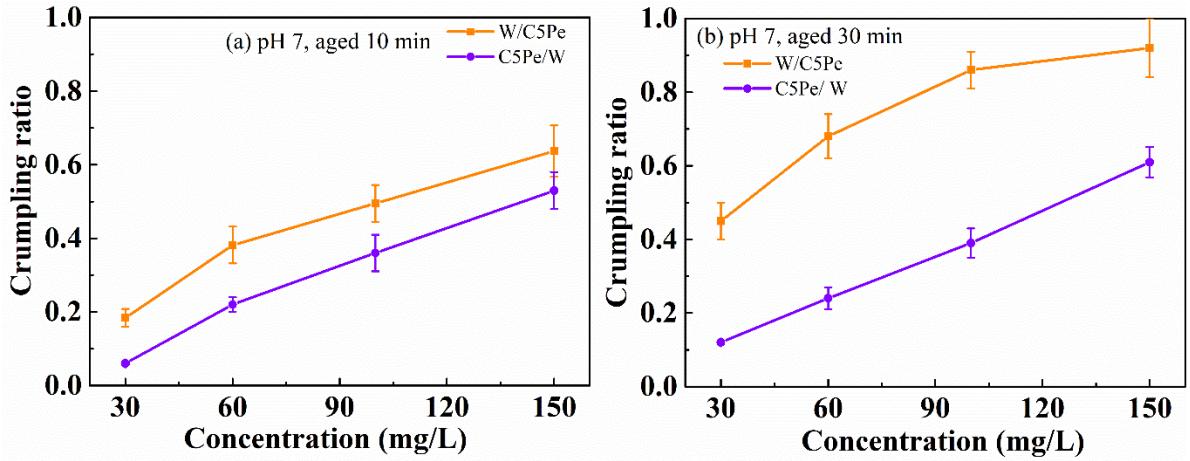

Figure 4-8 Crumpling ratio of water−C5Pe in xylene systems as a function of C5Pe concentration with the droplets of pH 7 being aged for 10 min (a) and 30 min (b).

4.3.3 Dilatational rheology

Dilatational rheology is an important physicochemical property of oil−water interfaces. By inducing a change in the interfacial area while measuring the interfacial tension, dilatational measurement provides important information on the dilatational viscoelasticity (viscoelastic modulus) of the interface, which arises in response to surface expansions and compressions.[149]

For dilatational measurements, experiments should be conducted in the linear viscoelastic regions where the viscoelastic properties observed are independent of the imposed frequency and amplitude levels. We measured the modulus as a function of frequency and amplitude as shown in **Figure 4-9**. The elastic modulus remains unchanged for amplitude between 8% and 16% and frequency between 0.1 to 0.4 Hz. Based on these results, the amplitude and frequency in dilatational rheology measurement were set at 10% and 0.1 Hz, respectively.

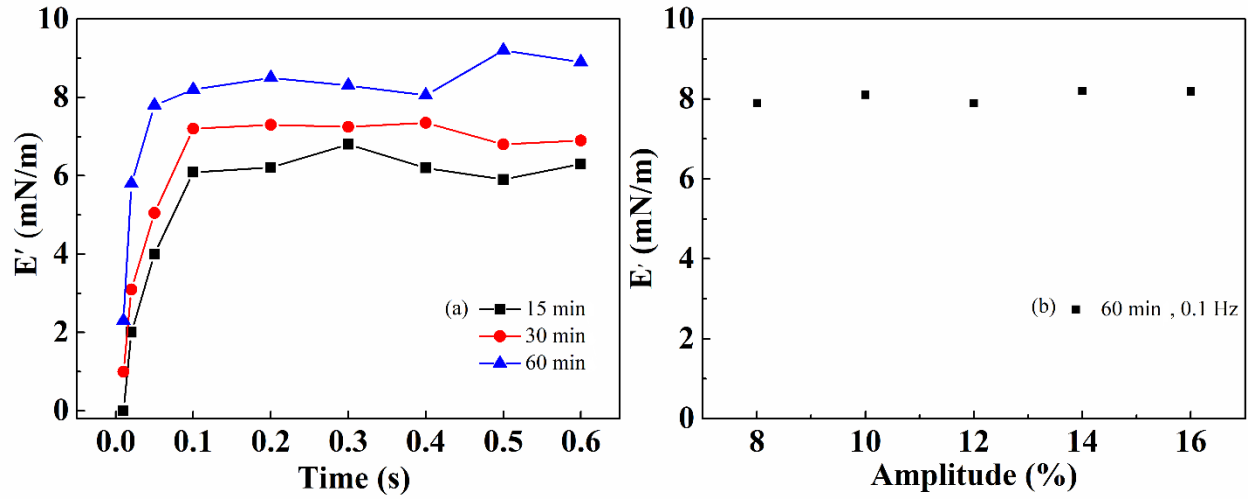

Figure 4-9 (a) Frequency dependence of elastic modulus of the interface for DI water in 100 mg/L C5Pe in xylene solution at different aging time; (b) Effect of amplitude (volume change) on the measured elastic modulus for DI water in 100 mg/L C5Pe in xylene solution: aging time 60 min; frequency 0.1 Hz.

Similar to crumpling ratio, only dilatational rheology of the C5Pe system was measurable and no viscoelasticity was detected for the C5PeC11 system up to a C5PeC11 concentration of 150 mg/L. The measured viscoelasticity of the W/O and O/W systems of C5Pe is shown in **Figure 4-10**. Each experiment was repeated for three times which showed the same trend. It is interesting to note a rapid increase in viscoelasticity of the interfacial films for the W/O system, followed by a gradual increase. In contrast, only a much slower and gradual increase in the

viscoelasticity of the interfacial films for the O/W system is observed, indicating a significant difference of interfacial rheological properties in O/W and W/O emulsion systems. The observed rapid increase in interfacial rheology would correspond to the increased adsorption of C5Pe molecules at the xylene−water interface to build stronger interfacial layers, while the gradual increase comes most likely from the molecular rearrangement with the further addition of a small amount of C5Pe molecules to the interface. For the W/O system, the viscoelasticity is observed at relatively small C5Pe concentrations (100 mg/L) and increases with increasing C5Pe concentration to 150 mg/L. For the O/W system, no viscoelasticity is measured for C5Pe concentrations less than 300 mg/L. Even for 300 mg/L C5Pe in xylene, the measured viscoelasticity of the interfacial film is still lower than that of 100 mg/L C5Pe in xylene for the W/O system. It can be concluded that the W/O system has higher viscoelasticity of the interfacial film compared with the O/W system, which is consistent with the crumpling ratio result. The dilatational result further confirms tighter packing and stronger association of C5Pe molecules at the interface for the W/O system than for the O/W system, most likely as a result of the increased amount of C5Pe molecules at the corresponding oil−water interface.

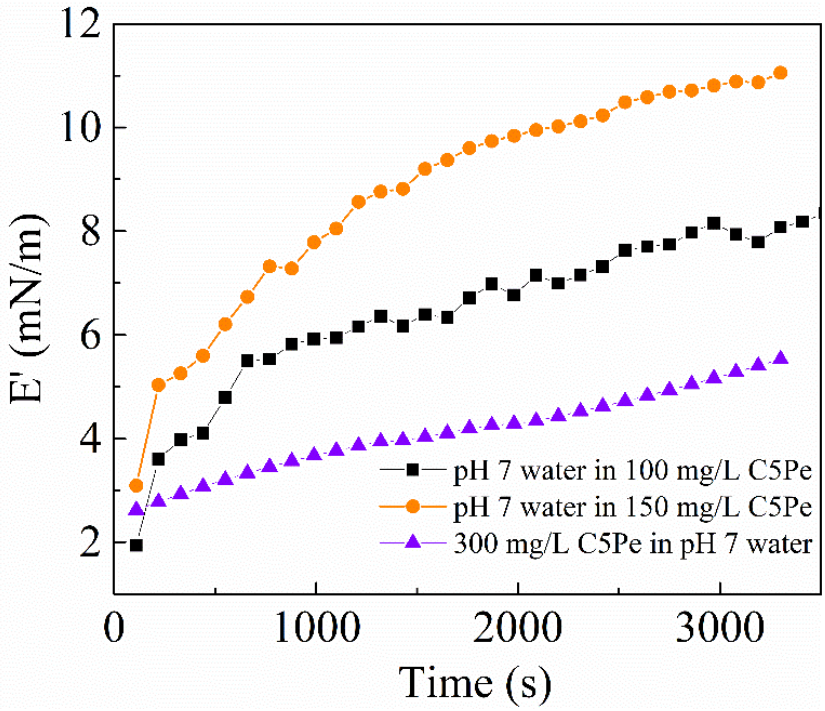

Figure 4-10 Dilatational modulus of water−C5Pe in xylene solution system as a function of measurement time.

4.3.4 Coalescence time

The coalescence times between the droplets were measured at different concentrations of C5Pe or C5PeC11 and the results are shown in **Figure 4-11**. Each data point in this figure is an average of five measurements with the error bars representing the standard deviation of the measurements.

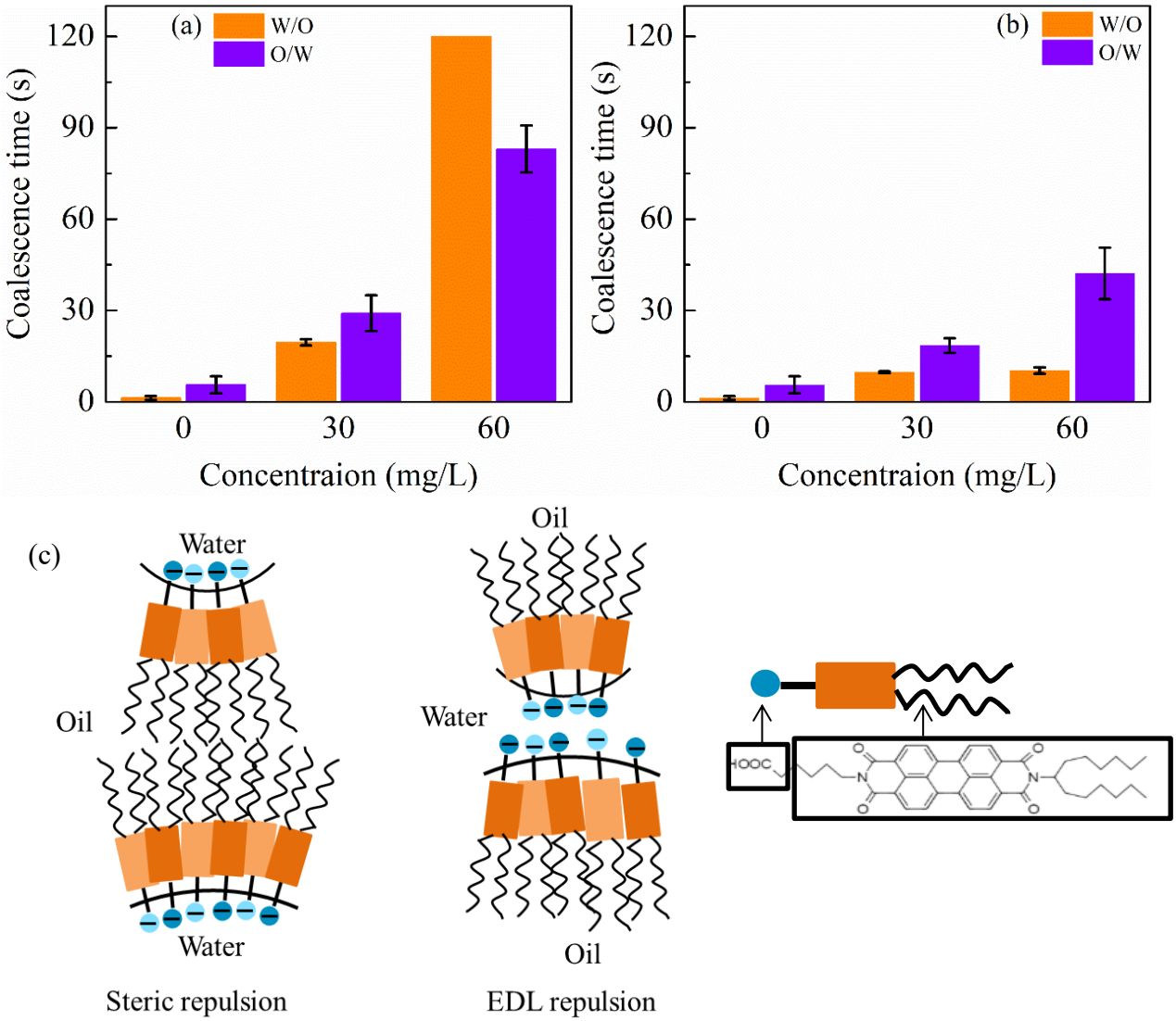

Figure 4-11 Experimental observations of coalescence time for (a) C5Pe, (b) C5PeC11 of various concentrations in the W/O and O/W systems. The viscosity of oil and water is 0.8 and 1 mPa·s, respectively, and (c) schematics showing steric repulsion for the W/O system and EDL repulsion for the O/W system, respectively (slightly colored molecules are used to demonstrate the stacking of polyaromatic cores).

In general, the coalescence time increases with increasing the concentration for both polyaromatic compounds. However, the droplets in C5PeC11−water system can coalesce much easier than in C5Pe−water system as shown by a shorter coalescence time for both W/O and O/W emulsion systems. The finding correlates well with the observed absence of droplet crumpling and low viscoelasticity of C5PeC11−water system. Interestingly, the coalescence of water droplets in the W/O emulsion system is always faster than that of oil droplets in the O/W emulsion system for C5PeC11−water system. The absence of electrostatic repulsion of water droplets in oil along with favorable migration of C5PeC11 molecules on water droplets into the oil phase than oil droplets into water seem to be responsible for such difference.

For C5Pe − water system, the advantage of W/O system is diminished with the increasing concentration of C5Pe (60 mg/L), as shown by the longer coalescence time of water droplets (W/O system) than the oil droplets (O/W system), when the steric repulsion as well as film rigidity and viscoelasticity, become so significant (as indicated by the crumpling ratio (**Figure 4-8**) and dilatational rheology results (**Figure 4-10**)) to hinder coalescence. Specifically, the coalescence time for O/W system at 60 mg/L C5Pe concentration was around 80 s, while for W/O case coalescence did not happen during the experimental time of 120 s. As the measurement limit for ITFDA is 120s, systems with coalescence time higher than 120 s are considered stable. It should be noted that at higher concentration (i.e., 100 mg/L and 150 mg/L), the coalescence times for both W/O and O/W systems were all over 120 s.

Theoretically, the coalescence time is related to the time it takes for the thin liquid film between the droplets to drain to a critical thickness where surface forces become relevant for the film to thin and rupture. The disjoining pressure (Π),[161-163] which generally arises from electric double layer (EDL) interaction, van der Waals (vdW) interaction, steric interaction, hydrophobic (HB) interaction, and so on, is system dependent and is responsible for the liquid film rupture when the film is sufficiently thin to make an attractive disjoining pressure. It should be noted that the forces contributing to the disjoining pressure are not exactly the same in the two systems. In the O/W system, the electrostatic double layer force (**Figure 4-11** (c)) and steric repulsion that stabilize the oil droplets are overcome by the attractive vdW force to realize the rupture of the thin liquid film. The hydrophobic attraction between oil droplets in the current systems is negligible due to the orientation of polar groups facing the aqueous phase to impart hydrophilic

nature of the oil droplet surface. Therefore, vdW force is considered to be the driving force to induce the film rupture between the oil droplets. On the other hand, steric interaction is the main repulsive force in the W/O system, attributed to the adsorption of C5Pe molecules (Figure 4-11 (c)). This steric force originated from the adsorbed C5Pe or C5PeC11 molecules at the xylene−water interfaces should be much weaker in the O/W system due to the orientation and compaction of polyaromatic molecules at the interface.[164] Similar to the O/W system, the attractive vdW force in the W/O system is responsible for the film rupture at low concentrations. At high concentrations, the larger steric repulsive force due to the formation of a steric layer from stacking of molecules at the interface would override the attractive surface force and prevent the droplets from coalescence.

By investigating O/W and W/O configurations of the same chemistry, it becomes evident that the different adsorption amount due to the reservoir effect that affects the arrangement of molecules at the interface is important and has effects on measurements such as crumpling ratio, dilatational rheology and coalescence time that could have not been observed using flat oil−water interfaces. In general, though similar trends are observed in most situations, the O/W configuration does not quantitatively represent the W/O system in terms of crumpling ratio, dilatational rheology and coalescence time. In particular, due to different film drainage process as well as the different interfacial film rigidity and viscoelasticity, coalescence time of the W/O system cannot be represented by the reversed O/W system.

4.4 Conclusions

A systematic study of O/W and W/O systems has been performed to understand their difference using asphaltene model compounds. Interfacial tension measurements indicated that the used asphaltene model compounds are very interfacially active and the adsorption amounts of C5Pe molecules at the oil−water interface for W/O and O/W systems are different due to the reservoir effect when oil is used as the continuous phase. The measurements of the crumpling ratio of the W/O system showed the presence of ‘skin-like’ structures around the droplet, which became more pronounced with increased concentration. On the other hand, the reversed O/W system showed less pronounced crumpling, which was attributed to less adsorption amount and therefore loose packing of the C5Pe molecules at the interface. A similar trend was found for

interfacial dilatational rheology measurement, further confirming tighter and stronger molecular packing at the oil−water interface of the W/O system.

Regarding the coalescence time, a longer coalescence time of oil droplets in water than that of water droplets in oil for both C5PeC11−water and C5Pe−water systems at low C5Pe concentration was observed. The role of film rigidity, film viscoelasticity, and steric repulsion on the coalescence time was especially significant for the high concentration of C5Pe model compound (60 mg/L), leading to longer coalescence time of water droplets in oil for the C5Pe−water system.

In summary, our results are consistent with previous literature about the accepted understanding that asphaltenes cause stabilization of the emulsion by creating a ‘skin’ around the water drops, which prevents coalescence. We have shown that many characteristics change for the reversed W/O system. Results obtained in this work indicate that the investigation of the stability of W/O emulsions by using O/W emulsions that have much better visualization features can only give qualitative trends.

Chapter 5 Changing the Interface Between an Asphaltene Model Compound and Water by Addition of an EO-PO Demulsifier through Adsorption Competition or Adsorption Replacement

5.1 Introduction

Emulsions widely exist in various industries, such as food, cosmetics, medicines, and petroleum.[165-167] The production of viscous emulsions in petroleum industry causes various problems, such as increased pumping costs, equipment or pipework corrosion, and poisoning of the downstream refinery catalysts.[168] Efficient emulsion breakup is usually realized by the addition of chemical demulsifiers. Consequently, factors that affect the emulsion stability and the role played by the demulsifiers in demulsification are of great significance to the oil industry.

It has been reported that a rigid film, which is formed around a water droplet, is the determining factor for the stability of W/O emulsions[169, 170] and asphaltenes are widely accepted as the major components of this rigid film.[11, 137, 171-174] Based on SARA analysis, asphaltenes are defined as a solubility class. They are soluble in aromatic solvents but insoluble in paraffinic solvents. This definition inherently indicates that the properties of crude oil or bitumen and the components of asphaltene samples may not be the same between different oil fields and even different wells. Nowadays, asphaltenes are widely reported to be the polyaromatic hydrocarbons (PAH) with amphiphilic properties, which consist of fused aromatic rings with alkyl branches attached on both sides.[95, 175, 176] Based on this, several PAH surfactants have been synthesized as the asphaltene models, which are characterized by a central perylene core with the lipophilic branch(es) to one and hydrophilic alkyl branch(es) to the other side.[99, 100, 154]

Nordgård and coauthors reported that both W/O and O/W emulsions can be stabilized by the synthesized PAH surfactants.[99, 100, 154] C5Pe and C5PeC11, as a kind of the PAH surfactants, were reported to be suitable asphaltene model compounds[103-107, 177, 178] as they behave similarly as asphaltenes. For the synthesized C5Pe asphaltene model compound, its interfacial activities,[99] adsorption behavior at interfaces,[100] Langmuir films, and fluorescent properties[154] have all been reported. The intermolecular forces between the C5Pe molecules in solvents and the adsorption behavior of the C5Pe molecules on a mica surface were similar to that of asphaltenes, despite the quantitative differences between them. Simon and coauthors reported the association of C5PeC11 molecules.[179] By isothermal titration calorimetry and nuclear magnetic resonance

investigations, they concluded that the aggregation of C5PeC11 molecules was mainly due to the π–π stacking of the polyaromatic rings and hydrogen bonding of the carboxylic groups. Molecular dynamics simulations were also used to study the aggregation behavior of the PAH surfactants in organic solvents and their adsorption behavior at the toluene or heptane−water interface. Teklebrhan et al.[180] showed that C5Pe molecules aggregated into large particles in both heptane and toluene, although their self-aggregation behavior was weaker in toluene because the aromatic solvent weakened the π–π stacking between C5Pe molecules for the molecular association. Although the interfacial activity of asphaltene model compounds has been thoroughly studied, no investigation has been conducted on the interaction between demulsifier molecules and asphaltene model compounds.

W/O (crude oil or bitumen) emulsions are black in nature; therefore, the reverse crude oil or bitumen in water system (O/W) has been used for the investigations of most interfacial properties. When studying the demulsification mechanism, it is essential to know whether the demulsifier would work similarly on the oil−water interfacial film for both systems. In a real dewatering process of W/O emulsions, the demulsifier diffusion through the continuous oil phase to the interface of the dispersed aqueous droplet indicates the adsorption replacement of the emulsifier molecules by the demulsifier molecules at the interface. When using the reverse O/W system, we have to premix the emulsifier and demulsifier molecules as the oil phase, indicating the adsorption competition between them. Therefore, an investigation on the adsorption replacement and competitive adsorption between emulsifier and demulsifier molecules should be conducted.

Asphaltene model compounds C5Pe and C5PeC11, which have better visibility when used as the oil sample, enable us to study the interfacial properties of both W/O and O/W systems, as discussed in **Chapter 4**. This study aimed to investigate how the properties of the C5Pe or C5PeC11−water interface were changed by an EO-PO copolymer demulsifier, which would enhance the understanding of the dewatering of emulsions from the molecular perspective. The EO-PO block copolymer has been chosen as the demulsifier as it has been extensively investigated[45, 181] and previously reported to be an effective chemical in the dewatering of W/O emulsions stabilized by asphaltenes.[71]

Within the main goal, there are three sub-goals: (1) compare the similarities and differences of the oil−water interfaces for water droplet in xylene diluted C5Pe or C5PeC11 solution (W/O) and

xylene diluted C5Pe or C5PeC11 droplet in water (O/W) systems with EO-PO demulsifier addition by interfacial tension (IFT) and crumpling ratio measurements; (2) study how the flat C5Pe−water interface was changed by the addition of the EO-PO demulsifier using Langmuir trough, atomic force microscopy (AFM), and Rheometer techniques through spreading (simulating competitive adsorption in O/W system) and diffusion (simulating adsorption replacement in the W/O system) protocols; and (3) investigate whether the asphaltene model compound C5Pe could interact with demulsifier molecules in a similar way as that of real asphaltenes and demulsifier molecules.

5.2 Materials and Methods

5.2.1 Materials

The chemical structures of the PAH surfactants C5Pe and C5PeC11 are shown in **Figure 2-5**. As can be seen, two types of alkyl chains are attached to the condensed polyaromatic rings through nitrogen atoms. Specifically, a hydrophilic carboxylic acid alkyl chain is bonded to one end and the other end is bonded to a hydrophobic double alkyl chain. The longer alkyl chains of the C5PeC11 molecule make it more soluble in organic solvents than the C5Pe molecule. The detailed synthetic procedures for the C5Pe and C5PeC11 molecules have been reported elsewhere.[154, 182] For the preparation of the xylene diluted C5Pe or C5PeC11 solution, C5Pe or C5PeC11 was dissolved in xylene and sonicated for 30 min.

The EO-PO demulsifier supplied by Baker Hughes was used in this study, and its chemical properties have been reported elsewhere in detail.[183] The purification of the deionized (DI) water was conducted by the Barnstead Nanopure Millipore system. Xylene (assay: ≥98.5%, Certified ACS, Fisher Chemical) used in this study is composed of m-, o-, and p-xylene with the ratio of each compound around 60, 20, and 20%, respectively.

5.2.2 Methods

5.2.2.1 Tensiometer (Biolin Scientific, Sweden)

The Tensiometer T200 was applied in this study for the interfacial tension and crumpling ratio measurements for both W/O and O/W systems (xylene diluted C5Pe or C5PeC11 solution was used as the oil sample) in the presence or absence of the EO-PO demulsifier.

Interfacial tension

For W/O and O/W systems, dynamic interfacial tensions (DIFT) were measured using the pendant drop technique to investigate the competitive adsorption and adsorption replacement between C5Pe (or C5PeC11) molecules and the EO-PO demulsifier molecules at different concentrations of the EO-PO demulsifier. For the W/O system, 3 mL of C5Pe or C5PeC11 xylene solution (30 mg/L) was added to a quartz cuvette as the oil sample. After that, a DI water droplet with a volume of 18 μL was produced by a gastight syringe and immersed in the oil solution. The IFT of the W/O system was monitored for 1200 s in total at 23 °C. After aging the water droplet in the C5Pe or C5PeC11 xylene solution for 600 s, the EO-PO demulsifier was injected in the continuous oil phase. The IFT was monitored for another 600 s after EO-PO demulsifier addition. For the O/W system, the oil sample was prepared by mixing the EO-PO copolymer with xylene diluted C5Pe or C5PeC11. A droplet of the oil mixture with a volume of 18 μL was immersed in DI water, and the IFT was recorded for 1200 s in total. The IFT of the EO-PO demulsifier-only solution was also measured for comparison.

Crumpling ratio

The contraction behavior of the asphaltene film around the surface of the water droplet in emulsions could demonstrate the role of this film in preventing the coalescence of the emulsion droplets.[58, 158, 159] Crumpling ratio (CR), which characterizes the extent of the interfacial steric layer (film) formation,[128] can be obtained by comparing the projected area of an oil droplet right before 'crumpling' was observed (A_f) on this droplet with the area at initial state (A_i). Similar to that for IFT measurement, the volume of the oil (or water) droplet for the CR measurements was also maintained at 18 μL. The oil samples used in this measurement were xylene diluted C5Pe solution with and without the EO-PO copolymer. The oil (or water) droplet was contracted steadily after aging it for 3600 s, and a simultaneous recording of the whole retracting process was initiated. It should be noted that for the W/O system, the demulsifier was added after aging the droplet for 1800 s, and demulsifier diffusion was allowed for 1800 s before contraction. Through a frame-by-frame video playback, the points at the initial state and right before crumpling of the droplet were determined.

5.2.2.2 Interfacial pressure−area isotherm

To investigate the compressional properties of the C5Pe interfacial layer in the presence or absence of the EO-PO demulsifier, the interfacial pressure of this layer was measured by a KSV

Langmuir trough in terms of the trough area. The IFT difference between the clean interface (σ_0) and the interface with the adsorption of interfacially active materials (σ) is defined as the interfacial pressure (π), which can be expressed as $\pi = \sigma_0 - \sigma$. 120 mL of aqueous subphase was filled in the bottom of the trough. A pressure increase of less than 0.2 mN/m indicated that the trough is well cleaned by compressing the water surface to the minimum trough area (25 cm^2).

Both diffusion and spreading protocols[184] were adopted to study the compressibility of the C5Pe interfacial films in the presence of the EO-PO demulsifier. The diffusion method allowed us to elucidate whether the EO-PO demulsifier could break the C5Pe interfacial layer that is already formed prior to the introduction of the EO-PO demulsifier, whereas the spreading protocol enabled us to probe the inhibition of the complete C5Pe interfacial layer formation by the EO-PO demulsifier. In other words, the diffusion protocol aimed to investigate the replacement of C5Pe molecules by the EO-PO demulsifier, whereas the spreading protocol studied the competitive adsorption between the EO-PO demulsifier and C5Pe molecules. In the diffusion protocol, the EO-PO demulsifier diffused from the continuous oil phase to the interface to mimic a real demulsification process, which is also the case for the IFT and CR measurements for the W/O system. In the spreading protocol, the mixture of the C5Pe molecule and EO-PO demulsifier was used as the oil phase, which is the same as that of the O/W case.

For the diffusion protocol, 100 mL of xylene diluted C5Pe solution (30 mg/L) was covered on the aqueous subphase. Then, the EO-PO demulsifier at different concentrations was injected into the top oil phase after equilibrating the system for 1800 s. The EO-PO demulsifier was allowed to diffuse for 1800 s prior to compression. For the spreading protocol, xylene diluted C5Pe solution was premixed with the EO-PO demulsifier at the desired concentrations. A total of 100 mL of the mixture of the C5Pe solution and EO-PO demulsifier was placed on the water subphase. The interfacial layer was compressed after spreading the molecules for 3600 s. For comparison, the interfacial pressure−area isotherm of the demulsifier-only solution−water interface was collected. The isotherm of a clean xylene−water interface was also determined. A low compression rate of 10 mm/min was used in our work as it is commonly used in the interfacial pressure isotherm measurement for the asphaltene system. [185, 186]

5.2.2.3 Atomic Force Microscopy (AFM) Imaging

The C5Pe interfacial films in the presence and absence of the EO-PO demulsifier under both diffusion and spreading protocols were prepared using the Langmuir−Blodgett (LB) technique. A silicon wafer, which was thoroughly cleaned by piranha solution and DI water, was the substrate for film deposition. While maintaining the interfacial pressure at 2 mN/m, the LB films were transferred on the clean wafers and pulled up through the oil−water interface at a rate of 8.6 mm/min. The topography of the dried LB films was acquired by the Dimension Icon AFM (Bruker Dimension Icon-PT, Bruker Corporation) under tapping mode in air at 23 °C. The LB films were imaged using an AFM silica probe (NCHV-A) at the scan rate of 1 Hz. The NanoScope Software V8.15 was used to control the sample imaging process. The demulsifier-only LB film and silicon wafer surface were also imaged by AFM.

5.2.2.4 Rheology

Interfacial shear rheology, which is measured by a rheometer, is used to study the flow and deformation behavior of liquid interfaces by external forces. In other words, the shear rheology consists of measuring how much the sample deforms or how fast the sample flows after inducing a shear stress on it.[132] An AR-G2 rheometer was used in this study to measure the interfacial viscoelastic properties of the C5Pe interfacial layer, monitoring its formation and breakdown by the addition of the EO-PO demulsifier. The double wall ring (DWR) setup used in this study has been illustrated in **Chapter 3 3.7**.[133] The Pt/Ir ring was flamed to remove organic contaminants on it prior to use.

The experimental procedure is described as following. After instrument calibration, 19.2 mL of the aqueous subphase was injected into the lower part of the rheometer trough, and the DWR was then lowered and positioned at the water surface. Similar to Langmuir trough experiments, both diffusion and spreading protocols were adopted. For diffusion protocol, 15 mL of 30 mg/L freshly prepared C5Pe in xylene solution was injected into the trough as the top phase and a Teflon cap was used to avoid evaporation. After equilibrating the interface for 3600 s, the EO-PO demulsifier at different concentrations was added dropwise to the top C5Pe in xylene solution. Meanwhile, the changes of G″ (loss or viscous modulus) and G′ (storage or elastic modulus) were measured. For spreading protocol, 15 mL of the mixture of the EO-PO demulsifier and xylene diluted C5Pe solution was injected into the trough as the top phase. The duration of all the experiments was set to 7200 s in total. The shear rheology of the demulsifier-

only system was also measured. The frequency and strain in the interfacial shear rheology measurement were set at 0.5 Hz and 0.8%, respectively. The experimental temperature was controlled by a water bath at 23° C. Detailed procedures of the experiments can be found elsewhere.[187]

5.3 Results and Discussion

5.3.1 Interfacial tension

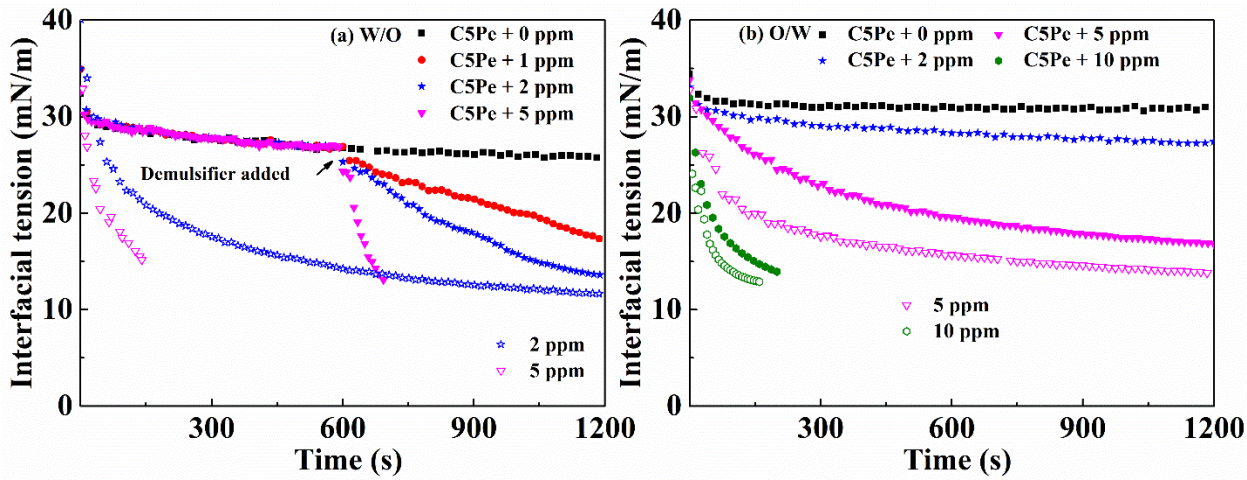

Figure 5-1 (a) DIFT of the DI water droplet in xylene diluted C5Pe solution (30 mg/L) with the addition of EO-PO demulsifier at different concentrations and (b) DIFT of the xylene diluted C5Pe droplet (30 mg/L) mixed with the EO-PO demulsifier at varied dosages in water.

To study the difference between adsorption competition and adsorption replacement, the changes in the dynamic interfacial tension (DIFT) for both W/O and O/W systems were recorded, and the results are shown in **Figure 5-1**. Three parallel experiments were conducted for each measurement, and the difference in IFT between different measurements was less than 0.2 mN/m under the same condition. **Figure 5-1** (a) shows the DIFT of the W/O system (DI water droplet in C5Pe xylene solution at 30 mg/L) at varied EO-PO demulsifier dosages. Different concentrations of the EO-PO demulsifier were added at the 600th s. The addition of the EO-PO demulsifier at 1, 2, and 5 ppm all led to rapid reduction of the IFTs, showing faster kinetics at higher EO-PO demulsifier concentration. When 5 ppm EO-PO demulsifier was added, the IFT decreased rapidly to a very low value that the droplet could not remain at the tip of the syringe 100 s after EO-PO demulsifier addition. The slope of the DIFT curve of the C5Pe/EO-PO system was very similar to that of the DIFT curve for the demulsifier-only system (for example, the

slope of C5Pe + 5 ppm EO-PO demulsifier system was almost the same as that of the 5 ppm EO-PO demulsifier), suggesting the dominant adsorption of the EO-PO demulsifier at the interface. It should be noted that the IFT of the EO-PO demulsifier/C5Pe system fell between the EO-PO demulsifier-only and C5Pe-only system, implying that the interface was occupied by both C5Pe molecules and the EO-PO demulsifier, which agreed well with that of the asphaltene/demulsifier system.[71] The asphaltene/demulsifier−water or diluted bitumen/demulsifier−water systems were also reported to have lower IFTs than those of the asphaltene−water or diluted bitumen−water systems.[71, 184, 188]

Figure 5-1 (b) shows the IFT of the O/W system (the mixture of the EO-PO demulsifier and xylene diluted C5Pe solution was used as the oil phase). Compared with that of C5Pe molecules, the adsorption of the EO-PO demulsifier at the interface was much easier, which led to a further decrease in the IFT compared with the C5Pe-only system. The more the EO-PO demulsifier added, the lower the IFT measured, which is very similar to the case of the W/O system. The C5Pe/EO-PO system and EO-PO demulsifier-only system showed similar adsorption kinetics, as indicated by the similar slope of their IFT curves. It should be noted that at the same C5Pe or EO-PO concentration, for the corresponding W/O and O/W systems, the IFTs were quantitatively different, whereas the reservoir effect[157] should be responsible for this difference.

Similar to that of the C5Pe system, the measurement of the IFT for the C5PeC11 system was also conducted. The IFT of the DI water droplet in xylene diluted C5PeC11 solution (30 mg/L) was measured for 1200 s, and the EO-PO demulsifier at different concentrations was added into this system at the 600th s (**Figure 5-2** (a)). Generally, rapid decrease for all IFTs after EO-PO demulsifier addition was observed at all used demulsifier dosages (0.5, 1, and 2 ppm), showing faster kinetics at higher EO-PO concentrations. For the C5PeC11 droplet in water (**Figure 5-2** (b)), EO-PO demulsifier addition could further decrease the IFT in contrast with the C5PeC11-only system. By comparing the slopes of the IFT curves, it can be seen that the C5PeC11/EO-PO system had almost the same adsorption kinetics as that of the demulsifier-only system, which implied much better surface-active properties of the EO-PO demulsifier than that of the C5PeC11 molecules.

Overall, EO-PO molecules can compete with (indicated by the IFT decrease of the O/W system) and replace (indicated by the IFT decrease of the W/O system) the asphaltene model compounds

C5Pe or C5PeC11 at the interface. It should be noted that no synergistic effect, i.e., further reduction of the IFT for the EO-PO/C5Pe−water system compared with that of the EO-PO−water system, was found between the EO-PO demulsifier and C5Pe molecules.

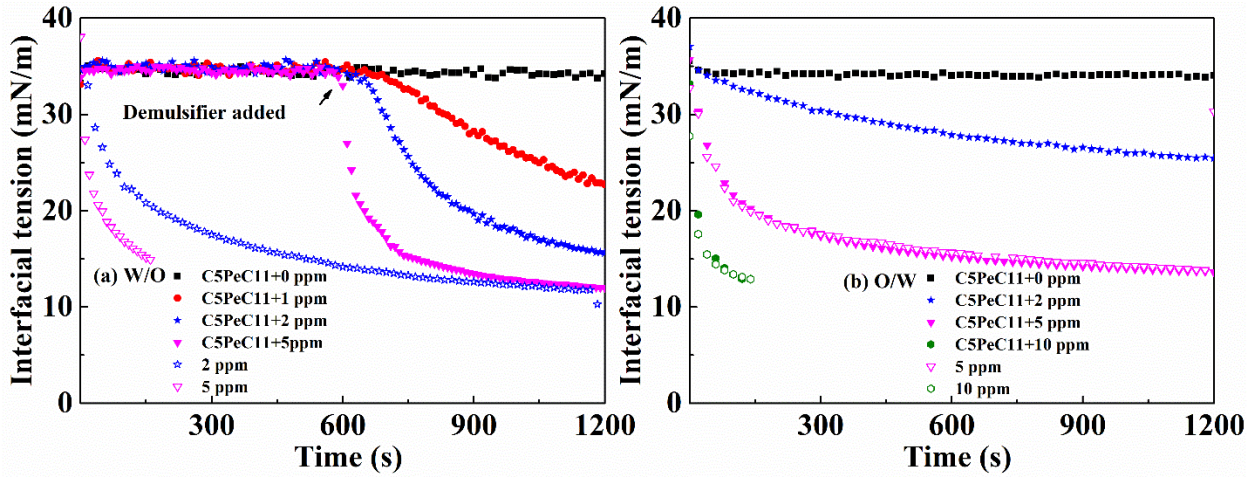

Figure 5-2 (a) DIFT of the DI water droplet in xylene diluted C5PeC11 solution (30 mg/L) with the addition of the EO-PO demulsifier at different dosages and (b) DIFT of the xylene diluted C5PeC11 droplet (30 mg/L) mixed with the EO-PO demulsifier at different dosages in water.

5.3.2 Crumpling ratio

Crumpling experiments were conducted to investigate the adsorption and interaction of C5Pe molecules at the interface. No crumpling of the C5PeC11 interfacial film was observed. Each crumpling ratio (CR) value in **Figure 5-3** corresponds to an average of three independent experimental results, and the difference between the measurements is around 0.05. DI water droplets (or oil droplets) of approximately 18 μL in volume were aged in the oil solution (or DI water) for 3600 s. The oil samples consisted of xylene diluted C5Pe solution (30 mg/L) with the EO-PO demulsifier at different concentrations. The CR results for the C5Pe/EO-PO−water interface are summarized in **Figure 5-3**. When the liquid inside the water droplets was retracted, the presence of the C5Pe interfacial films could be observed as wrinkles outside these water droplets. For the W/O system, the CR was around 0.30 after aging for 3600 s, whereas it decreased to 0 with 2 ppm EO-PO demulsifier addition (**Figure 5-3** (a), (b)). The EO-PO demulsifier was also capable of reducing the interfacial film rigidity for the O/W system, as indicated by the absence of the CR with the EO-PO demulsifier addition (**Figure 5-3** (c), (d)). As indicated by the IFT and CR results, the EO-PO demulsifier was more surface-active when compared to the C5Pe molecules and capable of softening the C5Pe interfacial film after

adsorption. It should be noted that the CRs of the C5Pe-only system for both W/O and O/W systems were different (**Figure 5-3** (a), (c)), which should be due to the larger adsorption amount of C5Pe molecules for the W/O system that led to denser molecular packing at the interface of the same interfacial area as discussed in **4.3.2**. Overall, the EO-PO demulsifier worked similarly through adsorption competition and adsorption replacement for both W/O and O/W systems to soften and weaken the C5Pe interfacial film.

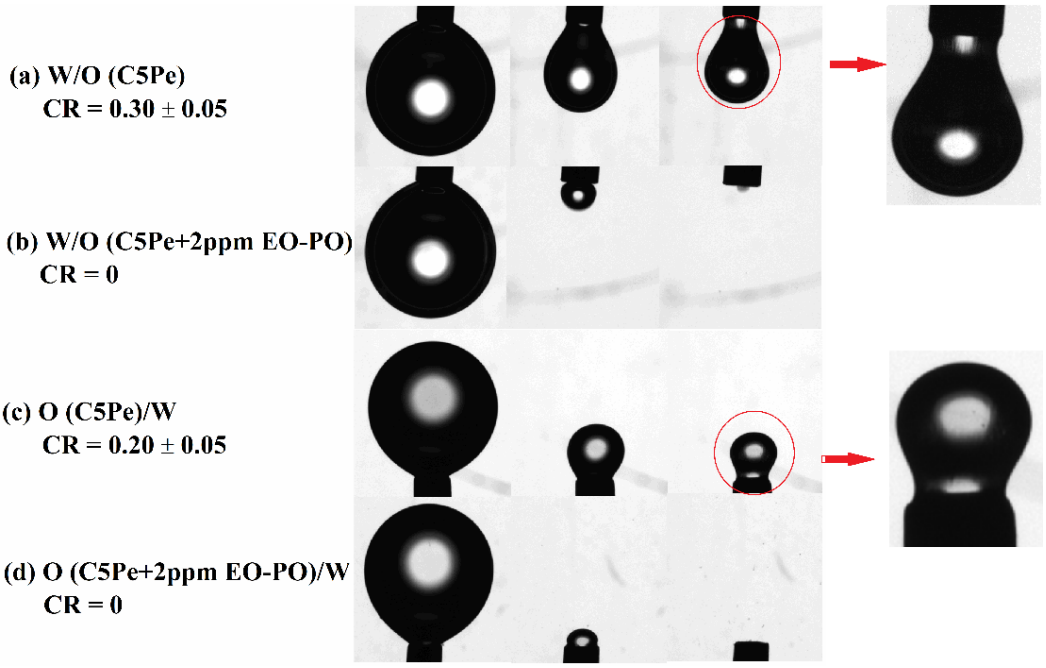

Figure 5-3 Crumpling ratio of (a, b) W/O system, DI water droplet in xylene diluted C5Pe solution at 30 mg/L with the addition of the EO-PO demulsifier at 0 and 2 ppm, and (c, d) O/W system, xylene diluted C5Pe droplet at 30 mg/L mixed with the EO-PO demulsifier at 0 and 2 ppm in water.

5.3.3 Interfacial pressure-area isotherm

It has been reported that the compressional behavior of the interface is linked to the emulsion stability.[185] The interfacial pressure−area isotherm of the C5Pe−water interface was measured with and without EO-PO demulsifier addition to demonstrate the interfacial pressure in terms of the trough area (**Figure 5-4**). Both diffusion and spreading protocols were used for the interfacial pressure measurements. The higher the increase of the interfacial pressure upon compression, the less compressible the interfacial film. Three parallel experiments were conducted to ensure the reproducibility of the measurement.

The clean xylene–water interface without surface-active materials has a stable interfacial pressure of 11 mN/m, which remained almost unchanged under the whole compression process. As can be observed in **Figure 5-4**, at the largest trough area (243 cm^2), adding the EO-PO demulsifier (2 and 5 ppm) to the xylene–water system resulted in significant growth of the interfacial pressure, which was consistent with the reduction in IFT (**Figure 5-1**).

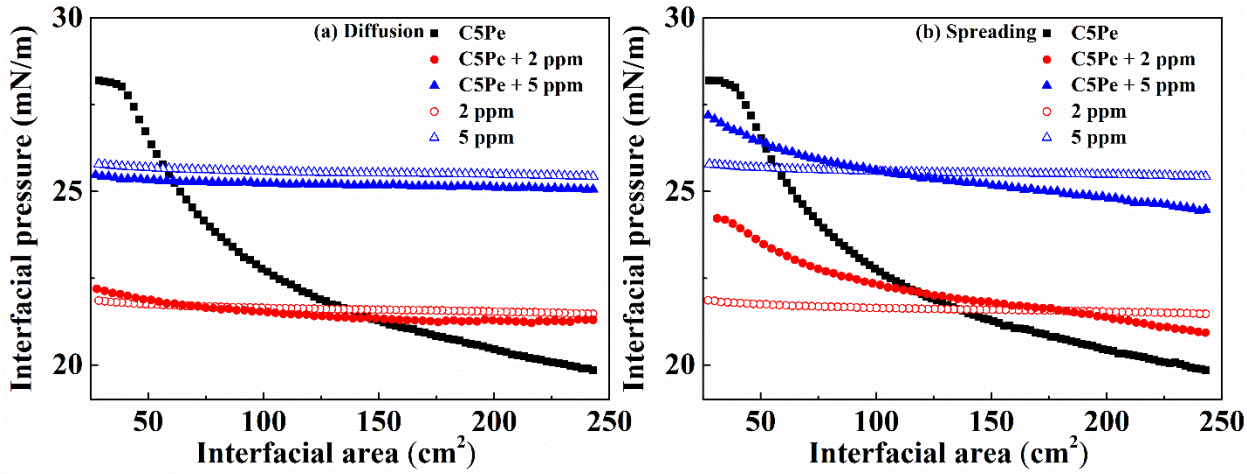

Figure 5-4 Interfacial pressure–area isotherm for the C5Pe-only, C5Pe with the EO-PO demulsifier, and EO-PO demulsifier-only system: (a) diffusion protocol and (b) spreading protocol.

For the demulsifier-only system, the growth of the interfacial pressure under compression was negligible, indicating the formation of a demulsifier film with high compressibility. The C5Pe interfacial film was characterized by the dramatic growth of the interfacial pressure upon compression, which indicated low compressibility of this film. Generally, the interfacial film for the C5Pe/EO-PO system became much more compressible than that of the C5Pe-only system, indicated by the smaller interfacial pressure increase with EO-PO demulsifier addition. Similarly, it has been widely reported that the asphaltene–water interfacial film becomes more compressible by adding chemical demulsifiers.[11, 71, 145, 189] In the diffusion protocol, the isotherm slope of the C5Pe xylene solution with the EO-PO demulsifier of 2 ppm was similar to that of the EO-PO demulsifier-only system at low compression (larger interfacial area). At high compression, a slight increase in the slope of the isotherm was observed, implying that some C5Pe film structures remained at the interface. After adding 5 ppm EO-PO demulsifier into the C5Pe xylene solution, the shape of the isotherm was similar to that of the isotherm of the pure

EO-PO demulsifier at 5 ppm, indicating that EO-PO demulsifier molecules had dominantly occupied the oil−water interface, which corresponded well with the IFT measured for the W/O system in **Figure 5-1**. It can be inferred that the C5Pe interfacial layer was almost completely broken. In the spreading protocol, the isotherm resembled that of the EO-PO system at low compression and the C5Pe system at high compression, a similar trend as in the diffusion protocol that was mentioned above. It should be noted that the diffusion and spreading protocols show results that appeared to be inconsistent, which should be attributed to the difference between competitive adsorption and adsorption replacement. In the diffusion protocol, the demulsifier works on breaking the already formed C5Pe interfacial film. Once cracks appear on the C5Pe interfacial film, EO-PO molecules would accumulate along the fissure, to further widen and extend the fissure until the whole film breakage occurs. In the spreading protocol, EO-PO demulsifier molecules compete with the C5Pe molecules and adsorb relatively evenly at the interface, which prevents the whole C5Pe interfacial film formation but does not introduce severe cracks on the C5Pe film as in the diffusion protocol.

5.3.4 Morphology of the C5Pe interfacial film

The LB films of the C5Pe-only, C5Pe with the EO-PO demulsifier, and EO-PO demulsifier-only systems were investigated by AFM imaging to visually observe their morphological changes. The films were prepared by both diffusion and spreading protocols. The AFM image of the LB film for the C5Pe−water interface is shown in **Figure 5-5** (a). The C5Pe interfacial film was found to be composed of tightly packed nanoaggregates, and similar AFM images for the asphaltene or bitumen LB films have been reported elsewhere.[184, 190]

The AFM images formed by the diffusion method are shown in **Figure 5-5** (b) and (c). With 2 ppm EO-PO addition, many cracks appeared on the C5Pe interfacial film. On increasing the EO-PO concentration to 5 ppm, film pieces were sporadically distributed on the interface. The surface area that is not covered by the C5Pe interfacial film provides the opportunity for two water droplets to coalesce in the case of emulsions. Obviously, the EO-PO demulsifier was capable of destroying the C5Pe interfacial layer and performed better at high concentration. The observed breakage of the C5Pe interfacial film from the AFM images agreed well with the high compressibility of this film with EO-PO addition as shown by the surface pressure results in **Figure 5-4**. **Figure 5-5** (d) and (e) shows the morphological characteristics of the LB films

prepared by the mixture of C5Pe and EO-PO molecules under spreading protocol. It can be observed that the EO-PO addition prevented the continuous C5Pe interfacial film formation that was observed in **Figure 5-5** (a) and film debris was formed instead. On increasing the EO-PO concentration from 2 to 5 ppm, the film debris became smaller and much more dispersed. Chemical additives were also reported to introduce similar changes in an asphaltene film or a diluted bitumen film.[184, 188, 190, 191] For the demulsifier-only system, no film structure was detected, as shown in **Figure 5-5** (f). The silicon surface was also imaged, and no film structure was observed.

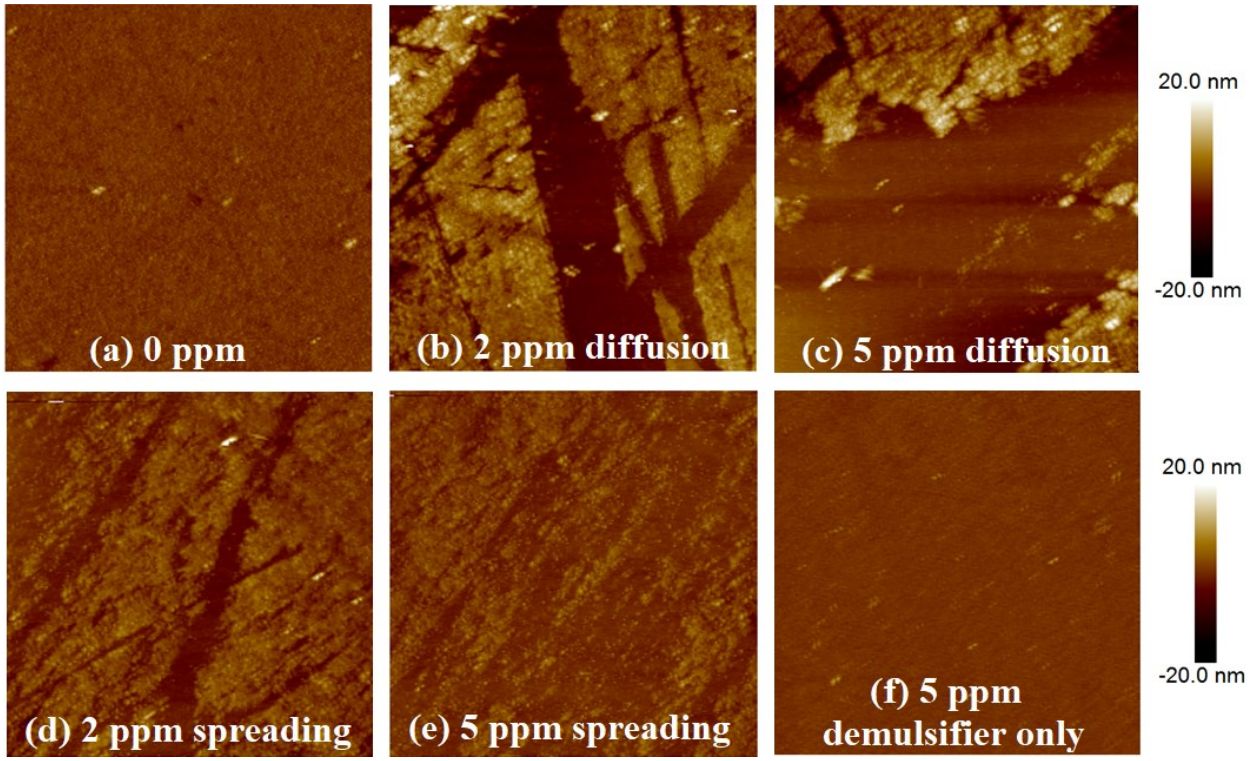

Figure 5-5 AFM image of the LB film: (a) C5Pe interfacial film; (b) and (c) films prepared by diffusing the EO-PO demulsifier at different concentrations (2 and 5 ppm) to the already formed C5Pe interfacial film; (d) and (e) films prepared by spreading the mixture of C5Pe solution and the EO-PO demulsifier (2 and 5 ppm) at the interface; and (f) 5 ppm demulsifier-only film (2 ppm demulsifier-only film was similar to 5 ppm demulsifier-only system and is not shown here). The scale of all images is 5 μm.

By analyzing AFM images of the LB films, it can be concluded that EO-PO could prevent the formation of a continuous interfacial film or break the already formed interfacial film. Overall, data obtained from spreading protocol (mimic adsorption competition in the O/W system) can

represent the diffusion protocol (mimic adsorption replacement in the W/O system) to a certain degree.

5.3.5 Interfacial shear rheology

In this study, the rheological properties of the C5Pe/EO-PO system were measured by DWR rheometer geometry. Both spreading and diffusion protocols were applied for the shear rheology measurements. Here, only diffusion results are shown because the moduli measured for the spreading protocol were similar to those of the clean xylene−water interface or demulsifier-only system. In the diffusion protocol, the variations of G″ (loss or viscous modulus) and G′ (storage or elastic modulus) were measured for C5Pe, C5Pe/EO-PO, EO-PO, and clean xylene−water interfaces (**Figure 5-6**). The interfacial shear rheology measurements were repeated three times, and the reproducibility was adequate because for all measurements either the storage modulus or the loss modulus of the C5Pe interfacial film overlapped before demulsifier addition, as shown in **Figure 5-6**.

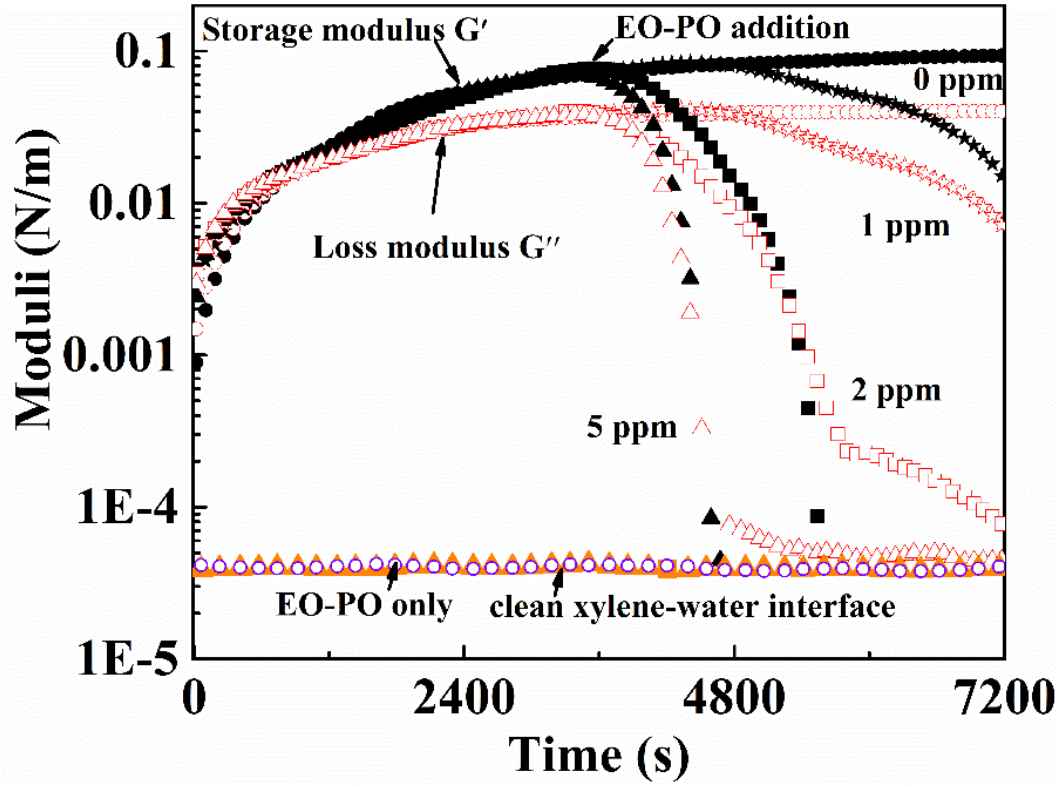

Figure 5-6 G″ (loss or viscous moduli) and G′ (storage or elastic moduli) of C5Pe layers with EO-PO demulsifier addition at varied dosages.

Without the EO-PO demulsifier, the C5Pe interfacial film was dominantly viscous at the very beginning and the viscous modulus G″ started at around 10^{-3} N/m. The elastic modulus G′ began to develop afterward. The growth of the elastic modulus was faster than that of the viscous contribution because C5Pe molecules gradually accumulated at the interface, leading to a crossover at around the 600th s (G″ = G′). Then, G′ became greater than G″ and both moduli kept increasing slowly with time, indicating that the interface exhibited more elastic properties rather than viscous properties. It has been reported that the elastic modulus can be considered as a good indicator of the strong interaction and cross-linking of interfacial molecules. In addition, the intensive interaction and cross-linking of interfacial molecules change the interfacial film from soft to rigid.[192, 193]

After aging the C5Pe−water interface for 3600 s, the EO-PO demulsifier was added to the top C5Pe xylene solution. Reductions of the elastic and viscous moduli were observed for all dosages used (1, 2, and 5 ppm) as shown in **Figure 5-6**, although to a different extent. After 1 ppm EO-PO addition, both G′ and G″ decreased immediately. After 3600 s of diffusion, G″ and G′ decreased to values that were still higher than those of the clean xylene−water interface, representing a small change of viscoelastic properties of the C5Pe/1 ppm EO-PO film with aging. Moreover, G′ was still higher than G″ after 3600 s demulsifier addition, indicating the insufficient amount of the EO-PO demulsifier. When 2 ppm EO-PO demulsifier was added, both G′ and G″ decreased rapidly, although G′ declined much more rapidly and a crossover was found at around the 5200th s (1600 s after EO-PO copolymer addition). Further increasing the demulsifier dosage to 5 ppm made the crossover of G′ and G″ appear much faster, at around the 700th s after EO-PO demulsifier addition. G′ of the C5Pe layer with the addition of EO-PO demulsifier at 2 and 5 ppm could finally reduce to an unmeasurable value, suggesting that the strong network of C5Pe molecules was almost completely disrupted, which is consistent with the interfacial pressure−area results. G″ of the C5Pe layer with 2 ppm EO-PO demulsifier was still measurable and higher than those of the clean xylene−water interface, indicating that some residual C5Pe molecules were still active at the xylene−water interface, even though they could no longer form a rigid film because of the weak interactions. For 5 ppm EO-PO demulsifier addition, G″ reduced to a value similar to that of the demulsifier-only or clean xylene−water system, illustrating that the EO-PO demulsifier was dominant at the interface.

By summarizing the results of interfacial tension, crumpling ratio, surface pressure, AFM images, and interfacial shear rheology, it is clear that the EO-PO demulsifier was capable of destroying the interfacial C5Pe film after adsorbing at the interface. In addition, it can be inferred that although residual C5Pe molecules and the EO-PO demulsifier co-existed at the interface they did not interact with each other to form a strong interfacial film network. The decrease of the moduli after EO− PO demulsifier addition in the diffusion protocol and the fact that moduli measured in the spreading protocol are equivalent to those of the clean xylene−water system or demulsifier-only system further confirmed that the EO-PO molecules performed similarly through adsorption competition and adsorption replacement. The absence of G′ and the decrease of G″ for the asphaltene/demulsifier−water interfacial film compared with the asphaltene−water interfacial film were also observed by other researchers.[39]

5.4 Conclusions

This study revealed a consistent destabilization mechanism of the stable C5Pe interfacial film by the EO-PO demulsifier. In addition, the changes in the asphaltene model compound−water interface due to the EO-PO demulsifier addition through adsorption competition or adsorption replacement were compared.

Due to its high interfacial activity, the EO-PO demulsifier was able to further reduce the interfacial tension by competing with or replacing the C5Pe or C5PeC11 molecules at the interface for both W/O and O/W systems. The interfacial characteristics of the C5Pe−water interface were changed dramatically by adding the EO-PO demulsifier in the C5Pe xylene solution. The EO-PO demulsifier could cause the reduction or even elimination of the C5Pe−water interfacial film rigidity, for both W/O and O/W systems. Interfacial pressure−area isotherm, AFM imaging, and shear rheology studied using diffusion (simulate adsorption replacement in the W/O system) and spreading (simulate adsorption competition in the O/W system) protocols further confirmed that the EO-PO demulsifier could introduce similar changes on the C5Pe interfacial film through adsorption competition or adsorption replacement.

Overall, C5Pe compound, as one of the important polyaromatic asphaltene models, stabilized the interfacial film and the EO-PO demulsifier was capable of disrupting this stable C5Pe interfacial film through adsorption replacement or adsorption competition. This research should enhance our understanding of the feasibility of using the reverse O/W system to represent the

W/O system when a demulsifier is introduced. In addition, the interaction between the demulsifier and C5Pe molecules was similar to that of the asphaltene/demulsifier system, providing further justification for using C5Pe as the asphaltene model compound.

Chapter 6 Molecular Destabilization Mechanism of Asphaltene Model Compound C5Pe Interfacial Film by EO-PO Copolymer: Experiments and MD Simulation

6.1 Introduction

In the crude oil industry, water-in-oil emulsions (W/O) are usually formed when crude oil and water are intimately mixed at the wellhead, production well, valves, and pumps. The same is true in bitumen recovery by both in situ and open pit mining recovery methods. However, the formation of the stable W/O emulsions in the petroleum industry is highly undesirable because salts and brine carried with the emulsified water cause corrosion, poison catalysts, reduce throughput, and lead to equipment failure in downstream operation.[19, 168] Understanding the emulsion stability and demulsification mechanisms is thus fundamental in the petroleum industry.

It is widely accepted that the emulsion stability is due to the formation of a mechanically strong, rigid, and viscoelastic interfacial film by the accumulation of surface-active components, such as asphaltenes, resins, naphthenic acids and inorganic solids from the bitumen or crude oil.[169, 194, 195] These components stabilize the emulsion by preventing the direct contact between droplets or the drainage of the thin film between them.[23, 24] Asphaltenes are believed to be the main components that contribute to the formation of the rigid film which stabilizes W/O emulsions.[171-173, 196, 197] For efficient breakup of the W/O emulsions, the use of demulsifier has been regarded as an economical and efficient method that is widely used in the petroleum industry.[28, 29] Modern demulsifiers are usually mixtures of surface-active macromolecular chemicals, such as acid- or base-catalyzed phenol-formaldehyde polymers, ethoxylated and/or propyloxylated polyamines, di-epoxides, polyols, and silicone copolymers.[40, 41, 198] Most of the active ingredients in the chemicals used as demulsifiers are copolymers of ethylene oxide (EO) and propylene oxide (PO) of different molecular weight and EO-to-PO ratio.[42-44]

However, investigations of the demulsification mechanism at the molecular level are still lacking. Therefore, we aim to reveal the molecular demulsification mechanism by both experiments and molecular dynamics (MD) simulations. EO-PO copolymer was used as the demulsifier because it has been extensively investigated[42, 44-46] and reported as an effective additive in breaking

asphaltene/bitumen-stabilized W/O emulsions.[44, 71] As asphaltenes are merely a solubility class having undefined chemical composition and molecular structure, different asphaltene model compounds have been used as models in MD simulations.[199-201] C5Pe is a suitable model compound as it shows very similar interfacial activities as asphaltenes. Nenningsland et al.[200] have extensively investigated factors affecting the emulsion stability by an array of techniques and concluded that the formation of a rigid network/layer of polycyclic aromatic compounds, such as asphaltene model compound C5Pe, was responsible for enhancing the emulsion stability. Jiebin et al.[106] have systematically studied the interfacial layer properties of the polyaromatic asphaltene model compound C5Pe and its role in stabilizing W/O emulsions. Their findings confirmed that the formation of an elastically dominant interfacial microstructure by the continuous accumulation of C5Pe molecules and rearrangement of C5Pe aggregates are requirements to prevent the rupture of the intervening liquid film that results in droplet coalescence. It should be noted that there still remains a gap between the model system and the real heavy oil in which a mixture of different types of hydrocarbons is likely present.

In this paper, the interfacial tension was measured to investigate the interfacial activity of EO-PO copolymer and C5Pe molecules at the oil−water interface. Brewster angle microscopy was used to study the effect of EO-PO molecules on the morphology of the C5Pe interfacial film. The experimental results were confirmed by MD simulations. In addition, the MD simulations provided new insights into the molecular mechanism of interfacial film destabilization and how different groups of the EO-PO demulsifier behaved at the interface, so as to provide information on how to design efficient demulsifiers for dewatering.

6.2 Materials and Methods

6.2.1 Materials

C5Pe (N-(1-hexylheptyl)-N′-(5-carboxylicpentyl) perylene-3,4,9,10-tetracarboxylic bisimide), as one of the model compounds, consists of four aromatic rings fused together with three cyclic rings containing heteroatoms of O and N (**Figure 2-5**).

Solutions of C5Pe in xylene (≥98.5%, ACS grade, Fisher Scientific, Canada) were prepared by dissolving C5Pe in xylene and sonicating for 30 min. The EO-PO block copolymer demulsifier (provided by Bake Hughes) had a star-like structure of three arms, a molecular weight of 6145

g/mol, an EO content of 35% (weight percent) and the relative solubility number of the demulsifier was 16.92. Deionized (DI) water of a resistivity > 18.5 MΩ·cm was purified with a Millipore system and used throughout this study.

6.2.2 Methods

6.2.2.1 Interfacial tension

The static interfacial tension of oil−water interface can be measured using Du Noüy ring method.[125] 20 mL DI water was loaded in the cell first and the ring is immersed in the water phase. The water phase is then covered by 15 mL xylene diluted C5Pe solution. After aging the interface for 600 s, EO-PO copolymer with different concentrations was added into this system through the top oil phase. After the demulsifier diffusion for 600 s, the immersed ring is gradually directed towards the interface while monitoring force applied to the ring. At the point when the oil−water interface is vertical, the largest detachment force can be detected by the electronic balance, which can be converted to interfacial tension.

6.2.2.2 Brewster Angle Microscopy (BAM)

Brewster Angle Microscopy (Model EP3, Accurion GmbH, Goettingen, Germany) was used to study the morphological changes of the interfacial film. BAM is an imaging method that is particularly well-suited to study liquid-liquid interfaces[71, 134, 135] without transferring the film to a solid substrate. At the Brewster angle θ_B, the p-polarized light is not reflected for the clean interface, while the light will be reflected to the detector once the interface supports a film. The reflected light provides an image of the film, which is a good characterization of the interface.

The following procedure was used when running BAM experiments: 28.5 mL of water was poured into the trough, and 80 mL of 30 mg/L xylene diluted C5Pe was then added on top of the aqueous phase. After aging for 3600 s, the interfacial films were imaged at the angle of incidence (AOI) of 41.6° (Brewster Angle) with the polarizer and analyzer set to around 2° and 10°, respectively. 2, 5, and 10 ppm of EO-PO copolymer were added dropwise from the top oil phase and images were taken after demulsifier diffusion for 600 s. The EO-PO copolymer film and clean xylene−water were also imaged to elucidate a possible dependence between demulsifier concentration (or xylene) and film structure.

6.2.2.3 Simulation Method

To understand the interactions at the molecular level, molecular dynamics (MD) simulations were performed. The Material Studio 8.0 package was adopted, using the COMPASS (condensed-phase optimized molecular potentials for atomistic simulation studies) force field.[202] The COMPASS force field is widely used in exploring the molecular dynamics at the oil−water interface.[203, 204] All calculations were performed with the Forcite module in the Material Studio software package.

Molecular Models

C5Pe is a typical asphaltene model that was reported in several studies.[115, 180] Xylene model was based on the proportion of each component (60% of m-xylene, 20% of o-xylene, and 20% of p-xylene). The EO-PO copolymer was modeled as a star-like structure with three arms[44] (**Figure 6-1**). Glycerol was used as the base compound with 35% of EO percent in total weight. All models were built using built-in modeling tools in the Material Studio software package.

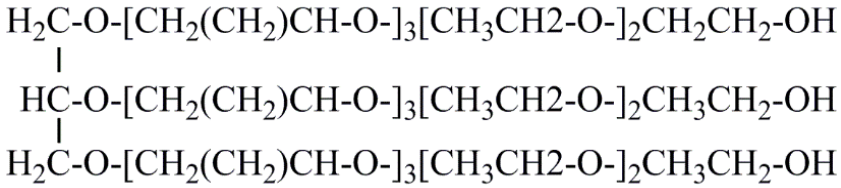

Figure 6-1 EO-PO copolymer model used in the MD simulation.

Initial Simulation Configuration

In this work, simulations were performed for four different configurations, named as systems A, B, C, and D (**Figure 6-2**). The initial configuration for each system was defined as follows:

System A: Molecules of C5Pe placed near the oil−water interface.

System B: Mixture of EO-PO and C5Pe molecules placed near the oil−water interface.

System C: Separate layers of C5Pe and EO-PO, with C5Pe near water.

System D: Separate layers of C5Pe and EO-PO, with C5Pe near oil.

The simulation details are summarized in **Table 6-1** and **Figure 6-2**. In the simulation of system A, xylene molecules were randomly put into a cubic box of 5×5×1.5 nm^3. C5Pe molecules were

assumed at the vicinity of the oil−water interface since it was shown that C5Pe molecules tend to aggregate at the oil−water interface.[115, 205] Then NVT ensemble (N, conserved number of particles; V, constant volume; T, constant temperature) was carried out to obtain a reasonable density. Systems B, C, and D were explored to study the interaction of EO-PO molecules with C5Pe molecules at the oil−water interface. For all systems, a vacuum layer of 40 Å in thickness was introduced at the top of the oil layer.

Table 6-1 Simulation parameters of different systems

System	$N_{o\text{-}xylene} : N_{m\text{-}xylene} : N_{m\text{-}xylene}$	N_{C5Pe}	N_{Water}	$N_{EO\text{-}PO}$
A	240:80:80	18	2000	0
B, C, D	240:80:80	18	2000	9

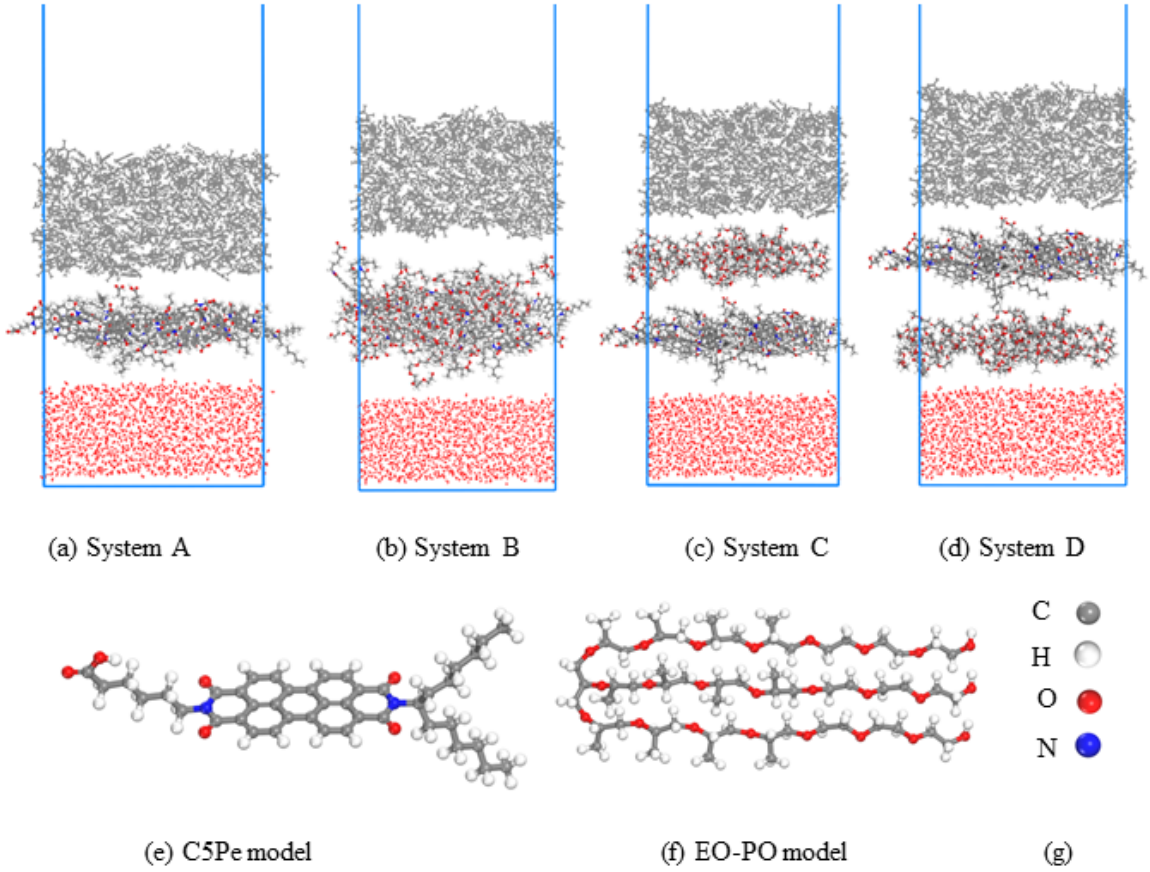

Figure 6-2. Initial configuration of systems (a) A, (b) B, (c) C, and (d) D. The C5Pe and EO-PO copolymer model are displayed in parts (e) and (f). (g) Color scheme: C, gray; H, white; N, blue; O, red.

Details of Molecular Dynamics

The initial configurations were minimized by the steepest descent and conjugate gradient methods. After the models were geometrically optimized, MD simulations were performed to obtain the final model structures for analysis.

During the geometry optimization, the cut off of the Coulomb and van der Waals interactions was 15.5 Å. When the maximum force of the system was converged to a threshold of less than 5×10^{-3} kJ·mol^{-1}·Å^{-1} and the maximum energy of the system was converged to less than 1×10^{-4} kcal·mol^{-1}, the system was considered to be stabilized. Finally, 10,000 ps NVT simulations were carried out at 298 K with a time step of 1 fs. In the NVT ensembles, the periodic boundary condition was applied in all directions. The Nose-Hoover thermostat temperature control with a Q ratio of 0.01 was used. The reciprocal space particle–particle–particle–mesh (PPPM) method[206, 207] was adopted to calculate the electrostatic interactions while the van der Waals interaction was calculated by the atom-based method. The hydrogen-bonding interaction is considered as a form of electrostatic interactions in molecular modeling.

6.3 Results and Discussion

6.3.1 Interfacial tension

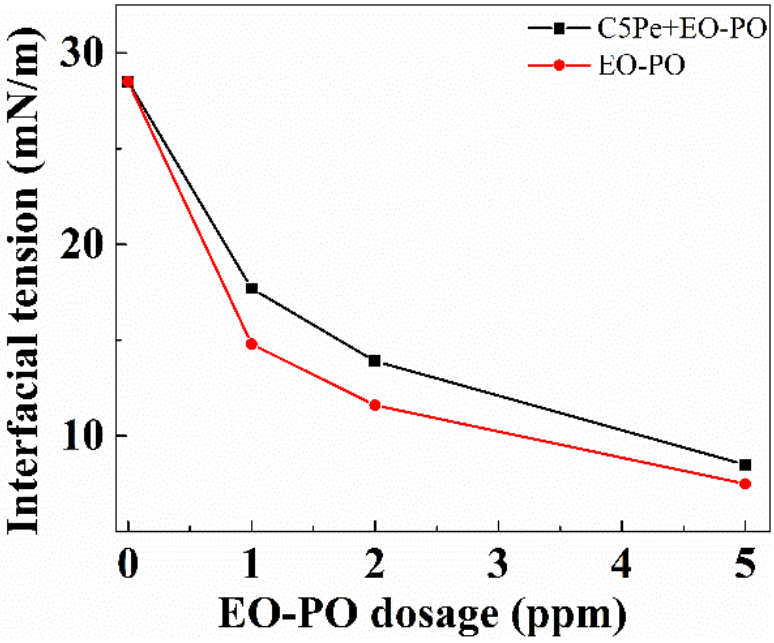

Figure 6-3 Interfacial tension of 30 mg/L xylene diluted C5Pe–water interface and pure demulsifier–water interface as a function of the EO-PO dosage.

The xylene−water interfacial tension in the presence of C5Pe or EO-PO copolymer was measured to study the adsorption behavior of C5Pe and EO-PO copolymer at the oil−water interface. **Figure 6-3** shows the interfacial tensions of the xylene-diluted C5Pe−water interface at different demulsifier dosages. It was found that EO-PO addition could decrease the interfacial tensions at all selected concentrations (1, 2, and 5 ppm). The higher the EO-PO copolymer dosage, the more the interfacial tension decreased. The decrease of the interfacial tension after EO-PO addition indicated that EO-PO molecules could compete and replace the asphaltene model compound C5Pe at the interface. The interfacial tensions of the C5Pe + EO-PO/water system were always lower than those of the C5Pe/water system, but higher than the EO-PO/water system, indicating the coexistence of the EO-PO copolymer with C5Pe molecules at the oil−water interface when EO-PO molecules were added in the oil phase.

6.3.2 Interfacial morphology

The morphological changes of the xylene diluted C5Pe−water interfacial film after demulsifier addition were characterized in real time without disturbing the films by Brewster angle microscopy (BAM). In the current study, C5Pe interfacial film was diffused and aged for 3600 s in order to have high rigidity.

The BAM images in **Figure 6-4** provide the characteristics of C5Pe films at the xylene−water interface and changes of morphological features in situ during the demulsification by EO-PO addition. **Figure 6-4** (a) shows a typical BAM image of the demulsifier-free xylene diluted C5Pe−water interface with the structure being indicated by the pale gray color. The film did not show different gray levels, indicating the same thickness of structures at the interface. Therefore, it can be inferred that a uniform, immobile, and interconnected interfacial layer was formed at the interface after aging the interface for 3600 s.

With the addition of 2 ppm of EO-PO copolymer from the oil phase to the formed xylene diluted C5Pe film, small cracks appeared on the C5Pe films, as shown in **Figure 6-4** (b). At this concentration, the C5Pe film appeared to be partially broken by the EO-PO copolymer as the majority of the C5Pe film remained unchanged, indicating insufficient EO-PO copolymer to act on the entire area of the C5Pe film at the interface. When the EO-PO copolymer concentration was increased to 5 ppm, the whole C5Pe interfacial film started to fall apart to chunks of variable sizes and shapes at the oil−water interface (**Figure 6-4** (c)). Increasing EO-PO dosage to 10 ppm

further ruptured large C5Pe chunks to small C5Pe pieces (**Figure 6-4** (d)). Note that for a clean interface, the BAM image should appear as a dark field as shown by **Figure 6-4** (e). The interfacial film with only 10 ppm demulsifier (**Figure 6-4** (f)) appeared similarly as clean xylene−water interface (**Figure 6-4** (e)). The trend of the C5Pe interfacial film breakage is consistent with the interfacial tension results: more EO-PO molecules were adsorbed at the oil−water interface at higher demulsifier dosage (as indicated by the lower interfacial tension in **Figure 6-3**), thereby leading to considerable film breakage.

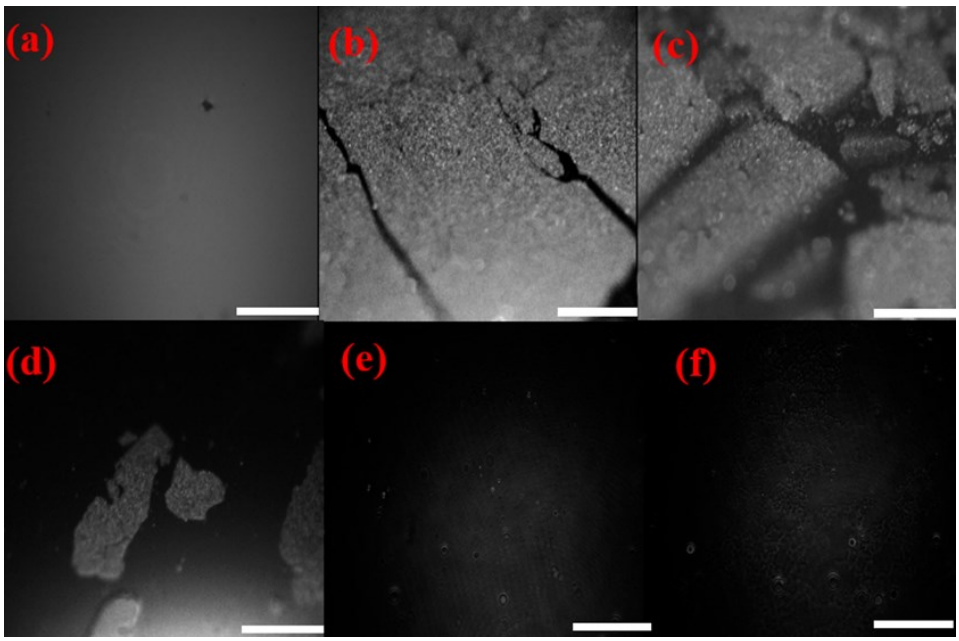

Figure 6-4 BAM images of xylene diluted C5Pe−water interface: (a) no EO-PO added; (b) 2 ppm, (c) 5 ppm, and (d) 10 ppm EO-PO added in the oil phase; in comparison with (e) 10 ppm EO-PO film and (f) clean xylene−water interface. The scale bar is 200 μm for all BAM images.

In conclusion, C5Pe molecules would penetrate the interfacial network, and hence break the film into micro chunks. The color of the remaining structure at the interface did not change, indicating the same film thickness before and after demulsifier addition. It is inferred that the C5Pe molecules would no longer stay at the interface once the demulsifiers are present, but would move to the oil phase. The properties of the C5Pe interfacial film are similar to those of the diluted bitumen film,[208] which further proved the representativeness and reasonability of this model compound. In an emulsion system, it can be inferred that the reduced coverage of the

interfacial protective film of the emulsion droplets increased the possibility for the coalescence of the droplets upon their collision.

6.3.3 MD simulation

The behavior of C5Pe molecules at the oil−water interface with and without EO-PO molecules was also investigated by MD simulations. Examination of the density profile (**Figure 6-5**) revealed the trend of C5Pe and EO-PO molecules adsorbing at the interface. Initially, water molecules are placed in the left-hand side and the solvent is placed in the right-hand side in each system with C5Pe and/or EO-PO in the middle as shown in **Figure 6-5**. The horizontal axis represents the position of each component while the vertical axis represents the relevant concentration of each component. Time starts from the back and increases toward the front, showing how each component evolves at the oil−water interface.

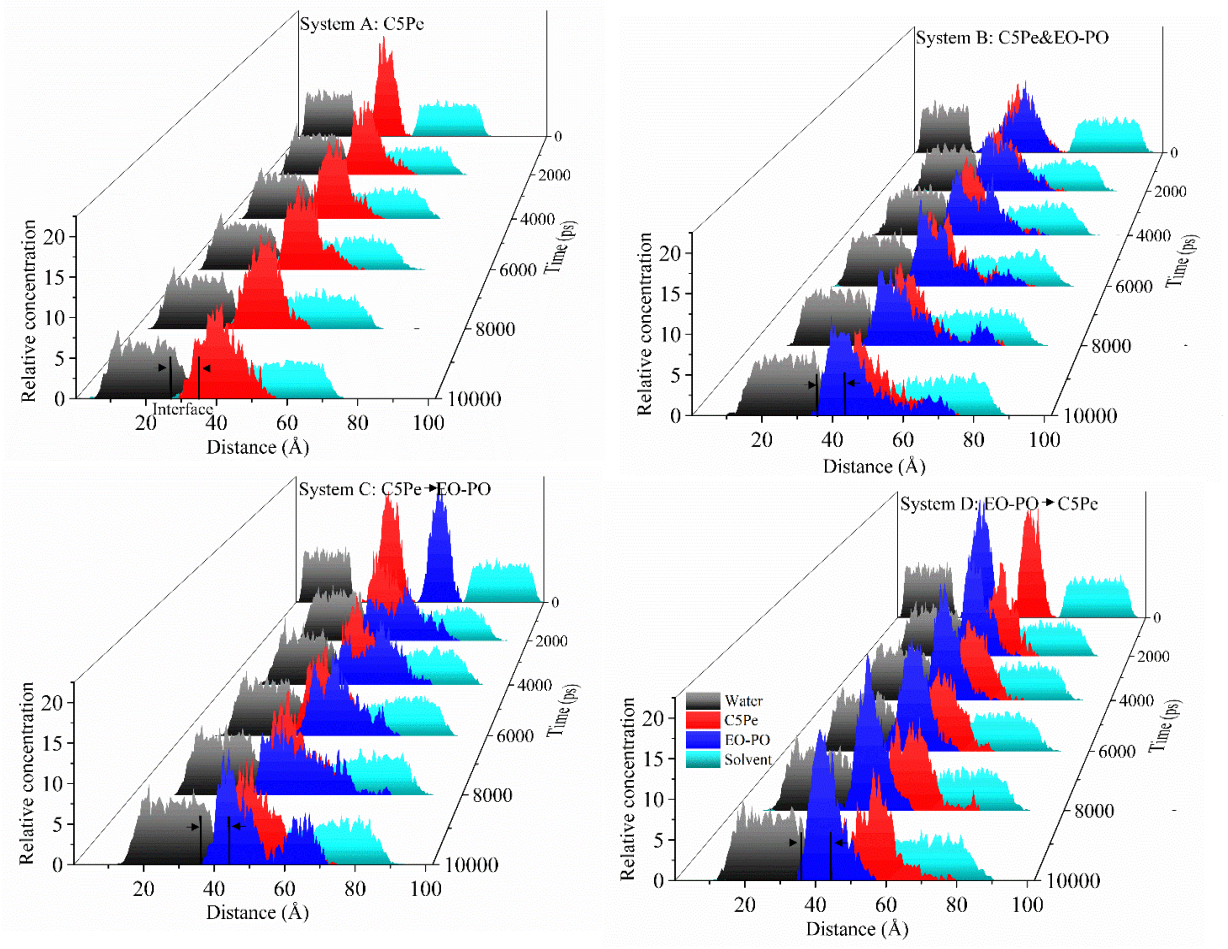

Figure 6-5 Density profiles of systems A, B, C, and D. Water, C5Pe, EO-PO copolymer, and solvent are shown in gray, red, blue, and green colors, respectively.

For system A, the solvation of water and xylene occurred during the simulation process, forming the xylene−water interface. C5Pe molecules were found to be adsorbed at the interface instead of totally dissolving in bulk xylene or water phase, as shown for system A.

System B is similar to system A, apart from replacing the C5Pe layer with a coexisting C5Pe and EO-PO layer. Initially, C5Pe and EO-PO molecules were distributed evenly in their colayer. Over time (from the very beginning until 10,000 ps of the simulation process), the density peak of EO-PO molecules gradually moved closer to the xylene−water interface compared to that of C5Pe molecules, indicating higher interfacial activity of EO-PO molecules, though both C5Pe and EO-PO molecules showed a preference to be adsorbed at the xylene−water interface.

Systems C and D showed that both EO-PO and C5Pe molecules have a tendency to move toward the interface, similar to system B. EO-PO molecules can penetrate the C5Pe layer at the interface step by step and even replace the C5Pe molecules at the xylene−water interface as shown in system C, while C5Pe molecules did not show much influence on the EO-PO layer at the interface as observed in system D, with EO-PO layer firmly absorbed at the interface and C5Pe dissolved back in xylene. The penetration of the C5Pe layer by the EO-PO molecules corresponded to the breakage of the C5Pe interfacial film in BAM images.

System B and C demonstrated that EO-PO molecules were more competitive for the oil−water interface than C5Pe molecules, which agreed well with the interfacial tension results. In addition, system D suggested that the adsorption of EO-PO molecules at the interface was very strong and was not affected by C5Pe molecules. Overall, the results imply that if we perform the simulation for a much longer time, the EO-PO molecules instead of the C5Pe molecules will take compelling advantage at the oil−water interface for all the systems.

Figure 6-6 depicts the radial distribution between the surface-active molecules and water. The results showed a monotonic increase of g(r) between C5Pe/EO-PO molecules and water as the separation between them was increased. For systems containing both EO-PO and C5Pe molecules, EO-PO showed a sharper increase/or stronger interaction with increasing the distance than that of C5Pe molecules, indicating that EO-PO is more interfacially active and tends to concentrate much near the oil−water interface, which is consistent with the interfacial tension results.

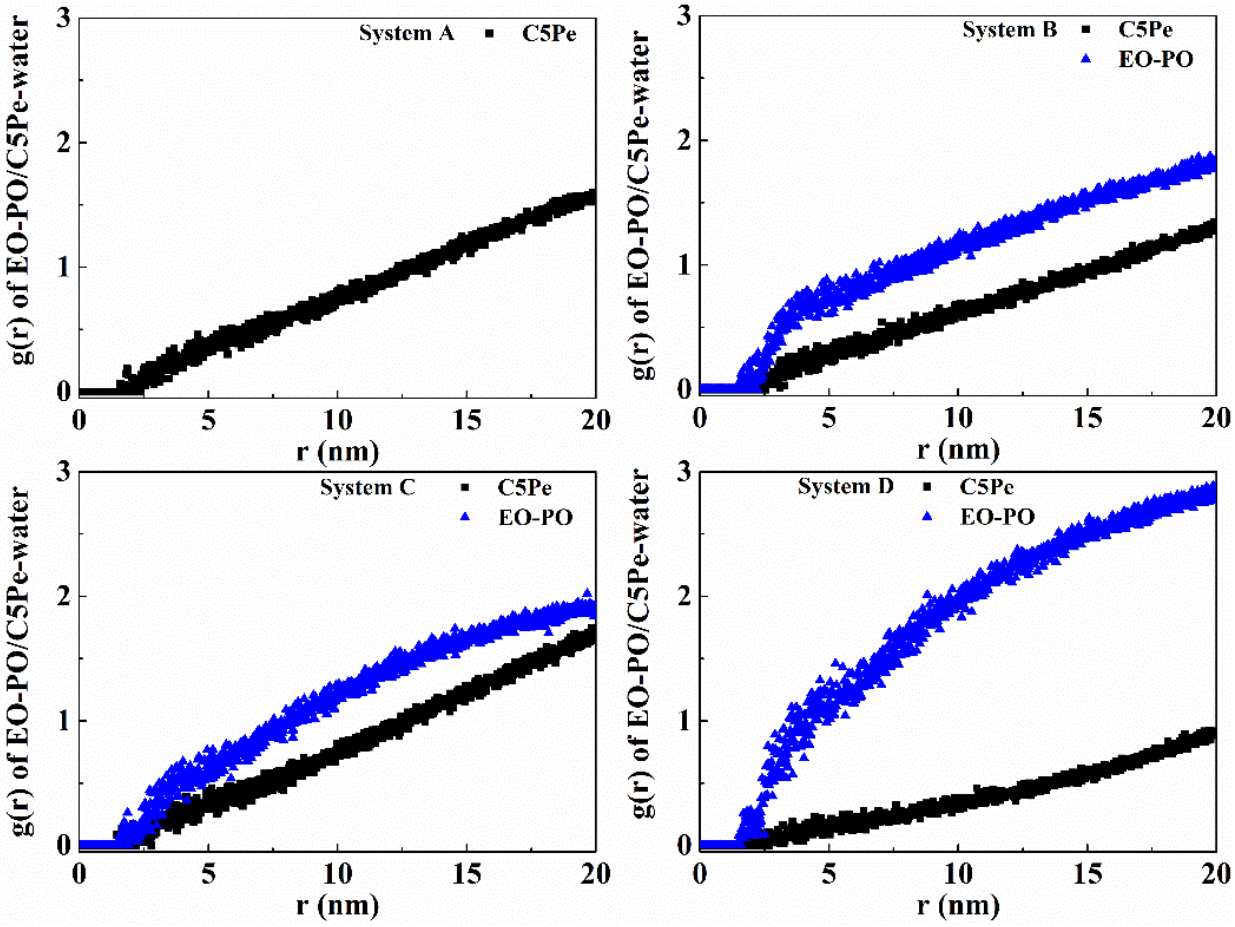

Figure 6-6 Radical distribution between the C5Pe/EO-PO molecules and water for system A, B, C, and D after 10,000 ps simulation.

A hypothesis is proposed that stronger hydrogen bonds can be formed between EO-PO molecules and water and that is the reason why the adsorption of EO-PO molecules is more favorable at the oil−water interface. To check this hypothesis, the hydrogen bonding energies for all the four systems were calculated using Dreiding force field[209] and the results are shown in **Figure 6-7**. It was found that the hydrogen bonding energy between EO-PO and water molecules was lower than that between C5Pe and water molecules in all relevant cases. Compared with C5Pe-only system (system A), the hydrogen bonding energy between C5Pe and water molecules was generally higher in the systems containing both C5Pe and EO-PO molecules. Indeed, the stronger hydrogen bonding interaction between EO-PO and water molecules would be one of the reasons for the higher interfacial activities of EO-PO molecules than C5Pe molecules.

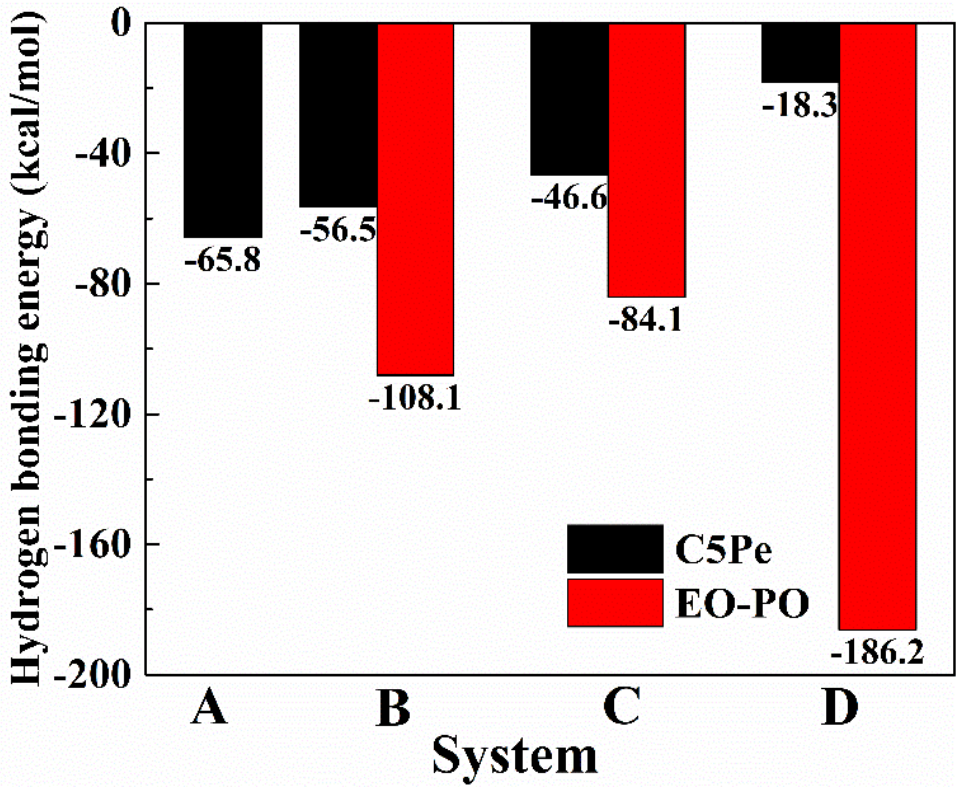

Figure 6-7 Hydrogen bonding energy for system A, B, C, and D.

The final configurations of systems A, B, C, and D are shown in **Figure 6-8**, which correspond to the density profiles in **Figure 6-5** at 10,000 ps. C5Pe molecules tended to be close to or adsorbed at the oil−water interface, as shown in **Figure 6-8**, system A. For systems with EO-PO addition (systems B, C, and D), EO-PO molecules are preferentially adsorbed at the interface, while C5Pe molecules are more likely to dissolve in the oil phase, especially for system D.

The distributions of the hydrophobic and hydrophilic groups of C5Pe or EO-PO molecules under different conditions are also shown in **Figure 6-8**, which demonstrates how different groups of the interfacial active molecules behave at the interface, therefore providing some information on how to design the demulsifier molecules. The interface is defined as the shared area for both oil and water. In system A, the hydrophilic groups of C5Pe molecules tended to stay at the interface, while most of the hydrophobic groups stayed in xylene. For the mixture of C5Pe and EO-PO layer, while most of the hydrophobic groups of C5Pe preferred to dissolve in xylene, a large portion of both EO and PO units appeared at the interface, with some EO units even dissolving in water. Results for systems C and D showed that EO units have stronger affinity to water than that of the hydrophilic groups of C5Pe molecules and PO units have much

better interfacial activity than the hydrophobic groups of C5Pe. The detailed adsorption proportion of each unit is shown in **Figure 6-9** by calculating the peak area ratio of the corresponding unit. The proportion of EO-PO molecules was larger than that of C5Pe molecules in systems B, C, and D. Specifically, for system D, EO-PO molecules (EO units + PO units) occupied 89% of the interface. The group distribution results clearly demonstrated that EO-PO molecules will be dominantly adsorbed at the interface once present though they are unable to completely replace the C5Pe molecules at the interface.

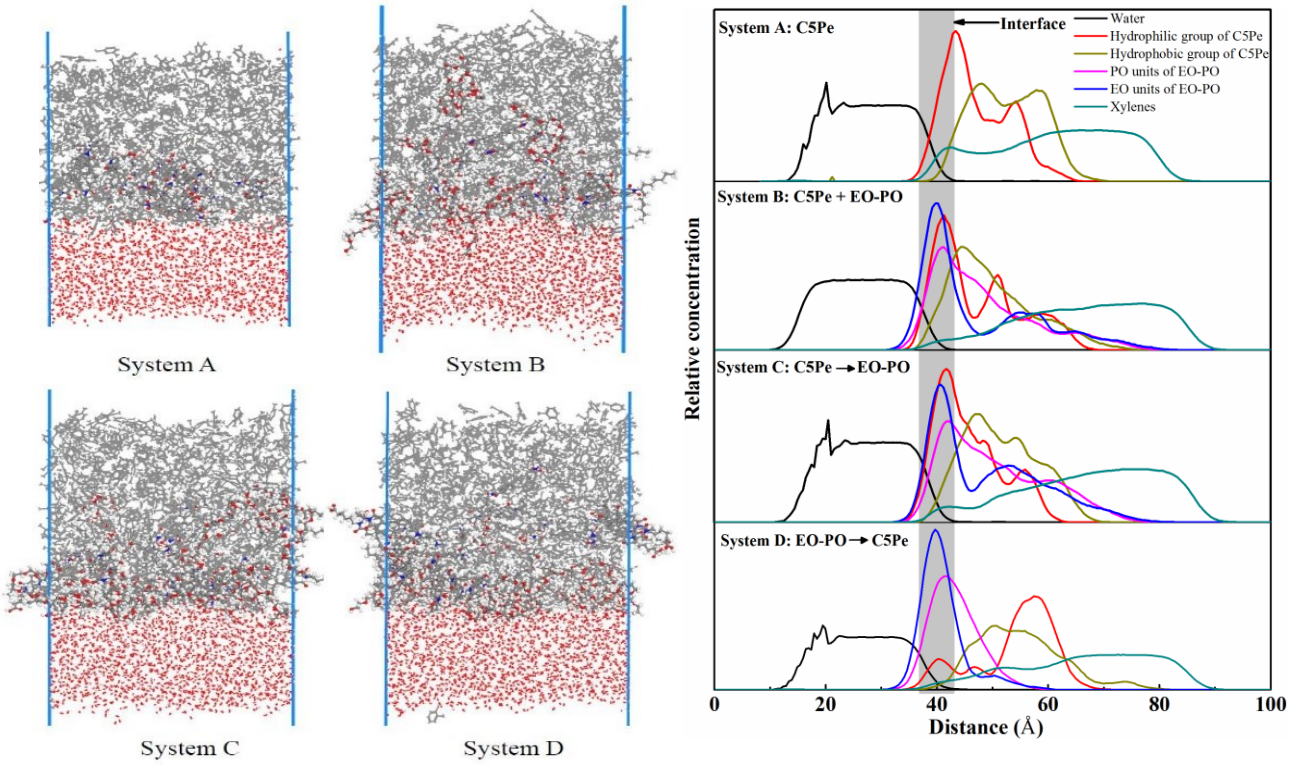

Figure 6-8 Final configurations and distributions of the hydrophobic and hydrophilic groups at the interface of systems A, B, C, and D.

Overall, both C5Pe and EO-PO molecules tend to be adsorbed at the interface, though EO-PO molecules show better performance, as confirmed by the interfacial tension measurements and MD simulations. Besides, EO-PO molecules, which have stronger hydrogen bonding with water, could penetrate and break the C5Pe interfacial film, as indicated by the BAM images and the density profile of systems A−D. Once EO-PO molecules replace C5Pe molecules at the interface, the strong steric repulsion from EO-PO molecules would significantly inhibit further adsorption of C5Pe molecules at the interface.

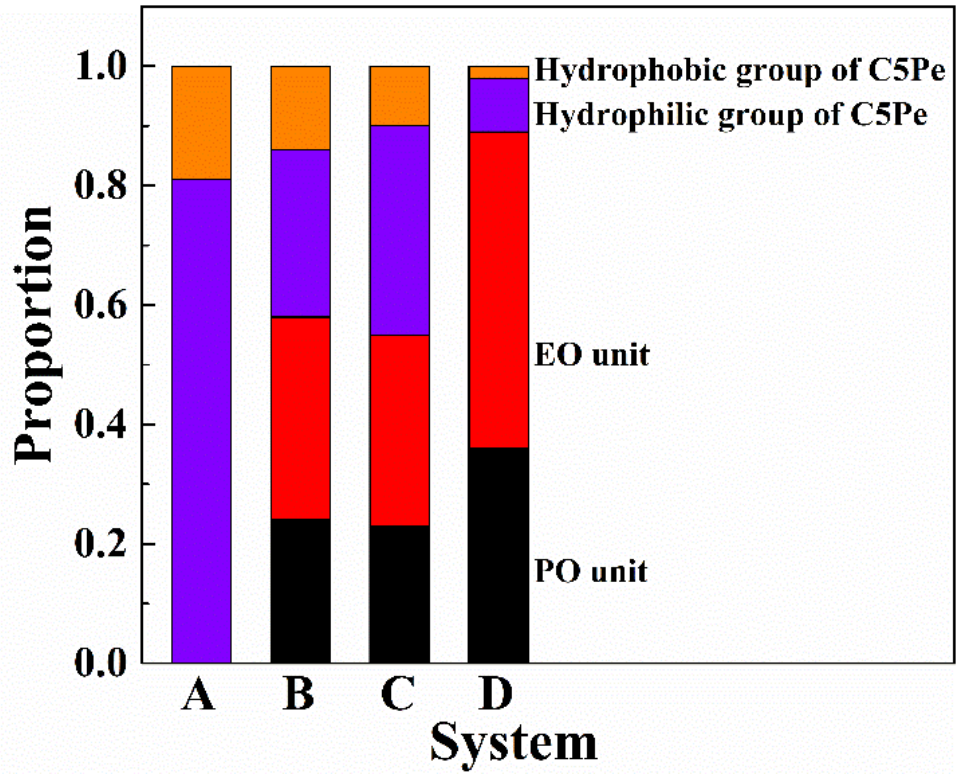

Figure 6-9 Proportion of hydrophilic or hydrophobic groups at the oil−water interface

6.4 Conclusions

Interfacial tension results, BAM images, and MD simulations have consistently revealed the destabilization mechanism of the rigid interfacial film formed by the asphaltene model compound C5Pe by EO-PO copolymer. EO-PO copolymer is more interfacially active and can replace most of the C5Pe molecules at the interface. Once adsorbed at the interface, EO-PO molecules could break the complete networked interfacial film, making the interfacial film unstable. MD simulation has confirmed that EO-PO molecules could replace the C5Pe molecules at the oil−water interface by forming stronger hydrogen bonding, penetrating the C5Pe interfacial film. The adsorbed EO-PO molecules at the interface form a new surface barrier and prevent further adsorption of C5Pe molecules, finally destroying the C5Pe interfacial film and making coalescence of two droplets possible. Both EO and PO units have strong interfacial activity and even affinity to water. Overall, as C5Pe has a known structure, the study of demulsification mechanism of water in asphaltene-stabilized emulsions is therefore simplified by MD simulation. This research provides an improved understanding of the demulsification mechanism at the molecular level as well as how to design efficient demulsifiers for better dewatering.

Chapter 7 Effect of Temperature on Demulsification of Water-in-Heavy Oil Emulsions Using EO-PO Copolymers

7.1 Introduction

Stable water-in-oil (W/O) emulsions are often encountered during the production of crude oils and bitumen. Formation of such stable emulsions in the oil industry is highly undesirable as salts, brine, and fines that are present in the emulsified water pose great threats to the downstream operations.[19] To achieve effective breakup of W/O emulsions, several methods including heat, electricity or chemicals have been applied in industrial operations to enhance the gravitational settling of the emulsified water. The most common method of emulsion treatment is chemical demulsification and EO-PO copolymer is used as the demulsifier in this chapter.

In this work, EO-PO copolymers were added to a water-in-naphtha diluted bitumen emulsion, and the effectiveness of the copolymer in breaking water-in-diluted bitumen emulsions was investigated by measuring the in situ emulsion droplet size, with the demulsifier dosage, water pH, and system temperature as the controlled parameters. The remaining water content was also measured to further determine the effect of demulsifier addition on emulsion demulsification. In addition, the interfacial properties of the oil−water interface with and without demulsifier addition were investigated to obtain a better understanding of the demulsification mechanism. The interfacial tensions of the O/W system for diluted bitumen, EO-PO copolymer, and the mixture of them were measured to detect the interfacial activities of the demulsifier molecules and surface-active species in diluted bitumen. The contraction experiments of the oil droplets in water were conducted to characterize the rigidity of the interfacial film. The morphological changes of the diluted bitumen film at the oil−water interface with the addition of the demulsifier were observed by Brewster angle microscopy to further understand the ability of demulsifier to penetrate into the interfacial films and to alter the film structure.

This study provides further understanding of the general behavior of such copolymers as a demulsifier, which is of great interest for a wide range of industrial applications.[46, 210] In addition, experiments are also conducted in combination with heat treatment to evaluate the effect of the elevated temperatures on the demulsification capacity of EO-PO copolymers.

7.2 Materials and Methods

7.2.1 Demulsifiers

Ethylene oxide (EO) and propylene oxide (PO) copolymers were purchased from Baker Hughes and used as received. The detailed physical properties of the demulsifiers are shown in **Table 7-1**. In this work, EO-PO copolymer samples were freshly prepared at the concentration of 1 wt.% in naphtha as a stock solution and diluted to desired concentrations prior to its use.

Table 7-1 Physical properties of EO-PO copolymers.

Demulsifier	EO (%)	Molecular weight (Dalton)	Arm number	RSN
C (16 H)	35	6145	3	16.92
B (E 20)	20	10003	5	10.59

❖ RSN (relative solubility number): the higher the RSN value, the greater the hydrophilicity of the surfactant.[31, 68]

7.2.2 Solvent and water

Heavy reformate, which is named as "naphtha" throughout this work, was provided by Champion Technologies, Ltd. and used as received. The Deionized water (DI water) was purified with a Millipore system.

7.2.3 Preparation of water in naphtha diluted bitumen emulsion

The vacuum distillation feed bitumen was provided by Syncrude Canada Ltd. It was mixed with naphtha to obtain a naphtha to bitumen mass ratio of 0.65 as the naphtha diluted bitumen oil samples, to mimic conditions of practical operations. After dilution, the mixture was shaken in a mechanical shaker overnight at 200 cycles/min. The diluted bitumen solution prepared by this protocol was used throughout this chapter.

5 wt.% deionized (DI) water was added into the diluted bitumen solution placed in the autoclave vessel and the mixture was homogenized by a PowerGen 1000 homogenizer at 30,000 rpm for 3 min. The emulsion prepared freshly each day using the procedure above was used in all experiments reported here. The resulting emulsified water droplets were found stable with several micrometers in size, as shown in **Figure 7-1**.

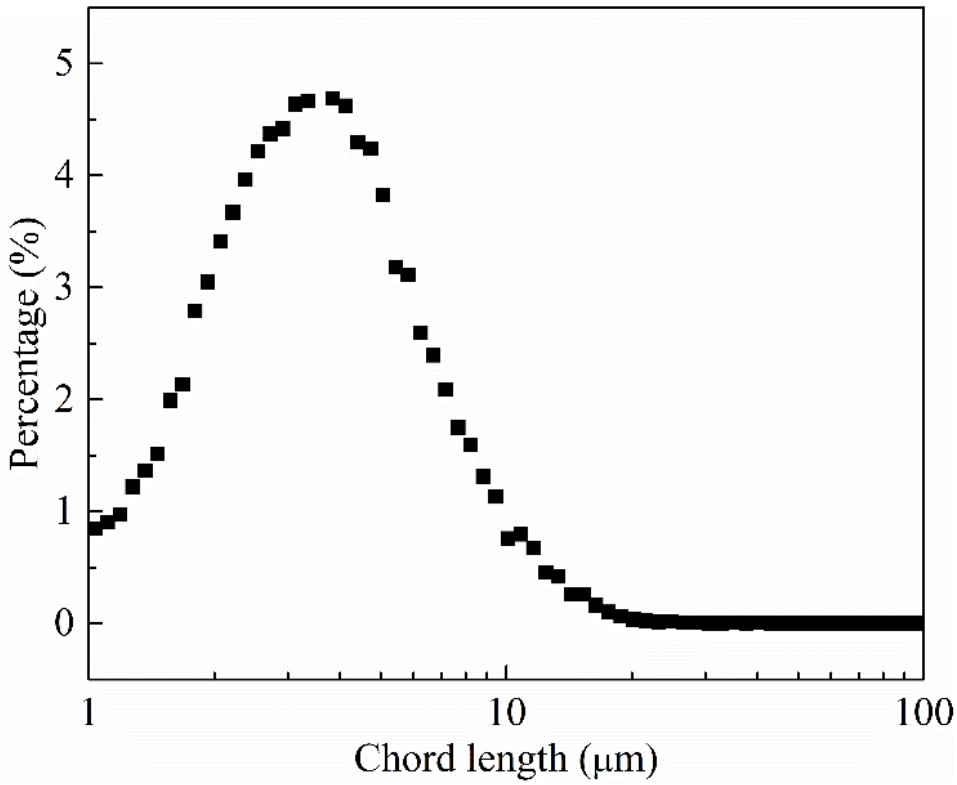

Figure 7-1 Size distribution of water droplets in diluted bitumen emulsions detected by FBRM.

7.2.4 Demulsification study using FBRM and Karl Fisher Titrator

The effectiveness of the EO-PO demulsifier can be evaluated by measuring the emulsion droplet size during the demulsification process. Focused Beam Reflectance Measurement (FBRM) is a powerful technique which gives an online and in situ measurement of the particle/droplet size distribution over a wide range of concentrations.[211]

The effects of dosage, pH, and temperature were investigated. All demulsification tests were repeated for at least three times. **Table 7-2** lists all experimental conditions used in these tests. The same amount of water-in-naphtha diluted bitumen emulsion (90 g) was used in each demulsification tests. For each measurement, the emulsion sample was stirred for 5 min at the beginning. At the 5th min, a desired amount of demulsifier was injected into the reactor and the size of emulsion droplets was monitored by FBRM for another 55 min. The blank test (room temperature without demulsifier addition) was also conducted for comparison. When running experiments at high temperature, a heating mantle and an external water bath were used to keep the temperature constant.

Table 7-2 Experimental conditions used in autoclave demulsification tests

	Demulsifier C (16H)	Demulsifier B (E20)
Dosage (ppm)	20, 50, 100, 125, 150	50, 100
pH	4.5, 6.5, 8.5, 10.5	6.5
Temperature (°C)	23, 40, 50, 60, 80	23, 50, 80

In addition, the amount of water that remained in the system after the demulsification process was measured using titration method with a Karl Fisher Titrator (Cou-Lo 2000, GR Scientific Canada). Emulsion samples were transferred to the 11cm Pyrex glass 35 tubes (16×100 mm) after demulsification process for gravity settling. The water content of the emulsion sample was measured at 2.5 cm below the top surface of the emulsion sample as a function of the settling time. At least three measurements were performed for each sample and the average was taken for data analysis.

7.2.5 Analysis from a pendant drop

In order to study the adsorption of the demulsifier at the water-diluted bitumen interface, the interfacial tension of this system was measured using the pendant drop technique (Theta Optical Tensiometer T200). The effects of concentrations of the EO-PO copolymers (0, 20, 50, and 100 ppm) and temperatures (23 °C to 80 °C) were studied. The naphtha diluted bitumen mixed with different dosages of EO-PO copolymers was used as the oil sample. An oil drop of 18 μL in volume was immersed in 3 mL DI water placed in a quartz cuvette. The interfacial tension was recorded for 3,600 s.

In addition, the pendant drop shape analysis allows us to study the degree of steric layer (skin) formation at the interface, by analyzing the crumpling ratio (CR) of the droplets.[128] In general, larger crumpling ratio indicates a more rigid skin on the surface of an oil droplet. In this study, the naphtha diluted bitumen was mixed with different dosages of EO-PO copolymers (0, 50, and 100 ppm) and the aging time of the oil droplets was set to 3,600 s for all measurements. Similar to interfacial tension measurement, the crumpling ratio was also measured for the oil droplets of 18 μL in volume in water at both 23°C and 50 °C. Each data point was obtained as an average of four measurements with the error bar representing the standard deviation.

7.2.6 Brewster angle microscopy

The morphology of the interfacial film was studied by Brewster angle microscopy (Model EP3, Accurion GmbH, Goettingen, Germany). The following procedures were used when running BAM experiments: 28.5 mL of DI water was poured into the trough, then 50 μL of diluted bitumen was added on the water phase, followed by gently pipetting 80 mL of naphtha along the sidewall of the trough to cover the water subphase. After equilibrating for 3,600 s, the interfacial films were imaged at the angle of incidence of 41.8° (Brewster Angle) with the polarizer and analyzer set to around 2° and 10°, respectively. The EO-PO copolymer at concentrations of 0.5, 1, and 5 ppm was added dropwise and images were taken after demulsifier diffusion. EO-PO copolymer film at 5 ppm was also imaged to elucidate a possible dependence between demulsifier concentration and film structure.

7.3 Demulsification performance of the EO-PO copolymers on dewatering water-in-naphtha diluted bitumen emulsions

EO-PO copolymer was proven to be effective in breaking asphaltene-stabilized W/O emulsions by Pensini et al.[71] Since the diluted bitumen−water interface is much more complicated than the asphaltene−water interface, the study of the diluted bitumen system allows us to further investigate the effectiveness of EO-PO copolymers in breaking emulsions of more practical relevance. The overall demulsification performance of EO-PO copolymers was firstly evaluated by measuring the size of the emulsion droplets during the demulsification process. After the demulsification process, the remaining water content in the emulsion was measured to further evaluate the demulsification efficiency.

An example is given when demulsifier dosage is 100 ppm (demulsifier C) to show the results of FBRM measurements. **Figure 7-2** shows that the number of droplet counts as a function of time. The dotted line denotes the point when demulsifier was added into the system. It is evident that the number of the droplet counts with droplet size smaller than 10 μm decreased dramatically after the demulsifier was added into the system. However, for the droplets with size ranging from 10 to 50 μm, a noticeable increase in the number of droplet counts was detected, which indicates rapid droplet coalescence or flocculation after the addition of the demulsifier. An increase in counts number of the droplets with sizes ranging from 50 to 150 μm was also observed as shown in the inset of **Figure 7-2**. Although the counts number in this size range was not as high as that

of the droplets with size ranging from 10 to 50 μm, it was still a good indication of effective emulsion breaking.

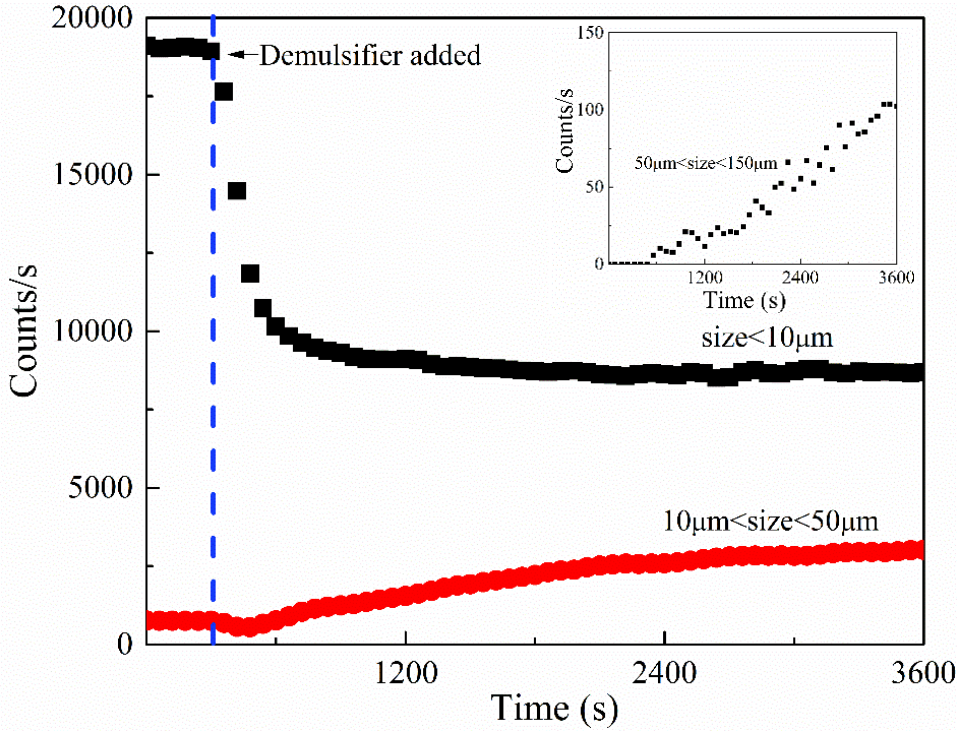

Figure 7-2 Counts number of the water droplets in emulsions as a function of time, detected by FBRM (100 ppm of demulsifier C). The dashed line represents the point when the demulsifier was added to the system. The inset shows the counts number of the droplet with size ranging from 50 to 150 μm.

The chord length distributions were plotted in **Figure 7-3** and **Figure 7-4**. **Figure 7-3** shows the unweighted chord length distribution (UWT CLD) at different demulsification periods. As can be seen, the percentage of small droplets continued to decrease while the percentage of large droplets kept increasing, which led to the increase in the average emulsion droplet size during the dewatering process as observed by FBRM. Square weighted chord length distribution (SWT CLD) is provided to analyze the influence of the presence of large droplets on the emulsion droplet size (**Figure 7-4)**. A significant shift of the droplet size distribution, from small droplet area (peak at around 7 μm) to large droplet area (peak at around 50 μm), is observed. It is also evident that demulsifier C (100 ppm) worked immediately after its addition (added at the 5th min). At the 5th min, the SWT CLD showed a significant increase with the addition of 100 ppm demulsifier C.

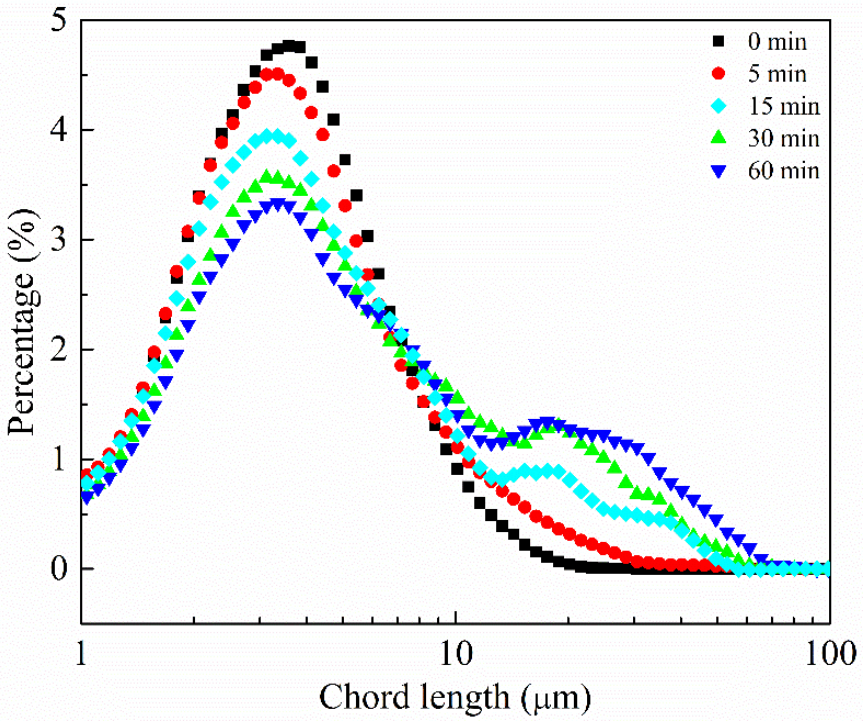

Figure 7-3 UWT CLD during demulsification of the water-in-naphtha diluted bitumen emulsions using 100 ppm demulsifier C at different demulsification time.

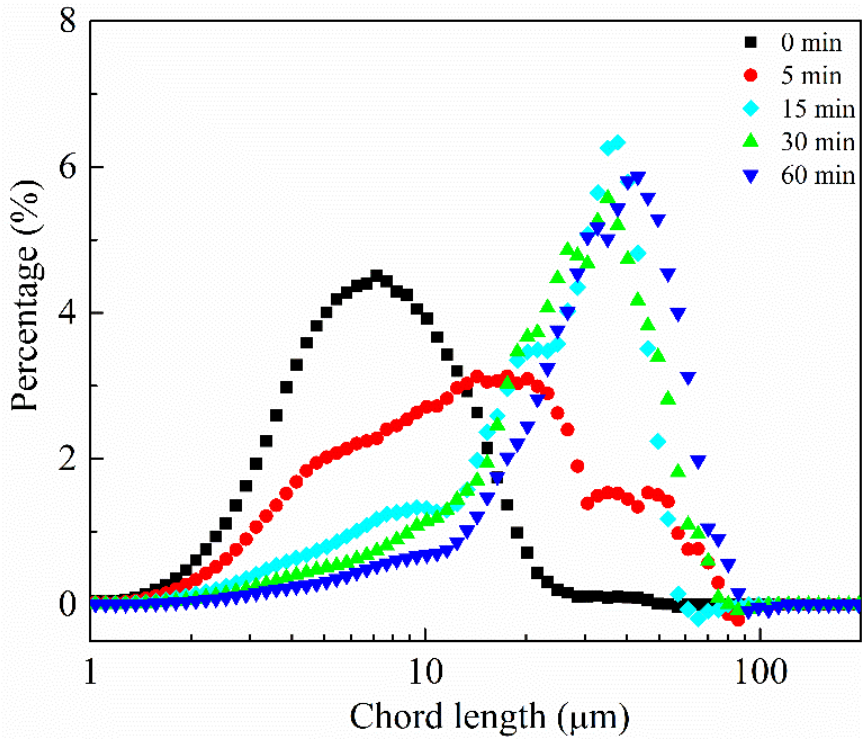

Figure 7-4 SWT CLD during demulsification of the water-in-naphtha diluted bitumen emulsions using 100 ppm demulsifier C at different demulsification time.

7.3.1 Performance of demulsifier C

7.3.1.1 Effect of dosage

Using FBRM, droplet sizes of the water-in-naphtha diluted bitumen emulsions were measured for 3,600 s upon addition of the EO-PO copolymer at the 5th min. As shown in **Figure 7-5**, increased droplet sizes can be found for all copolymer added systems, which clearly indicates coalescence or flocculation of the emulsion droplets (i.e., demulsification). For the system without the addition of the demulsifier (blank), the chord length was nearly unchanged over this period due to inhibited coalescence or flocculation of the emulsion droplets.

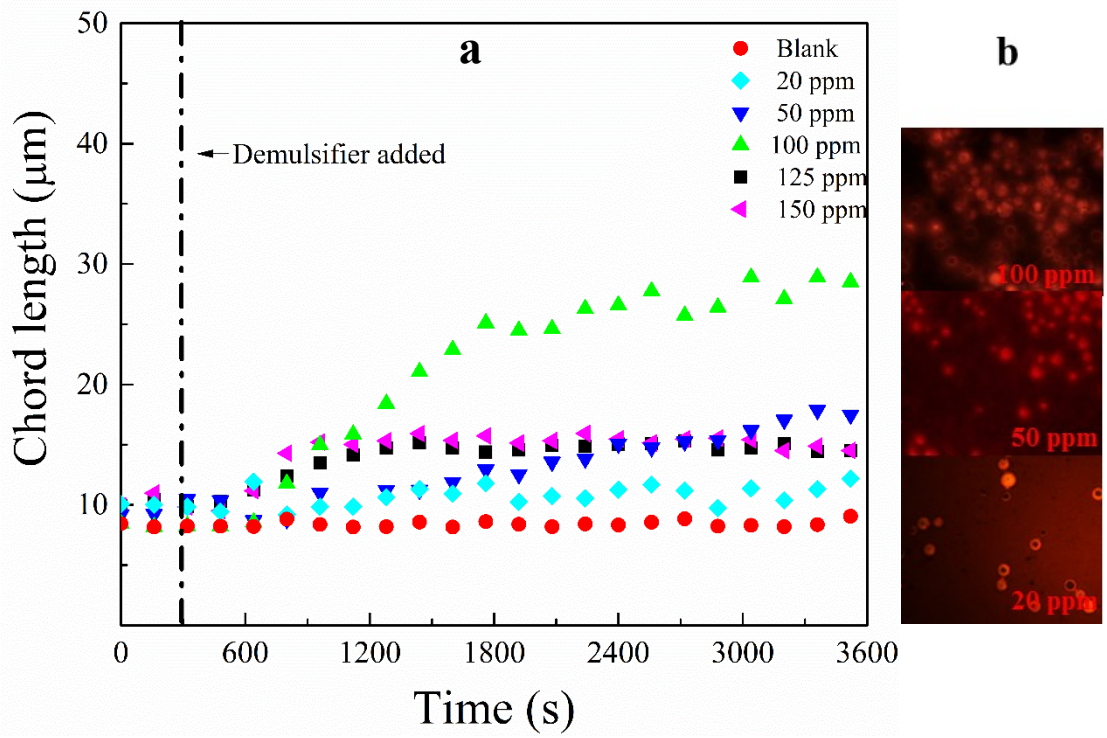

Figure 7-5 (a) SWT CL during demulsification of the water-in-naphtha diluted bitumen emulsions at different dosages of demulsifier C as a function of the demulsification time and (b) microscopy pictures of the emulsion droplets at the bottom of the autoclave vessel.

By comparing the 'chord length' at the end of the demulsification process (3, 600 s) for systems in **Figure 7-5**, the effectiveness of the demulsifier at different dosage can be evaluated as indicated by the increased final chord length. We can conclude that the demulsification performance of the EO-PO copolymer can be enhanced with increasing dosage up to 100 ppm. As shown by the microscopy pictures of the emulsion sample which was obtained from the bottom of the vessel, the amount of the water droplets was notably more significant at high

demulsifier concentration (100 ppm). However, at higher polymer dosages (125 and 150 ppm), smaller emulsion droplets were obtained at the end of the demulsification process, which seemed to suggest an overdose effect, as previously reported.[29, 71] At the overdosed concentrations, it is plausible that the adsorption of polymer molecules at the oil−water interface leads to larger steric repulsion and thus prevents coalescence between the emulsion droplets.

An increase in the droplet size after demulsification was observed from the UWT CLD (**Figure 7-6**). It should be noted that large droplets between 20 to 60 μm in size were not detected when the demulsifier dosage was at 125 or 150 ppm while these large droplets can be found when the demulsifier dosage was below 100 ppm. The SWT CLD of the emulsion droplets after the demulsification process is shown in **Figure 7-7**. Similarly, relatively large droplets (20−100 μm) can only be observed when the demulsifier dosage was lower than 100 ppm.

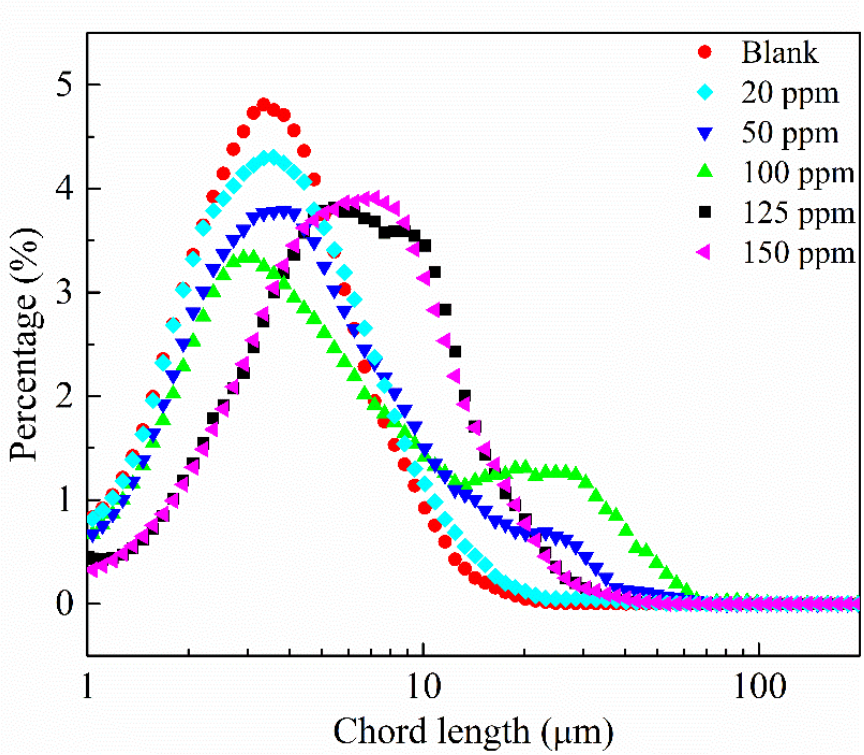

Figure 7-6 UWT CLD at the steady state of the demulsification process at different dosages of demulsifier C.

As is well known, flocculation is a very fast process while coalescence is a relatively slow process. The overdose effect might be explained as 1) at high dosage, coalescence occurs to form relatively large droplets but the steric repulsion caused by demulsifier adsorption between

droplets prevents further coalescence; 2) at high dosage, large droplet did form during the demulsification process but the droplet was too large that it settled very fast before it could be detected by FBRM.

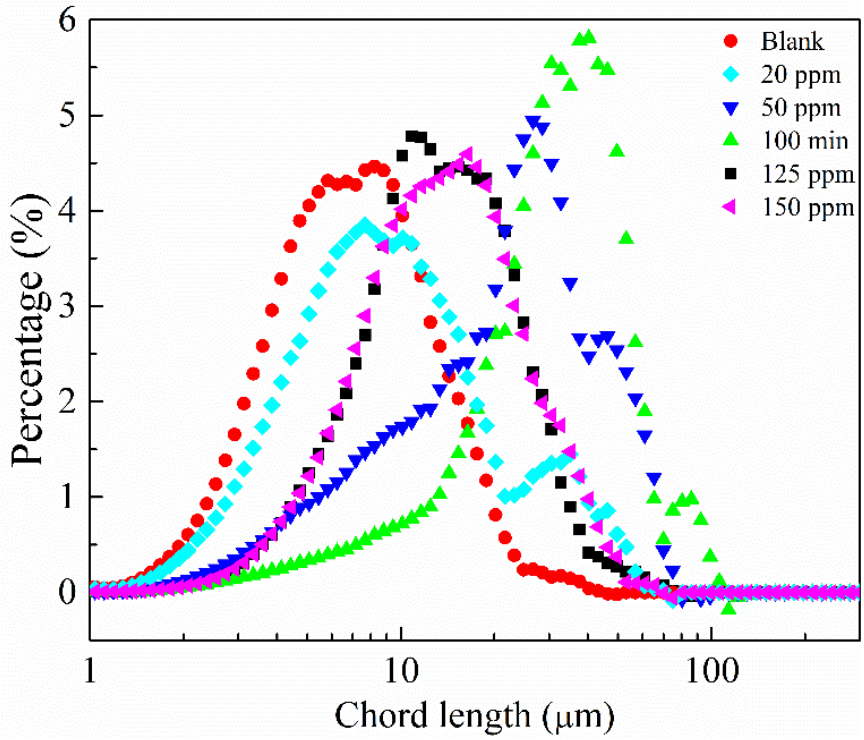

Figure 7-7 SWT CLD at the steady state of the demulsification process at different dosages of demulsifier C.

The water-in-naphtha diluted bitumen emulsions remained stable without EO-PO copolymer addition. The remaining water content in the water-in-naphtha diluted bitumen emulsions after demulsification is presented as a function of settling time in **Figure 7-8**. The comparison in **Figure 7-8** shows a general enhancement of water removal from systems with increased dosage of the demulsifier. In particular, with the demulsifier dosage at 100 ppm, a significant 60% reduction of the water content (5wt.% at the origin) was achieved after 2 h of settling. Interestingly, the water removal at this settling time was found to be very similar even for those systems with an 'overdosed' demulsifier content (125-150 ppm) as suggested by the FBRM measurements (**Figure 7-5**). This appeared to confirm the fact that at overdosed concentrations, the extra copolymers merely offer a weak steric stabilization to the colloidal droplets, which becomes less effective at a longer time. Nevertheless, the result seems to agree that 100 ppm was the optimum demulsifier dosage since the water removal was significantly more effective as

compared to systems with lower demulsifier dosage, and the water removal was notably enhanced with further increased dosage.

Moreover, with a further extended period of settling (~4 h), the system with 50 ppm demulsifier dosage, which was initially less effective in water removal during the period of 1-2 h, also achieved an over 75% water removal, comparable to systems with a higher demulsifier dosage. Such increase in the resolved water at an extended period of settling is actually a reasonable observation, as emulsions are thermodynamically unstable systems and phase separation should eventually occur if sufficient time is given for the settling. This process, as also confirmed by our results, can be significantly accelerated with the addition of an effective demulsifier (e.g. the EO-PO copolymer as applied in this study).

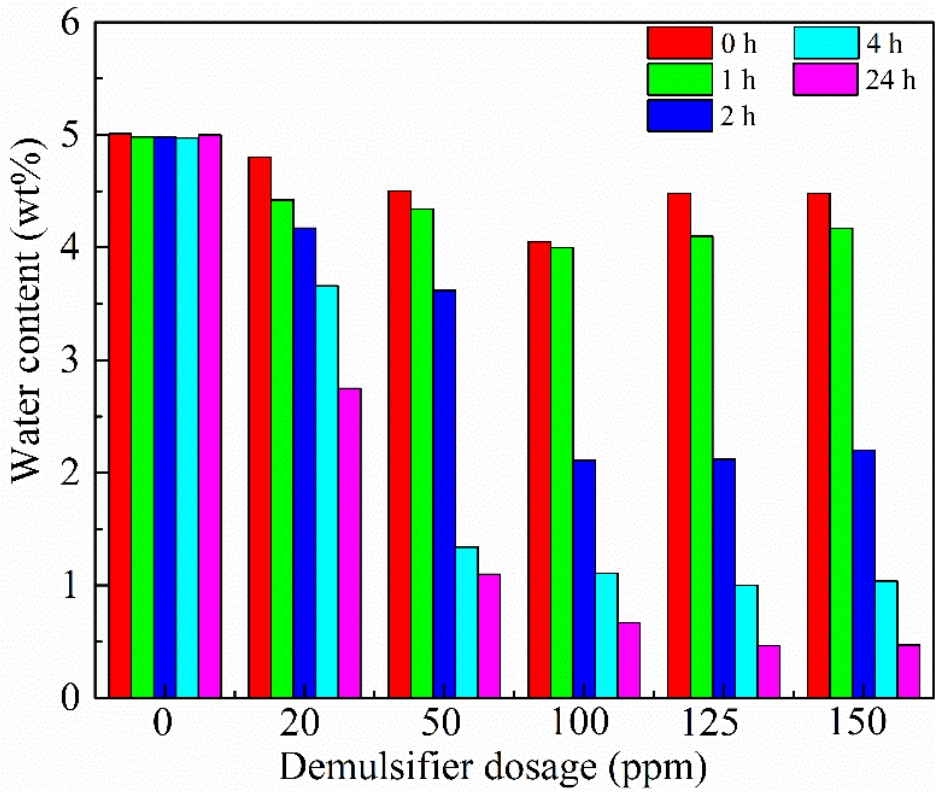

Figure 7-8 Water content remained in the water-in-naphtha diluted bitumen emulsions after the demulsification process at different dosages of demulsifier C.

7.3.1.2 pH effect

Experiments were also conducted at various pH with 50 ppm demulsifier C addition to study the pH effect. FBRM results in **Figure 7-9** shows that demulsifier C performed the best over the neutral pH range. When the pH was equal to 4.5 or 8.5, demulsifier C was less effective than that

at pH 6.5. At pH 10.5, the EO-PO demulsifier merely showed little effect. Obviously, the maximum demulsification efficiency was obtained at a neutral pH whereas it decreased in both directions. We speculate that this trend may happen as follows: more surface-active components in bitumen adsorb at the interface to make the interfacial film much more stable at high pH, making it harder for the demulsifier to penetrate or weaken the interfacial film.

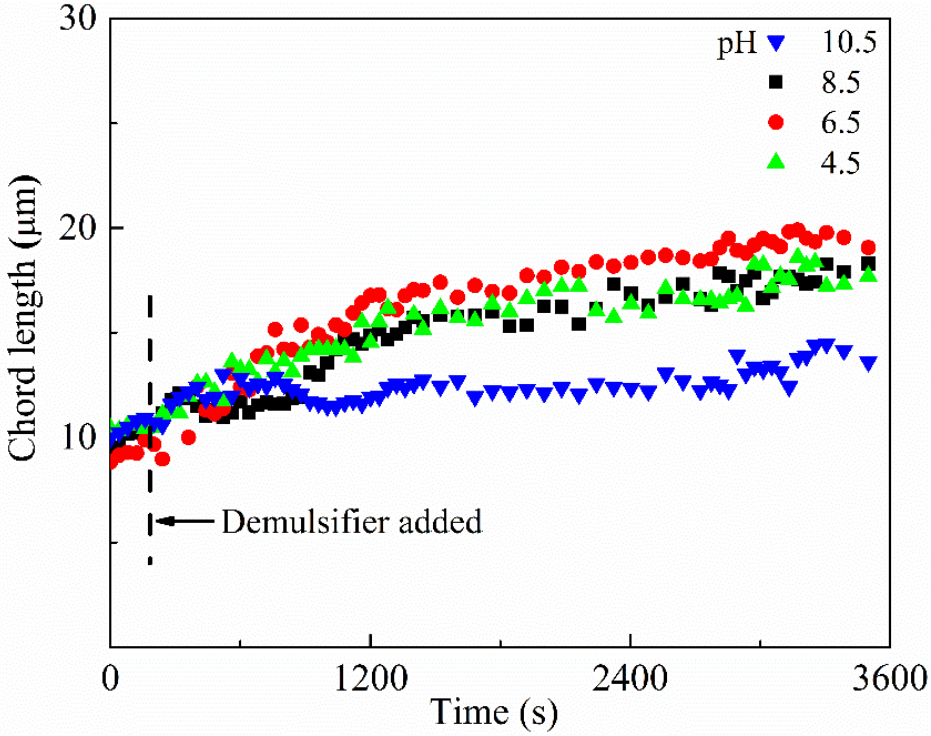

Figure 7-9 SWT CL during demulsification of the water-in-naphtha diluted bitumen emulsions using 50 ppm demulsifier C as a function of the demulsification time at different pH.

The UWT CLD in **Figure 7-10** shows the formation of large droplets when pH was at 6.5. When pH was at 10.5, the CLD remained almost the same as that of the original case. From SWT CLD shown in **Figure 7-11**, it could be further confirmed that demulsifier C performed the best in the neutral environment.

To confirm the demulsification performance of demulsifier C determined by the FBRM measurements, the remaining water contents were also measured. The results in **Figure 7-12** showed that even allowing the emulsion sample to settle for a long period (up to 24 h), the water content of emulsions at aqueous pH of 10.5 remained higher than that at other pH values. The optimum pH for demulsification was found to be 6.5, which was consistent with the results from the CLD measurement.

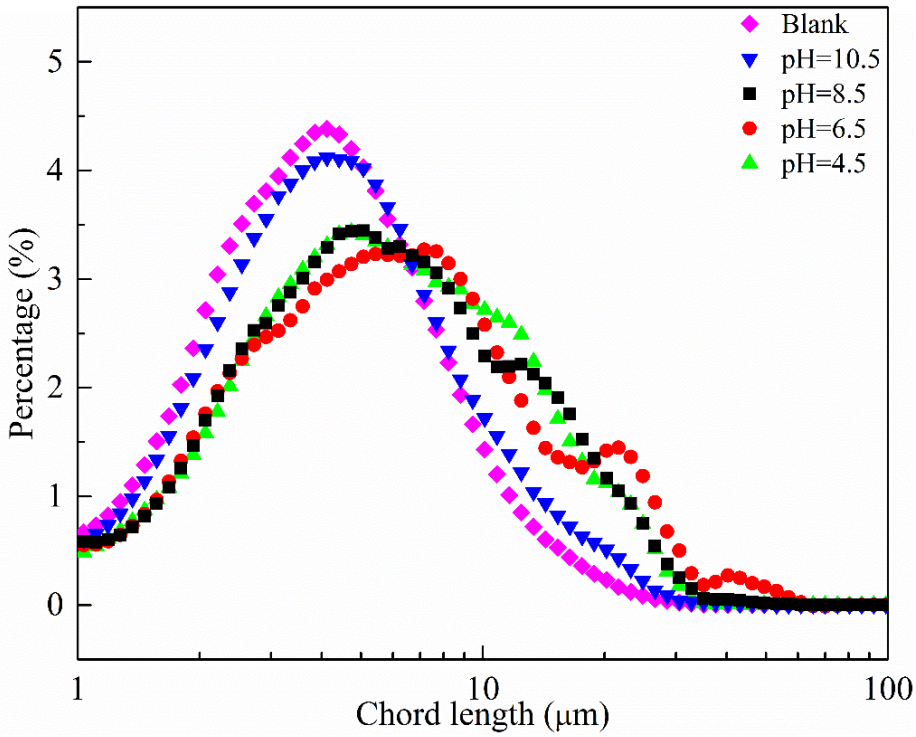

Figure 7-10 UWT CLD at steady state of the demulsification process using 50 ppm demulsifier C at different pH.

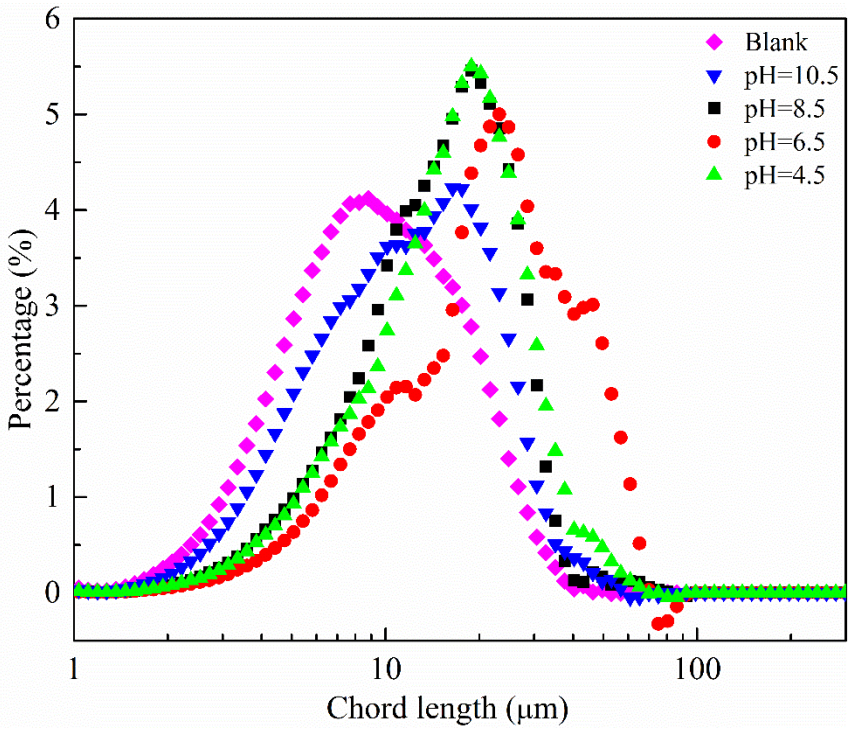

Figure 7-11 SWT CLD at steady state of the demulsification process using 50 ppm demulsifier C at different pH.

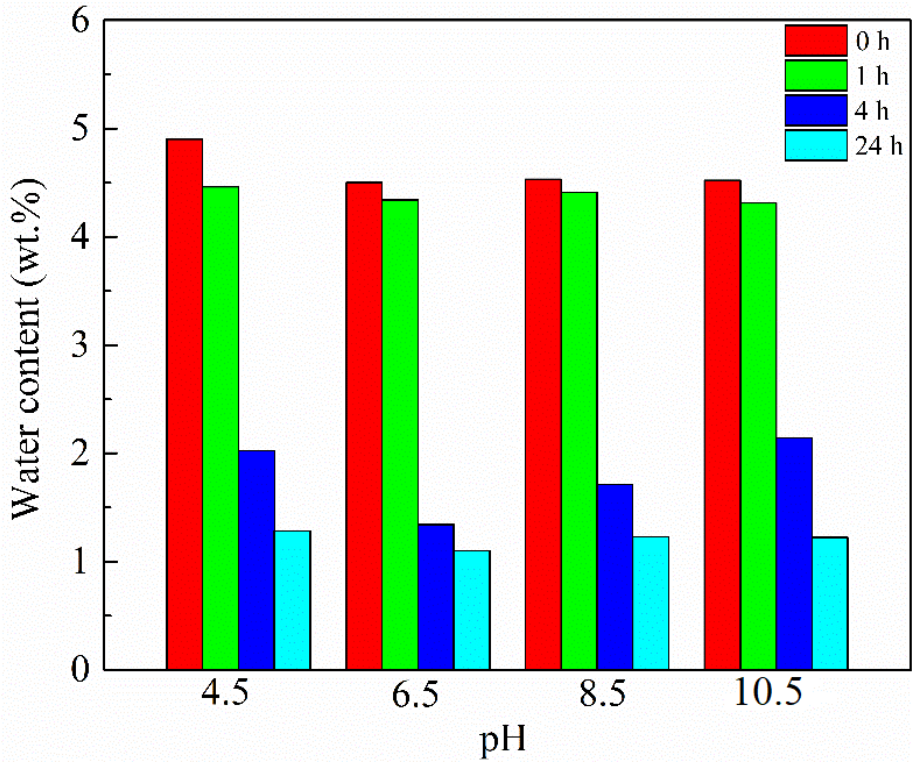

Figure 7-12 Water content remained in the water-in-naphtha diluted bitumen emulsions after the demulsification process by 50 ppm demulsifier C at different pH.

7.3.1.3 Temperature effect

In order to achieve better demulsification efficiency, the effect of 'heat treatment' in combination with the demulsifier was also studied. All the experiments in this section were conducted at 50 ppm demulsifier concentration and neutral pH. FBRM was used to measure the size of the emulsion droplets in real time. The emulsion sample was loaded into the autoclave vessel and an external heating mantle was wrapped around it to heat up the sample. After equilibrating for 5 min at the desired temperature, 50 ppm of EO-PO copolymer was added into the vessel to demulsify the emulsions.

As shown in **Figure 7-13**, elevating the temperature resulted in increased emulsion droplet size in general. By comparing the droplet size at steady states (obtained after 1,000 s of temperature increase), different emulsion behavior was obtained over three ranges of the temperature:

(1) At 23°C, the emulsion droplet radius remained mostly steady at ~17 μm. (2) For temperatures between 40 °C to 60 °C, the droplet radius was relatively stable at ~50 μm. (3) At 80 °C, however, the droplet size was found to increase again to 70 μm. These three ranges of

temperature corresponding to the different behaviors of emulsion droplets may indicate two demulsification mechanisms: (1) From 23 to 60 °C, the demulsification process is dominated by flocculation, which can be enhanced by elevating temperature up to 60 °C for the maximum effect; (2) At temperatures close to 80 ºC or higher, coalescence becomes the dominant effect, where droplet with larger size appears.

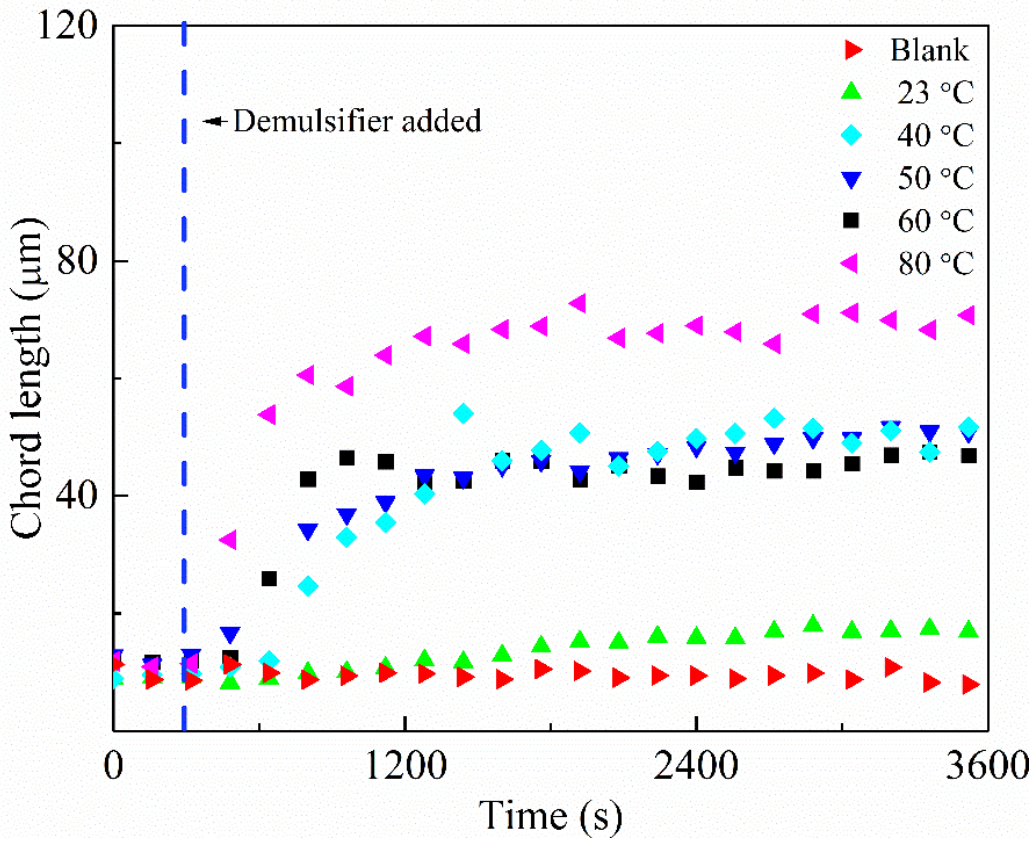

Figure 7-13 SWT CL during demulsification of water-in-naphtha diluted bitumen emulsions using 50 ppm demulsifier C as a function of the demulsification time at different temperatures (Blank represents the condition when the experiment was run at room temperature without demulsifier addition).

As shown in **Figure 7-14**, a less significant difference in UWT CLD was observed for the demulsification at elevated temperatures. As long as the temperature was increased, even only to 40 °C, an obvious decrease in the percentage of small droplets and an increase in the percentage of large droplets were seen. In contrast, a clear increase in the size of the droplets was found at 80 °C from SWT CLD (**Figure 7-15**). This finding indicates the formation of much larger droplets of around 100 μm at 80 °C, though the number of such larger droplets is much smaller.

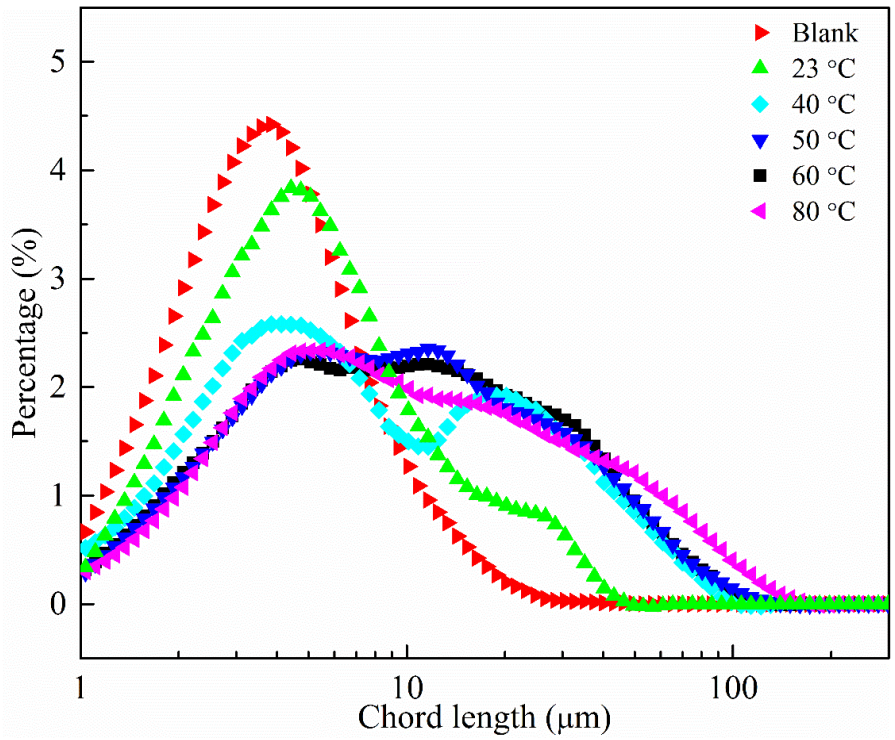

Figure 7-14 UWT CLD at steady state of the demulsification process using 50 ppm demulsifier C at different temperatures.

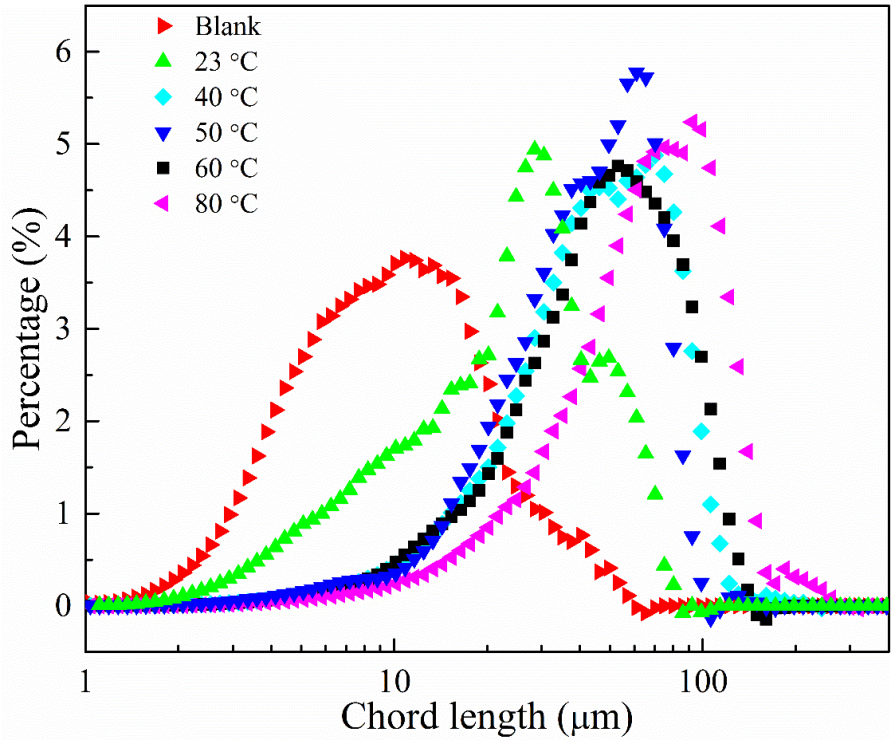

Figure 7-15 SWT CLD at steady state of the demulsification process using 50 ppm demulsifier C at different temperatures.

The remaining water contents for systems demulsified at elevated temperature were also recorded and compared in **Figure 7-16**. It should be noted that instead of keeping at the temperature of demulsification, all the demulsified samples were settled at room temperature (23 °C). In general, water removal was enhanced when emulsions were treated with demulsifiers at elevated temperatures. Particularly, a significant 80% reduction of water content from original 5 wt.% to less than 1 wt.% immediately after demulsification at 80 °C was achieved even without settling at 80 °C, further proving the presence of much larger droplets that were formed during the demulsification process, indicating coalescence of the emulsion droplets.

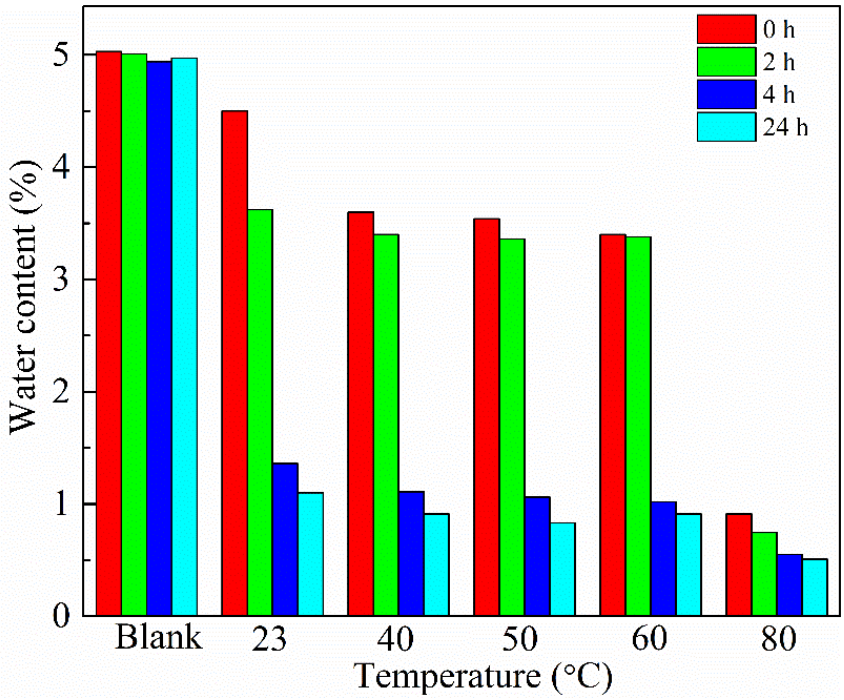

Figure 7-16 Water content remained in the water-in-naphtha diluted bitumen emulsions after the demulsification process by 50 ppm demulsifier C at different temperatures.

7.3.2 Performance of demulsifier B

7.3.2.1 Dosage effect

The changes in the emulsion droplet size during the demulsification process using 100 ppm demulsifier B is shown in **Figure 7-17** and **Figure 7-18**. Both the square weighted chord length (SWT CL) and unweighted chord length (UWT CL) increased immediately after the addition of the demulsifier. Interesting, a decrease in the droplet size was observed a few minutes later after the demulsifier addition. To find out the possible reasons, it is necessary to analyze the counts number of the emulsions droplets in different size ranges.

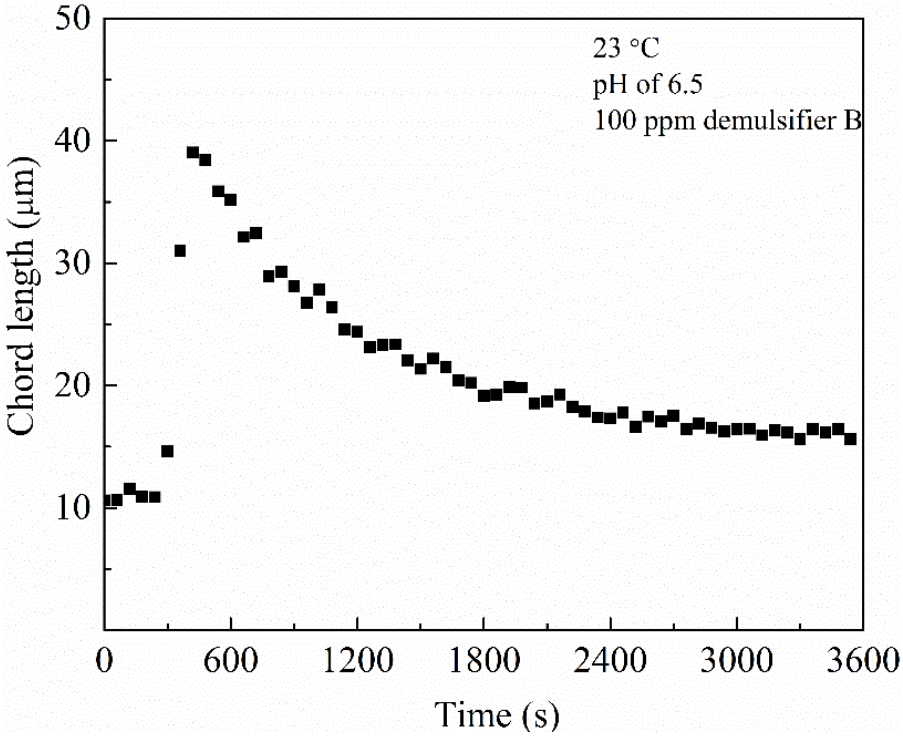

Figure 7-17 SWT CL during demulsification of the water-in-naphtha diluted bitumen emulsions using 100 ppm demulsifier B as a function of the demulsification time.

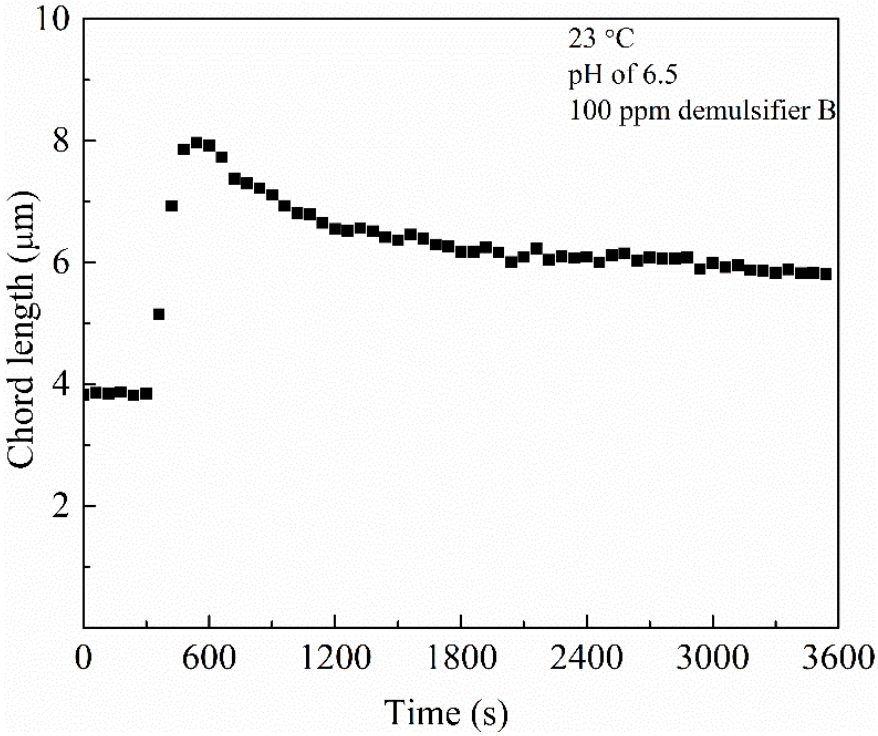

Figure 7-18 UWT CL during demulsification of the water-in-naphtha diluted bitumen emulsions using 100 ppm demulsifier B as a function of the demulsification time.

The counts number of the emulsion droplets as a function of time is given in **Figure 7-19**, **Figure 7-20**, and **Figure 7-21**, respectively. The counts number of small droplets (1<size<10 μm) decreased first and then increased (**Figure 7-19**). It is speculated that smaller droplets (size<1μm), which are below the detection limit of FBRM, can flocculate or coalesce at high demulsifier dosage (100 ppm of demulsifier B) to form relatively larger droplets (size>1 μm).

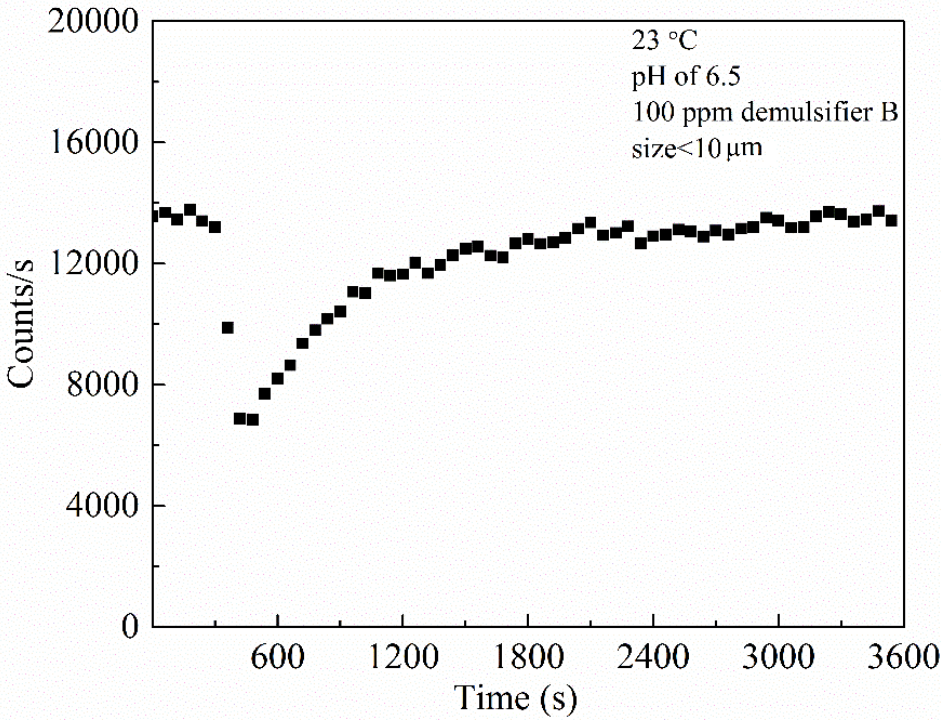

Figure 7-19 Counts number of the emulsion droplets with size less than 10 μm during demulsification of the water-in-naphtha diluted bitumen emulsions using 100 ppm demulsifier B as a function of the demulsification time.

As discussed in **3.1.2**, the change of the counts number in much larger droplets (10<size<50 μm or 50<size<150 μm) would influence the SWT CL dramatically. As can be seen in **Figure 7-20**, the counts number of the emulsion droplets (10<size<50 μm) shows an overall increasing trend, reaching an equilibrium of around 4000 counts/s, though a decrease was observed a few minutes after the demulsifier addition. The counts number of the emulsion droplets with the size larger than 50 μm (**Figure 7-21)** increased first, followed by a dramatic decrease. Therefore, the decrease in the counts number of droplets with sizes ranging from 10 to 150 μm led to the observed decrease in the SWT CL. As for why the counts number of droplets in this size range decreased over time, a possible reason is that the large droplets are consumed to form even larger droplets, which can settle down quickly and are not detected by FBRM.

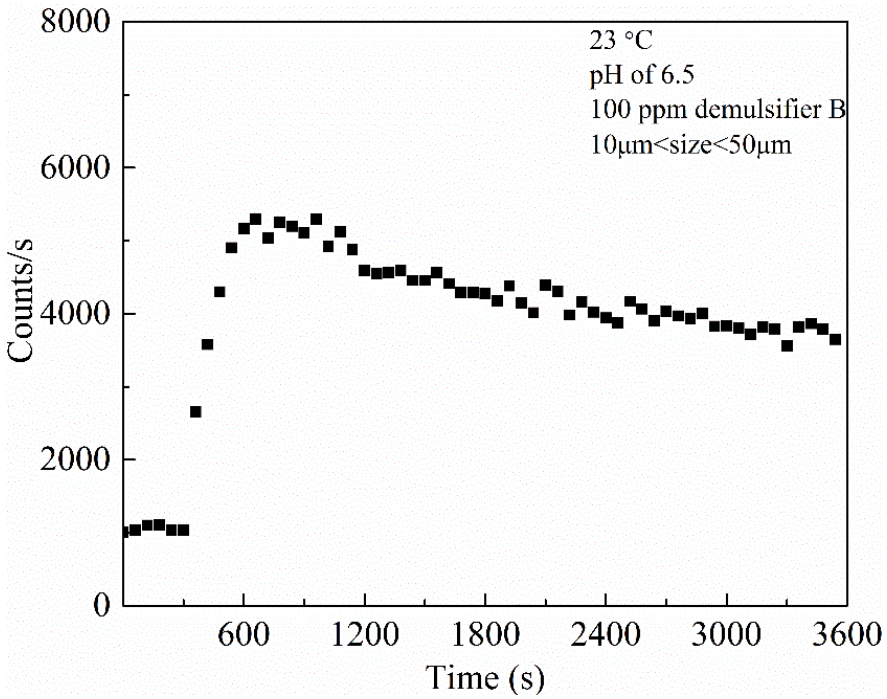

Figure 7-20 Counts number of emulsion droplets with size ranging from 10 to 50 μm during demulsification of the water-in-naphtha diluted bitumen emulsions using 100 ppm demulsifier B as a function of the demulsification time.

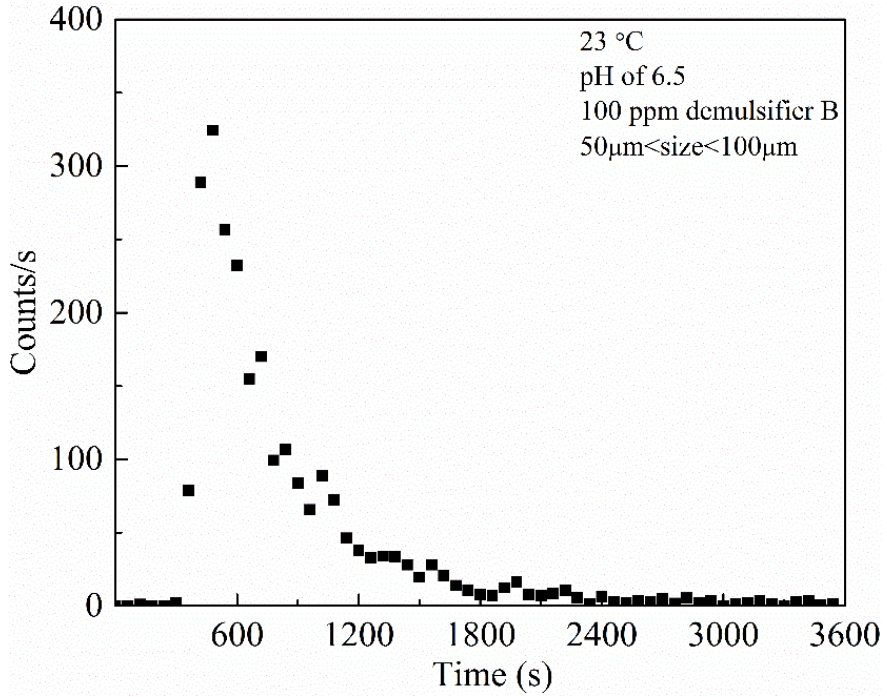

Figure 7-21 Counts number of emulsion droplets of size ranging from 50 to 150 μm during demulsification of the water-in-naphtha diluted bitumen emulsions using 100 ppm demulsifier B as a function of the demulsification time.

The CLDs in **Figure 7-22** and **Figure 7-23** appear to show that large droplets disappeared while the percentage of small droplets increased during the demulsification process. This, to some extent, proved the hypothesis that large droplets became further flocculated or coalesced to form even larger ones which cannot be detected by FBRM due to gravity settling. The increase of small droplets was mainly due to the flocculation or coalescence of smaller droplets originally below 1 μm.

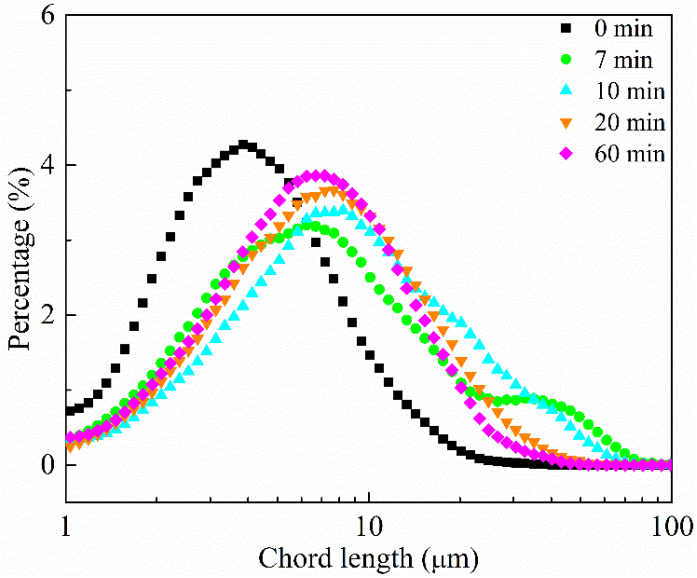

Figure 7-22 UWT CLD during demulsification of the water-in-naphtha diluted bitumen emulsions using 100 ppm demulsifier B at different demulsification time.

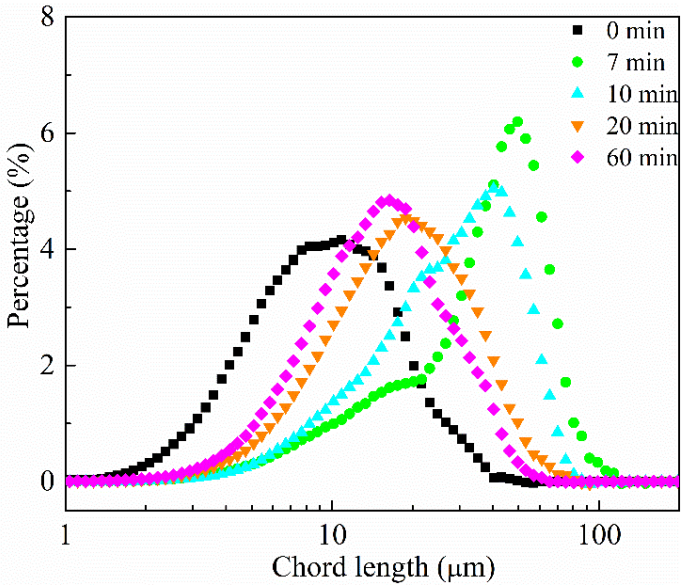

Figure 7-23 SWT CLD during demulsification of the water-in-naphtha diluted bitumen emulsions using 100 ppm demulsifier B at different demulsification time.

The results of the remaining water content (**Figure 7-24**) show that for each given settling time, 100 ppm of demulsifier B performed better than 50 ppm in dewatering the emulsions.

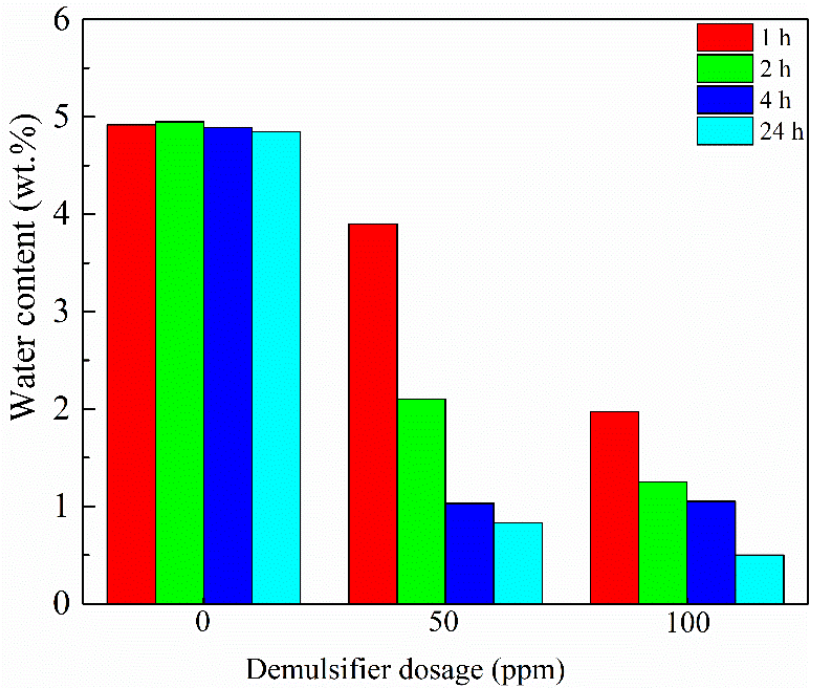

Figure 7-24 Water content remained in the water-in-naphtha diluted bitumen emulsions after the demulsification process at different dosages of demulsifier B.

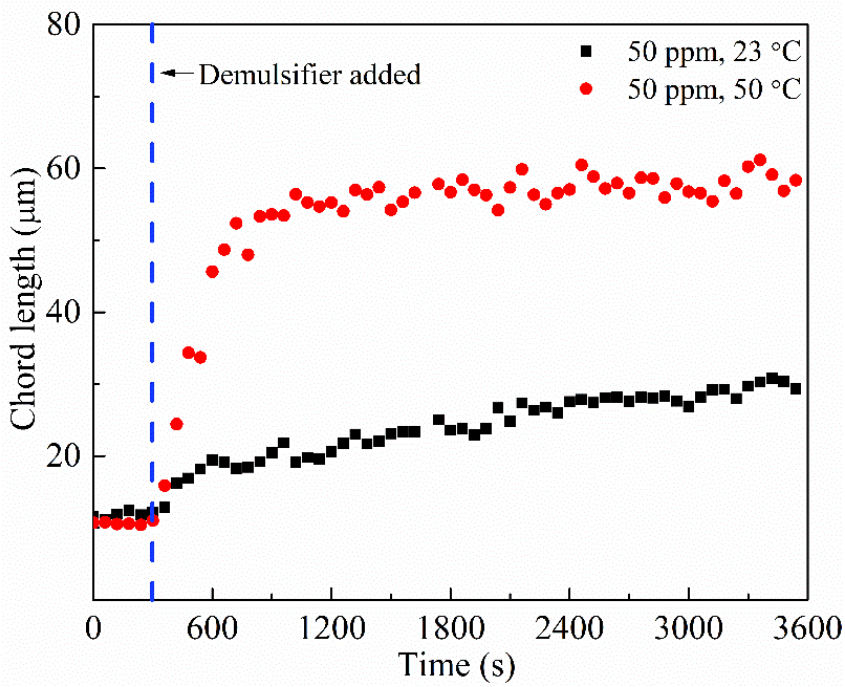

Figure 7-25 SWT CL during demulsification of the water-in-naphtha diluted bitumen emulsions using 50 ppm demulsifier B as a function of the demulsification time at different temperatures.

7.3.2.2 Temperature effect

As can be seen from **Figure 7-25**, the emulsion droplet size increased from 25 to 60 μm when increasing temperature from 23 °C to 50 °C. At 80 °C, very large water droplets, which can be seen even with naked eyes (**Figure 7-26**), were formed during the demulsification process. The large droplets settled so fast to the bottom of the sample after formation that they were not detected by FBRM. The chord length at 80 °C given by FBRM was therefore not representative for the system. However, it is safe to say that demulsifier B exhibited better performance in breaking the emulsion at 80 °C than lower temperatures (23 °C and 50 °C).

Figure 7-26 View of the emulsion sample at the bottom of autoclave after dewatering by 50 ppm demulsifier B at 80 °C.

From the UWT CLD and SWT CLD that are shown in **Figure 7-27** and **Figure 7-28**, it can be seen that there were more large droplets in the system after demulsification at 50 °C than that at 23 °C, indicating better dewatering efficiency at elevated temperature.

By analyzing the water content remained in the emulsions (**Figure 7-29)**, it is clear that the water content of the emulsion sample at 80 °C was the lowest, further confirming that high temperature can improve the demulsification performance of demulsifier B.

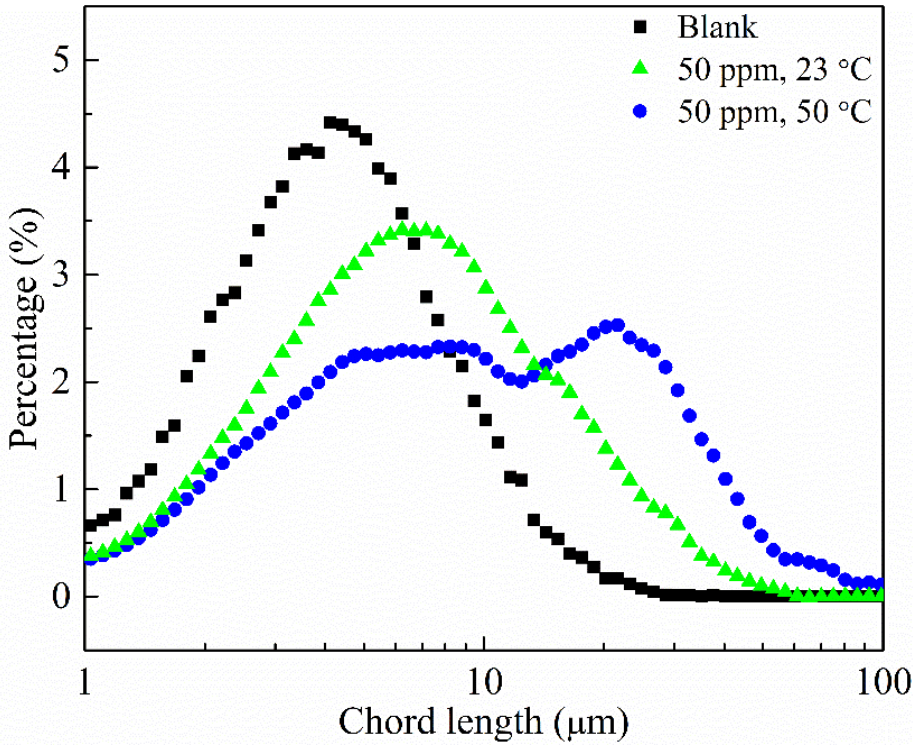

Figure 7-27 UWT CLD at steady state of the demulsification process using 50 ppm demulsifier B at different temperatures.

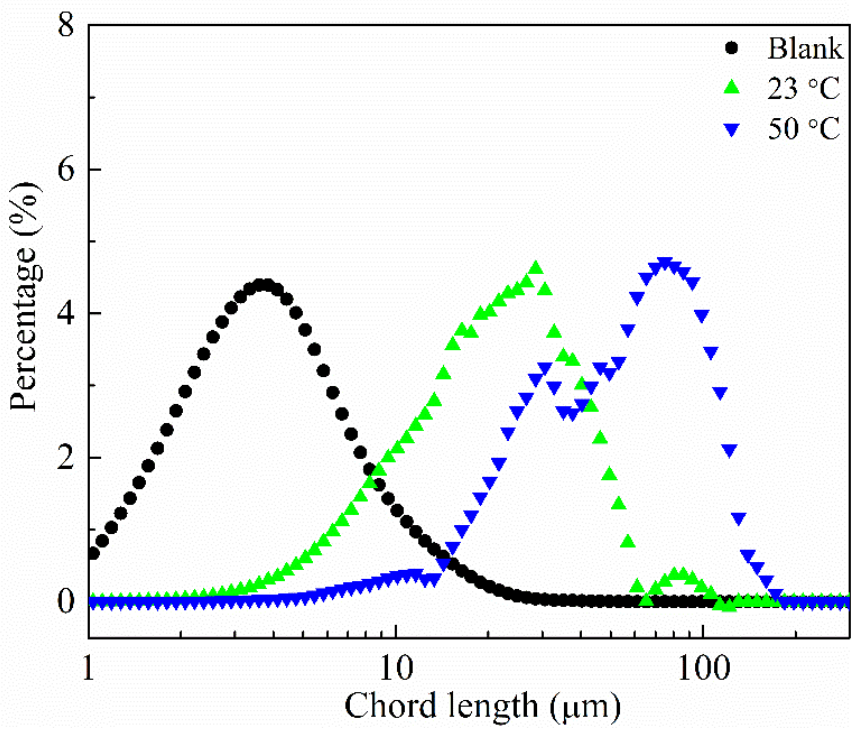

Figure 7-28 SWT CLD at steady state of the demulsification process using 50 ppm demulsifier B at different temperatures.

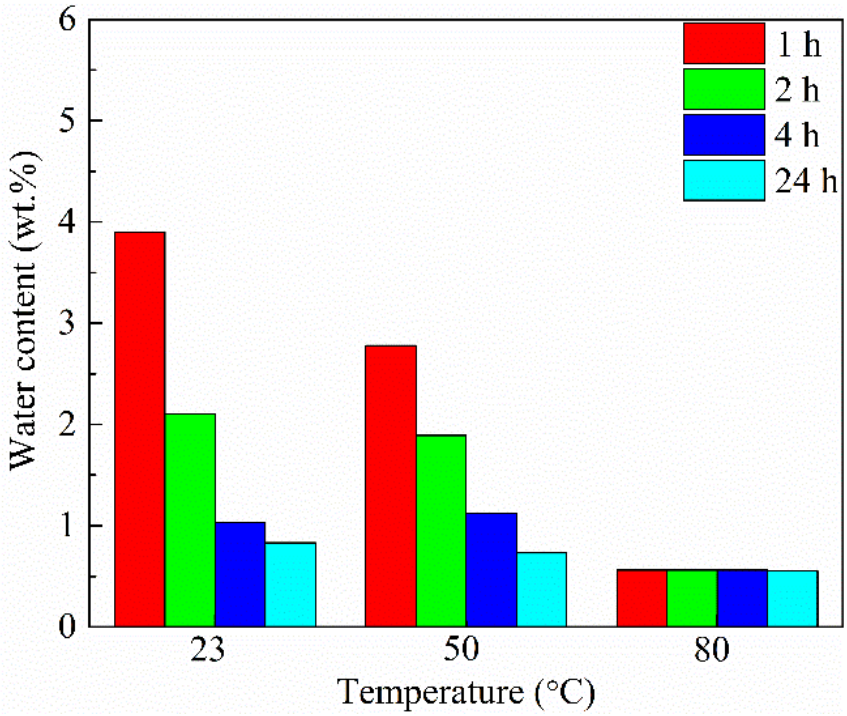

Figure 7-29 Water content remained in the water-in-naphtha diluted bitumen emulsions after the demulsification process by 50 ppm demulsifier B at different temperatures.

7.3.3 Comparison between demulsifier B and C

To compare the demulsification performance of demulsifier B and C, the emulsion droplet size measured by FBRM are compared in **Figure 7-30**. At each given temperature, the emulsion samples with the addition of demulsifier B always had larger droplet size than that of demulsifier C.

The UWT CLD and SWT CLD of the emulsion samples with the addition of demulsifier B or C are shown in **Figure 7-31** and **Figure 7-32**, respectively. It is observed that the emulsion samples with the addition of demulsifier B had less small droplets and more big droplets. The water content is compared in **Figure 7-33**, and the emulsion samples with the addition of demulsifier B always had lower water content than that with the addition of demulsifier C, as expected. Overall, demulsifier B showed better performance in emulsion breakup than demulsifier C. It was reported in the literature that demulsifier with higher molecular weight and larger arm number usually performs better in breaking emulsions (**Chapter 2**). As can be seen from **Table 7-1**, demulsifier B does have a higher molecular weight and larger arm number, which appears to be the reason for its better dewatering performance than that of demulsifier C.

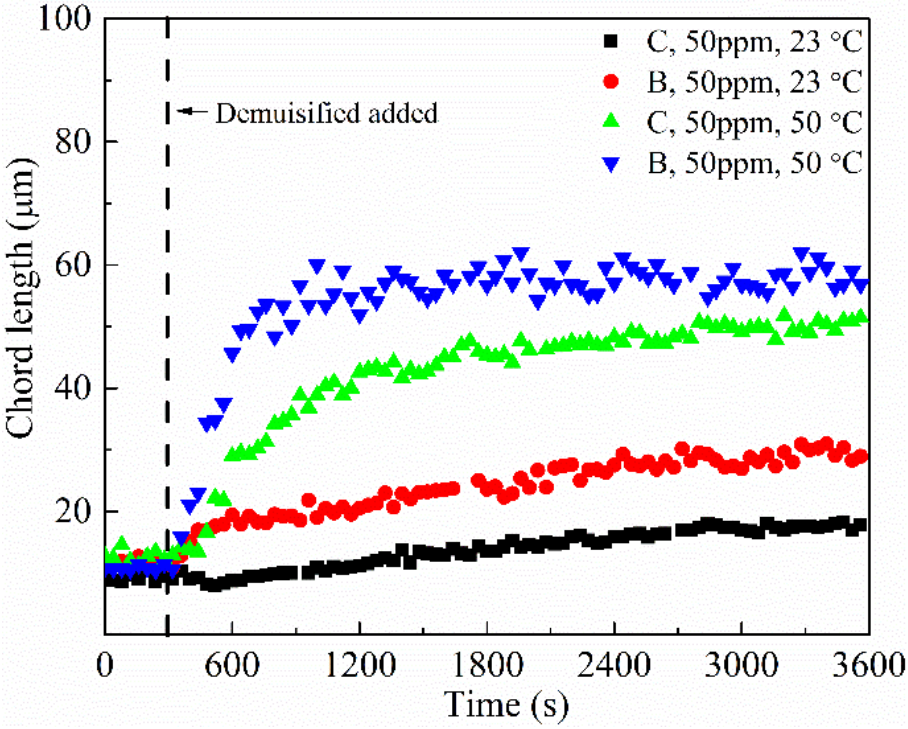

Figure 7-30 SWT CL during demulsification of the water-in-naphtha diluted bitumen emulsions using 50 ppm demulsifier B or C as a function of the demulsification time at different temperatures.

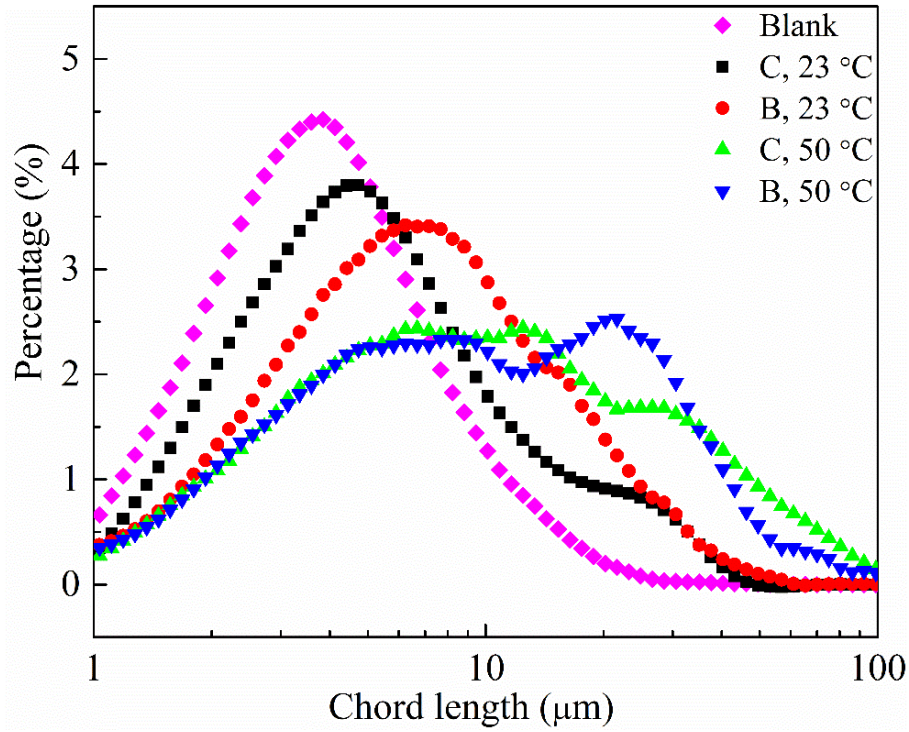

Figure 7-31 UWT CLD at steady state of the demulsification process using 50 ppm demulsifier B or C at different temperatures.

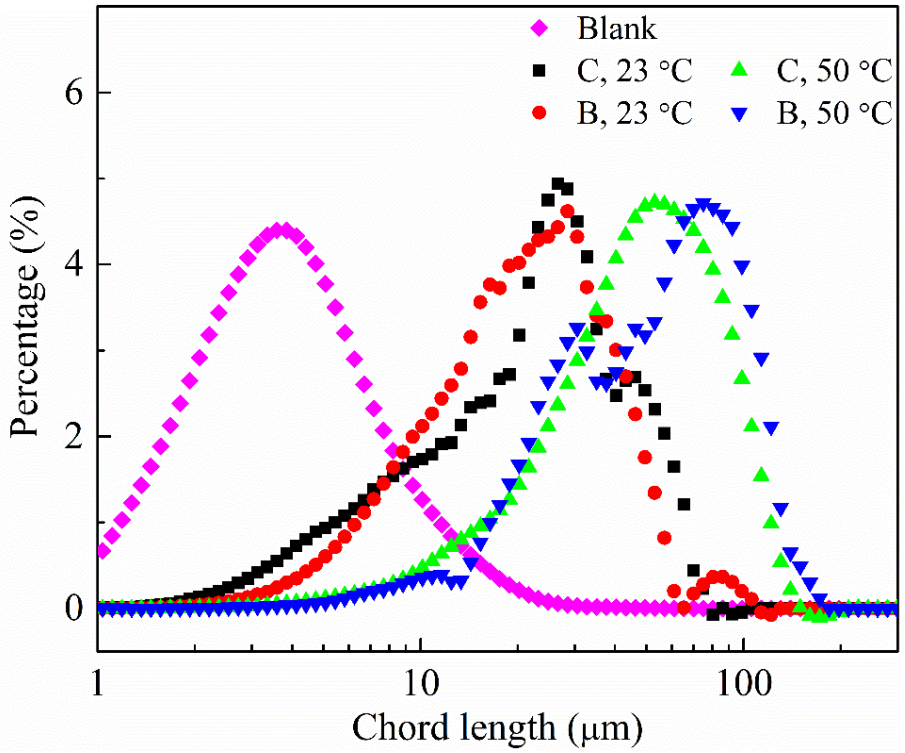

Figure 7-32 SWT CLD at steady state of the demulsification process using 50 ppm demulsifier B or C at different temperatures.

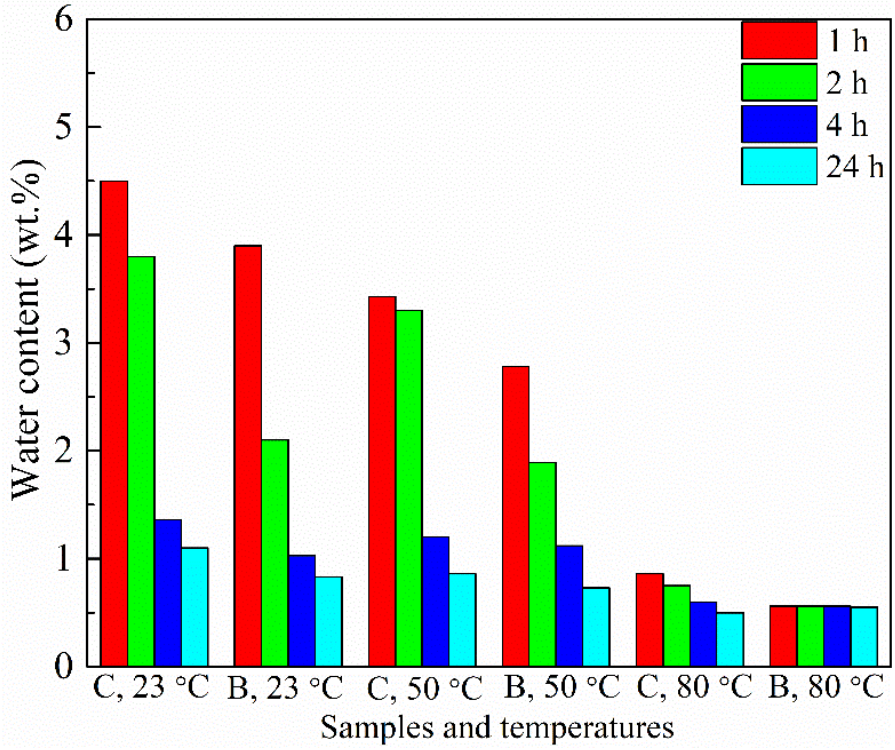

Figure 7-33 Water content remained in the water-in-naphtha diluted bitumen emulsions after demulsification by 50 ppm demulsifier B or C at different temperatures.

7.4 Interfacial properties

Having demonstrated that in a water-in-naphtha diluted bitumen system, the stability of the colloidal droplets can be significantly affected by adding EO-PO copolymer and increasing temperature, experiments were carried out to further investigate the interfacial properties of the systems with both the demulsifier concentration and temperature as the controlled parameters. The interfacial properties were studied in three different aspects: interfacial tension, crumpling ratio, and morphology of the water−diluted bitumen interfacial film. All the experiments discussed in this section were conducted on droplets of oil in water medium, as the measurements require good optical visibility of studied objects, and due to the dark and non-transparent nature of bitumen even in diluted samples, these measurements cannot be conducted in the reversed system (i.e., a water droplet in diluted bitumen). The feasibility of using the reversed O/W system to represent the original W/O system has been discussed in **Chapter 4** and **Chapter 5**. For interfacial tension and crumpling ratio measurements, the reversed O/W system can provide valuable qualitative information (**Chapter 4)** and the results obtained can be accepted as a demonstration of the general properties of the water−diluted bitumen interface. The effects of EO-PO molecules on the interfacial properties of the oil−water interface using asphaltene model compound as the oil phase have also been investigated and the results showed that EO-PO copolymer can work similarly to reduce the interfacial tension and crumpling ratio for both O/W and W/O systems (**Chapter 5**).

7.4.1 Dynamic interfacial tension

It is believed that the demulsification performance of EO-PO copolymers should arise from their interfacial activity at the diluted bitumen films, which competes against and displace the pre-adsorbed materials (i.e., asphaltene) at the interface to reduce the interfacial tension of the system.[15, 184, 212] To further probe the action of EO-PO copolymers at the interface between water and diluted bitumen, dynamic interfacial tension measurements were conducted using the pendant drop method and the dynamic interfacial tensions of the oil drop in DI water at 23 °C and 50 °C are shown in **Figure 7-34**. The naphtha diluted bitumen mixed with EO-PO copolymer at different dosage was used as the oil sample. Notable reduction of the interfacial tension was obtained with the increase in the demulsifier dosage, which was attributed to the effective penetration of the EO-PO molecules into the diluted bitumen films at the oil−water

interface. It should be noted that interfacial tensions that were obtained at elevated temperature (50 °C) were lower in general. The reduction of the interfacial tension became relatively less significant with the addition of demulsifier at high temperature (the equilibrium interfacial tension decrease by ~ 10 and 7 mN/m at 23 °C and 50 °C with 100 ppm demulsifier addition, respectively, in comparison with the demulsifier-free systems). This can be attributed to the enhanced interfacial activity of the active species in diluted bitumen, which in turn became more competitive at the interface and thus inhibited the adsorption of EO-PO copolymers. Furthermore, the results show a small decline in the interfacial tension within the first few minutes for all samples, indicating the diffusion process of the interfacial active species to the interface. However, for the samples with demulsifiers, such decline occurred within a relatively short time, as indicated by the larger slope at the initial stage. This observation corresponds to a faster adsorption kinetic at the interface, which further confirms the preferential adsorption of EO-PO copolymers at the oil−water interface. It should be noted that for bitumen-free systems with only the demulsifier as the interfacial active material, the interfacial tension was much lower as compared to the mixed system (diluted bitumen with demulsifier), which seems to imply that the adsorption of surface-active species from bitumen cannot be fully prevented by the demulsifier molecules at the interface, and hence these two species always coexist in a mixed system.

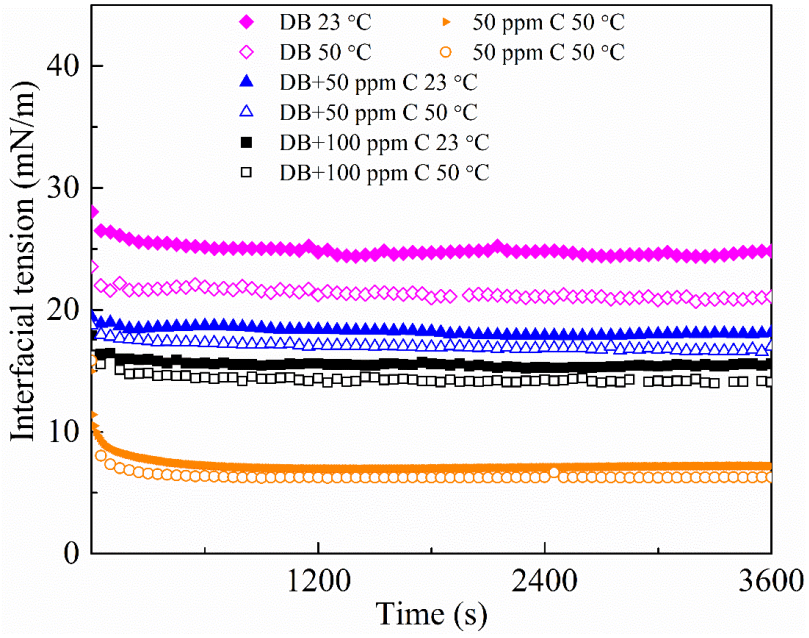

Figure 7-34 Dynamic oil−water interfacial tension of diluted bitumen, demulsifier C solution, and their mixture in naphtha at different temperatures. Note that DB denotes diluted bitumen.

Overall, the data revealed that the EO-PO copolymer has the potential to compete with the surface-active species in diluted bitumen for the naphtha−water interface, thereby softening or destroying the rigid film formed by these surface-active species contained in diluted bitumen (as indicated by the morphological changes and contraction behavior of the diluted bitumen film in the presence of EO-PO copolymer which will be discussed later). This finding also implies that increasing temperature can facilitate demulsification efficiency more effectively than merely increasing the demulsifier dosage.

Atta et al.[212] studied the demulsification performance of some EO-PO copolymers and linked the ability of the demulsifier to lower the interfacial tension with their demulsification performance. They found that successful dewatering occurred when the interfacial tension of the system was effectively reduced by the addition of EO-PO copolymers. However, although lower interfacial tension indicates lower interfacial energy, it does not necessarily link directly to high demulsification performance, with a lot of studies showing a lack of correlation between emulsion breakup efficiency and reduction of interfacial tension by demulsifier addition.[29, 44, 68, 213] More techniques should be used to investigate the demulsification mechanism.

7.4.2 Morphology of diluted bitumen−water interfacial film

Using Brewster Angle Microscopy (BAM), the effect of EO-PO demulsifier at the interface was further studied by characterizing the morphological effect of such demulsifiers on the diluted bitumen film.

For diluted bitumen, it is reported that the pale grey region in BAM image corresponds to the film structures[208, 214] while a dark appearance indicates no film structures. **Figure 7-35** (a) shows a BAM image for a demulsifier-free diluted bitumen film at the naphtha−water interface. As indicated by the pale grey region in **Figure 7-35** (a), a significant amount of film clusters was formed at the interface after aging for 1 h. Those clusters did not present different grey level, indicating the same thickness of film structures at the interface. It should be noted that for a clean interface, such as naphtha−water interface, the obtained BAM image showed a generally dark appearance which represents a surface with no cluster structures.

With the addition of EO-PO copolymer to the formed naphtha diluted bitumen film, these clusters observed in **Figure 7-35** (a) started to gradually disappear with increasing concentration

of demulsifier C (**Figure 7-35** (b) to **Figure 7-35** (d)). A clean interface was eventually obtained with 5 ppm demulsifier C added into the oil phase, as indicated by the entirely diminished light area from the dark background in **Figure 7-35** (d). These morphological changes of the interface with the addition of demulsifier C implied that the surface-active species, such as asphaltenes or resins in the diluted bitumen, would no longer stay at the interface once they were replaced. The interfacial film with 5 ppm demulsifier C-only system appeared to be the same as compared with clean naphtha−water interface (**Figure 7-35** (d)). No EO-PO aggregates could be observed at this concentration.

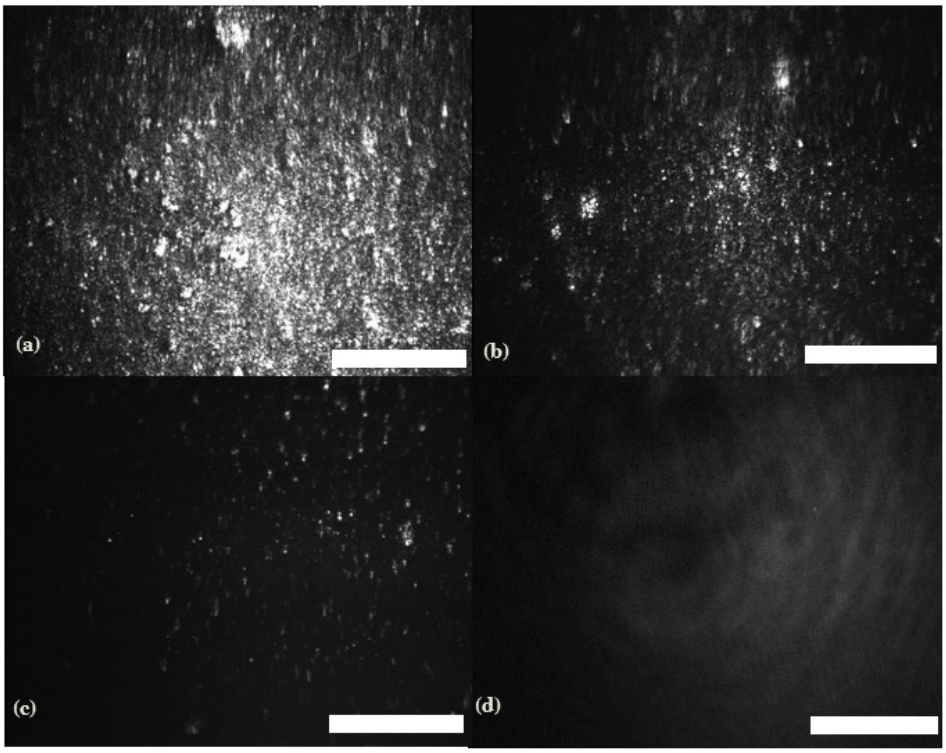

Figure 7-35 BAM images of diluted bitumen film (a) No demulsifier added, (b) 0.5 ppm, (c) 1 ppm, and (d) 5 ppm demulsifier added in the oil phase. The scale bar is 200 μm for all BAM images.

As indicated by the interfacial tension results, both surface-active molecules from diluted bitumen and EO-PO molecules should coexist at the interface. However, it should be noted that the interface studied in BAM experiments was different from those in other experiments discussed above. A flat oil−water interface was investigated in BAM experiments while the interface of an oil droplet in water was studied in all other experiments. Also, the concentration of the diluted bitumen was adjusted (~0.06 vol%) in order to optimize the contrast for BAM

images and therefore was very different from the systems discussed earlier. However, with the distinctively different morphology at the interface, results clearly demonstrated the presence of a protective film formed by the surface-active species from bitumen even at a very low concentration (~0.06 vol%), and also the ability of EO-PO copolymer to disrupt such species from the interface. This effect can be considered as a general interfacial behavior for both bitumen and the EO-PO copolymer, which should not be limited to the current studied system. Therefore, the same effect is also expected for much smaller structures, such as emulsion droplets. Nevertheless, it can be inferred that the displacement of surface-active species from diluted bitumen at the interface by EO-PO copolymer would reduce the coverage of the protective film of the emulsion droplets, and hence increase the possibility for the coalescence of emulsion droplets upon their collision. It is also possible that the EO-PO copolymer adsorbed at the interface could bridge two nearby droplets, enhancing the chance for coalescence.

7.4.3 Contraction behavior

Measurements of the dynamic interfacial tension proved that both surface-active species in diluted bitumen and EO-PO copolymers could adsorb at the oil−water interface though EO-PO copolymers exhibited a better interfacial activity. For the flat diluted bitumen−water interface, BAM was employed to observe the morphology of interfacial films with EO-PO copolymer addition. However, the effect of the EO-PO copolymer on the mechanical properties of the interfacial film around the emulsion water droplets has not been investigated. Volume contraction experiments were used to study the rigidity of the interfacial film of emulsion droplets. It is reported that by contracting the asphaltene films at the oil−water interface, an interfacial film of elastic nature was observed, which could prevent coalescence of emulsion droplets.[58, 215] Similarly, by studying the crumpling ratio obtained from volume contraction experiments on a pendant drop of naphtha diluted bitumen in water, we could further develop a better understanding on the behavior of diluted bitumen films and the effect of EO-PO polymers at interfaces.

In **Figure 7-36**, photos of the oil droplet captured in the crumping experiments are shown, in which I represents the initial state of an equilibrated oil droplet after aging for a desired time, II is the status right before crumpling, and III shows the first visible sign of crumpling for systems A−F. For systems N and O, no crumpling was detected and the droplet detached from the needle.

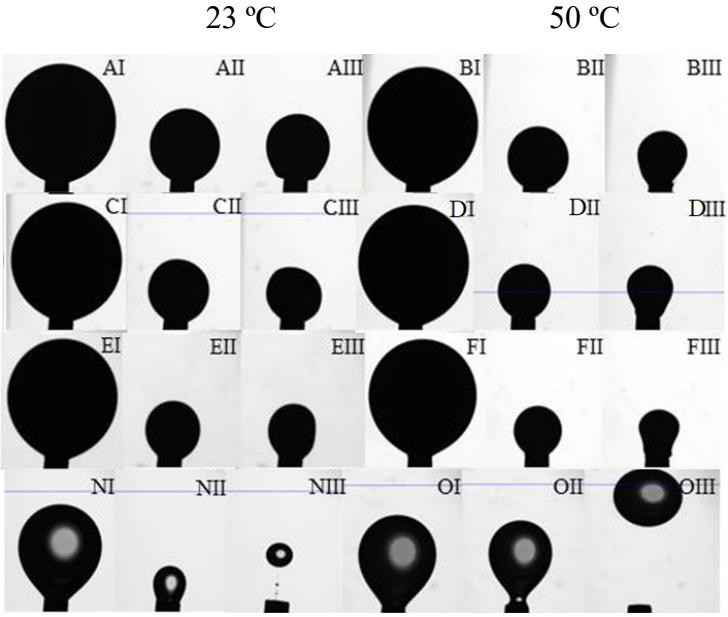

Figure 7-36 Crumpling of oil droplets measured by the pendant drop technique. Oil droplets aged for 1 h without demulsifier (A and B), with 50 ppm demulsifier C (C and D), with 100 ppm demulsifier C (E and F), and 50 ppm pure demulsifier C (N and O), respectively.

Results of volume contraction experiments are summarized in **Figure 7-37**. Each data point in **Figure 7-37** is an average of at least four independent measurements, and the error bars represent the standard deviation of all measurements. For the naphtha diluted bitumen droplet without the addition of demulsifier, the crumpling ratio was 0.39 at 23 ºC and 0.29 at 50 ºC, implying a reduced rigidity of the water-diluted bitumen interfacial film at high temperature. Upon mixing with EO-PO copolymers, the crumpling ratio was found to decrease with increasing dosage of the demulsifier at both 23 ºC and 50 ºC. The elevated temperature was more efficient in reducing the film rigidity than merely increasing the demulsifier dosage. It should be noted that the main contribution to the rigidity of the film should come from the asphaltene molecules present in the oil phase[128] whereas, for a surface fully adsorbed by the EO-PO copolymer, the film rigidity of the copolymer itself should be significantly lower and hence would not result in 'crumpling' of the drops.

The obtained crumpling ratios are consistent with the earlier conclusion obtained from the interfacial tension experiments: at room temperature, the EO-PO copolymers readily adsorb onto the water-diluted bitumen film and relax its rigidity, and high temperature/concentration enhanced this relaxation.

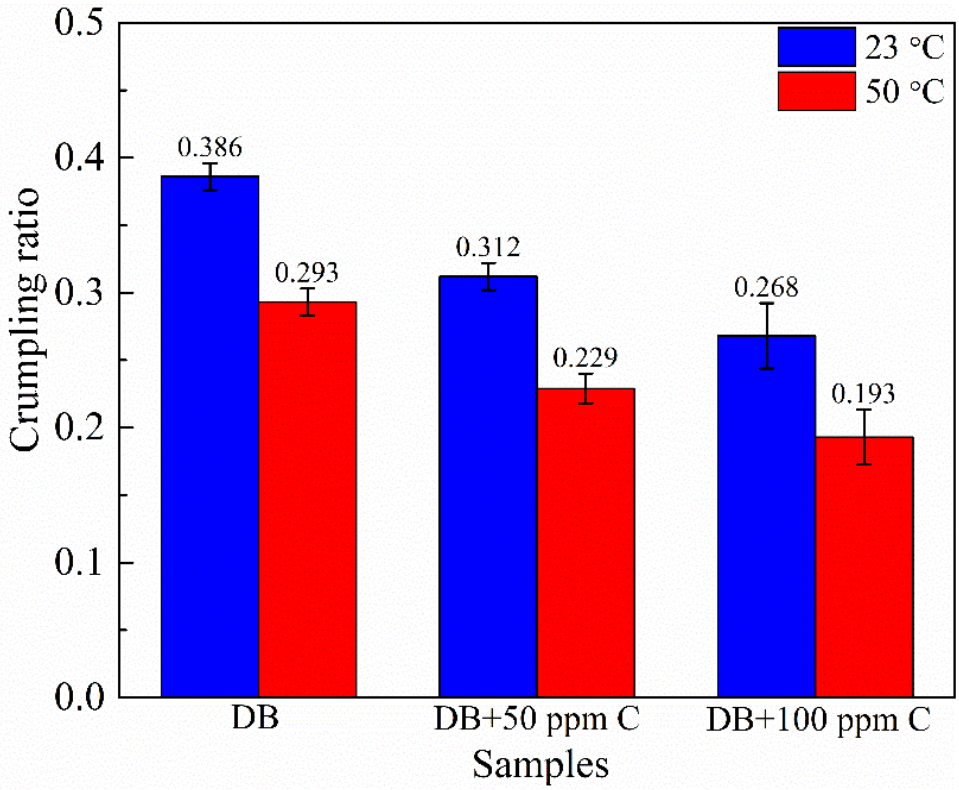

Figure 7-37 Crumpling ratio of naphtha diluted bitumen with and without demulsifier addition (DB denotes diluted bitumen, DB+50 ppm C denotes diluted bitumen containing 50 ppm demulsifier C, and so on)

7.5 Conclusions

By measuring the size of the emulsion droplets using FBRM during the demulsification process and determining the remaining water content in the emulsion samples using Karl Fisher Titrator after dewatering, the demulsification performance of the EO-PO copolymers in dewatering water-in-naphtha diluted bitumen emulsions was evaluated. The results of FBRM and remaining water content measurements showed an optimum performance of demulsifier C at 100 ppm. Increasing the dosage of demulsifier C resulted in a more efficient emulsion breakup. However, at higher dosages of demulsifier C (125 or 150 ppm), the demulsification performance degraded, showing overdose effect. It was also found that demulsifier C showed maximum performance over the neutral pH range. Increasing the temperature significantly increased the emulsion droplet size and decreased the remaining water content in emulsions, leading to a higher dewatering efficiency of demulsifier C. Demulsifier B showed a general better dewatering performance than demulsifier C. At 80 ºC for demulsifier B, very large water droplets, which can be seen even with naked eyes, were formed during the demulsification process. The better

demulsification performance of demulsifier B should be attributed to its higher molecular weight and larger arm number.

The properties of the diluted bitumen interfacial film and the effect of EO-PO demulsifiers on this film were probed by the dynamic interfacial tension, Brewster angle morphology, and volume contraction measurements. Reversed O/W system was used for the study of the interfacial properties. The results of interfacial tension measurement proved that EO-PO copolymers were more interfacially active than surface-active species in diluted bitumen and could compete effectively for the interface, especially at elevated temperatures. The results also indicated the co-existence of EO-PO copolymer and surface-active species in diluted bitumen at the oil−water interface. Brewster Angle Microscope results suggested the formation of interfacial film structures after aging and those film structures can be destroyed by EO-PO copolymers. Crumpling ratio measurements showed that the film rigidity reduced with the increase in the demulsifier dosage, indicating the ability of the EO-PO molecules to soften the interfacial film, and high temperature improved the performance of the EO-PO copolymer.

Chapter 8 Conclusions and Future Work

8.1 Conclusions

Establishing interfacial science to understand molecular mechanisms of stabilizing water in heavy crude oil (W/O) emulsions is challenging due to non-transparent nature of crude oil even in diluted systems, as most of the interfacial property measurements are based on visualization of the experimental systems. This study investigated whether interfacial properties measured using transparent O/W emulsion systems could be used to understand the stability of W/O emulsion systems. With the same chemistry of interfacially active polyaromatic compounds (C5Pe and C5PeC11) in xylene as the model oil, the interfacial tension, crumpling ratio, dilatational rheology, and coalescence time of W/O and O/W systems were measured. For less surface-active C5PeC11, the interfacial tensions for W/O and O/W systems were similar. For more surface-active C5Pe, the interfacial tension of the W/O system was always lower than that of the O/W system, while the film rigidity and viscoelasticity of the W/O system were higher than that of the O/W system. At low C5Pe concentration, the coalescence time for the W/O system was lower than that for the O/W system with the coalescence time for the W/O system being higher at higher C5Pe concentrations. The results revealed that even though the interfacial properties measured using reverse O/W system exhibit similar qualitative trends, care should be taken when quantitatively studying W/O emulsions using interfacial property measurements of the O/W emulsions due to the difference in most of the interfacial properties.

The effect of the EO-PO copolymer on the interfacial properties of the water−asphaltene model compound C5Pe/C5PeC11 interface was also investigated. By adding the EO-PO demulsifier, the interface between the asphaltene model compounds and water was changed. This study focused on investigating the adsorption replacement of C5Pe or C5PeC11 molecules by the EO-PO demulsifier molecules and the competitive adsorption between them. A reduction of the interfacial tension of the C5Pe or C5PeC11−water interface by EO-PO demulsifier addition for the W/O and O/W systems was observed, suggesting higher interfacial activities of the EO-PO demulsifier, especially at high EO-PO demulsifier concentrations. Crumpling ratios of the flat C5Pe−water interfacial film for W/O and O/W systems were also measured, and the results showed that the EO-PO demulsifier was capable of softening and weakening the interfacial films for both systems. The EO-PO demulsifier showed similar performance on changing the C5Pe

interfacial film through both diffusion (simulating the W/O system) and spreading (simulating the O/W system) protocols. By investigating the Langmuir interfacial−area isotherms, it was found that the C5Pe−water interfacial film became much more compressible with the addition of the EO-PO demulsifier. The EO-PO demulsifier could also destroy the integrity of the C5Pe interfacial film or avoid a networked film formation as indicated by atomic force microscopy images. In addition, shear rheology measurements showed that the rigidity of the C5Pe interfacial film was dramatically reduced or even absent in the presence of the EO-PO demulsifier. Moreover, the changes in the C5Pe−water interface by the EO-PO demulsifier were similar to those of the EO-PO/asphaltene system, providing further justification for using C5Pe as the asphaltene model compound.

In order to investigate the demulsification mechanism at the molecular level, molecular dynamics (MD) simulation was used to investigate the destabilization mechanism of the interfacial film. Asphaltene model compound C5Pe and EO-PO block copolymer were used as the emulsifier and demulsifier, respectively. Numerical results showed that C5Pe molecules are adsorbed at the oil−water interface in the form of C5Pe aggregates and EO-PO molecules could replace some of the adsorbed C5Pe molecules at the interface. In addition, the adsorbed EO-PO molecules could form a new surface barrier at the interface, which inhibited the adsorption of C5Pe molecules. The investigation of the EO-PO behavior at the oil−water interface in this study also provided information on how to design efficient demulsifiers.

In order to confirm if the demulsification performance could be enhanced by combining thermal energy and chemical treatment together, the demulsification performance of the EO-PO demulsifiers in dewatering the water-in-diluted bitumen emulsions at high temperature was studied. The naphtha diluted bitumen system was used as it is relatively close to the conditions in the oil industry. EO-PO copolymer was used as a demulsifier because it is a promising additive in breaking W/O emulsions. By applying FBRM and water content measurement, results have clearly demonstrated the effectiveness of the EO-PO copolymer as demulsifier in the diluted bitumen system, and with heat treatment applied in combination, the demulsification power can be further enhanced. The interfacial properties of the diluted bitumen droplets in water were studied by Theta Optical Tensiometer T200 and Brewster Angle Microscopy. In general, results confirmed that the surface-active species from bitumen formed a rigid film at the water−oil

interface that inhibited the coalescence of emulsion droplets. With the addition of the EO-PO copolymer, such surface-active species could be displaced from the interface and are no longer effective in stabilizing the emulsions. Furthermore, with elevated temperature, two possible demulsification mechanisms have been proposed regarding the different behaviors of the demulsifier: 1. A flocculation dominated process at low temperature, and 2. A coalescence dominated process at high temperature (above 80 °C), or for a long time scale (> 2 h) at low temperature.

Overall, by using asphaltene model compounds that have much better optical transparency as the oil samples, it was found that the interfacial properties of the W/O emulsions had the same qualitative trends as that of the O/W emulsions. When adding the EO-PO demulsifier to the W/O and O/W systems, similar changes were introduced to the stable C5Pe interfacial films by the EO-PO molecules through adsorption replacement or adsorption competition. Thus, our understanding regarding the feasibility of using the reverse O/W system to represent the W/O system was enhanced, especially when demulsifier is introduced. This enabled us to perform the demulsification tests using the water in diluted bitumen emulsions while studying the interfacial properties using the diluted bitumen droplets in water. The demulsification process could be greatly improved by high temperature as the adsorption of EO-PO molecules at the oil−water interface were enhanced at elevated temperatures. Through this study, a relationship between demulsification efficiency and operational factors is established that allows us to better design real industrial operations.

8.2 Future work

To distinguish between flocculation and coalescence of the droplets, interactions of the water droplets should be investigated by the micropipette technique.[184] In the case of flocculation, when separating two water droplets after bringing them into contact, the stretching and deformation of the water droplets due to the adhesion force between them can be observed before final separation. While in the case of coalescence, two water droplets will coalesce into one large droplet.

Experiment results showed that demulsifier B always shows better demulsification performance than demulsifier C. It is worth investigating the reason behind in order to design more effective

demulsifiers. EO-PO copolymers with various molecular weight, arm number, and EO content should be tested to achieve this objective.

Additionally, it is interesting to study the effect of pressure on dewatering efficiency, which can help to optimize the operational factors in the real industry. Pressure can be increased by increasing the demulsification temperature in a closed vessel or by injecting compressed air into a closed vessel.

Reference

1. Deffeyes K.S. Hubbert's Peak: The Impending World Oil Shortage (New Edition). *Princeton University Press* **2008**.

2. Hallock, J.L.; Tharakan, P.J.; Hall, C.A.S.; Jefferson, M.; Wu, W. Forecasting the Limits to the Availability and Diversity of Global Conventional Oil Supply. *Energy* **2004**, 29(11), 1673-1696.

3. Bentley, R.W. Global Oil & Gas Depletion: an Overview. *Energy Policy* **2002**, 30(3), 189-205.

4. Masliyah, J.H.; Czarnecki, J.; Xu, Z. Handbook on Theory and Practice of Bitumen Recovery From Athabasca Oil Sands, Volume 1: Theoretical Basis. *Canada: Kingsley Knowledge Publishing* **2011**, 1-39.

5. Alberta Culture and Tourism. Available at: http://www.history.alberta.ca.

6. Solovyev, A.; Zhang, L.Y.; Xu, Z.; Masliyah J. H. Langmuir Films of Bitumen at Oil/Water Interfaces. *Energy Fuels* **2006**, 20(4), 1572-1578.

7. Strausz, O. P. Bitumen and Heavy Oil chemistry. AOSTRA Technical Handbook on Oil Sands, Bitumens and Heavy Oils. *Alberta Oil Sands Technology and Research Authority*, **1989**.

8. Sjoblom, J.; Aske, N.; Auflem, I.H.; Brandala, Ø.; Havrea, T.E.; Sæthera, Ø.; Westvikb, A.; Johnsenb, E.E.; Kallevikb, H. Our Current Understanding of Water-in-Crude Oil Emulsions. Recent characterization techniques and high pressure performance. *Adv. Colloid Interface Sci.* **2003**, 100, 399-473.

9. Speight J.G. Petroleum Asphaltenes-Part 1: Asphaltenes, Resins and the Structure of Petroleum. *Oil Gas Sci. Technol.* **2004**, 59(5), 467-477.

10. Speight J.G. The Chemistry and Technology of coal. *CRC Press* **2012**.

11. Ortiz, D.P.; Baydak, E.N.; Yarranton, H.W. Effect of Surfactants on Interfacial Films and Stability of Water-in-Oil Emulsions Stabilized by Asphaltenes. *J. Colloid Interface Sci.* **2010**, 351(2), 542-555.

12. Akbarzadeh, K.; Bressler, D.C.; Wang, J.N.; Gawrys, K.L.; Gray, M.R.; Kilpatrick, P.K.; Yarranton, H.W. Association Behavior of Pyrene Compounds as Models for Asphaltenes. *Energy Fuels* **2005**, 19(4), 1268-1271.

13. Lopez-Linares, F.; Carbognani, L.; Gonzalez, M.F.;, Sosa-Stull, C.; Figueras, M.; Pereira-Almao, P. Quinolin 65 and Violanthrone-79 as Model Molecules for the Kinetics of the Adsorption of C7 Athabasca Asphaltene on Macroporous Solid Surfaces. *Energy Fuels,* **2006**, 20(6), 2748-2750.

14. Rakotondradany, F.; Fenniri, H.; Rahimi, P.; Gawrys, K.L.; Kilpatrick, P.K.; Gray, M.R. Hexabenzocoronene Model Compounds for Asphaltene Fractions: Synthesis & Characterization. *Energy Fuels* **2006**, 20(6), 2439-2447.

15. Masliyah, J.H.; Czarnecki, J.; Xu, Z. Handbook on Theory and Practice of Bitumen Recovery From Athabasca Oil Sands, Volume 1: Theoretical Basis. *Canada: Kingsley Knowledge Publishing* **2011**, 349-386.

16. Saadatmand, M.; Yarranton, H.W.; Moran, K. Rag Layers in Oil Sand Froths. *Ind. Eng. Chem. Res.* **2008**, 47(22), 8828-8839.

17. Masliyah, J.H.; Czarnecki, J.; Xu, Z. Handbook on Theory and Practice of Bitumen Recovery From Athabasca Oil Sands, Volume 1: Theoretical Basis. *Canada: Kingsley Knowledge Publishing* **2011**, 211-250.

18. Pandey, S.C.; Ralli, D.K.; Saxena, A.K.; Alamkhan, W.K. Physicochemical Characterization and Applications of Naphtha. *J. Sci. Ind. Res. India* **2004**, 63(3), 276-282.

19. McLean, J.D.; Kilpatrick, P.K. Effects of Asphaltene Solvency on Stability of Water-in-Crude-Oil Emulsions. *J. Colloid Interface Sci.* **1997**, 189(2), 242-253.

20. Farah, M.A.; Oliveira, R.C.; Caldas, J.N.; Rajagopal, K. Viscosity of Water-in-Oil Emulsions: Variation with Temperature and Water Volume Fraction. *J. Petrol. Sci. Eng.* **2005**, 48(3-4), 169-184.

21. Aomari, N.; Gaudu, R.; Cabioc'h, F.; Omari, A. Rheology of Water in Crude Oil Emulsions. *Colloid Surf. A-Physicochem. Eng. Asp.* **1998**, 139(1), 13-20.

22. Eley, D.D.; Hey, M.J.; Symonds, J.D. Emulsions of Water in Asphaltene-Containing Oils 2. Rheology. *Colloids Surf.* **1988**, 32(1-2), 103-112.

23. Hunter, R.J. Foundations of Colloid Science. *Clarendon, Oxford* **1987**.

24. Everett, D. Basic Principles of Colloid Science. *Royal Soc. Chem.* **1988**.

25. Lissant, K.J. Demulsification Industrial Applications. *Marcel Dekker, New York* **1983**.

26. Sjöblom, J.; Johnsen, E.; Westvik, A.; Ese, M.; Djuve, J.; Auflem, I.; Kallevik, H. Demulsifiers in the Oil Industry. *Encyclopedic handbook of emulsion technology, CRC Press* **2001**, 595-620.

27. Schramm, L.L. Emulsions: Fundamentals and Applications in the Petroleum Industry. *ACS, Washington* **1992**,1-49.

28. Zhang, L.Y.; Xu, Z.; Mashyah, J.H. Langmuir and Langmuir-Blodgett Films of Mixed Asphaltene and a Demulsifier. *Langmuir* **2003**, 19(23), 9730-9741.

29. Xu, Y.M.; Wu, J.Y.; Dabros, T.; Hamza, H.; Venter, J. Optimizing the Polyethylene Oxide and Polypropylene Oxide Contents in Diethylenetriamine-Based Surfactants for Destabilization of a Water-in-Oil Emulsion. *Energy Fuels* **2005**, 19(3), 916-921.

30. Wu, J.; Xu, Y.; Dabros, T.; Hamza, H. Effect of Demulsifier Properties on Destabilization of Water-in-Oil Emulsion. *Energy Fuels* **2003**, 17(6), 1554-1559.

31. Xu, Y.; Wu, J.; Dabros, T.; Hamza, H.; Wang, S.; Bidal, M.; Venter, J. Tran, T. Breaking Water-in-Bitumen Emulsions Using Polyoxyalkylated DETA Demulsifier. *Can. J. Chem. Eng.* **2004**, 82(4), 829-835.

32. Feng, J.; Fang, H.B.; Zong, H.; Zhang, L.; Zhang, L.; Zhao, S.; Yu, J.Y. Interfacial Dilational Properties of Two Different Structure Demulsifiers at Oil−Water Interfaces. *J. Dispersion Sci. Technol.* **2011**, 32(10), 1416-1421.

33. Kim, Y.H.; Wasan, D.T. Effect of Demulsifier Partitioning on the Destabilization of Water-in-Oil Emulsions. *Ind. Eng. Chem. Res.* **1996**, 35(4), 1141-1149.

34. Sun, T.; Zhang, L.; Wang, Y.; Zhao, S.; Peng, B.; Li, M.; Yu, J. Influence of Demulsifiers of Different Structures on Interfacial Dilational Properties of an Oil−Water Interface Containing Surface-Active Fractions from Crude Oil. *J. Colloid Interface Sci.* **2002**, 255(2), 241-247.

35. Feng, X.; Xu, Z.; Masliyah, J.H. Biodegradable Polymer for Demulsification of Water-in-Bitumen Emulsions. *Energy Fuels* **2008**, 23(1), 451-456.

36. Hou, J.; Feng, X.; Masliyah, J.H.; Xu, Z. Understanding Interfacial Behavior of Ethylcellulose at the Water-Diluted Bitumen Interface. *Energy Fuels* **2012**, 26(3):1740-1745.

37. Fan, Y.R.; Simon, S.; Sjoblom, J. Chemical Destabilization of Crude Oil Emulsions: Effect of Nonionic Surfactants as Emulsion Inhibitors. *Energy Fuels* **2009**, 23(9), 4575-4583.

38. Ese, M.H. Sjoblom, J.; Djuve, J.; Pugh, R. An Atomic Force Microscopy Study of Asphaltenes on Mica Surfaces. Influence of Added Resins and Demulsifiers. *Colloid Polym. Sci.* **2000**, 278(6), 532-538.

39. Fan, Y.R.; Simon, S.; Sjoblom, J. Interfacial Shear Rheology of Asphaltenes at Oil−Water Interface and its Relation to Emulsion Stability: Influence of Concentration, Solvent Rromaticity and Nonionic surfactant. *Colloid Surf. A-Physicochem. Eng. Asp.* **2010**, 366(1-3), 120-128.

40. Rondon, M.; Bouriat, P.; Lachaise, J.; Salager, J.L. Breaking of Water-in-Crude Oil Emulsions. 1. Physicochemical Phenomenology of Demulsifier Action. *Energy Fuels* **2006**, 20(4), 1600-1604.

41. Nguyen, D.; Sadeghi, N.; Houston, C. Chemical Interactions and Demulsifier Characteristics for Enhanced Oil Recovery Applications. *Energy Fuels* **2012**, 26(5), 2742-2750.

42. Angle, C.W.; Dabros, T.; Hamza, H.A. Demulsifier Effectiveness in Treating Heavy Oil Emulsion in The Presence of Fine Sands in the Production Fluids. *Energy Fuels* **2007**, 21(2), 912-919.

43. Wu, J.Y.; Xu, Y.M.; Dabros, T.; Hamza, H. Effect of EO and PO Positions in Nonionic Surfactants on Surfactant Properties and Demulsification Performance. *Colloid Surf. A-Physicochem. Eng. Asp.* **2005**, 252(1), 79-85.

44. Ramalho, J.B.; Ramos, N.; Lucas, E. The Influence of Some Interfacial Properties of PEO-b-PPO Copolymers on Dewatering of Water-in-Oil Asphaltene Model Emulsions. *Chem. Chem. Technol.* **2009**, 3, 53-58.

45. Abdel-Azim, A.-A. A.; Zaki, N. N.; Maysour, N. E. S. Polyoxyalkylenated Amines for Breaking Water-in-Oil Emulsions: Effect of Structural Variations on the Demulsification Efficiency. *Polym. Adv. Technol.* **1998**, 9(2), 159-166.

46. Zaki, N.; Abdel-Raouf, M. E.; Abdci-Azim, A.-A. A. Propylene Oxide-Ethylene Oxide Block Copolymers as Demulsifiers for Water-in-Oil Emulsions, II. Effects of

Temperature, Salinity, pH-Value, and Solvents on the Demulsification Efficiency. *Monatsh. Chem.* **1996**, 127 (12), 1239−1245.

47. Sullivan, A.P. Kilpatrick, P.K. The Effects of Inorganic Solid Particles on Water and Crude Oil Emulsion Stability. *Ind. Eng. Chem. Res.* **2002**, 41(14), 3389-3404.

48. Shetty, C.S.; Nikolov, A.D.; Wasan, D.T.; Bhattacharyya, B.R. Demulsification of Water in Oil-Emulsions Using Water-Soluble Demulsifiers. *J. Dispersion Sci. Technol.* **1992**, 13(2), 121-133.

49. Krawczyk, M.A.; Wasan, D.T.; Shetty, C.S. Chemical Demulsification of Petroleum Emulsions Using Oil-Soluble Demulsifiers. *Ind Eng Chem Res* **1991**, 30(2), 367-375.

50. Wasan D. Destabilization of Water-in-Oil Emulsions. *Emulsions: A Fundamental and Practical Approach, Springer* **1992**, 283-295.

51. Kim, Y.H.; Wasan, D.T.; Breen, P.J. A Study of Dynamic Interfacial Mechanisms for Demulsification of Water-in-Oil Emulsions. *Colloid Surf. A-Physicochem. Eng. Asp.* **1995**, 95(2-3), 235-247.

52. Hirato, T.; Koyama, K.; Tanaka, T.; Awakura, Y.; Majima, H. Demulsification of Water-in-Oil Emulsion by an Electrostatic Coalescence Method. *Mater. Trans.* **1991**, 32(3), 257-263.

53. Malhotra, A.K.; Wasan, D.T. Stability of Foam and Emulsion Films - Effects of the Drainage and Film Size on Critical Thickness of Rupture. *Chem. Eng. Commun.* **1986**, 48(1-3), 35-56.

54. Mukherjee, S.; Kushnick, A.P. Effect of Demulsifiers on the Interfacial Rheological Properties Governing Crude-Oil Demulsification. *Prepr.-Am. Chem. Soc., Div. Pet. Chem.* **1988**, 33 (1), 205.

55. Moran, K.; Czarnecki, J. Competitive Adsorption of Sodium Naphthenates and Naturally Occurring Species at Water-in-Crude Oil Emulsion Droplet Surfaces. *Colloid Surf. A-Physicochem. Eng. Asp.* **2007**, 292(2-3), 87-98.

56. Gelot, A.; Friesen, W.; Hamza, H.A. Emulsification of Oil and Water in the Presence of Finely Divided Solids and Surface-Active Agents. *Colloids Surf.* **1984**, 12(3-4), 271-303.

57. Tambe, D.E.; Sharma, M.M. Factors Controlling the Stability of Colloid-Stabilized Emulsions: I. An Experimental Investigation. *J. Colloid Interface Sci.* **1993**, 157(1), 244-253.

58. Tsamantakis, C.; Masliyah, J.h.; Yeung, A.; Gentzis, T. Investigation of the Interfacial Properties of Water-in-Diluted-Bitumen Emulsions Using Micropipette Techniques. *J. Colloid Interface Sci.* **2005**, 284(1), 176-183.

59. Menon, V.; Wasan, D. Particle-Fluid Interactions With Application to Solid-Stabilized Emulsions Part I. The Effect of Asphaltene Adsorption. *Colloid Surf.* **1986**, 19(1), 89-105.

60. Kimbler, O.K.; Reed, R.; Silberberg, I. Physical Characteristics of Natural Films Formed at Crude Oil−Water Interfaces. *SPE J.* **1966**, 6(02), 153-165.

61. Pfeiffer, J.P.; Saal R.N.J. Asphaltic Bitumen as Colloid System. *J. Phys. Chem.* **1940**, 44(2), 139-165.

62. Sjoblom, J.; Urdahl, O.; Borve, K.G.N.; Li, M.Y.; Saeten, J.O.; Christy, A.A.; Gu, T.R. Stabilization and Destabilization of Water-in-Crude Oil-Emulsions from the Norwegian Continental-Shelf - Correlation with Model Systems. *Adv. Colloid Interface Sci.* **1992**, 41, 241-271.

63. Ese, M.H.; Kilpatrick, P.K. Stabilization of Water-in-Oil Emulsions by Naphthenic Acids and Their Salts: Model Compounds, Role of pH, and Soap: Acid Ratio. *J. Dispersion Sci. Technol.* **2004**, 25(3), 253-261.

64. Mediaas, H.; Wolf, N.O.; Baugh, T.D.; Grande, K.V.; Vinstad, J.E. The Discovery of High Molecular Weight Naphthenic Acids (ARN Acid) Responsible for Calcium Naphthenate Deposits. Proceedings of the 7th Society of Petroleum Engineers (SPE) Oilfield Scale Symposium; Aberdeen, U.K., **2005**.

65. Verruto, V.J.; Le, R.K.; Kilpatrick, P.K. Adsorption and Molecular Rearrangement of Amphoteric Species at Oil−Water Interfaces. *J. Phys. Chem. B* **2009**, 113(42), 13788-13799.

66. Pena, A.A.; Hirasaki, G.J.; Miller, C.A. Chemically Induced Destabilization of Water-in-Crude Oil Emulsions. *Ind. Eng. Chem. Res.* **2005**, 44(5), 1139-1149.

67. Pelssers, E.G.M.; Stuart, M.A.C.; Fleer, G.J. Kinetic Aspects of Polymer Bridging - Equilibrium Flocculation and Nonequilibrium Flocculation. *Colloid Surf.* **1989**, 38(1-3), 15-25.

68. Kailey, I.; Feng, X. Influence of Structural Variations of Demulsifiers on their Performance. *Ind Eng Chem Res* **2013**, 52(2), 785-793.

69. Feng, X.; Wang, S.Q.; Hou, J.; Wang, L.X.; Cepuch, C.; Masliyah, J.H.; Xu, Z. Effect of Hydroxyl Content and Molecular Weight of Biodegradable Ethylcellulose on Demulsification of Water-in-Diluted Bitumen Emulsions. *Ind. Eng. Chem. Res.* **2011**, 50(10), 6347-6354.

70. Wu, H.Y.; Xu, Y.M.; Dabros, T.; Hamza, H. Development of a Method for Measurement of Relative Solubility of Nonionic Surfactants. *Colloid Surf. A-Physicochem. Eng. Asp.* **2004**, 232(2-3), 229-237.

71. Pensini, E.; Harbottle, D.; Yang, F.; Tchoukov,P.; Li, Z.; Kailey, I.; Behles, J. Masliyah, J.H.; Xu, Z. Demulsification Mechanism of Asphaltene-Stabilized Water-in-Oil Emulsions by a Polymeric Ethylene Oxide Propylene Oxide Demulsifier. *Energy Fuels* **2014**, 28(11), 6760-6771.

72. Romanova, U.G.; Yarranton, H.W.; Schramm, L.L.; Shelfantook, W.E. Investigation of Oil Sands Froth Treatment. *Can. J. Chem. Eng.* **2004**, 82(4), 710-721.

73. Menon, V.B.; Wasan, D.T. Characterization of Oil−Water Interfaces Containing Finely Divided Solids with Applications to the Coalescence of Water-in-Oil Emulsions: a Review. *Colloid Surf.* **1988**, 29(1), 7-27.

74. Barre, L.; Espinat, D.; Rosenberg, E.; Scarsella, M. Colloidal Structure of Heavy Crudes and Asphaltene Solutions. *Rev. Inst. Fr. Pet.* **1997**, 52(2), 161-175.

75. Acevedo, S.; Gutierrez, L.B.; Negrin, G.; Pereira, J.C.; Mendez, B.; Delolme, F.; Dessalces, G.; Broseta, D. Molecular Weight of Petroleum Asphaltenes: A Comparison Between Mass Spectrometry and Vapor Pressure Osmometry. *Energy Fuels* **2005**, 19(4), 1548-1560.

76. Sato, S.; Takanohashi, T.; Tanaka, R. Molecular Weight Calibration of Asphaltenes Using Gel Permeation Chromatography/Mass Spectrometry. *Energy Fuels* **2005**, 19(5), 1991-1994.

77. Pomerantz, A.E.; Hammond, M.R.; Morrow, A.L.; Mullins, O.C. Zare, R.N. Asphaltene Molecular-Mass Distribution Determined by Two-Step Laser Mass Spectrometry. *Energy Fuels* **2008**, 23(3), 1162-1168.

78. Andrews, A.B.; Shih, W.C.; Mullins, O.C.; Norinaga, K. Molecular Size Determination of Coal-Derived Asphaltene by Fluorescence Correlation Spectroscopy. *Appl. Spectrosc.* **2011**, 65(12), 1348-1356.

79. Schneider, M.H.; Andrews, A.B.; Mitra-Kirtley, S.; Mullins, O.C. Asphaltene Molecular Size by Fluorescence Correlation Spectroscopy. *Energy Fuels* **2007**, 21(5), 2875-2882.

80. Strausz, O.P.; Mojelsky, T.W.; Lown, E.M. The Molecular-Structure of Asphaltene: an Unfolding Story. *Fuel* **1992**, 71(12), 1355-1363.

81. Mojelsky, T.W.; Ignasiak, T.M.; Frakman, Z.; Mcintyre, D.D.; Lown, E.M.; Montgomery, D.S.; Strausz, O.P. Structural Features of Alberta Oil Sand Bitumen and Heavy Oil Asphaltenes. *Energy Fuels* **1992**, 6(1), 83-96.

82. Groenzin, H.; Mullins, O.C. Asphaltene Molecular Size and Weight by Time-Resolved Fluorescence Depolarization. *Asphaltenes, Heavy oils, and Petroleomics, Springer* **2007**, 17-62.

83. Sharma, A.; Groenzin, H.; Tomita, A.; Mullins, O.C. Probing Order in Asphaltenes and Aromatic Ring Systems by HRTEM. *Energy Fuels* **2002**, 16(2), 490-496.

84. Ruiz-Morales, Y.; Mullins, O.C. Measured and Simulated Electronic Absorption and Emission Spectra of Asphaltenes. *Energy Fuels* **2009**, 23(3-4), 1169-1177.

85. Betancourt, S.S.; Ventura, G.T.; Pomerantz, A.E.; Viloria, O.; Dubost, F.X.; Zuo, J.; Monson, G.; Bustamant, D.; Purcell, J.M.; Nelson, R.K.; Rodgers, R.P.; Reddy, C.M.; Marshall, A.G.; Mullins, O.C. Nanoaggregates of Asphaltenes in a Reservoir Crude oil and Reservoir Connectivity. *Energy Fuels* **2008**, 23(3), 1178-1188.

86. Fenistein, D.; Barre, L.; Experimental Measurement of the Mass Distribution of Petroleum Asphaltene Aggregates Using Ultracentrifugation and Small-Angle X-ray Scattering. *Fuel* **2001**, 80(2), 283-287.

87. Simon, S.B.; Jestin, J.; Palermo, T.; Barré, L.C. Relation Between Solution and Interfacial Properties of Asphaltene Aggregates. *Energy Fuels* **2008**, 23(1), 306-313.

88. Espinat, D.; Fenistein, D.; Barre, L.; Frot, D.; Briolant, Y. Effects of Temperature and Pressure on Asphaltenes Agglomeration in Toluene. A light, X-ray, and Neutron Scattering Investigation. *Energy Fuels* **2004**, 18(5), 1243-1249.

89. Spiecker, P.M.; Gawrys, K.L.; Trail, C.B.; Kilpatrick, P.K. Effects of Petroleum Resins on Asphaltene Aggregation and Water-in-Oil Emulsion Formation. *Colloid Surf. A-Physicochem. Eng. Asp* **2003**, 220(1-3), 9-27.

90. Dickie, J.P.; Yen, T.F. Macrostructures of the Asphaltic Fractions by Various Instrumental Methods. *Anal. Chem.* **1967**, 39(14), 1847-1852.

91. Mullins, O.C. The Modified Yen Model. *Energy Fuels* **2010**, 24(4), 2179-2207.

92. Gray, M.R.; Tykwinski, R.R.; Stryker, J.M.; Tan, X.L. Supramolecular Assembly Model for Aggregation of Petroleum Asphaltenes. *Energy Fuels* **2011**, 25(7), 3125-3134.

93. Yarranton, H.W.; Ortiz, D.P.; Barrera, D.M.; Baydak, E. N.; Barré, L.; Frot, D.; Eyssautier, J.; Zeng, H.; Xu, Z.; Dechaine, G.; Becerra, M.; Shaw, J. M.; McKenna, A. M.; Mapolelo, M. M.; Bohne, C. ; Yang, Z.; Oake, J. On the Size Distribution of Self-Associated Asphaltenes. *Energy Fuels* **2013**, 27(9), 5083-5106.

94. Liu, J.J.; Zhang, L.Y.; Xu, Z.; Masliyah, J.H. Colloidal Interactions Between Asphaltene Surfaces in Aqueous Solutions. *Langmuir* **2006**, 22(4), 1485-1492.

95. Wang, S.; Liu, J.; Zhang, L.; Masliyah, J.H.; Xu, Z. Interaction Forces Between Asphaltene Surfaces in Organic Solvents. *Langmuir* **2009**, 26(1), 183-190.

96. Sheremata, J.M.; Gray, M.R.; Dettman, H.D.; McCaffrey, W.C. Quantitative Molecular Representation and Sequential Optimization of Athabasca Asphaltenes. *Energy Fuels* **2004**, 18(5), 1377-1384.

97. Boek, E.S.; Yakovlev, D.S.; Headen, T.F. Quantitative Molecular Representation of Asphaltenes and Molecular Dynamics Simulation of their Aggregation. *Energy Fuels* **2009**, 23(3-4), 1209-1219.

98. Nordgard, E.L.; Landsem, E.; Sjoblom, J. Langmuir Films of Asphaltene Model Compounds and their Fluorescent Properties. *Langmuir* **2008**, 24(16), 8742-8751.

99. Nordgård E.L.; Sjöblom, J. Model Compounds for Asphaltenes and C80 Isoprenoid Tetraacids. Part I: Synthesis and Interfacial Activities. *J. Dispersion Sci. Technol.* **2008**, 29(8), 1114-1122.

100. Nordgård, E.L.; Sørland, G.; Sjöblom, J. Behavior of Asphaltene Model Compounds at W/O Interfaces. *Langmuir* **2009**, 26(4), 2352-2360.

101. Rogel, E. Asphaltene Aggregation: A Molecular Thermodynamic Approach. *Langmuir,* **2002**, 18(5), 1928-1937.

102. Gawrys, K.L.; Spiecker, P.M.; Kilpatrick, P.K. The Role of Asphaltene Solubility and Chemical Composition on Asphaltene Aggregation. *Pet. Sci. Technol.* **2003**, 21(3-4), 461-489.

103. Pradilla, D.; Subramanian, S.; Simon, S.; Sjoblom. J.; Beurroies, I.; Denoyel, R. Microcalorimetry Study of the Adsorption of Asphaltenes and Asphaltene Model Compounds at the Liquid-Solid Surface. *Langmuir* **2016**, 32(29), 7294-7305.

104. Wang, J.; Opedal, N.V.D.T.; Lu, Q.; Xu, Z.; Zeng. H.; Sjöblom, J. Probing Molecular Interactions of an Asphaltene Model Compound in Organic Solvents Using a Surface Forces Apparatus (SFA). *Energy Fuels* **2011**, 26(5), 2591-2599.

105. Wang, J.; Lu, Q.; Harbottle, D.; Sjoblom, J.; Xu, Z.; Zeng, H. Molecular Interactions of a Polyaromatic Surfactant C5Pe in Aqueous Solutions Studied by a Surface Forces Apparatus. *J. Phys. Chem. B* **2012**, 116(36), 11187-11196.

106. Bi, J.; Yang, F.; Harbottle, D.; Pensini, E.; Tchoukov, P. Simon, S.; Sjöblom, J.; Dabros, T.; Czarnecki, J.; Liu, Q.; Xu, Z. Interfacial Layer Properties of a Polyaromatic Compound and its Role in Stabilizing Water-in-Oil Emulsions. *Langmuir* **2015**, 31(38), 10382-10391.

107. Pradilla, D.; Simon, S.; Sjoblom, J.; Samaniuk, J.; Skrzypiec, M.; Vermant, J. Sorption and Interfacial Rheology Study of Model Asphaltene Compounds. *Langmuir* **2016**, 32(12), 2900-2911.

108. Grimes, B.; Dorao, C.; Simon, S.; Nordgård, E.; Sjöblom, J. Analysis of Dynamic Surfactant Mass Transfer and its Relationship to the Transient Stabilization of Coalescing Liquid–Liquid Dispersions. *J. Colloid Interface Sci.* **2010**, 348(2), 479-490.

109. Barre, L.; Jestin, J.; Morisset, A.; Palermo, T.; Simon, S. Relation Between Nanoscale Structure of Asphaltene Aggregates and their Macroscopic Solution Properties. *Oil Gas Sci. Technol.* **2009**, 64(5), 617-628.

110. Liu, L.; Sjoblom, J.; Xu, Z. Nanoaggregation of Polyaromatic Compounds Probed by Electrospray Ionization Mass Spectrometry. *Energy Fuels* **2016**, 30(5), 3742-3751.

111. Teklebrhan, R.B.; Ge, L.L.; Bhattacharjee, S.; Xu, Z.; Sjoblom, J. Initial Partition and Aggregation of Uncharged Polyaromatic Molecules at the Oil−Water Interface: A Molecular Dynamics Simulation Study. *J. Phys. Chem. B* **2014**, 118(4), 1040-1051.

112. Jian, C.Y.; Tang, T.; Bhattacharjee, S. Probing the Effect of Side-Chain Length on the Aggregation of a Model Asphaltene Using Molecular Dynamics Simulations. *Energy Fuels* **2013**, 27(4), 2057-2067.

113. Kuznicki, T.; Masliyah, J.H.; Bhattacharjee, S. Aggregation and Partitioning of Model Asphaltenes at Toluene−Water Interfaces: Molecular Dynamics Simulations. *Energy Fuels* **2009**, 23(10), 5027-5035.

114. Kuznicki, T.; Masliyah, J.H.; Bhattacharjee, S. Molecular Dynamics Study of Model Molecules Resembling Asphaltene-Like Structures in Aqueous Organic Solvent Systems. *Energy Fuels* **2008**, 22(4), 2379-2389.

115. Gao, F.; Xu, Z.; Liu, G.; Yuan, S. Molecular Dynamics Simulation: the Behavior of Asphaltene in Crude Oil and at the Oil/Water Interface. *Energy Fuels* **2014**, 28(12), 7368-7376.

116. Jian, C.Y.; Zeng, H.; Liu, Q.; Tang, T. Probing the Adsorption of Polycyclic Aromatic Compounds onto Water Droplets Using Molecular Dynamics Simulations. *J. Phys. Chem. C* **2016**, 120(26), 14170-4179.

117. Andrews, A.B.; McClelland, A.; Korkeila, O.; Demidov, A.; Krummel, A.; Mullins, O.C.; Chen, Z. Molecular Orientation of Asphaltenes and PAH Model Compounds in Langmuir−Blodgett Films Using Sum Frequency Generation Spectroscopy. *Langmuir* **2011**; 27(10), 6049-6058.

118. FBRM. Available at: www.mt.com/distribution/fbrm

119. Li, M.; Wilkinson, D.; Patchigolla, K. Comparison of Particle Size Distributions Measured Using Different Techniques. *Part. Sci. Technol.* **2005**, 23(3), 265-284.

120. Ruf, A.; Worlitschek, J.; Mazzotti, M. Modeling and Experimental Analysis of PSD Measurements through FBRM. *Part. Part. Syst. Char.* **2000**, 17(4), 167-179.

121. Worlitschek. J.; Hocker, T.; Mazzotti, M. Restoration of PSD From Chord Length Distribution Data Using the Method of Projections onto Convex Sets. *Part. Part. Syst. Char.* **2005**, 22(2), 81-98.

122. Hu. X.; Cunningham, J.C.; Winstead, D. Study Growth Kinetics in Fluidized Bed Granulation with at-Line FBRM. *Int. J. Pharm.* **2008**, 347(1), 54-61.

123. Chen, Z.; Peng, J.; Ge, L.; Xu, Z. Demulsifying Water-in-Oil Emulsions by Ethyl Cellulose Demulsifiers Studied Using Focused Beam Reflectance Measurement. *Chem. Eng. Sci.* **2015**, 130, 254-263.

124. Wang, L.; Sharp, D.; Masliyah, J.H.; Xu, Z. Measurement of Interactions Between Solid Particles, Liquid Droplets, and/or Gas Bubbles in a Liquid Using an Integrated Thin Film Drainage Apparatus. *Langmuir* **2013**, 29(11), 3594-3603.

125. Gao, S. Stability of Water-in-Diluted Bitumen Emulsion Droplets. *University of Alberta* **2010**.

126. Stauffer, C.E. The Measurement of Surface Tension by the Pendant Drop Technique. *J. Phys. Chem.* **1965**, 69(6), 1933-1938.

127. Yeung, A.; Dabros, T.; Masliyah, J.H.; Czarnecki, J. Micropipette: a New Technique in Emulsion Research. *Colloid Surf. A-Physicochem. Eng. Asp* **2000**, 174(1-2), 169-181.

128. Yeung, A.; Dabros, T.; Czarnecki, J.; Masliyah, J.H. On the Interfacial Properties of Micrometre–Sized Water Droplets in Crude Oil. *Proceedings of the Royal Society of London. Series A: Mathematical, Physical and Engineering Sciences 455* **1990**, 3709-3723.

129. Shaw, R.C.; Schramm, L.L.; Czarnecki, J. Suspensions in the Hot Water Flotation Process for Canadian Oil sands. *Adv. Chem. Ser.* **1996**, 251(251), 639-675.

130. Liggieri, L.; Ferrari, M.; Mondelli, D.; Ravera, F. Surface Rheology as a Tool For the Investigation of Processes Internal to Surfactant Adsorption Layers. *Faraday Discuss.* **2005**, 129, 125-140.

131. Myrvold, R.; Hansen, F.K. Surface Elasticity and Viscosity from Oscillating Bubbles Measured by Automatic Axisymmetric Drop Shape Analysis. *J. Colloid Interface Sci.* **1998**, 207(1), 97-105.

132. Kragel, J.; Derkatch, S.R. Interfacial Shear Rheology. *Curr. Opin. Colloid Interface Sci.* **2010**, 15(4), 246-255.

133. Vandebril, S.; Franck, A.; Fuller, G.G.; Moldenaers, P.; Vermant, J. A double Wall-Ring Geometry for Interfacial Shear Rheometry. *Rheol. Acta* **2010**, 49(2), 131-144.

134. Xu, R.; Dickinson, E.; Murray, B.S. Morphological Changes in Adsorbed Protein Films at the Oil−Water Interface Subjected to Compression, Expansion, and Heat Processing. *Langmuir* **2008**, 24(5), 1979-1988.

135. Murray, B.S.; Xu, R,.; Dickinson, E. Brewster Angle Microscopy of Adsorbed Protein Films at Air–Water and Oil–Water Interfaces After Compression, Expansion and Heat Processing. *Food Hydrocolloids* **2009**, 23(4), 1190-1197.

136. Yan, Z.; Elliott, J.A.; Masliyah, J.H. Roles of Various Bitumen Components in the Stability of Water-in-Diluted-Bitumen Emulsions. *J. Colloid Interface Sci.* **1999**, 220(2), 329-337.

137. Yarranton, H.W.; Hussein, H.; Masliyah, J.H. Water-in-Hydrocarbon Emulsions Stabilized by Asphaltenes at Low Concentrations. *J. Colloid Interface Sci.* **2000**, 228(1), 52-63.

138. Angle, C.W. Chemical Demulsification of Stable Crude Oil and Bitumen Emulsions in Petroleum Recovery: a Review. *Encyclopedic handbook of emulsion technology*: *CRC Press* **2001**, 541-594.

139. Siffert, B.; Bourgeois, C.; Papirer, E. Structure and Water—Oil Emulsifying Properties of Asphaltenes. *Fuel* **1984**, 63(6), 834-837.

140. Nordli, K.G.; Sjöblom, J.; Kizling, J.; Stenius, P. Water-in-Crude Oil Emulsions From the Norwegian Continental Shelf 4. Monolayer Properties of the Interfacially Active Crude Oil Fraction. *Colloids Surf.* **1991**, 57(1), 83-98.

141. Sheu, E.Y.; Maureen, M.; Storm, D.A.; DeCanio, S.J. Aggregation and Kinetics of Asphaltenes in Organic Solvents. *Fuel* **1992**, 71(3), 299-302.

142. Mohammed, R.; Bailey, A.; Luckham, P.; Taylor, S. Dewatering of Crude Oil Emulsions 2. Interfacial Properties of the Asphaltic Constituents of Crude Oil. *Colloid Surf. A-Physicochem. Eng. Asp.* **1993**, 80(2), 237-242.

143. Mohammed, R.; Bailey, A.; Luckham, P.; Taylor, S. Dewatering of Crude Oil Emulsions 3. Emulsion Resolution by Chemical Means. *Colloid Surf. A-Physicochem. Eng. Asp* **1994**, 83(3), 261-271.

144. Sun, T.; Zhang, L.; Wang, Y.; Zhao, S.; Peng. B.; Li, M.; Yu, J. Influence of Demulsifiers of Different Structures on Interfacial Dilational Properties of an Oil–Water Interface Containing Surface-Active Fractions from Crude Oil. *J. Colloid Interface Sci.* **2002**, 255(2), 241-247.

145. Ese M-H, Galet L, Clausse D, Sjöblom J. Properties of Langmuir Surface and Interfacial Films Built up by Asphaltenes and Resins: Influence of Chemical Demulsifiers. *J. Colloid Interface Sci.* **1999**, 220(2), 293-301.

146. Fan, Y.; Simon, S.; Sjöblom, J. Chemical Destabilization of Crude Oil Emulsions: Effect of Nonionic Surfactants as Emulsion Inhibitors. *Energy Fuels* **2009**, 23(9), 4575-4583.

147. Rane, J.P.; Harbottle, D.; Pauchard, V.; Couzis, A.; Banerjee, S. Adsorption Kinetics of Asphaltenes at the Oil–Water Interface and Nanoaggregation in the Bulk. *Langmuir* **2012**, 28(26), 9986-9995.

148. Firoozabadi, A.; Ramey, Jr. H.J. Surface Tension of Water-Hydrocarbon Systems at Reservoir Conditions. *J. Can. Pet. Technol.* **1988**, 27(03).

149. Ravera, F.; Loglio, G.; Kovalchuk, V.I. Interfacial Dilational Rheology by Oscillating Bubble/Drop Methods. *Curr. Opin. Colloid Interface Sci.* **2010**, 15(4), 217-228.

150. Noskov, B.A. Dilational Surface Rheology of Polymer and Polymer/Surfactant Solutions. *Curr. Opin. Colloid Interface Sci.* **2010**, 15(4), 229-236.

151. Ivanov I. Thin Liquid Films. *CRC Press* **1988**.

152. Liang, Y. Dynamic Demulsification Mechanism of Asphaltene-stabilized Water-in-oil Emulsions by Ethylcellulose. *University of Alberta* **2015**.

153. Zhang, X.; Tchoukov, P.; Manica, R.; Wang, L.; Liu, Q.; Xu, Z. Simultaneous Measurement of Dynamic Force and Spatial Thin Film Thickness Between Deformable and Solid Surfaces by Integrated Thin Liquid Film Force Apparatus. *Soft Matter* **2016**, 12(44), 9105-9114.

154. Nordgård, E.L.; Landsem, E.; Sjöblom, J. Langmuir Films of Asphaltene Model Compounds and their Fluorescent Properties. *Langmuir* **2008**, 24(16), 8742-8751.

155. Rane, J.P.; Pauchard, V.; Couzis, A.; Banerjee, S. Interfacial Rheology of Asphaltenes at Oil–Water Interfaces and Interpretation of the Equation of State. *Langmuir* **2013**, 29(15), 4750-4759.

156. Wang, J.; Lu, Q.; Harbottle, D.; Sjöblom, J.; Xu, Z.; Zeng, H. Molecular Interactions of a Polyaromatic Surfactant C5Pe in Aqueous Solutions Studied by a Surface Forces Apparatus. *J. Phys. Chem. B* **2012**, 116(36), 11187-11196.

157. Kairaliyeva, T.; Aksenenko, E.; Mucic, N.; Makievski, A.; Fainerman, V.; Miller, R. Surface Tension and Adsorption Studies by Drop Profile Analysis Tensiometry. *J. Surfactants Deterg.* **2017**, 20(6), 1225-1241.

158. Yeung, A.; Dabros, T.; Masliyah, J.; Czarnecki, J. Micropipette: a New Technique in Emulsion Research. *Colloid Surf. A-Physicochem. Eng. Asp* **2000**, 174(1), 169-181.

159. Moran, K.; Yeung, A.; Masliyah, J. The Viscoplastic Properties of Crude Oil–Water Interfaces. *Chem. Eng. Sci.* **2006**, 61(18), 6016-6028.

160. Wang, X.; Zhang, R.; Liu, L.; Qiao, P.; Simon, S.; Sjöblom, J.; Xu, Z.; Jiang, B. Interactions of Polyaromatic Compounds. Part 2. Flocculation Probed by Dynamic Light Scattering and Molecular Dynamics Simulation. *Energy Fuels* **2017**, 31(9), 9201-9212.

161. Israelachvili, J.N. Intermolecular and surface forces. *Academic Press* **2015**.

162. Tabor, R.F.; Wu, C.; Grieser, F.; Dagastine, R.R.; Chan, D.Y. Measurement of the Hydrophobic Force in a Soft Matter System. *J. Phys. Chem. Lett.* **2013**, 4(22), 3872-3877.

163. Shi, C.; Chan, D.Y.; Liu, Q.; Zeng, H. Probing the Hydrophobic Interaction Between Air Bubbles and Partially Hydrophobic Surfaces Using Atomic Force Microscopy. *J. Phys. Chem. C* **2014**, 118(43), 25000-25008.

164. Shi, C.; Zhang, L.; Xie, L.; Lu, X.; Liu, Q.; Mantilla, C.A.; van den Berg. F.G.A.; Zeng, H. Interaction Mechanism of Oil-in-Water Emulsions with Asphaltenes Determined Using Droplet Probe AFM. *Langmuir* **2016**, 32(10), 2302-2310.

165. Mikula, R.; Munoz, V. Characterization of Emulsions and Suspensions in the Petroleum Industry Using Cryo-SEM and CLSM. *Colloid Surf. A-Physicochem. Eng. Asp.* **2000**, 174(1), 23-36.

166. Ghosh, S.; Rousseau, D. Fat Crystals and Water-in-Oil Emulsion Stability. *Curr. Opin. Colloid Interface Sci.* **2011**, 16(5), 421-431.

167. Reed, S. G.; Bertholet, S.; Coler, R. N.; Friede, M. New Horizons in Adjuvants for Vaccine Development. *Trends Immunol.* **2009**, 30(1), 23-32.

168. Li, X.; He, L.; Wu, G.; Sun, W.; Li, H.; Sui, H. Operational Parameters, Evaluation Methods, and Fundamental Mechanisms: Aspects of Nonaqueous Extraction of Bitumen From Oil Sands. *Energy Fuels* **2012**, 26(6), 3553-3563.

169. Little R. C. Breaking Emulsions of Water in Navy Fuel Oils. *Fuel* **1974**, 53(4), 246-252.

170. Shetty, C.; Nikolov, A.; Wasan, D.; Bhattacharyya, B. Demulsification of Water in Oil Emulsions Using Water Soluble Demulsifiers. *J. Dispersion Sci. Technol.* **1992**, 13(2), 121-133.

171. Tchoukov, P.; Czarnecki, J.; Dabros, T. Study of Water-in-Oil Thin Liquid Films: Implications for the Stability of Petroleum Emulsions. *Colloid Surf. A-Physicochem. Eng.* **2010**, 372(1), 15-21.

172. Czarnecki, J; Tchoukov, P.; Dabros, T. Possible Role of Asphaltenes in the Stabilization of Water-in-Crude Oil Emulsions. *Energy Fuels* **2012**, 26(9), 5782-5786.

173. Gafonova, O. V.; Yarranton H. W. The Stabilization of Water-in-Hydrocarbon Emulsions by Asphaltenes and Resins. *J. Colloid Interface Sci.* **2001**, 241(2), 469-478.

174. Kang, W.; Xu, B.; Wang, Y.; Li, Y.; Shan, X.; An, F.; Liu, J. Stability Mechanism of W/O Crude Oil Emulsion Stabilized by Polymer and Surfactant. *Colloid Surf. A-Physicochem. Eng.* **2011**, 384(1-3), 555-560.

175. Mullins, O. C.; Sabbah, H.; Eyssautier, J.; Pomerantz, A. E.; Barre, L.; Andrews, A. B.; Ruiz-Morales, Y.; Mostowfi, F.; McFarlane, R.; Goual, L.; Lepkowicz, R.; Cooper, T.; Orbulescu, J.; Leblanc, R. M.; Edwards, J.; Zare, R. N. Advances in Asphaltene Science and the Yen–Mullins Model. *Energy Fuels* **2012**, 26(7), 3986-4003.

176. Hosseini-Dastgerdi, Z.; Tabatabaei-Nejad, S.; Khodapanah, E.; Sahraei, E. A Comprehensive Study on Mechanism of Formation and Techniques to Diagnose Asphaltene Structure; Molecular and Aggregates: a Review. *Asia-Pac. J. Chem. Eng.* **2015**, 10(1), 1-14.

177. Xiong Y.; Cao, T.; Chen, Q.; Li, Z.;, Yang, Y.; Xu, S.; Yuan, S.; Sjöblom, J.; Xu, Z. Adsorption of a Polyaromatic Compound on Silica Surfaces from Organic Solvents Studied by Molecular Dynamics Simulation and AFM Imaging. *J. Phys. Chem. C* **2017**, 121(9), 5020-5028.

178. Xiong, Y.; Li, Z.; Cao, T.; Xu, S.; Yuan, S.; Sjöblom, J.; Xu, Z. Synergistic Adsorption of Polyaromatic Compounds on Silica Surfaces Studied by Molecular Dynamics Simulation. *J. Phys. Chem. C* **2018**, 122(8), 4290-4299.

179. Simon, S.; Wei, D.; Barriet, M.; Sjöblom, J. An ITC and NMR Study of Interaction and Complexation of Asphaltene Model Compounds in Apolar Solvent I: Self-association Pattern. *Colloid Surf. A-Physicochem. Eng.* **2016**, 494, 108-115.

180. Teklebrhan, R. B.; Ge, L.; Bhattacharjee, S.; Xu, Z.; Sjöblom, J. Probing Structure-Nanoaggregation Relations of Polyaromatic Surfactants: a Molecular Dynamics Simulation and Dynamic Light Scattering Study. *J. Phys. Chem. B* **2012**, 116(20), 5907-5918.

181. Zhang, W.; Dong, G.; Yang, H.; Sun, J.; Zhou, J.; Wang, J. Synthesis, Surface and Aggregation Properties of a Series of Amphiphilic Dendritic Copolymers. *Colloid Surf. A-Physicochem. Eng.* **2009**, 348(1-3), 45-48.

182. Pradilla, D.; Simon, S.; Sjöblom, J.; Samaniuk, J.; Skrzypiec, M.; Vermant, J. Sorption and Interfacial Rheology Study of Model Asphaltene Compounds. *Langmuir* **2016**, 32(12), 2900-2911.

183. Niu, Z.; Ma, X.; Manica, R.; Yue, T. Molecular Destabilization Mechanism of Asphaltene Model Compound C5Pe Interfacial Film by EO-PO Copolymer: Experiments and MD Simulation. *The J. Phys. Chem. C* **2019**, 123, 10501-10508.

184. Feng, X.; Mussone, P.; Gao, S.; Wang, S.; Wu, S-Y.; Masliyah, J. H.; Xu, Z. Mechanistic Study on Demulsification of Water-in-Diluted Bitumen Emulsions by Ethylcellulose. *Langmuir* **2009**, 26(5), 3050-3057.

185. Zhang, L. Y.; Xu, Z.; Masliyah, J. H. Characterization of Adsorbed Athabasca Asphaltene Films at Solvent−Water Interfaces Using a Langmuir Interfacial Trough. *Ind. Eng. Chem. Res.* **2005**, 44(5), 1160-1174.

186. Zhang, L. Y.; Lawrence, S.; Xu, Z.; Masliyah, J. H. Studies of Athabasca Asphaltene Langmuir films at air–water interface. *J. Colloid Interface Sci.* **2003**, 264(1), 128-140.

187. Harbottle, D.; Chen, Q.; Moorthy, K.; Wang, L.; Xu, S.; Liu, Q.; Sjöblom, J.; Xu, Z. Problematic Stabilizing Films in Petroleum Emulsions: Shear Rheological Response of Viscoelastic Asphaltene Films and the Effect on Drop Coalescence. *Langmuir* **2014**, 30(23), 6730-6738.

188. Feng, X.; Wang, S.; Hou, J.; Wang, L.; Cepuch, C.; Masliyah, J.; Xu, Z. Effect of Hydroxyl Content and Molecular Weight of Biodegradable Ethylcellulose on Demulsification of Water-in-Diluted Bitumen Emulsions. *Ind. Eng. Chem. Res.* **2011**, 50(10), 6347-6354.

189. Zhang L. Y.; Xu, Z.; Masliyah, J. H. Langmuir and Langmuir-Blodgett Films of Mixed Asphaltene and a Demulsifier. *Langmuir* **2003**, 19(23), 9730-9741.

190. Ese, M-H.; Sjöblom, J.; Djuve, J.; Pugh, R. An Atomic Force Microscopy Study of Asphaltenes on Mica Surfaces. Influence of Added Resins and Demulsifiers. *Colloid Polym. Sci.* **2000**, 278(6), 532-538.

191. Daniel-David, D.; Le Follotec, A.; Pezron, I.; Dalmazzone, C. N.; Noïk, C.; Barré, L.; Komunjer, L. Destabilisation of Water-in-Crude Oil Emulsions by Silicone Copolymer Demulsifiers. *Oil Gas Sci. Technol.* **2008**, 63(1), 165-173.

192. Spiecker P. M.; Kilpatrick, P. K. Interfacial Rheology of Petroleum Asphaltenes at the Oil−Water Interface. *Langmuir* **2004**, 20(10), 4022-4032.

193. Freer, E.; Radke, C. Relaxation of Asphaltenes at the Toluene/Water Interface: Diffusion Exchange and Surface Rearrangement. *J. Adhes.* **2004**, 80(6), 481-496.

194. He, L.; Li, X.; Wu, G.; Lin, F.; Sui, H. Distribution of Saturates, Aromatics, Resins, and Asphaltenes Fractions in the Bituminous Layer of Athabasca Oil Sands. *Energy Fuels* **2013**, 27, 4677−4683.

195. Qiao, P.; Harbottle, D.; Tchoukov, P.; Masliyah, J.; Sjoblom, J.; Liu, Q.; Xu, Z. Fractionation of Asphaltenes in Understanding Their Role in Petroleum Emulsion Stability and Fouling. *Energy Fuels* **2017**, 31, 3330−3337.

196. Yang, X.; Hamza, H.; Czarnecki, J. Investigation of Subfractions of Athabasca Asphaltenes and Their Role in Emulsion Stability. *Energy Fuels* **2004**, 18, 770−777.

197. Papirer, E.; Bourgeois, C.; Siffert, B.; Balard, H. Chemical Nature and Water/Oil Emulsifying Properties of Asphaltenes. *Fuel* **1982**, 61, 732−734.

198. Phukan, M.; Koczo, K.; Falk, B.; Palumbo, A. New Silicon Copolymers for Efficient Demulsification. SPE Oil and Gas India Conference and Exhibition **2010**, SPE-128553-MS.

199. Wu, G.; He, L.; Chen, D. Sorption and Distribution of Asphaltene, Resin, Aromatic and Saturate Fractions of Heavy Crude Oil on Quartz Surface: Molecular Dynamic Simulation. *Chemosphere* **2013**, 92, 1465−1471.

200. Nenningsland, A. L.; Gao, B.; Simon, S.; Sjöblom, J. Comparative Study of Stabilizing Agents for Water-in-Oil Emulsions. *Energy Fuels* **2011**, 25, 5746−5754.

201. Bai, Y.; Sui, H.; Liu, X.; He, L.; Li, X.; Thormann, E. Effects of the N, O, and S Heteroatoms on the Adsorption and Desorption of Asphaltenes on Silica Surface: A Molecular Dynamics Simulation. *Fuel* **2019**, 240, 252−261.

202. Sun, H. Compass: An Ab Initio Force-Field Optimized for Condensed-Phase Applications Overview with Details on Alkane and Benzene Compounds. *J. Phys. Chem. B* **1998**, 102, 7338−7364.

203. Deguillard, E.; Pannacci, N.; Creton, B.; Rousseau, B. Interfacial Tension in Oil−Water−Surfactant Systems: On the Role of Intra-Molecular Forces on Interfacial Tension Values Using Dpd Simulations. *J. Chem. Phys.* **2013**, 138, 144102.

204. Dong, F.-L.; Li, Y.; Zhang, P. Mesoscopic Simulation Study on the Orientation of Surfactants Adsorbed at the Liquid/Liquid Interface. *Chem. Phys. Lett.* **2004**, 399, 215−219.

205. Teklebrhan, R.B.; Ge, L.; Bhattacharjee, S.; Xu, Z.; Sjöblom, J. Initial Partition and Aggregation of Uncharged Polyaromatic Molecules at the Oil–Water Interface: a Molecular Dynamics Simulation Study. *J. Phys. Chem. B* **2014**, 118(4), 1040-1051.

206. Jang, S.S.; Lin, S.-T.; Maiti, P.K.; Blanco, M.; Goddard, W.A.; Shuler, P.; Tang, Y. Molecular Dynamics Study of a Surfactant-Mediated Decane−Water Interface: Effect of Molecular Architecture of Alkyl Benzene Sulfonate. *J. Phys. Chem. B* **2004**, 108(32), 12130-12140.

207. Hockney R.; Eastwood, J. Computer Simulations Using Particles Mcgraw-Hill. *New York* **1981**.

208. Fan, Y.; Simon, S.; Sjöblom, J. Influence of Nonionic Surfactants on the Surface and Interfacial Film properties of Asphaltenes Investigated by Langmuir Balance and Brewster Angle Microscopy. *Langmuir* **2010**, 26(13), 10497-10505.

209. Mayo, S. L.; Olafson, B. D.; Goddard, W. A. Dreiding: A Generic Force Field for Molecular Simulations. *J. Phys. Chem.* **1990**, 94, 8897−8909.

210. Peña, A.A.; Hirasaki, G.J.; Miller, C.A. Chemically Induced Destabilization of Water-in-Crude Oil Emulsions. *Ind. Eng. Chem. Res.* **2005**, 44(5), 1139-1149.

211. Heath, A.R.; Fawell, P.D.; Bahri, P.A.; Swift, J.D. Estimating Average Particle Size by Focused Beam Reflectance Measurement (FBRM). *Part. Part. Syst. Char.* **2002**, 19(2), 84-95.

212. Atta, A.M.; Fadda, A.A.; Abdel-Rahman, A.A.H.; Ismail, H.S.; Fouad, R.R. Application of New Modified Poly(ethylene Oxide)-Block-Poly(propylene oxide)-Block-Poly(ethylene oxide) Copolymers as Demulsifier for Petroleum Crude Oil Emulsion. *J. Dispersion Sci. Technol.* **2012**, 33(6), 775-785.

213. Singh, B.P. Performance of Demulsifiers−Prediction Based on Film Pressure-Area Isotherms and Solvent Properties. *Energ Sources* **1994**, 16(3), 377-385.

214. Á lvarez, L.; Díaz, M. E.; Montes, F. J.; Galan, M. A. Langmuir´ Technique and Brewster Angle Microscope Studies of the Interfacial Behavior of Bitumen, Asphaltenes and

Maltenes at the Air−Water Interface. I. Effect of Different Spreading Solution Volumes. *Fuel* **2010**, 89, 691−702.

215. Moran, K.; Yeung, A.; Masliyah, J. The Viscoplastic Properties of Crude Oil−Water Interfaces. *Chem. Eng. Sci.* **2006**, 61(18), 6016-6028.

216. Agrawala, M.; Yarranton, H.W. An asphaltene association model analogous to linear polymerization. *Ind. Eng. Chem. Res.* **2001**, 40(21), 4664-4672.